UC Santa Barbara
UC Santa Barbara Electronic Theses and Dissertations

Title

Using Photoredox Catalysis to Expand Atom Transfer Radical Polymerizations and Radical Dehalogenations

Permalink

Author

Treat, Nicolas

Publication Date

2016

Peer reviewed|Thesis/dissertation

UNIVERSITY OF CALIFORNIA

Santa Barbara

Using Photoredox Catalysis to Expand Atom Transfer Radical Polymerizations and Radical

Dehalogenations

A dissertation submitted in partial satisfaction of the

requirements for the degree Doctor of Philosophy

in Materials

by

Nicolas John Treat

Committee in charge:

Professor Craig J. Hawker, Chair

Professor Javier Read de Alaniz

Professor Rachel A. Segalman

Professor Michael L. Chabinyc

June 2016

The dissertation of Nicolas John Treat is approved.

_____

Michael L. Chabinyc

_____

Rachel A. Segalman

_____

Javier Read de Alaniz

_____

Craig Hawker, Committee Chair

June 2016

Using Photoredox Catalysis to Expand Atom Transfer Radical Polymerizations and Radical

Dehalogenations

ACKNOWLEDGEMENTS

First, I would like to acknowledge both of my advisors, Craig and Javier. They have both been very supportive throughout my Ph.D. and have inspired me to be a better scientist. Craig has given me freedom to think and conduct research independently. He has taught me to care about every presentation I make, ever. And he has taught me to make sure to convert to PDF files when giving a presentation on a PC that was put together on a mac. He has also taught me to take a lot of pride in my work, and how to frame a story well so I can convince other people my work is important. I'll forever be grateful for getting to work in his group among some awesome scientists from a large variety of backgrounds. I could go on and on about what I'm thankful I got to learn in Craig's group- both from him and from the environment he seeks to create in the group. I'll be looking back at this experience for the rest of my life, remembering how much fun it was.

Javier has been a wonderful co-advisor to Craig. I've learned a lot more about mechanisms and organic synthetic methodology from him and his group, making me a much more well-rounded chemist. Javier has always believed in the work I did, encouraging me and motivating me to work even harder. He has put up with my complaints about the ins and outs of academic science, as well as some of the ridiculous things I've been asked to do during my Ph.d. He has been extremely supportive, letting me move away from a nitroso project that I spent my first year and a half working on that was doomed for failure (or maybe we can still publish something on that?). His reasonableness is overwhelming, and he's been an incredibly great source to go to talk to about experiments that aren't working or any needed guidance.

Brett Fors was a post-doc in the group when I joined. I thank Craig for pairing me with Brett, a brilliant organic chemist. Brett was tirelessly optimistic, believing that literally every experiment he did would work. I am incredibly lucky to have worked with such a smart, motivated scientist. I also learned the art of efficiency from Brett. He could do 10 experiments and all 10 would end up in his manuscript being published. Brett is still a great resource for me, even though he has moved on to Cornell as an assistant professor. I can't emphasize enough how lucky I was to start grad school by working with such a great scientist that I got along with really well. People need to joke and laugh more like Brett does.

My entire tenure at UCSB I've been surrounded with very smart people from both Craig and Javier's groups. People like Max Robb, Jason Spruell, Frank Leibfarth, Johannes and Hazel Sprafke, and Will Gutekunst have been incredibly good resources to go to with ideas to be challenged/ scrutinized. Damien Montarnal worked with my during my first year on a project that failed miserably, but he taught me a lot about rheology and dynamic covalent chemistry. His understanding of polymer physics was a great resource.

From Javier's group, I learned a ton of organic chemistry from Chuck Frazier and Dave Sandovol. I surfed a lot these past few months with Jimmy Hemmer, and I am grateful that Jimmy let me work on some awesome photoswitch research that he recently uncovered.

In the Dow lab where I sat for 4 of the past 5 years, I shared an office with up to 6 other people. We had some of the nicest desks of any students at UCSB thanks to Craig. These office mates included Brett Fors, Jetsuda Areephong, Saemi Poelma, Sameh Helmy, Andrey Samoshin, Yingdong Luo, Emre Discekici, Yvonne Diaz, Les Burnett, and a variety of undergraduates. It has been such a fun environment to be in. I'm grateful to my office

mates for putting up with me talking a lot about random things, and allowing me to interrupt them all the time asking questions about research. It is an incredibly gifted group of researchers, and we did some great research in that grungy old lab. Keep up the good work!

I have to specially thank Yingdong Luo, who was always quick to help me when I had questions. He is an incredible organic chemist, and can tell me what is going on in my NMR in an instant. He was a great resource to talk to about virtually everything under the sun, and can be incredibly stubborn if he disagrees with you. He became a great friend, and was a great coworker.

I'd also like to say thanks to my family. My parents are the best you could ask for. My older brothers Neil and Nathan were both inspiring to me as they both went into science fields. Neil in particular was a large reason I ever came to UCSB, as he was a part of Craig's lab before me, and told me to come work for a summer out in Santa Barbara. He definitely has inspired me as a scientist to do good work, and has been a huge resource throughout my Ph.D. for everything under the sun. Don't know where I'd be without my whole family.

Finally, last but definitely most importantly I'd like to thank my wife Bea. She has been so supportive of all I've done, even if she doesn't understand it. Her joy in life is so contagious. Her love and support have been invaluable over the course of our relationship. I wouldn't be able to work like I have or think like I have without her support and love. Pumped I get to spend my life with her.

VITA OF NICOLAS JOHN TREAT
June 2016

EDUCATION

Bachelor of Science, University of Southern Mississippi, May 2011 (*Summa Cum Laude*)
Doctor of Philosophy in Materials, University of California, Santa Barbara, June 2016
(expected)

PROFESSIONAL EMPLOYMENT

Graduate Research Assistant
University of California Santa Barbara, Professors Craig J. Hawker and Javier Read de
Alaniz (August 2011 – June 2016)

Undergraduate Research Assistant
University of Southern Mississippi, Hattiesburg, MS Professor Charles L. McCormick
(August 2007 – May 2011)
University of California, Santa Barbara, Professor Craig J. Hawker (Summer 2010)

PUBLICATIONS

Emre H. Discekici, Christian W. Pester, **Nicolas J. Treat**, Jimmy Lawrence, Kaila M.
Mattson, Benjaporn Narupai, Edward P. Toumaya, Yingdong Luo, Alaina J. McGrath, Paul
G. Clark, Javier Read de Alaniz, Craig J. Hawker *"Simple Benchtop Approach to Polymer
Brush Nanostructures Using Visible-Light-Mediated Metal-Free Atom Transfer Radical
Polymerization" ACS Macro Lett.* **2016**, *5, 258.*

Jetsuda Areephong, Kaila M. Mattson, **Nicolas J. Treat**, Saemi O. Poelma, John W.
Kramer, Hazel A. Sprafke, Allegra A. Latimer, Javier Read de Alaniz, Craig J. Hawker
*"Triazine-Mediated Controlled Radical Polymerization: New Unimolecular Initiators"
Polym. Chem.* **2016**, *7, 370.*

Yingdong Luo, Damien Montarnal, **Nicolas J. Treat**, Phillip D. Hustad, Matthew D.
Christianson, Edward J. Kramer, Glenn H. Fredrickson, Craig J. Hawker *"Enhanced Block
Copolymer Phase Separation Using Click Chemistry and Ionic Junctions" ACS Macro Lett.*
2015, *4,* 1332.

Nicolas J. Treat,* Emre H. Discekici,* Saemi O. Poelma, Kaila M. Mattson, Zachary M.
Hudson, Yingdong Luo, Craig J. Hawker, Javier Read de Alaniz *"A Highly Reducing Metal-
free Photoredox Catalyst: Design and Application in Radical Dehalogenations" Chem.
Commun.* **2015,** *51,* 11705.

Nicolas J. Treat, Hazel Sprafke, John W. Kramer, Paul G. Clark, Bryan E. Barton, Javier
Read de Alaniz, Brett P. Fors, Craig J. Hawker *"Metal-Free Atom Transfer Radical
Polymerization" J. Am. Chem. Soc.* **2014**, *136*, 16096. *Highlighted in C&EN, JACS
Spotlight, UC Convergence.*

Nicolas J. Treat, Brett P. Fors, John W. Kramer, Matthew Christianson, Chien-Yang Chiu, Javier Read de Alaniz, Craig J. Hawker *"Controlled Radical Polymerization of Acrylates Regulated by Visible Light" ACS Macro Lett*. **2014**, *3*, 580.

Frank A. Leibfarth, Martin Wolffs, Luis M. Campos, Kris Delany, **Nicolas J. Treat**, Matthew J. Kade, Bongjin Moon, Craig J. Hawker *"Low-temperature Ketene Formation in Materials Chemistry Through Molecular Engineering" Chem. Sci.* **2012,** *3*, 766.

Nicolas J. Treat, Deedee Smith, Chengwen Teng, Joel D. Flores, Brooks A. Abel, Adam W. York, Faqing Huang, Charles L. McCormick *"Guanidine-Containing Methacrylamide (Co)polymers via aRAFT: Toward a Cell-Penetrating Peptide Mimic" ACS Macro Lett.* **2011,** *1*, 100.

Joel D. Flores, **Nicolas J. Treat**, Adam W. York, Charles L. McCormick *"Facile, Modular Transformations of RAFT Block Copolymers via Sequential Isocyanate and Thiol-ene Reactions" Polym. Chem.* **2011**, *9*, 1976.

Joel D. Flores, Xuewei Xu, **Nicolas J. Treat**, Charles L. McCormick *"'Self-Locked' Micelles from a Zwitterion-Containing Triblock Copolymer" Macromolecules* **2009**, *42*, 4941.

Shawn D. McConaughy, Stacy E. Kirkland, **Nicolas J. Treat**, Paul A. Stroud, Charles L. McCormick *"Tailoring the Network Properties of Ca^{2+} Crosslinked Aloe vera Polysaccharide Hydrogels for in Situ Release of Therapeutic Agents" Biomacromolecules* **2008**, *9*, 3277.

AWARDS

MRL/Dow Travel Fellowship – 2013
National Science Foundation Graduate Research Fellowship – 2011
Who's Who In American Colleges and Universities – 2011
NASA Space Grant Scholar – 2010
Goldwater Scholar – 2009
Honors College Scholar – 2007
Mississippi Eminent Scholar Grant – 2007
Mississippi Resident Tuition Assistance Grant – 2007
Presidential Scholar – 2007

ABSTRACT

Using Photoredox Catalysis to Expand Atom Transfer Radical Polymerizations and Radical

Dehalogenations

by

Nicolas John Treat

Developing methodology for both polymer and small molecule synthesis is

tremendously valuable to society, as these methodologies lead to improvements in lifestyle.

This can be observed in the fields of olefin polymerizations leading to low-cost plastics, or

small molecule methodology allowing the synthesis of novel pharmaceuticals and additives

for polymer processing. These chemical transformations have played a large role in the

advancement of society.

A methodology that has been of particular interest in recent years is the field of

photoredox chemistry, unlocking a variety of new chemical transformations under mild

conditions. However, there remains a large area to explore with respect to applying

photoredox catalysis towards controlled chain-growth polymerizations. This dissertation's

focus is largely upon photoredox-based polymerizations, particularly in the area of atom

transfer radical polymerizations (ATRP). Using photoredox chemistry allows an

unprecedented level of temporal control over polymerization, and unlocks the ability to use

metal-free catalysts to conduct ATRP. Further, metal-free photocatalysts identified for

polymerization were also found to be useful for the development of reductive dehalogenations. The oxygen tolerant nature of metal-free ATRP was also examined, and structure-property relationships were explored with respect to the metal-free photocatalyst. Finally, a deeper mechanistic understanding of the system was developed, and used to alter polymerization properties.

TABLE OF CONTENTS

xiv

LIST OF FIGURES

1. Introduction

I. Motivation

Polymer and small molecule methodologies serve as the backbone for a multitude of societal needs: ranging from life-saving pharmaceuticals to the plastic we encounter ubiquitously. Thus, developing new methodologies for chemical transformations opens doors to better our lives through a myriad of applications.

In recent years the field of synthetic organic chemistry has seen a large renewed interest in photoredox catalysis.[1,2] This interest is due to the mild nature of reactivity that can be achieved by coupling visible light to a photocatalyst system, allowing the development of a number of novel transformations. However, many aspects of this chemistry are underdeveloped. Most notably, taking advantage of photoredox chemistries for controlled polymerization has been underdeveloped. In addition, the majority of the chemistry that has been developed relies on expensive, transition metal photocatalysts. This dissertation seeks to address these two areas, with an emphasis on developing novel photomediated polymerization techniques and highly reducing metal-free photocatalysts.

II. Photomediated Polymerization

A variety of controlled chain-growth methods have been developed in recent years that allow the production of low dispersity polymers with targeted molecular weights and complex macromolecular architectures, giving non-experts access to powerful functional materials. At the forefront of these methods are controlled radical and ring opening methods, including atom transfer radical polymerization (ATRP),[3-6] reversible addition-

fragmentation chain transfer polymerization (RAFT),[4,7-9] nitroxide mediated polymerization (NMP),[10-12] and ring opening metathesis polymerization (ROMP).[3,4]

Further inspired by nature's elegant and complex synthetic approach to macromolecules, researchers have recently become interested in developing externally regulated polymerizations.[7,10-12] To this end, many groups have reported the use of allosteric, chemical, electrochemical, mechanical, and photochemical methods for activating/deactivating polymerizations.[7,13] Of these, light is an exceptionally attractive external stimulus as it can be easily tuned via wavelength and intensity, and it provides a non-invasive method for temporal regulation. Importantly, for many decades photoinitiated polymerizations have been used industrially in areas such as coatings, adhesives, inks, and microelectronics.[4,14,15] These methods rely on the photoinitiation of free radical or cationic polymerizations to produce polymers with ill-defined dispersities and molecular weights.[4,9,16] Significantly, these prior developments in photolithography and photocuring provide a platform of infrastructure that may lead to rapid development of spatially and temporally controlled light-mediated strategies.

For these reasons as well as many others, there has been a surge of interest in the field of photomediated controlled polymerizations. Typically, these reactions exhibit accurate molecular weight control, low polydispersities, living chain ends, and efficient regulation of the chain-growth process with light (Figure 1.1). Ideally, the most mild conditions should be used in these methods, including room temperature reactions, a low intensity as well as low energy light source, and the ability to polymerize a variety of monomer families (i.e. methacrylates, acrylates, styrenics, etc…) while maintaining excellent functional group tolerance (i.e. amines, alcohols, halides). This introduction will

highlight recent advances in photocontrolled polymerizations with special emphasis on the aforementioned attributes, as well as the mechanisms involved in each system described.

Within the field of photomediated controlled polymerizations, two primary modes of photoregulation have been developed: photocatalyst activation and activation of a photoreactive chain-end (Figure 1.2). Special emphasis will be put on photocatalyst-activated systems, as they do not require specialized chain ends for polymerization to occur, and provide more robust polymers. However, chain-end photoactivated systems will also be described, as they remain an important area of photoregulated polymerizations.
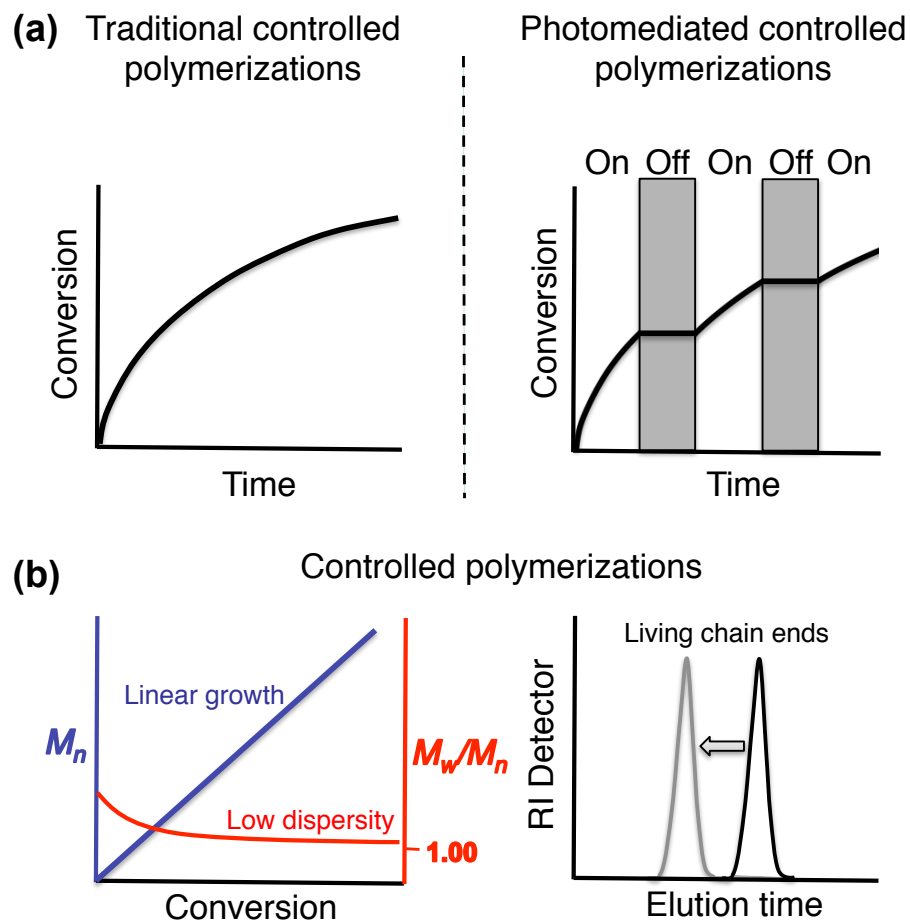
Figure 1.1 (a) Comparison of expected kinetic behavior for controlled polymerizations vs. photomediated controlled polymerizations and (b) characteristics expected for typical controlled polymerizations
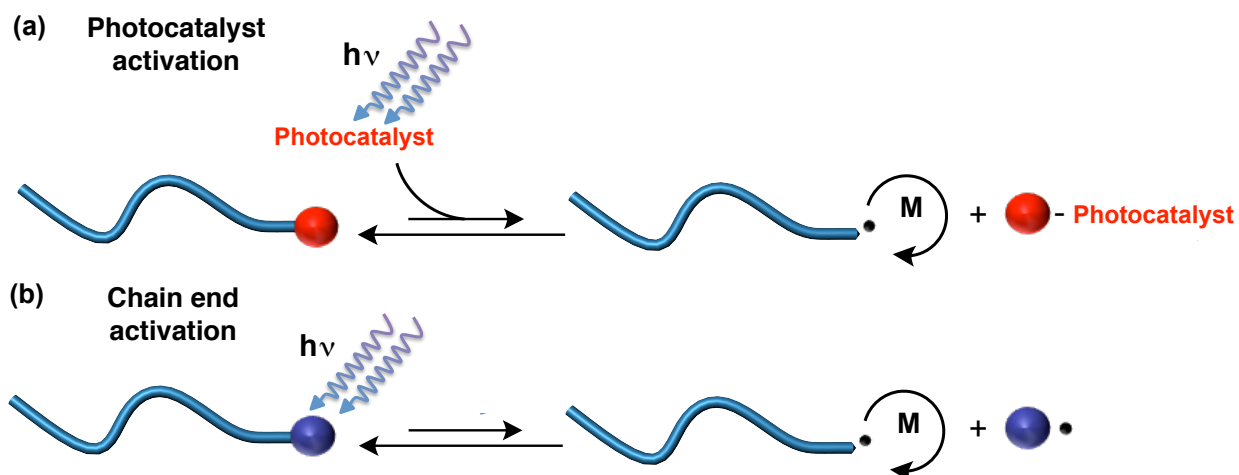
Figure 1.2 (a) Representative photocatalyst activation for photomediated polymerization and (b) chain-end activated polymerizations

III. Catalyst Activation by Light

A. Cu-Catalyzed Photoregulated Atom Transfer Radical Polymerizations (photoATRP):

ATRP is one of the most powerful methods for synthesizing well-defined materials, providing access to an array of functional polymers with varying architectures using commercially available catalyst-ligand systems. The classical form of ATRP takes advantage of a transition metal mediated redox equilibrium with an alkyl bromide initiator to gain control over polymerization. Mechanistically, these reactions rely on the reversible formation of propagating radicals in sufficiently low concentration to avoid termination events (Figure 3).

Although ATRP has been worked on for over 20 years, it wasn't until 2010 that initial efforts to perform photoATRP were conducted by employing a dithiocarbamate as

initiator in place of the traditionally used activated halide intiators.[10,17] The use of a dithiocarbamate was inspired by the iniferter (initiator- transfer –termination) chemistry developed in the Otsu lab in the 1980s,[13,18] wherein dithiocarbamates were cleaved photochemically to reversibly initiate and terminate chain ends. The initial photoATRP system employed CuBr to activate a dithiocarbamate upon UV irradiation at room temperature and was shown to exhibit moderate control ($M_w/M_n < 1.30$) at low conversions (<25%). Furthermore, the polymerization rate was greatly retarded (25-fold) when the light was removed from the system (Figure 1.4). However, due to residual CuBr, polymerization continued in the dark, and the low molecular weight distributions were only reported for low conversions. Nonethless, this was a significant step forward in demonstrating a photomediated ATRP process.
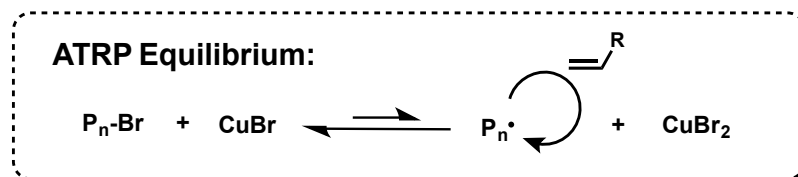
Figure 1.3 Traditional ATRP redox equilibrium

6
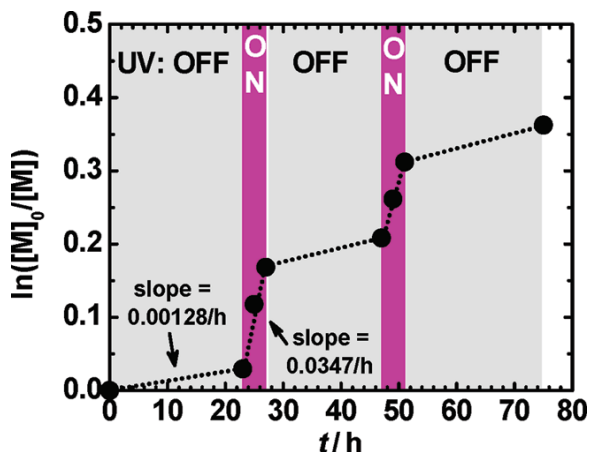
Figure 1.4 Photocontrolled ATRP using alkyl dithiocarbamates showing rate retardation and enhancement with cycling of the light source. Reprinted with permission from reference 10. Copyright 2010 American Chemical Society.

Following this, Yagci and coworkers were first to report a photoregulated ATRP process using a typical alkyl bromide initiator.[14,15,19] A 350 nm light source (3 mW/cm^2) was used to activate Cu(II)Br$_2$ with *N,N,N',N',N''*-pentamethyldiethylenetriamine (PMDETA) as a ligand for the polymerization of methyl methacrylate (MMA). These reactions showed good control ($M_w/M_n < 1.30$) up to moderate conversions (60-80%), with a linear increase of molecular weight with conversion and first order kinetics. Control experiments in the absence of light showed no polymerization, and importantly, when the reaction's exposure to light was cycled, very little polymerization occurred in the dark. Chain extension experiments were also conducted to further confirm the living nature of the polymerization. Importantly, this was the first example of photochemical formation of Cu(I)Br from Cu(II)Br$_2$. However, these polymerizations had an inhibition period which was attributed to the time to generate an appreciable amount of Cu(I) species., and furthermore, these experiments needed high catalyst loadings (1:1 Cu(II) to initiator).

Following this report, Mosnacek et al. developed a photoATRP using only 50-100 ppm of $Cu(II)Br_2$ for the polymerization of MMA using a mercury lamp coupled with a pyrex filter ($\lambda > 350$ nm, 20 mW/cm^2).[16,20] In this system, catalysts based both PMDETA and tris(2-pyridylmethyl)amine (TPMA) were shown to exhibit controlled polymerization behavior even at high (60-80 %) conversions. An initial proof of photoregulation was demonstrated, with little conversion observed when the light was turned off. Living chain ends were demonstrated using chain extension experiments. However, because of the intense light source used in these reactions, temperatures from 30-35 °C were typically observed.
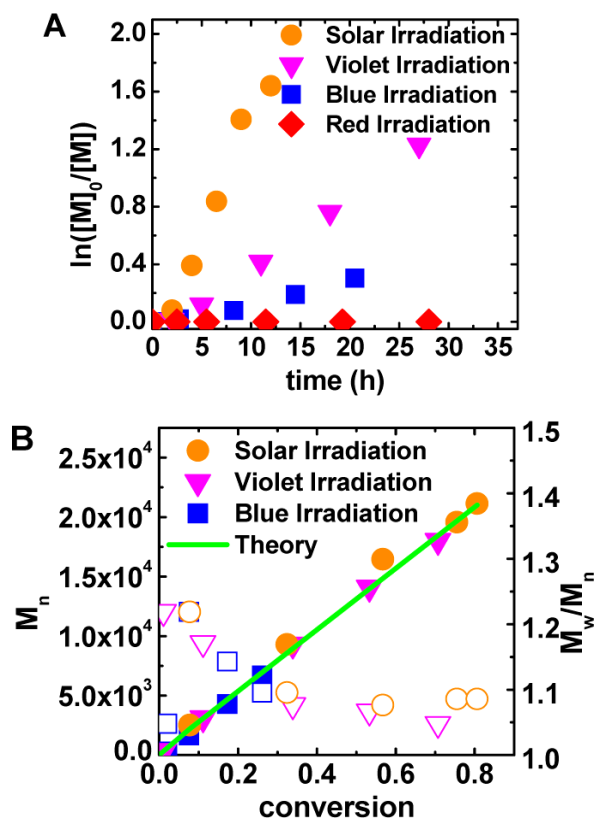
Figure 1.5 a) Kinetics and b) M_n and M_w/M_n evolution in polymerization of methyl acrylate using different irradiation sources under the following conditions: [MA]/[EBiB]/[CuBr$_2$]/[TPMA*] = 300:1:0.03:0.135 in 50 vol% DMF at room temperature. Reprinted with permission from reference 15. Copyright 2012 American Chemical Society.

Matyjaszewski and coworkers further extended the photoATRP system using 100 ppm of Cu(II)Br$_2$ to polymerize acrylates.[17,21] Various acrylate monomers were polymerized using tris((4-methoxy-3,5-dimetylpyridin-2-yl)methyl)amine (TPMA*) as ligand with blue (450 nm LEDs), violet (392 nm LEDs), and solar irradiation (Figure 1.5), where Solar irradiation showed the fastest kinetics. Lower energy red light (650 nm LEDs) showed no polymerization. Importantly, this was the first example of efficient photoregulation being observed using a Cu-based catalyst under such mild light sources,

with no polymerization observed in the absence of light. These conditions also enabled these polymerizations to be conducted in water giving oligoethylene oxide based methacrylate polymers. Analogously, Yagci and coworkers developed a photomediated ATRP in inverse micromemulsions that showed good control over the polymerization of oligoethyloxide methacrylates.[18,22]

Jordan and coworkers extended Cu-based photoATRP to the use of a standard fluorescent lamp for the polymerization of MMA.[19,23] Further, visible light was used to activate $Cu(II)Br_2$/PMDETA for surface initiated polymerizations on silicon surfaces that were functionalized with a pre-patterned ATRP initiator. Spatial control over this process was also demonstrated by using photomasks to selectively grow polymer brushes. This was the first example of using a Cu-based catalyst to achieve spatial control of polymer brush growth on surfaces.

Haddleton and coworkers also reported a photoinduced living radical polymerization of acrylates, using both sunlight and a UV light source (λ_{max} =360 nm).[20,24] Methyl acrylate was shown to be effectively polymerized using the UV light source and $CuBr_2$ in DMSO. This system gave similar characteristics to the traditional single electron transfer living radical polymerizations that have been performed in DMSO previously, with living behavior up to very high conversions (>95%), and with low dispersities ($M_w/M_n < 1.10$). This method also allowed for one-pot block copolymer formation and was shown to polymerize a variety of acrylate monomers. This initial report was expanded to also include the photoinduced living radical polymerization of a variety of acrylates including lauryl, octadecyl, and diethylene glycol ethyl ether acrylate.[21,25-29] Further, this method was then used to synthesize decablock copolymers.[22,27]

Haddleton and coworkers expanded on their initial work by isolating a pre-formed Cu(II) formate complex which could be used without any additional reducing agents or ligand to give identical photoregulated controlled radical polymerizations.[23,30] Control experiments showed that having equimolar amounts of Cu(II)Br$_2$ and Me$_6$TREN gave no polymerization, but in the presence of either excess ligand or sodium formate control over the polymerization was achieved with similar characteristics to the optimized system. Ishihara and coworkers have also expanded this Cu(II)Br$_2$ photomediated system to using tris(2-pyridylmethyl)amine (TPMA) in methanol to polymerize zwitterionic monomers such as 2-methacryloyloxyethyl phosphorylcholine.[24,31] Importantly, this extends the scope of Cu-based photomediated ATRP to more difficult monomer types.

A vast body of mechanistic work has been conducted to better understand photoregulated Cu-catalyzed ATRP.[25-29,32] Perhaps the most experimentally rigorous evaluation of the mechanism came from the groups of Haddleton and Barner-Kowollik, where a combination of pulsed-laser polymerization ($\lambda = 350$ nm) and high resolution mass spectrometry were used to study the Cu(II)/Me$_6$TREN/DMSO system. Through this evaluation, it was found that initiation of polymerization can be through the following: UV light-induced C–Br bond scission of the initiator (at 350 nm), Cu(I) activation of initiators after it's reduction from Cu(II) via an electron transfer from a photoexcited amine ligand, and the reduction of Cu(II) to Cu(I) via an excited copper species oxidizing the amine ligand (Figure 1.6). The combination of these processes and their relative contributions can vary based upon light sources and reaction conditions. For example, a fluorescent lamp will likely not be capable of directly inducing C–Br bond scission, and complexes based on ligands such as PMDETA will likely not absorb as much light as those comprised of TPMA.

11

Further, using a high intensity lasers to induce polymerization for these studies, likely causes some experimental differences from less intense light sources typically employed. UV-Vis spectroscopy was also used to verify that the Cu(II) was being consumed under experimental conditions, showing a decrease in absorption upon irradiation both in the presence and absence of monomer (Figure 1.7). In a separate study, Matyjaszewski and coworkers reported a mechanistic analysis using a combination of experimental and theoretical data to confirm under their light source that a photoreduction of Cu(II) with excess tertiary amine-based ligand is the primary mode of generating Cu(I) for polymerization in their system.[27,33]

Photomediated ATRP Mechanism:
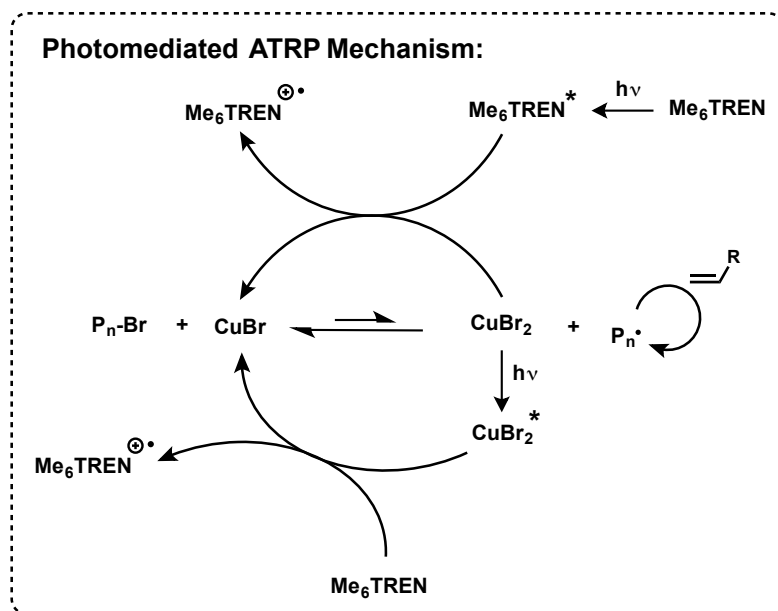
Figure 1.6 Mechanism for photomediated ATRP using Cu(II)Br$_2$ and electron-rich amine ligands
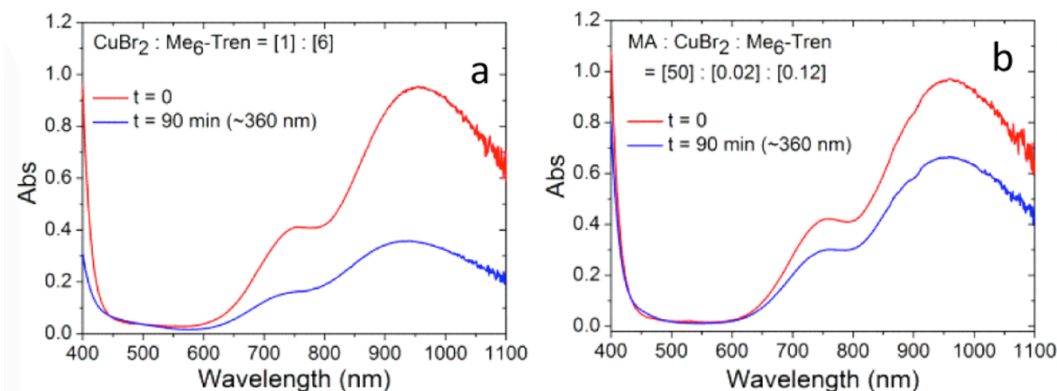
Figure 1.7 UV-Vis spectroscopy giving evidence for a decrease in Cu(II) concentration in the presence of excess ligand under irradiation

B. Photomediated ATRP with Non-Copper-Based Catalyst Systems

Hawker and coworkers (our group, or more specifically the legendary Brett P. Fors) reported one of the earliest truly photocontrolled polymerizations, which was catalyzed by an iridium-based catalyst.[30,34] 50 ppm of a *fac*-[Ir(ppy)$_3$] (Figure 1.8) was shown to efficiently control the polymerization of MMA in the presence of an alkyl bromide initiator. Excellent control over the polymerization was maintained even after multiple iterations of cycling the reactions exposure to light. Additionally, these polymerizations displayed living characteristics and enabled the efficient synthesis of block copolymers (PMMA M_w/M_n = 1.28, PMMA-*b*-PBnMA M_w/M_n = 1.30). Polymerization of methacrylic acid could also be performed with this system (M_w/M_n = 1.61), demonstrating the iridium catalyst's high functional group tolerance.

The mechanism of this process was proposed to occur through pathway previously reported for a photomediated atom transfer radical addition.[31,35] Excitation of the Ir(III)

complex with visible light affords a species that will reduce the alkyl bromide, resulting in the formation of an Ir(IV) complex and a propagating radical (Figure 1.9). The highly oxidizing Ir(IV) species can then deactivate polymerization via chain end oxidation to afford the dormant alkyl bromide. This process is fundamentally different from the previously discussed photoATRP using Cu-halide catalysts, as each propagating event is mediated by light, and does not rely on the traditional ATRP redox equilibrium. The extension of this work to acrylate systems will be the focus of chapter 2 of this dissertation.
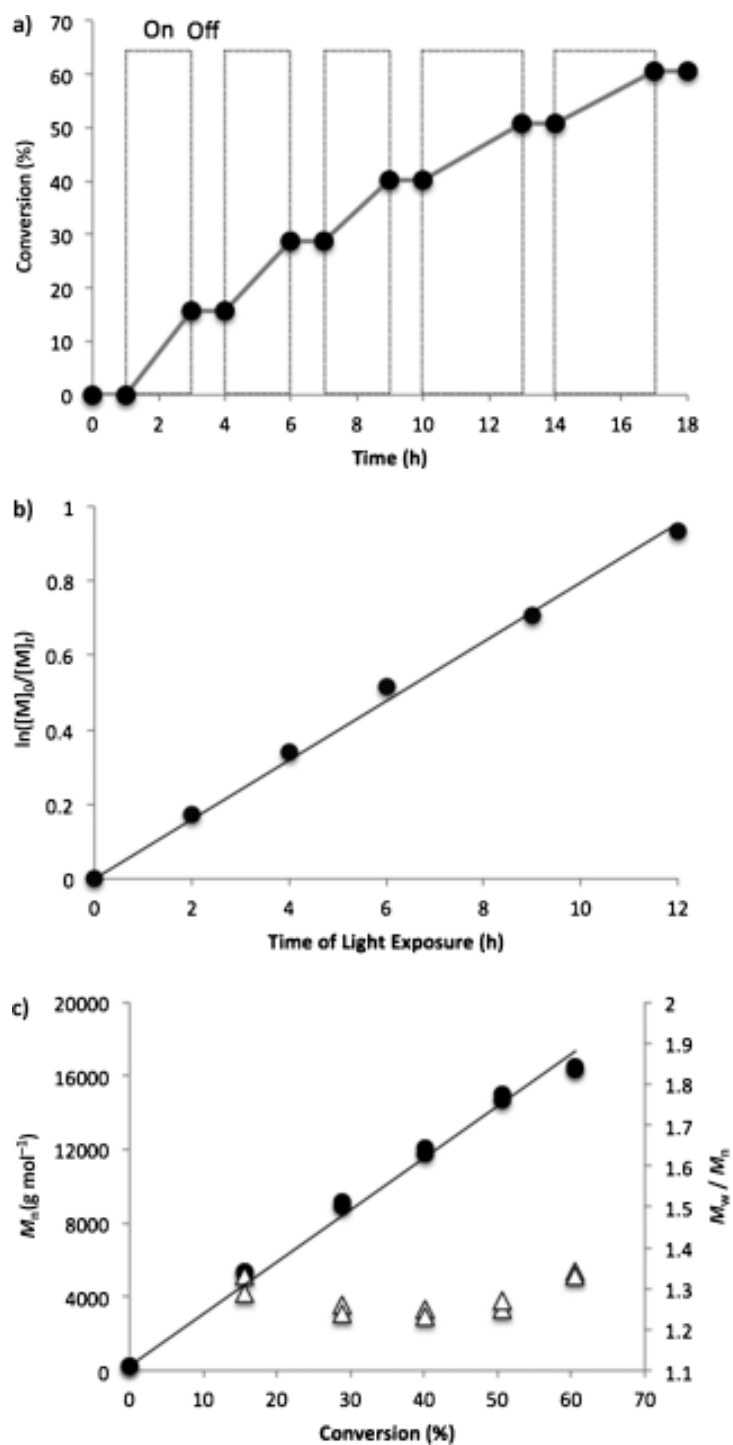
Figure 1.8 Polymerization of methyl methacrylate using Ir(ppy)₃ as a photocatalyst while cycling the reactions exposure to light

Further, a variety of other photocatalysts that have highly reducing excited states have also shown much promise to be useful for ATRP-type polymerizations. A dinuclear gold(I) complex, [Au$_2$(dppm))$_2$]Cl$_2$, was shown to very efficiently reduce alkyl bromide initiators when shining UV or sunlight on the solution.[33,36] Various wavelengths of UV light (i.e. 300, 350, 400 nm) were used to conduct polymerization with 1.25 mol % Au photocatalyst to polymerize MMA in DMF. Although dispersities were high ($M_w/M_n > 1.5$), chain extension of PMMA homopolymers showed living behavior. However, the molecular weight with conversion was not tracked for these experiments, and on/off kinetics were not demonstrated. Thus, this system appears to have promise for the development towards a photomediated ATRP, but further work is necessary.

A niobium nanoparticle system has also been developed for the polymerization of a variety of acrylate monomers using visible light.[34,37] Good polymerization characteristics were observed for this system when polymerizing N-isopropylacrylamide (NIPAAm), with a linear increase in molecular weight with conversion (up to 70%), and good on/off behavior, with no residual polymerization in the absence of light. Using niobium nanoparticles also allowed recycling of the photocatalyst through centrifugation. Further, niobium nanoparticles were shown to be tolerant to a variety of monomer systems, including methyl methacrylate, acrylic acid, and a variety of acrylates.

Recently, Poly and coworkers also reported a photomediated ATRP, employing a photoredox Cu catalyst.[35,38-40] Bis(1,10-phenanthroline)copper(I) was used as it has a strong absorption band in the visible regime, allowing a ~1 W blue LED to be used for polymerization. Mechanistically, this differs from previous photoATRP results as it relies on the copper complex to enter an excited state that will reduce the alkyl bromide to undergo

propagation. Controlled characteristics were observed during the polymerization, including

first order kinetics, linear increase in molecular weight with conversion (up to ~50%), and

low dispersities. It was also found that the addition of triethylamine as a reducing agent

helped speed up the reaction. Further, an Ir complex base on 2-(2'-benzothienyl)pyridine

ligands (Ir(btp)$_2$(tmd)) was also reported for controlled polymerization of MMA under a

similar mechanism with blue LEDs.[41,42] In each case, these catalysts were demonstrated to

efficiently stop and start polymerization in the absence and presence of light.
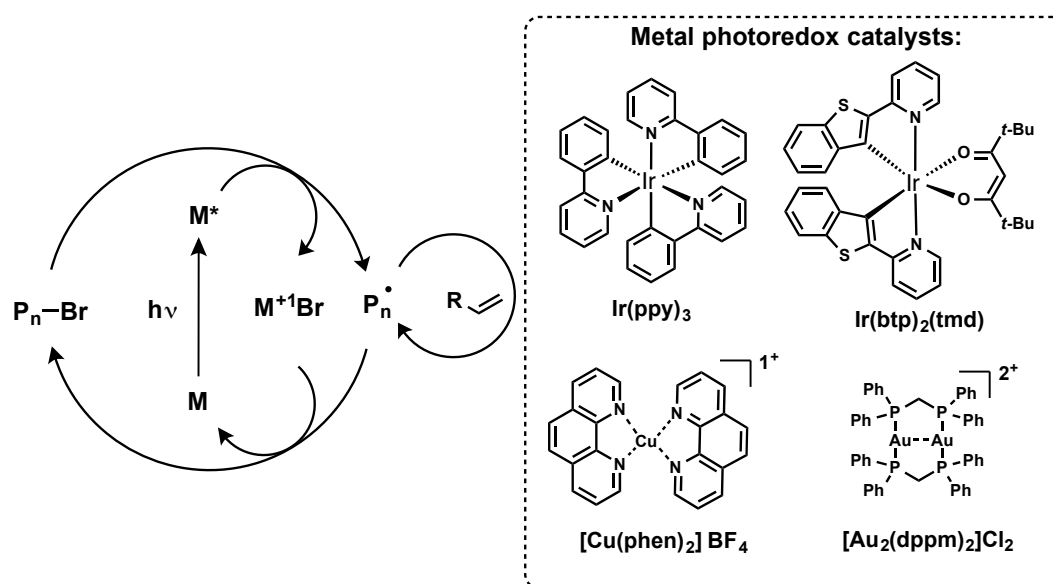
Figure 1.9 Photoredox catalysts used in photoATRP

A mechanistically distinct Ruthenium catalyst system has been developed that is photoregulated via ligand control.[37,43] Irradiation at 60 °C causes ligand dissociation from the metal-center, creating a 16-electron species that undergoes ATRP in the presence of an alkyl halide initiator (Figure 1.10). Light could be used to turn on and off these reactions due to the reversibility of the ligand coordination. However, broad molecular weight distributions (M_w/M_n = 1.4 - 1.6) were observed when polymerizing methyl methacrylate, styrene, and butyl acrylate. A combination of ^{1}H NMR and cyclic voltammetry provided good evidence for the proposed ligand dissociation mechanism. However, ^{1}H NMR also indicated some catalyst degradation, showing 35% decomposition after 6 h of irradiation. The authors propose that the degradation is likely the formation of a catalytically inactive dimeric Ru species. This is an interesting and promising form of photopolymerization, but further development is needed to fully demonstrate a living system.
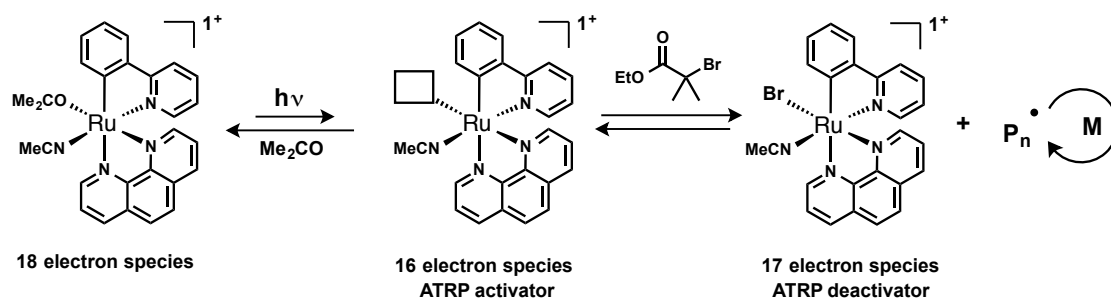
Figure 1.10 Photoregulated polymerization via ligand control

C. Iodine Mediated Photopolymerizations

Controlled radical polymerization using alkyl iodide initiators coupled with various catalyst systems have also been well studied. Due to the lability of the iodo chain-end, this

reduction event is much more facile than the carbon-bromide bond that is typically utilized for ATRP. However, this also leads to difficulty in livingness, as chain end degradation can readily occur.

The first report of light mediated iodo-chain end polymerization was from Koumura et al.[38-40,44] A dinuclear manganese carbonyl complex $[Mn_2(CO)_{10}]$ was shown to control polymerization of methyl acrylate, vinyl acetate, and styrene at 40 °C under a 27 W fluorescent bulb using an alkyl iodide initiator. Although photoregulation was observed for vinyl acetate, a steady loss in control was observed at higher conversion (i.e. increase in polydispersity), indicating that chain ends were not efficiently capped in the dark. Styrene gave the best control for this system, with a linear increase in molecular weight with conversion and acceptable molecular weight distributions ($M_w/M_n \sim 1.3$). Mechanistically, it was proposed that initiation was via the dinuclear manganese complex homolytically cleaving to form a manganese radical that then abstracted an iodo-radical from the initiator, forming an Mn-I bond and propagating chain-end. The Mn-I is proposed to recap the chain end when light is turned off.

Ma and coworkers have reported the visible light mediated polymerization of methacrylate monomers using perfluoro-1-iodohexane as initiator with $Ir(ppy)_3$ as catalyst.[41,45] Mechanistically, this work was proposed to be similar to the originally reported light mediated polymerizations of methacrylates using $Ir(ppy)_3$. This report demonstrated that the same Ir catalyst can be extended to iodo-chain ends and showed control over polymerization with fluorinated and glycidyl methacrylate monomers. Good photocontrol was observed for the system, with linear increase in molecular weight vs. conversion.

Vana and coworkers have reported the use of traditional photoinitiators coupled with alkyl iodide initiators for controlled radical polymerization of butyl methacrylate in bulk when irradiating with an 8 W mercury lamp ($\lambda > 366$ nm).[46-52] This study also explored thermal polymerization of iodo-chain ends, and found through a combination of experimental results and simulations that UV light gave polymers with lower dispersity and better control. It was hypothesized that the increase in control was due to the light induced C-I bond cleavage causing a nanomolar build-up of free iodine that led to both a reversible termination (i.e. ATRP) and degenerative transfer (i.e. RAFT) mechanism during polymerization. Good photocontrol was observed over the process with no reaction when the light was turned off, indicating that the chain ends were activated primarily by light. Finally, elevated temperatures were also be used in combination with UV light to increase polymerization rate but retain the added level of control afforded by light. This was an important demonstration of using an exceedingly simple system to gain control over polymerization, with light as activator and no added catalysts, ligand, or solvent necessary.

Another approach to gaining light control over iodine-based living radical polymerizations has been the use of amine catalysts.[53,54] This process used visible light ($\lambda = 350$-600 nm, 60 W xenon lamp) with tributylamine as catalyst (0.25-1 mol %). It was demonstrated that a variety of different methacrylates could be polymerized with low dispersities and targeted molecular weights. It was also shown that using different light intensities (300, 150, and 60 W) allowed for tuning the polymerization rate. A polymerization was conducted cycling the reactions exposure to light, but using different light intensities for each irradiation period, demonstrating disparate rates and illustrating good photoregulation. The same group also reported the use of various photocatalysts (12-25

mol %, λ_{max} = 530, 600, and 720 nm) for living radical polymerization over a range of wavelengths.[43,55] Further, it was shown for the first time that red light could be used in combination with a carbocyanine dye (λ_{max} = 720 nm) to induce controlled polymerization (Figure 1.11). The mechanism was proposed to occur via energy transfer and complexation of the catalyst with the iodo radical species upon homolysis to retain control over the reaction. A variety of methacrylate monomer functionalities (i.e. hydroxyethyl, glycidyl, polyethylene glycol, 2-ethylhexyl, and dimethylamino methacrylate) were tolerated using this method, and various block copolymers were produced as well. Finally, using an initiator that was capable of initiating ring-opening as well as radical polymerization, light wavelength was modulated to conduct a one-pot polymerization of both methyl methacrylate and δ-valerolactone, forming functional block copolymers.
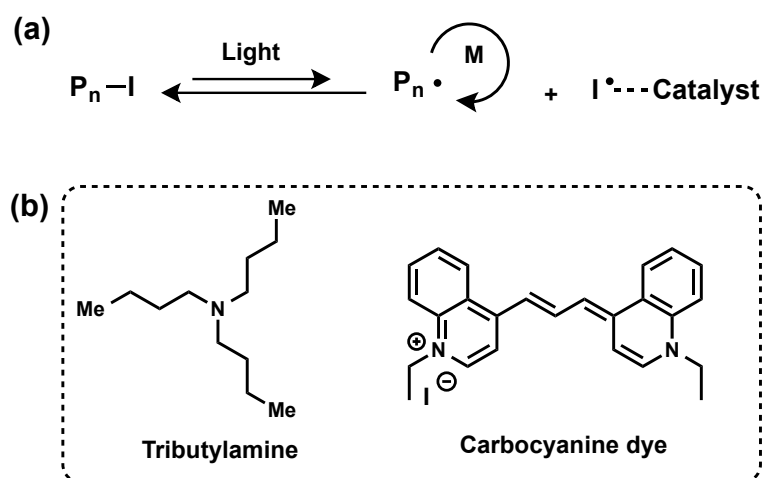
Figure 1.11 Proposed mechanism and representative catalysts for organic catalyzed iodine living radical polymerization

D. Metal-free Photomediated Ring Opening Metathesis Polymerization

Contrary to controlled radical polymerizations, ring opening metathesis polymerization (ROMP) utilizes cyclic monomers that are activated via ring strain. These polymerizations typically employ a metal-based catalyst (i.e. Ru, W, Mo) that propagate via metathesis reactions on the chain end. A longstanding challenge of this field has been the development of metal-free catalysts, which necessitated the development of new mechanistic approaches to ROMP.

Boydston and coworkers have recently demonstrated a controlled ring opening metathesis polymerization with organic photocatalysts.[44,56,57] This seminal work demonstrated that a metal-free ROMP process is possible, opening the doors to broader applications for ROMP-produced polymers. The key to this process is the use of a pyrylium photoredox catalyst that, upon absorption of visible light, enters a highly oxidizing excited state that can undergo single electron oxidation of a vinyl ether initiator (Figure 1.12). It was proposed that the oxidized vinyl ether forms a transient [2+2] complex with norbornene monomer that subsequently ring opens, undergoing an effective chain propagation. In the dark, the photocatalyst will reduce the chain end to form the stable vinyl ether and stop any propagation. A linear increase in molecular weight with conversion was demonstrated with norbornene, with dispersities from 1.3-1.5. Photoregulation was demonstrated, with very efficient stopping and starting of the reaction when the light was cycled on and off. The polymers prepared were compared to traditionally prepared ROMP polymers and shown have identical properties, as evidenced by glass transition temperatures and ^{1}H NMR. Following this initial work, it was then demonstrated that this system also tolerated the polymerization of dicyclopentadiene.[45,58] Random copolymerizations of norbornene and

dicyclopentadiene showed equivalent incorporations of the two monomers into the polymer backbone with no crosslinking. The resulting copolymers could then be subsequently crosslinked using thiol-ene click chemistry. One limitation was that homopolymerization of dicyclopentadiene stopped at low conversions (10-20 %), greatly limiting the molecular weights produced (2-4 kg/mol). Mechanistic studies demonstrated that the predominant *endo*-dicyclopentadiene caused both steric congestion and intramolecular side reactions of the radical cation with the pendant alkene, both of which contributed to the lack of conversion for the polymerization. Importantly, this work demonstrated the metal-free production of crosslinked ROMP-based polymers for the first time, and showed that this process is not limited to norbornene as monomer.

Metal-free ROMP still has several limitations to overcome. No evidence for the ability to form block copolymers has been given, indicating that the polymer chain ends aren't capable of being re-initiated, and the dispersities are higher than the metal ROMP processes, while the kinetics are much slower. Nonetheless, photoregulated metal-free ROMP is a significant advance for the field, nd it is anticipated that further development will lead to overcoming the aforementioned hurdles.
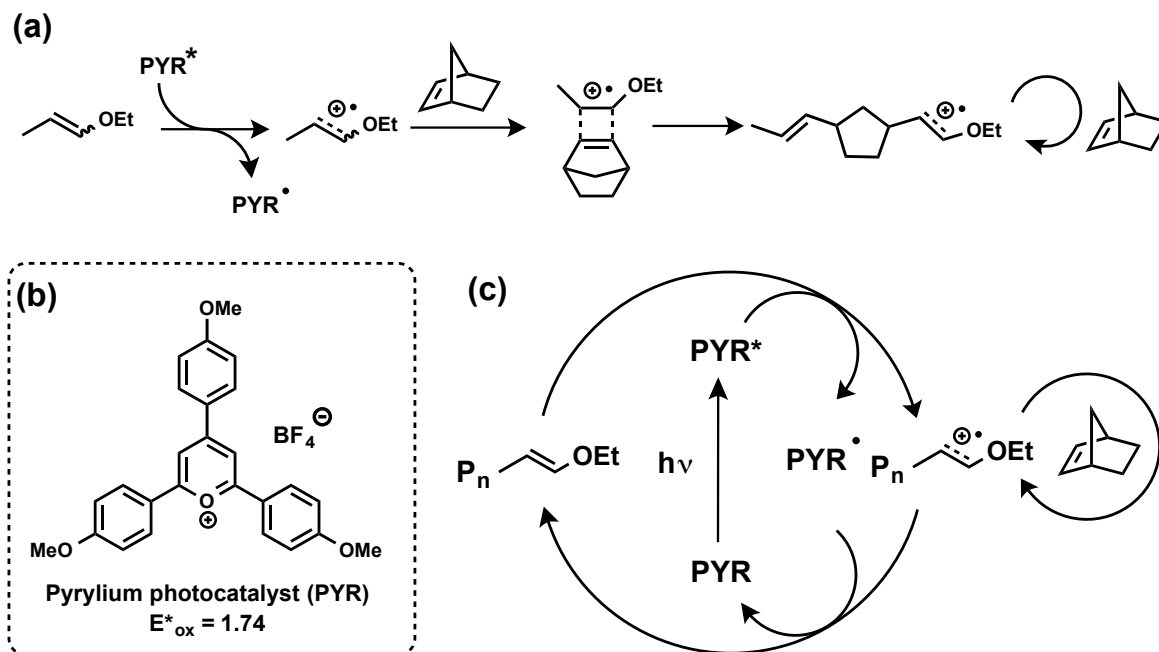
Figure 1.12 (a) Proposed mechanism for metal-free ROMP initiation and propagation (b) Pyrilium photoredox catalyst employed with excited state oxidation potential (vs. SCE) (c) Mechanistic rational for photoregulation

E. Photoregulated Reversible-addition Fragmentation Chain Transfer Polymerizations (photoRAFT)

Reversible-addition fragmentation chain transfer (RAFT) polymerization is one of the most commonly used techniques for producing well-defined polymers with access to advanced architecture and functionality.   The mechanism of RAFT relies on a high chain transfer constant of thiocarbonyl-thio (i.e. trithiocarbamate, dithioester, etc…) species to establish an equilibrium of growing radical chain-ends (Figure 1.13). RAFT is one of the most tolerant polymerization methods, allowing for a number of different functional groups to be polymerized with access to high conversions.
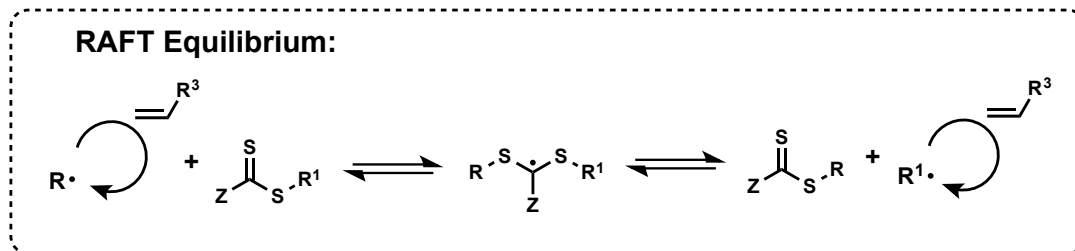
RAFT Equilibrium:

Figure 1.13 RAFT polymerization equilibrium operating via a chain (degenerative) transfer mechanism

Several groups have reported the use of photoinitiated UV[46,48-52,59] and visible[53,60] light RAFT polymerizations. However, these polymerizations were not demonstrated to be photomediated, and thus will not be the focus of this, although the potential for photomediation in these systems remains. In 2009, Cai and coworkers were the first to report a photomediated RAFT process.[55,61] Polymerizations were conducted in acidic aqueous solution using a water-soluble trithiocarbamate (EDMAT, see Figure 1.14), (2,4,6-trimethylbenzoyl)diphenylphosphine oxide (TPO) as the photoinitiator, and N-(2-acryloyloxyethyl) pyrrolidone (NAP) as a water-soluble acrylic monomer. A mercury vapor lamp equipped with an optical filter (λ = 405-577 nm, Intensity = 150 mW/cm^2) was used to irradiate the solution. A linear increase in molecular weight with conversion was demonstrated, with low dispersities and first order kinetics. Further, block copolymers were also produced, validating living chain-end fidelity. Finally, on-off kinetics were conducted at 7 °C, with very little conversion occurring in the dark, illustrating the first attempts at a photoregulated RAFT system. However, low temperatures were required in order to achieve photoregulation, and a photoinitator was present in the system, which may have aided in the re-initiation process when cycling the exposure to light. Later, the same group reported a

25

photocontrolled polymerization using a visible light absorbing RAFT agent (CPADB, see Figure 1.14) to polymerize amino-functional methacrylamide monomers in water. In this case, photoregulation was demonstrated at 25 °C, but the use of photoinitiator (TPO) was still required. In both of these initial reports, it was hypothesized that the origin of photocontrol was from a stabilized intermediate RAFT radical in the dark (Figure 1.13), although no experimental evidence was given to support this claim.[56,57,62]

Following this, a photocontrolled RAFT process in the absence of any additional photoinitiator was demonstrated by Johnson and coworkers.[58,63] A trithiocarbonate (bis-norbornene TTC, Figure 1.14) was irradiated with an 8 W black light (peak emission at 352 nm) in the presence of N-isopropylacrylamide (NIPAM) at room temperature. Due to lack of added external photoinitiator, this process relied solely on photocleavage of the C–S bond in the trithiocarbonate to initiate polymerization (Figure 1.14a). No reaction was observed in the dark, and efficient activation of the polymerization occurred upon exposure to light. Multiple "on"-"off" cycles were demonstrated with low dispersities (M_w/M_n < 1.2) observed up to 90% conversion. To verify livingness, a chain extension was carried out with NIPAM to form poly(NIPAM)-*b*-(NIPAM), with very efficient reinitiation of chain ends evidenced via the size exclusion chromatogram (SEC). These photopolymerizations were then used to synthesize a crosslinked polymer network of NIPAM utilizing the same RAFT agent. Subsequent chain extension of the network with sunlight demonstrated the novel concept for conversion of solar energy to mass in bulk materials.

A similar method was then adapted to the use of a continuous-flow setup, allowing access to rapid large scale synthesis of polymers.[59,64] TTC (Figure 1.14) was used as RAFT agent, and again irradiated using UV light (peak emission at 352 nm). The livingness

as well as photoregulation was demonstrated for the flow system (Figure 1.15), with various acrylamide and acrylate monomers being tolerated, enabling the synthesis of functional triblock copolymers. Importantly, by simply increasing the collection time, 3 g of poly(dimethylacrylamide) could be produced in 400 minutes, demonstrating a significant increase in reaction rate for the flow vs. bulk system without sacrificing any polymer properties. Further, this development opens the door for using flow systems to synthesize increasingly complex polymer structures.

Boyer and coworkers have reported photoregulated RAFT polymerization of methacrylate monomers under visible (green) light using low power (1-5 W) LEDs in combination with trithiocarbonate (CDTPA) RAFT agents.[60,65] Importantly, this was the first example of a photomediated RAFT polymerization controlling methacrylates using such mild visible light irradiation. Good photoregulation was observed with low dispersities throughout, and various organic solvents were tested (i.e. dioxane, acetonitrile, toluene, *N,N*-dimethylformamide), all showing good control over this process. One drawback of this system is the sensitivity of the RAFT agent (CDTPA) to chain end degradation, with the authors noting that polymers must be stored in the dark due to ambient light sensitivity. However, block copolymers are produced using this process, indicating that isolation and purification can be performed without adversely affecting chain ends.
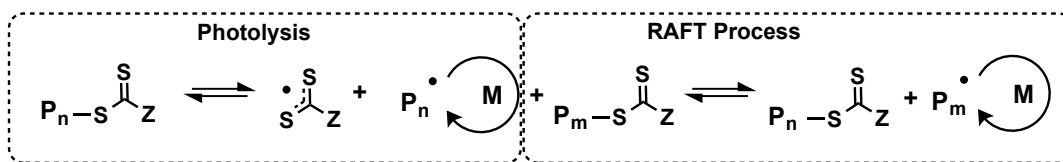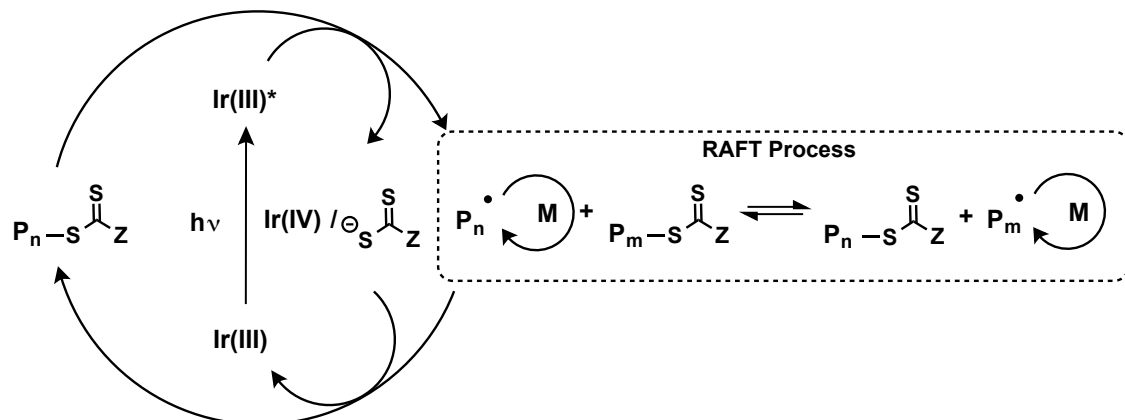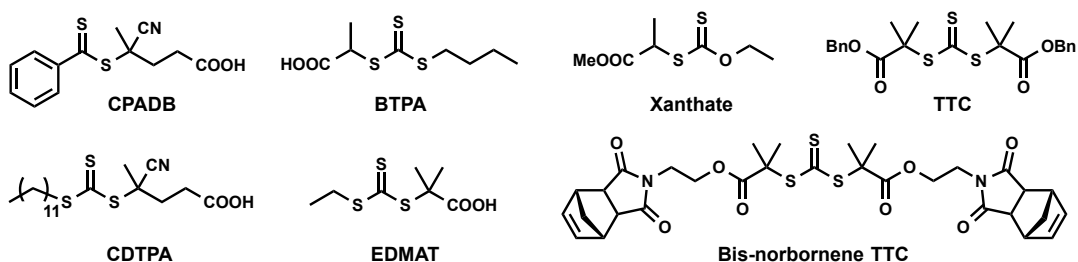
Figure 1.14 (a) Simplified mechanism of catalyst-free photomediated RAFT (b) Proposed mechanism of RAFT performed using photoredox catalysts (c) Examples of RAFT agents used in both catalyst-free and photoredox processes
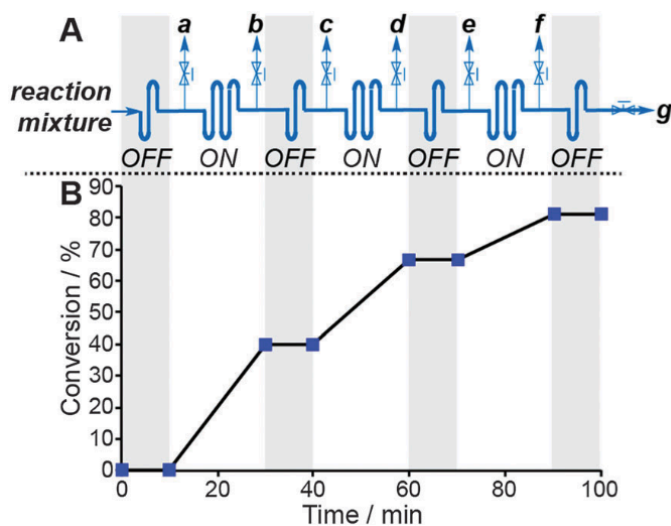
Figure 1.15 Photoregulated RAFT under continuous flow conditions using TTC as RAFT agent to polymerize NIPAM, taking aliquots before and after each "on" period. Reprinted with permission from reference 57. Copyright 2015 Royal Society of Chemistry.

Boyer and coworkers have also pioneered a photoredox-based RAFT system, employing small amounts (typically ppm) of photoredox catalysts in combination with RAFT agents to undergo living photomediated polymerization and extending photoRAFT to numerous monomer families and functionalities. Initially, their work focused on the use of Ir(ppy)$_3$ as a highly reducing photoredox catalyst (E^*_{red} = -1.7 V vs. SCE) for the reduction of a variety of RAFT agents (CPADB, E_{red} = -0.4 vs. SCE; BTPA, E_{red} = -0.6 vs. SCE; Xanthate, see Figure 1.14) to undergo polymerization of a large range of monomers, including methacrylates, acrylates, acrylamides, methacrylamides, styrenics, vinyl acetate, and *N*-vinyl pyrrolidone.[61,66] When conducting polymerizations, very low power (1-5 W) blue LEDs were used to give reasonable reaction rates (time = 2-48 h). Further, catalyst concentrations as low as 0.1 ppm were demonstrated to give control, although a lower rate was observed. Very good photoregulation was demonstrated for methyl methacrylate using

5 ppm of Ir(ppy)$_3$, with first order kinetics during light exposure and a linear increase in molecular weight with conversion (M_w/M_n = 1.05-1.3). Living chain ends were verified using ^{1}H NMR and UV-Vis absorbance to observe the presence of the RAFT agent in the purified polymer. Additionally, a variety of block copolymers were formed under these conditions, thoroughly demonstrating the ability to synthesize more complex materials.

Interestingly, it was discovered that these polymerizations were tolerant to oxygen due to the use of a photoredox catalyst that can directly react with molecular oxygen to form an inactive oxygen species. Thus, without degassing, polymerization of acrylates and methacrylates were demonstrated to be controlled, with only a moderate inhibition period observed (~1-3 h), likely due to the time it takes for the catalyst to convert the O$_2$ to an unreactive species (Figure 1.16). Finally, by letting conversion approach 99% and subsequently adding additional monomers multiblock acrylate copolymers were produced.[62,67]

Following Boyer and coworkers original report, a more thorough analysis was conducted for polymerizations mediated by Ru(bpy)$_3$Cl$_2$.[63] Extensive evidence for a controlled photomediated system was demonstrated for both methacrylate and acrylate monomers. Further, kinetic studies demonstrated that a 1-2 hour inhibition period was observed for polymerizations of acrylates, methacrylates, and acrylamides in the presence of oxygen. To confirm no catalyst degradation, the catalyst was pre-irradiated for 16 hours in solution before adding monomer and RAFT agent. Upon monomer and RAFT agent addition, polymerization was observed with identical characteristics to the non pre-irradiated solution, providing evidence that an insignificant amount of catalyst degradation occurs. Additionally, a more thorough analysis of the polymerization of vinyl acetate and N-

vinylpyrrolidinone was conducted using Ir(ppy)$_3$.[64] Again very similar characteristics for photoregulated polymerizations and block copolymerizations were demonstrated for unactivated monomers both in the presence and absence of oxygen. In nearly all cases, very good photoregulation and low dispersities (often < 1.2) were observed.
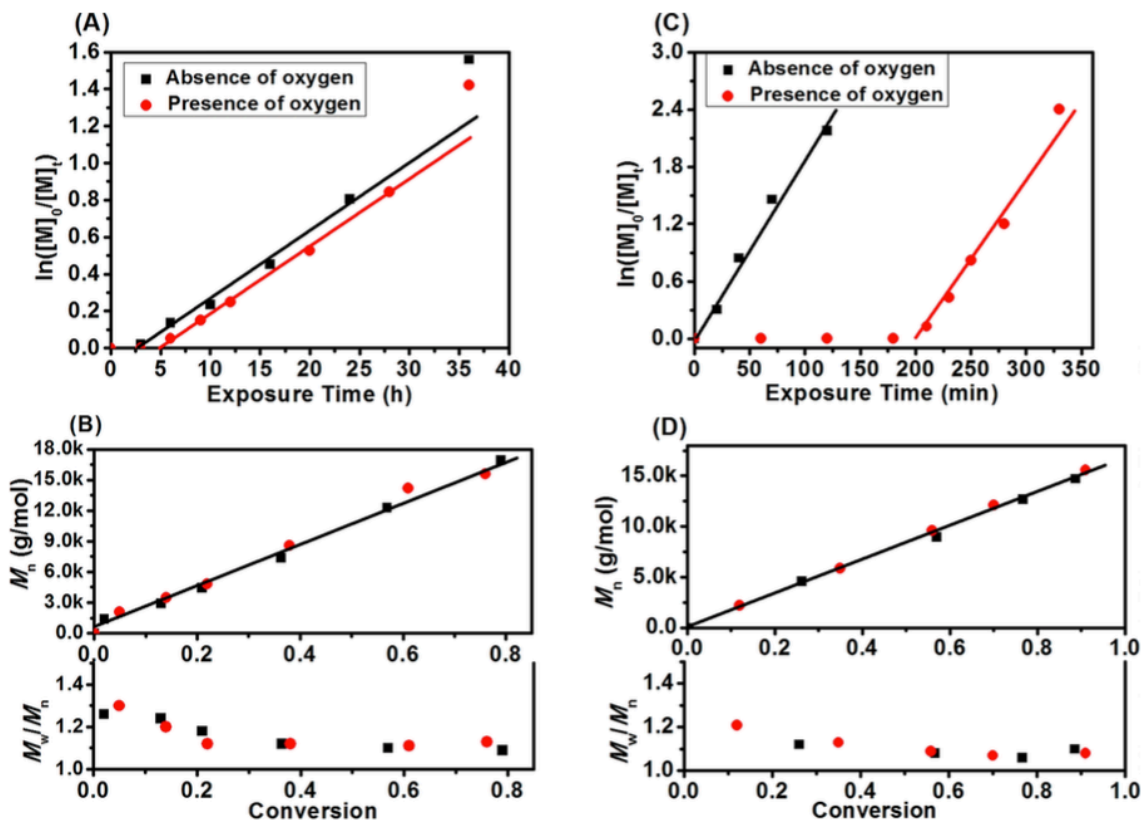
Figure 1.16   Kinetics and molecular weight control experiments conducted in the absence and presence of oxygen for (a) and (b) methyl methacrylate and (c) and (d) methyl acrylate using Ir(ppy)$_3$ in DMSO. Reprinted with permission from reference 59. Copyright 2014 American Chemical Society.

This system was then extended to conducting photoRAFT in the presence of water using Ru(bpy)$_3$Cl$_2$ as a water-soluble, biocompatible photocatalyst.[65] Typically 1-10 ppm

31

could be used to control the polymerization of dimethylacrylamide, with good photoregulation and living behavior. Further, in addition to extensive evidence for a controlled polymerization in water, protein polymer conjugates were synthesized using a grafting from approach (Figure 1.17). Bovine serum albumin (BSA) was chosen as a model protein, and the BTPA-based RAFT agent was synthesized containing a disulfide bond. The RAFT agent was subsequently attached to the BSA via a pyridyl disulfide exchange. Following this, polymerization was conducted under the optimized conditions to synthesize the protein-polymer conjugate. To verify livingness, SECs of the protein-polymer conjugate were obtained, demonstrating that chain extension occurred, although some unconjugated BSA remained in the solution due to the inefficiency of the disulfide exchange reaction. The polymers were then cleaved and run on the SEC independently, verifying a low dispersity and linear increase in molecular weight with conversion for polymerizations from the protein. Finally, BSA was shown to lose no activity after being subjected to the polymerization conditions.
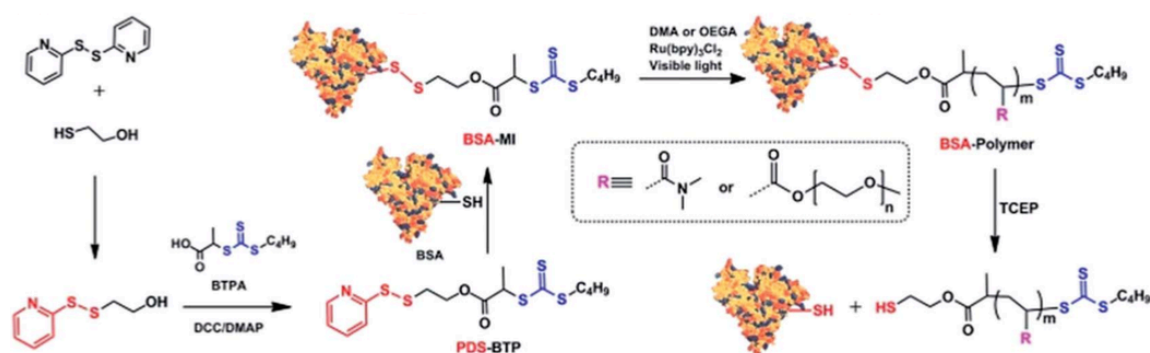
Figure 1.17 Synthetic approach for synthesis of polymer-protein conjugates using Ru(bpy)$_3$Cl$_2$ as photocatalyst. Reprinted with permission from reference 63. Copyright 2014 Royal Society of Chemistry.

PhotoRAFT was then extended to using a porphyrin-based chlorophyll catalyst in combination with various RAFT agents.[66] In this case, the most widely found form of chlororphyll (Clorophyll a, Figure 1.18) was extracted from spinach leaves and isolated via column chromatography. The naturally occurring catalyst was then employed for the polymerization of methacrylates, acrylates, and acrylamides with good control. An interesting aspect of this system is the catalyst's absorption (λ_{max} = 461 and 635 nm), which allowed the polymerization to occur under irradiation from both blue and red LED light sources. Photoregulation was observed for polymerizations under red light, and no conversion occurred when irradiating with green light due to the lack of photocatalyst absorption under that wavelength. The control of polymerization under red light indicates the ability of photoRAFT to occur under remarkably mild conditions, giving promise for future biological applications.

PhotoRAFT was also extended to organic photoredox catalysts, using fluorescein and Eosin Y to perform visible light mediated controlled polymerization. The excited state redox potentials of Eosin Y and fluorescein are -1.1 and -1.2 V vs. SCE, respectively, rendering them reducing enough to activate the RAFT agents (-0.4 to -0.8 V vs. SCE) in order to achieve controlled polymerization. Eosin Y proved to be the best organic photocatalyst. Further, triethylamine (TEA) could be added to improve the kinetics of the polymerization both in the presence and absence of oxygen. This is likely due to the oxidation of TEA by Eosin Y*, leading to the formation of a more reducing Eosin Y radical anion that will more efficiently initiate polymerization. Polymerization was well controlled from 10-100 ppm of Eosin Y, and block copolymers were formed using this process, verifying living chain ends.
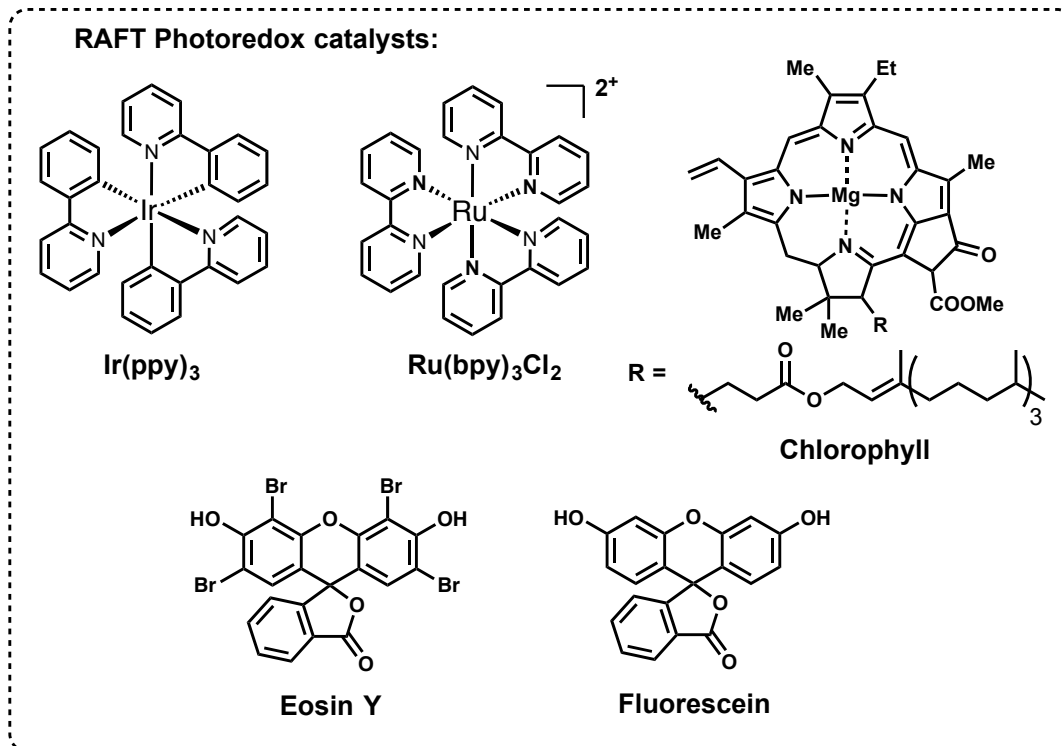
Figure 1.18 Photoredox catalysts used for photoRAFT polymerizations

PhotoRAFT is arguably the most general photomediated strategy to date, with a variety of organic and metal photoredox catalysts used for polymerization. This is potentially due to a heavier reliance on the RAFT mechanism for gaining control. Nonetheless, these systems are highly tolerant to numerous conditions, and exemplify how photoregulation can open up previously inaccessible levels of control over polymerization.

II. Polymerization via Light Activated Chain-ends

Another area of photoregulation has been achieved through using photosensitive chain ends. In each case, the chain end absorbs light, undergoing homolysis to form a propagating radical, and stable radical in solution that reversibly caps the growing polymer

chains. It should be noted that many of the RAFT and Iodine systems previously discussed also follow a light absorbing chain-end mechanism. Apart from these, three main systems have been reported for chain end photoregulated polymerizations.

First, Yang and coworkers reported a cycloketyl radical mediated living polymerization of methyl methacrylate and butyl acrylate using a 9,9'-bixanthene-9,9'-diol (BiXANDL) initiator (Figure 1.19).[67] These polymerizations followed a dissociation-combination mechanism, with UV light causing the BiXANDL chain end to undergo homolysis to initiate polymerization, and the resulting stable xanthone radicals capping the growing polymer chains. Also, due to UV light activation of chain ends, the polymerization conversion could be controlled by turning the light on and off, with control observed throughout the reaction.

Figure 1.19 Mechanism of dissociation-combination type polymerizations and examples of photoabsorbing chain ends

Another chain end activation system takes advantage of the lability of Cobalt-carbon bonds. Most commonly light has been used as an initiation source for cobalt polymerizations,[68-72] and, similar to photoRAFT, many of these systems still have potential for photoregulation. However, the only report to date of a photoregulated cobalt mediated radical polymerization has been using a cobalt porphyrin complex (Figure 1.19).[73] To gain control, these polymerizations required the preparation of a poly(methyl acrylate) macroinitiator. These initiators could be synthesized by combining methyl acrylate, AIBN, and the cobalt porphyrin at 60 °C and running the reaction to very low conversion. Although this is an unconventional form of an initiating species, these macroinitiators were demonstrated to polymerize *N,N*-dimethylacrylamide (DMA), *N,N*-diethylacrylamide (DEA), and *N*-acryloylmorpholine (AMO) with good control up to high conversions using

visible light (500 W Xe lamp, 400-800 nm optical filter). A kinetic experiment demonstrated first order kinetics and a linear increase in molecular weight up to 80% conversion with low polydispersities (M_w/M_n < 1.25). Furthermore, photomediation was demonstrated via an "on"/"off" experiment, with efficient stopping and starting of the reaction. Triblock copolymers between the PMA macroinitiator, DMA, and AMO or DEA were synthesized using visible light (PMA-*b*-DMA-*b*-DEA M_n = 69,100 g/mol, M_w/M_n = 1.25; PMA-*b*-DMA-*b*-AMO M_n = 84,100 g/mol, M_w/M_n = 1.28) to demonstrate livingness. A limitation of these polymerizations is the inherent lability of the Co–C bond, making the materials difficult to handle and therefore, requiring the preparation of an ill-defined macroinitiatior. However, this system remains a powerful method for producing functional materials and represents an important step for photoregulation using cobalt chain ends.

Another impressive light controlled polymerization is organotellerium living radical polymerization (TERP).[74] Yamago et al. have elegantly reported the use of a organotellerium transfer reagent with an absorption maximum at 351 nm, that, when irradiated with a 500 W high-pressure mercury lamp with a short-wavelength cutoff filter (>470 nm), underwent C–Te bond homolysis. The polymerization of butyl acrylate with the 500 W Hg lamp at ~50 °C reached 98% conversion in 2 hours. When using no cutoff filter from the same light source, uncontrolled polymerization was observed (M_w/M_n = 1.87). However, whenever using lower intensity light sources such as a 30-100 W black lamp, 6 W light emitting diode lamp,[75] or even sunlight, the polymerization was controlled, implying that a steady state equilibrium of polymer chain growth occurs with a variety of light sources. An "on-off" kinetic study was conducted to demonstrate the ability to retain chain ends through multiple cycles of stopping and starting the reaction. The polymerization was

stopped and started multiple times, in each case observing no conversion in the dark, and rapid re-initiation upon re-exposure to light, with good control. Higher molecular weight polymers (polybutylacrylate, M_n = 223,000 g/mol, PDI = 1.18) could be synthesized under identical conditions to those previously described. Another attractive feature of this system is the modularity of the organotellurium transfer agent. A single initiator was used for the synthesis of a variety of monomer families (acrylates, acrylamides, nonconjugated N-vinyl monomers).

III. Photoredox-based Dehalogenations

The field of photoredox catalysis has also unlocked a variety of key small molecule organic transformations.[2] Fundamentally, these reactions rely on single electron transfer events between organic substrates and a photocatalyst upon absorption of visible light. Key to this process is the fact that these photocatalysts are not strongly oxidizing or reducing in the ground state, but drastically change in character upon entering an excited state. By taking advantage of this, a number of different bonds have been oxidized and reduced.
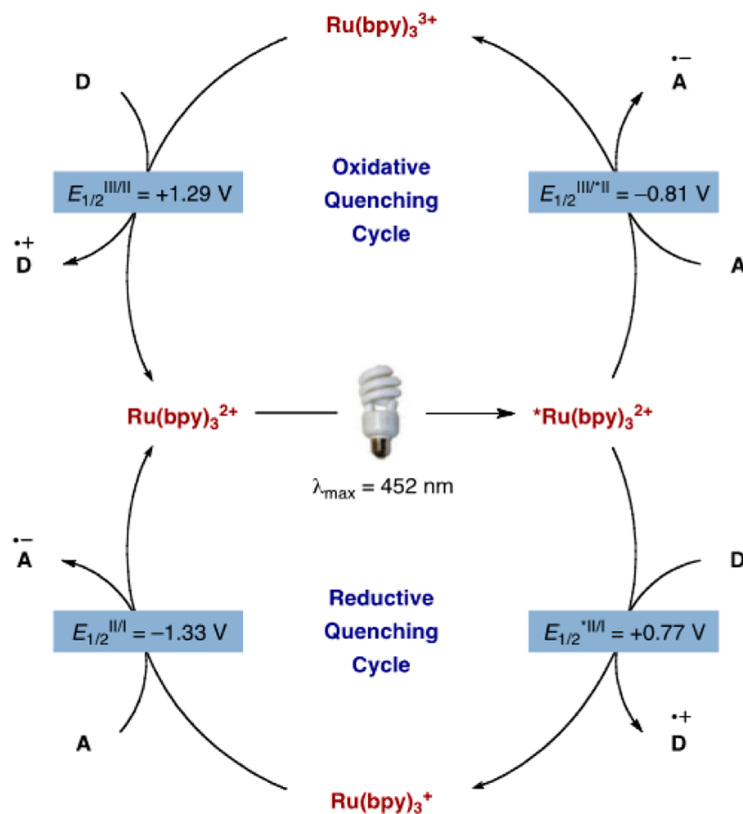
Scheme 1.1 Mechanistic routes of Ru(bpy)$_3$ when excited, demonstrating the ability to be both reducing and oxidizing in the excited state

For example, Ru(bpy)$_3$, a commonly used photocatalyst, when excited by visible light (λ_{max} = 452 nm) can be both oxidizing and reducing in its excited state (Scheme 1.1). These excited state redox potentials are estimated using a combination of ground state redox potentials and luminescence spectroscopy.[76] For Ru(bpy)$_3$, upon excitation it can act as a strong photoreductant (E*$_{red}$ = - 0.81 V vs. SCE), but it can also be oxidized to Ru(I), which is also a strong reductant (E$_{red}$ = -1.33 V vs. SCE). Such versatility allows photoredox catalysis to be an extremely powerful methodology. Further, substrates reduction and oxidation potentials can be measured using cyclic voltammetry, allowing researchers to estimate if a process is thermodynamically favorable.

An early example that took advantage of Ru(bpy)₃ for reductive processes was by Stephenson and coworkers, reporting the tin-free radical dehalogenation of a variety of activated halides (Scheme 1.2).[77] This work relied on an alkyl amine in combination with formic acid to act as both a terminal oxidant as well as hydrogen atom source. These conditions, working at ambient temperature with very mild sources of oxidants/reductants, pioneered a new form of reduction that moved away from conditions requiring tin hydrides in combination with free radical initiators (i.e. azobisisobutyronitrile).
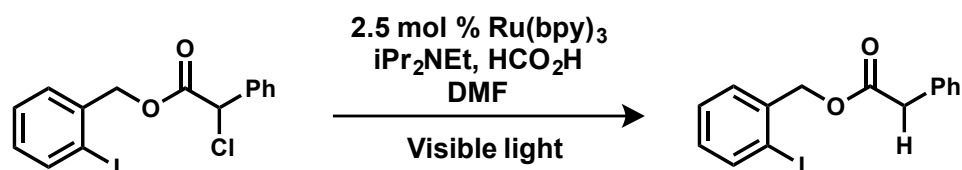
Scheme 1.2 Example of a tin-free reductive dehalogenation of an activated alkyl halide
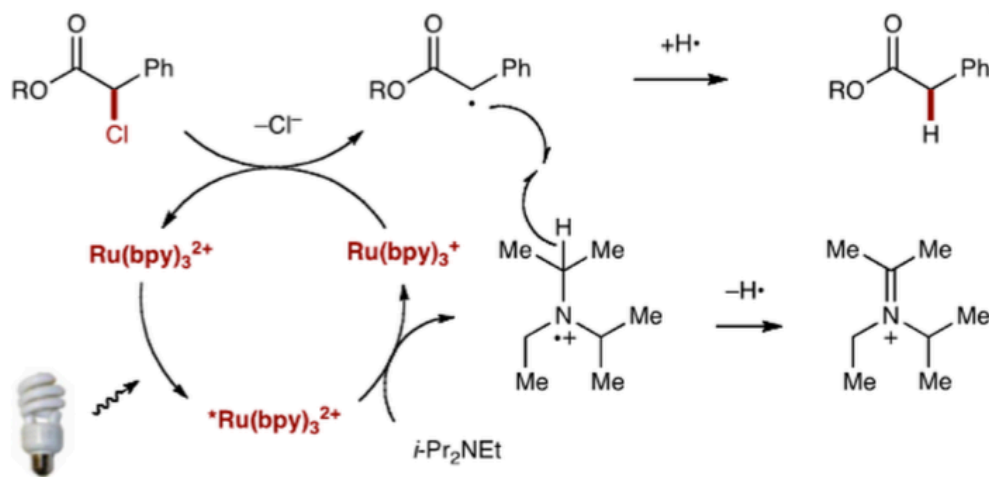
Scheme 1.3 Mechanism of reductive dehalogenations of activated halides using visible light photoredox catalysis

One illustrative reaction in this work is shown in Scheme 1.2, whereby the most easily reduced bond was C-Cl, due to its proximity to both ester and phenyl activating groups. Mechanistically, this occurs via photoexcitation of the Ru(II) catalyst, which is sufficiently oxidizing in the excited state to undergo a single electron transfer in the presence of a trialkyl amine (Scheme 1.3). This then forms a reducing Ru(I) species, that undergoes a reduction event in the presence of the activated halide. Following reduction, the radical abstracts hydrogen from the oxidized amine, closing the catalytic cycle and forming the dehalogenated product. It is notable that the less activated halide remained untouched in this process, due to its higher reduction potential (E_{red} = - 1.6 vs. SCE). However, this work served as a seminal report that demonstrated the potential power of visible light photocatalysis. Importantly, subsequent reports from the Stephenson group demonstrated the ability to intercept the intermediate carbon centered radicals with alkenes and alkynes to perform both atom transfer radical additions[31,78] and radical cyclizations.[79] These reports exemplified the potential of these reductions to be parlayed into carbon-carbon bond forming reactions, yielding access to complex molecules in an extremely mild manner.
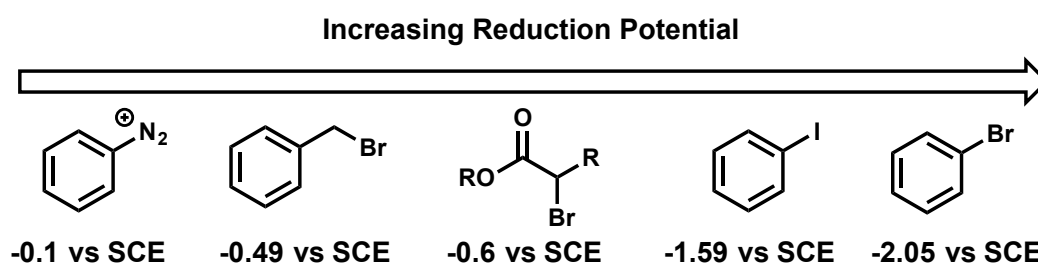
Scheme 1.4 Varying bonds with increasing reduction potentials relative to the saturated calomel electrode[80]

The aforementioned reports by Stephenson focused solely on highly activated carbon halide bonds (Scheme 1.4). In moving towards less activated halides, different photocatalyst systems were necessary. For this, Stephenson employed Ir(ppy)$_3$, a commercially available highly reducing transition metal photocatalyst, Ir(ppy)$_3$ ($E*_{1/2}^{red}$ = - 1.7 vs. SCE) (Scheme 1.5).[81] When employing Ir(ppy)$_3$ under similar conditions to those previously developed for radical dehalogenations, a variety of alkyl, alkenyl, and aryl iodides were reduced. Further, the resulting carbon centered radicals could also be intercepted intramolecularly with alkenes and alkynes, giving reductive cyclizations of unactivated alkyl, alkenyl, and aryl iodides. This again employed visible light at ambient temperatures, with tributylamine and formic acid as very mild terminal oxidants.
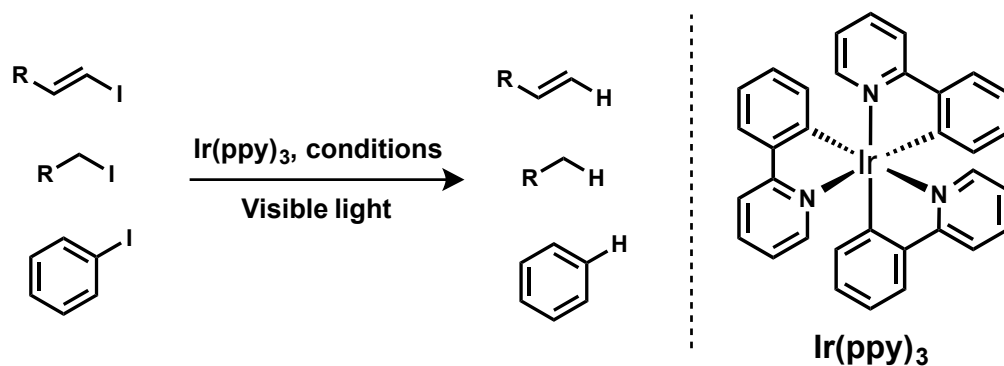
Scheme 1.5 Using a highly reducing Ir(ppy)$_3$ photocatalyst to reductively dehalogenate a variety of unactivated alkyl, alkenyl, and aryl iodides
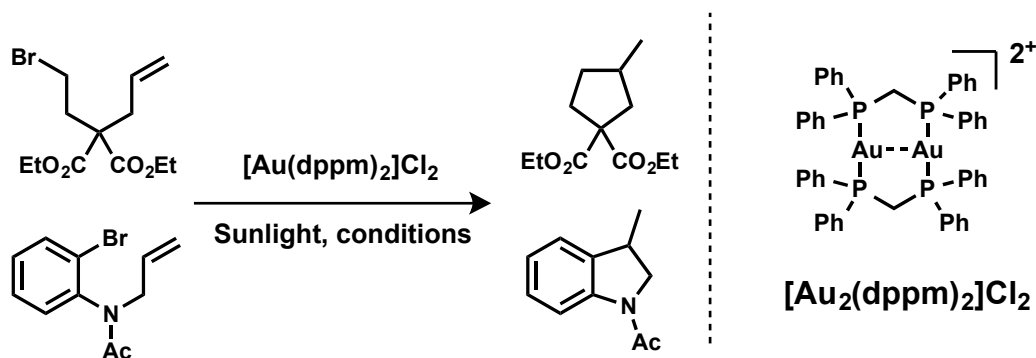
Scheme 1.6 A highly reducing gold photocatalyst that reduces unactivated alkyl and aryl carbon bromides to undergo radical cyclizations

Following Stephenson's work on reducing the unactivated carbon iodide bond (Scheme 1.4-1.5), Barriault and coworkers reported the use of a dimeric gold catalyst to undergo radical cyclization of unactivated bromides.[82] Again markedly mild conditions were employed, with a trialkyl amine as terminal oxidant. However, this work required the use of sunlight, and although an abundant source of energy, it likely relied upon higher energy UV irradiation to conduct the reactions, as it was not shown that visible light sources could mediate these reactions. To date, these radical dehalogenations and cyclizations are the most reducing photocatalysts developed, and demonstrate how far the field has come within only a few years.

The photocatalysts discussed above were primarily based on rare-earth transition metal (i.e. Ru and Ir) complexes. These catalyst complexes are used because they have broad absorption in the visible regime, as well as long-lived triplet excited states. Further, tuning the ligands surrounding the transition metals allows for tuning of their respective excited state redox potentials. However, although powerful, these catalysts also suffer from a variety of drawbacks. For example, they are commonly toxic in biological conditions and most are expensive due to being rare-earth transition metals. These drawbacks have spurred

the development of metal-free catalysts for photoredox processes (Figure 1.20).[83] Typically these catalysts are electron deficient and highly oxidizing in the excited state. This is due to their absorbance in the visible regime necessitating an electron deficient molecule. Although highly oxidizing in the excited state, they have also been employed for the reduction of activated alkyl halides[84] and diazoarenes.[85] In both of these cases, the photocatalysts are limited to reducing bonds with reduction potentials < 1 V (vs. SCE). Development of more reducing organic photocatalysts would extend the scope and applications of these processes.
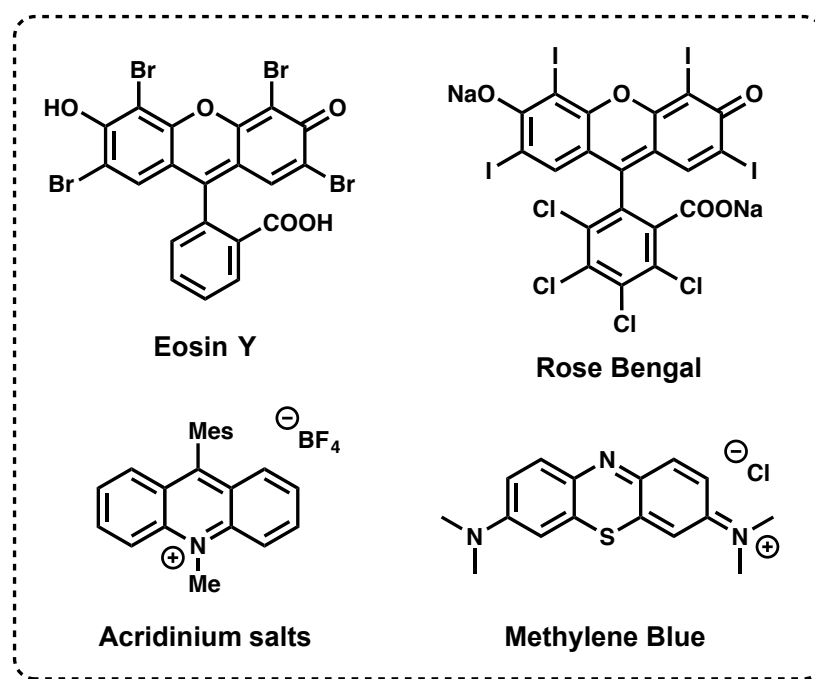
Figure 1.20 Commonly employed organic photocatalysts, which are all highly oxidizing in the excited state

IV. Conclusions

Light mediated polymerizations have emerged as an importance synthetic approach for the preparation of materials for a broad audience. These methods have advantages over

the previously held methods, including greater tolerance over a broad range of conditions. The extra dimension of control afforded by photomediation will surely continue to open doors to diverse multi-faceted materials applications at the interface of physics, biology, polymer chemistry, and materials science.

However, the area of photomediated atom transfer radical polymerizations using new catalyst systems (i.e. $Ir(ppy)_3$) is underdeveloped, only demonstrating the synthesis of polymethacrylates. The focus of chapter 2 is to address this issue by expanding these polymerizations to acrylic monomers. Further, the use of a metal-free photocatalyst would allow a metal-free atom transfer radical polymerization to be conducted, circumventing the issue of metal contamination in electronic and biological applications. The development of such a metal-free photocatalyst for controlled polymerization is the focus of chapter 3.

Photoredox-based dehalogenations have also opened doors for novel transformations and complex molecule syntheses. Such mild conditions employed allow for broader substrate scopes, and by judicious tuning of the catalysts, a wide range of activated and unactivated carbon-halide bonds may be accessed when using transition metal systems. However, there remains the need for highly reducing metal-free catalysts to be developed as well. This will be the focus of chapter 4.

The remaining chapters will focus on further developing the metal-free photocatalyst discussed in chapters 3 and 4 for its use in controlled polymerizations. Chapter 5 will focus on oxygen tolerant atom transfer radical polymerizations. Chapter 6 will explore structure-property relationships for optimization of the photocatalyst. Chapter 7 will seek to develop a deeper mechanistic understanding of the controlled polymerizations, and further explore catalyst characteristics.

V. References

[1]   J. M. R. Narayanam, C. R. J. Stephenson, *Chem. Soc. Rev.* **2010**, *40*, 102.

[2]   C. K. Prier, D. A. Rankic, D. W. C. MacMillan, *Chem. Rev.* **2013**, *113*, 5322–5363.

[3]   C. W. Bielawski, R. H. Grubbs, *Progress in Polymer Science* **2007**, *32*, 1–29.

[4]   Y. Yagci, S. Jockusch, N. J. Turro, *Macromolecules* **2010**, *43*, 6245–6260.

[5]   K. Matyjaszewski, N. V. Tsarevsky, *J. Am. Chem. Soc.* **2014**, *136*, 6513–6533.

[6]   M. Ouchi, T. Terashima, M. Sawamoto, *Chem. Rev.* **2009**, *109*, 4963–5050.

[7]   F. A. Leibfarth, K. M. Mattson, B. P. Fors, H. A. Collins, C. J. Hawker, *Angew. Chem. Int. Ed.* **2012**, *52*, 199–210.

[8]   G. Moad, Y. K. Chong, A. Postma, E. Rizzardo, S. H. Thang, *Polymer* **2005**, *46*, 8458–8468.

[9]   C. Dietlin, S. Schweizer, P. Xiao, J. Zhang, F. Morlet-Savary, B. Graff, J.-P. Fouassier, J. Lalevée, *Polym. Chem.* **2015**, *6*, 3895–3912.

[10]   Y. Kwak, K. Matyjaszewski, *Macromolecules* **2010**, *43*, 5180–5183.

[11]   C. J. Hawker, A. W. Bosman, E. Harth, *Chem. Rev.* **2001**, *101*, 3661–3688.

[12]   J. Nicolas, Y. Guillaneuf, C. Lefay, D. Bertin, D. Gigmes, B. Charleux, *Progress in Polymer Science* **2013**, *38*, 63–235.

[13]   T. Otsu, M. Yoshida, T. Tazaki, *Die Makromolekulare Chemie* **1982**, *3*, 133–140.

[14]   M. A. Tasdelen, M. Uygun, Y. Yagci, *Macromol. Rapid Commun.* **2010**, *32*, 58–62.

[15]   M. A. Tasdelen, M. Uygun, Y. Yagci, *Macromolecular Chemistry and Physics* **2010**, *211*, 2271–2275.

[16]   J. Mosnáček, M. Ilčíková, *Macromolecules* **2012**, 120719062410009.

[17]   D. Konkolewicz, K. Schröder, J. Buback, S. Bernhard, K. Matyjaszewski, *ACS Macro Lett.* **2012**, 1219–1223.

[18]   M. Ciftci, M. A. Tasdelen, W. Li, K. Matyjaszewski, Y. Yagci, *Macromolecules* **2013**, *46*, 9537–9543.

[19]   T. Zhang, T. Chen, I. Amin, R. Jordan, *Polym. Chem.* **2014**, *5*, 4790.

[20]   A. Anastasaki, V. Nikolaou, Q. Zhang, J. Burns, S. R. Samanta, C. Waldron, A. J. Haddleton, R. McHale, D. Fox, V. Percec, et al., *J. Am. Chem. Soc.* **2014**, *136*, 1141–1149.

[21]   A. Anastasaki, V. Nikolaou, A. Simula, J. Godfrey, M. Li, G. Nurumbetov, P. Wilson, D. M. Haddleton, *Macromolecules* **2014**, *47*, 3852–3859.

[22]   Y.-M. Chuang, A. Ethirajan, T. Junkers, *ACS Macro Lett.* **2014**, *3*, 732–737.

[23]   A. Anastasaki, V. Nikolaou, F. Brandford-Adams, G. Nurumbetov, Q. Zhang, G. J. Clarkson, D. J. Fox, P. Wilson, K. Kempe, D. M. Haddleton, *Chem. Commun.* **2015**, *51*, 5626–5629.

[24]   S. Chantasirichot, Y. Inoue, K. Ishihara, *Polymer* **2015**, *61*, 55–60.

[25]   E. Frick, A. Anastasaki, D. M. Haddleton, C. Barner-Kowollik, *J. Am. Chem. Soc.* **2015**, *137*, 6889–6896.

[26]   T. G. Ribelli, D. Konkolewicz, X. Pan, K. Matyjaszewski, *Macromolecules* **2014**, *47*, 6316–6321.

[27]   T. G. Ribelli, D. Konkolewicz, S. Bernhard, K. Matyjaszewski, *J. Am. Chem. Soc.* **2014**, *136*, 13303–13312.

[28]   Y.-N. Zhou, Z.-H. Luo, *AIChE J.* **2015**, *61*, 1947–1958.

[29]   J. Mosnáček, A. Eckstein-Andicsová, K. Borská, *Polym. Chem.* **2015**, *6*, 2523–

2530.

[30] B. P. Fors, C. J. Hawker, *Angew. Chem. Int. Ed.* **2012**, *51*, 8850–8853.

[31] J. D. Nguyen, J. W. Tucker, M. D. Konieczynska, C. R. J. Stephenson, *J. Am. Chem. Soc.* **2011**, *133*, 4160–4163.

[32] N. J. Treat, B. P. Fors, J. W. Kramer, M. Christianson, C.-Y. Chiu, J. R. de Alaniz, C. J. Hawker, *ACS Macro Lett.* **2014**, *3*, 580–584.

[33] J.-P. Goddard, L. Fensterbank, C. Ollivier, F. Nzulu, F. Stoffelbach, J. Lalevée, S. teliel, F. Morlet-Savary, B. Graff, *Polym. Chem.* **2015**, *6*, 4605–4611.

[34] Y. Cao, Y. Xu, J. Zhang, D. Yang, J. Liu, *Polymer* **2015**, *61*, 198–203.

[35] Q. Yang, F. Dumur, F. Morlet-Savary, J. Poly, J. Lalevée, *Macromolecules* **2015**, *48*, 1972–1980.

[36] X. Pan, M. Lamson, J. Yan, K. Matyjaszewski, *ACS Macro Lett.* **2015**, *4*, 192–196.

[37] N. V. Alfredo, N. E. Jalapa, S. L. Morales, A. D. Ryabov, R. Le Lagadec, L. Alexandrova, *Macromolecules* **2012**, *45*, 8135–8146.

[38] K. Koumura, K. Satoh, M. Kamigaito, *Macromolecules* **2008**, *41*, 7359–7367.

[39] K. Koumura, K. Satoh, M. Kamigaito, *Macromolecules* **2009**, *42*, 2497–2504.

[40] K. Koumura, K. Satoh, M. Kamigaito, *J. Polym. Sci. A Polym. Chem.* **2009**, *47*, 1343–1353.

[41] Q. Liu, L. Liu, Y. Ma, C. Zhao, W. Yang, *J. Polym. Sci. A Polym. Chem.* **2014**, *52*, 3283–3291.

[42] S. Telitel, F. Dumur, S. Telitel, O. Soppera, M. Lepeltier, Y. Guillaneuf, J. Poly, F. Morlet-Savary, P. Fioux, J.-P. Fouassier, et al., *Polym. Chem.* **2014**, DOI 10.1039/C4PY01358A.

[43]   A. Ohtsuki, L. Lei, M. Tanishima, A. Goto, H. Kaji, *J. Am. Chem. Soc.* **2015**, *137*, 5610–5617.

[44]   K. A. Ogawa, A. E. Goetz, A. J. Boydston, *J. Am. Chem. Soc.* **2015**, *137*, 1400–1403.

[45]   A. E. Goetz, A. J. Boydston, *J. Am. Chem. Soc.* **2015**, *137*, 7572–7575.

[46]   Y.-Z. You, C.-Y. Hong, R.-K. Bai, C.-Y. Pan, J. Wang, *Macromolecular Chemistry and Physics* **2002**, *203*, 477–483.

[47]   A. Wolpers, P. Vana, *Macromolecules* **2014**, *47*, 954–963.

[48]   J. F. Quinn, L. Barner, C. Barner-Kowollik, E. Rizzardo, T. P. Davis, *Macromolecules* **2002**, *35*, 7620–7627.

[49]   L. Lu, N. Yang, Y. Cai, *Chem. Commun.* **2005**, 5287–5288.

[50]   W. Jiang, L. Lu, Y. Cai, *Macromol. Rapid Commun.* **2007**, *28*, 725–728.

[51]   S. Muthukrishnan, E. H. Pan, M. H. Stenzel, C. Barner-Kowollik, T. P. Davis, D. Lewis, L. Barner, *Macromolecules* **2007**, *40*, 2978–2980.

[52]   M. Y. Khan, M.-S. Cho, Y.-J. Kwark, *Macromolecules* **2014**, *47*, 1929–1934.

[53]   T. G. McKenzie, Q. Fu, E. H. H. Wong, D. E. Dunstan, G. G. Qiao, *Macromolecules* **2015**, *48*, 3864–3872.

[54]   A. Ohtsuki, A. Goto, H. Kaji, *Macromolecules* **2013**, *46*, 96–102.

[55]   Y. Shi, G. Liu, H. Gao, L. Lu, Y. Cai, *Macromolecules* **2009**, *42*, 3917–3926.

[56]   Y. Shi, H. Gao, L. Lu, Y. Cai, *Chem. Commun.* **2009**, 1368.

[57]   G. Liu, H. Shi, Y. Cui, J. Tong, Y. Zhao, D. Wang, Y. Cai, *Polym. Chem.* **2013**, *4*, 1176.

[58]   *Angew. Chem. Int. Ed.* **2013**, *52*, 2235–2238.

[59]   M. Chen, J. A. Johnson, *Chem. Commun.* **2015**, *51*, 6742–6745.

[60]   K. Matyjaszewski, *Controlled/Living Radical Polymerization*, Amer Chemical Society, **2009**.

[61]   J. Xu, K. Jung, A. Atme, S. Shanmugam, C. Boyer, *J. Am. Chem. Soc.* **2014**, *136*, 5508–5519.

[62]   C. Fu, J. Xu, L. Tao, C. Boyer, *ACS Macro Lett.* **2014**, 633–638.

[63]   J. Xu, K. Jung, C. Boyer, *Macromolecules* **2014**, *47*, 4217–4229.

[64]   S. Shanmugam, J. Xu, C. Boyer, *Macromolecules* **2014**, *47*, 4930–4942.

[65]   J. Xu, K. Jung, N. A. Corrigan, C. Boyer, *Chem. Sci.* **2014**, *5*, 3568–3575.

[66]   S. Shanmugam, J. Xu, C. Boyer, *Chem. Sci.* **2015**, *6*, 1341–1349.

[67]   X. Zheng, M. Yue, P. Yang, Q. Li, W. Yang, *Polym. Chem.* **2012**, *3*, 1982.

[68]   C. Detrembleur, D.-L. Versace, Y. Piette, M. Hurtgen, C. Jérôme, J. Lalevée, A. Debuigne, *Polym. Chem.* **2012**, *3*, 1856.

[69]   A. Kermagoret, B. Wenn, A. Debuigne, C. Jérôme, T. Junkers, C. Detrembleur, *Polym. Chem.* **2015**, *6*, 3847–3857.

[70]   A. Debuigne, M. Schoumacher, N. Willet, R. Riva, X. Zhu, S. Rütten, C. Jérôme, C. Detrembleur, *Chem. Commun.* **2011**, *47*, 12703–12705.

[71]   X. Miao, W. Zhu, Z. Zhang, W. Zhang, X. Zhu, J. Zhu, *Polym. Chem.* **2013**, *5*, 551–557.

[72]   Y. Zhao, M. Yu, S. Zhang, Z. Wu, Y. Liu, C.-H. Peng, X. Fu, *Chem. Sci.* **2015**, *6*, 2979–2988.

[73]   Y. Zhao, M. Yu, X. Fu, *Chem. Commun.* **2013**, *49*, 5186–5188.

[74]   S. Yamago, Y. Ukai, A. Matsumoto, Y. Nakamura, *J. Am. Chem. Soc.* **2009**, *131*,

2100–2101.

[75]   Y. Nakamura, S. Yamago, *Beilstein J. Org. Chem.* **2013**, *9*, 1607–1612.

[76]   J. W. Tucker, C. R. J. Stephenson, *J. Org. Chem.* **2012**, *77*, 1617–1622.

[77]   J. M. R. Narayanam, J. W. Tucker, C. R. J. Stephenson, *J. Am. Chem. Soc.* **2009**, *131*, 8756–8757.

[78]   C.-J. Wallentin, J. D. Nguyen, P. Finkbeiner, C. R. J. Stephenson, *J. Am. Chem. Soc.* **2012**, *134*, 8875–8884.

[79]   J. W. Tucker, J. D. Nguyen, J. M. R. Narayanam, S. W. Krabbe, C. R. J. Stephenson, *Chem. Commun.* **2010**, *46*, 4985.

[80]   H. Roth, N. Romero, D. Nicewicz, *Synlett* **2016**, *27*, 714–723.

[81]   J. D. Nguyen, E. M. D'Amato, J. M. R. Narayanam, C. R. J. Stephenson, *Nature Chem* **2012**, *4*, 854–859.

[82]   G. Revol, T. McCallum, M. Morin, F. Gagosz, L. Barriault, *Angew. Chem. Int. Ed.* **2013**, *52*, 13342–13345.

[83]   D. A. Nicewicz, T. M. Nguyen, *ACS Catal.* **2014**, *4*, 355–360.

[84]   M. Neumann, S. Füldner, B. König, K. Zeitler, *Angew. Chem. Int. Ed. Engl.* **2011**, *50*, 951–954.

[85]   D. P. Hari, P. Schroll, B. König, *J. Am. Chem. Soc.* **2012**, *134*, 2958–2961.

2. Controlled Radical Polymerization of Acrylates Regulated by Visible Light

I. *Abstract*

The controlled radical polymerization of a variety of acrylate monomers is reported using an Ir-catalyzed visible light mediated process leading to well-defined homo-, random and block copolymers. The polymerizations could be efficiently activated and deactivated using light while maintaining a linear increase in molecular weight with conversion and first order kinetics. The robust nature of the *fac*-[Ir(ppy)$_3$] catalyst allows carboxylic acids to be directly introduced at the chain ends through functional initiators or along the backbone of random copolymers (controlled process up to 50 mol% acrylic acid incorporation). In contrast to traditional ATRP procedures, low polydispersity block copolymers - poly(acrylate)-*b*-(acrylate), poly(methacrylate)-*b*-(acrylate) and poly(acrylate)-*b*-(methacrylate) – could be prepared with no monomer sequence requirements. These results illustrate the increasing generality and utility of light mediated Ir-catalyzed polymerization as a platform for polymer synthesis.

"Light Off"   "Light On"

Highly Responsive

Fully Reversible

RO
Acrylates

Deactivation   Activation

▬▬▬ = polyacrylate   ● = bromine   • = free radical
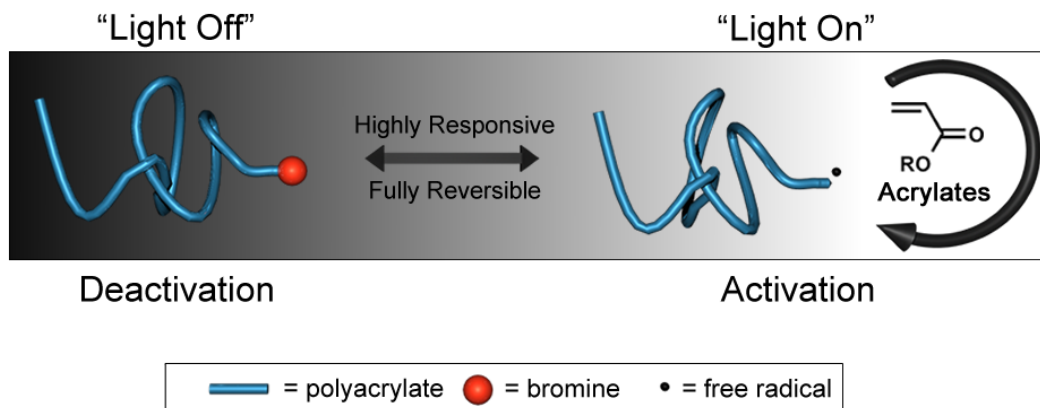
Figure 2.1 Representation of a photoregulated polymerization

II. Introduction

Controlled radical polymerizations (CRP), such as nitroxide mediated polymerization (NMP), [1,2] reversible-addition fragmentation chain transfer polymerization (RAFT),[1,3] and atom transfer radical polymerization (ATRP),[4] have revolutionized the field of polymer chemistry, allowing for the synthesis of well-defined macromolecular structures with excellent functional group tolerance. Perhaps of greater importance is the facile reaction conditions which allows non-experts access to these materials, enabling significant advances across a number of fields. More recently, additional control over living radical polymerizations has been achieved through regulation of the chain growth process by an external stimulus.[5] For example, electrochemical ATRP has been used to pattern polymer brushes on surfaces,[6-8] as well as gain control over aqueous polymerizations.[9] While the employment of externally regulated polymerizations is in its infancy, the potential for further innovation is significant.

53

In considering the wide range of possible external stimuli, light offers many attractive features such as readily available light sources, tunability and both spatial and temporal control. On this basis, significant work has been dedicated to the development of photoinitiated[10-17] and photoregulated radical polymerizations (i.e. photocontrolled RAFT, [18-20] ATRP,[21-24] organocatalytic,[25,26] cobalt-mediated,[27] and tellurium-mediated[28] methods). Recently, our group reported the controlled radical polymerization of methacrylates regulated by visible light and the photoredox catalyst, *fac*-[Ir(ppy)₃] (Figure 2.2).[29] This approach uses a simple reaction set-up with only ppm levels of Ir(ppy)₃ and enables efficient activation and deactivation of polymerization leading to control over molecular weight and molecular weight distributions. A fundamental element of this process is that in the absence of irradiation, the chain end rests as the dormant alkyl bromide, protected from deleterious radical reactions but available for reactivation upon re-exposure to light. Moreover, the spatial and temporal control of Ir-catalyzed photomediated processes has been exploited for patterning polymer brushes on surfaces to give novel, 3-D nanostructures.[30]
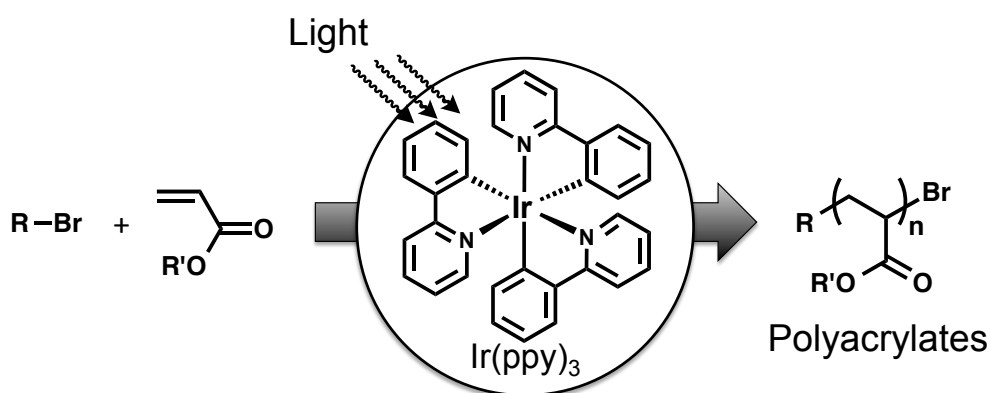
Figure 2.2.Controlled radical polymerization mediated by light employing *fac*-[Ir(ppy)₃] as the catalyst.

Our previous reports on photomediated radical polymerizations focused exclusively on methacrylates. In order to increase the scope and applicability of this strategy, extension to other monomer families is required. Our attention was therefore drawn to acrylate-based polymers as they offer broad opportunities in both academia and industry.[31,32] Despite this significance, controlled radical polymerization of acrylates represented a formidable challenge due to the increased propagation rate and difficulty in chain end reduction relative to methacrylate derivatives.[33]

III. Results and Discussion

A. Optimization of Conditions

Initial studies on methyl acrylate (MA) employed similar conditions to those developed for the polymerization of methacrylates: 0.005 mol % of Ir(ppy)$_3$, and benzyl α-bromoisobutyrate (**1**) as initiator in N,N-dimethylacetamide (DMA) with irradiation by either 380 nm LEDs or a 50 W fluorescent lamp for 4 hours (see Supporting Information). Encouragingly, our initial conditions indicated moderate control, showing an approximate agreement between theoretical and experimental molecular weights with $Đ$ = 1.45 (Table 2.1, entry 1), where $Đ = M_w / M_n$. However, the degree of control was inferior when compared to the polymerization of methacrylates. We hypothesized that increased control over these polymerizations could be achieved by varying the catalyst and monomer concentrations to account for the marked difference in k_p and k_t for acrylates vs. methacrylates. Indeed, increasing the monomer concentration to 3.5 M narrowed the molecular weight distribution to 1.30 (Table 2.1, entry 2). Further, increasing the catalyst

loading to 0.05 mol % provided additional improvement in polydispersity (Table 2.1, entries 3–5). It should be noted that even at Ir(ppy)$_3$ concentrations as high as 0.1 mol %, controlled polymerization was observed, whereas for methacrylates such high catalyst loadings resulted in uncontrolled polymerization.[29] This difference may be due to the known difficulty in acrylate chain end reduction compared to methacrylate systems. Control experiments without catalyst or in the absence of irradiation led to either uncontrolled or no polymerization, respectively (Table 2.1, entries 6 and 7).[34] These results clearly indicate that control over polymerization arises from the Ir catalyst with light as an external stimuli mediating the polymerization.

Table 2.1 Optimization of a light-mediated polymerization of methyl acrylate using Ir(ppy)$_3$.[a]
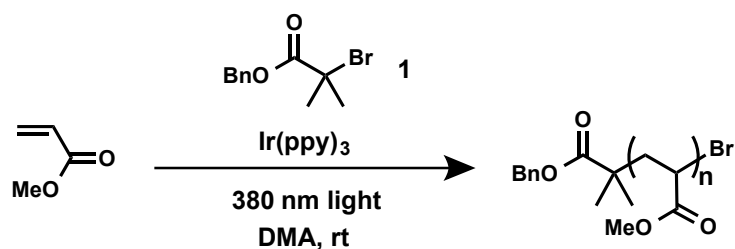
Entry	Ir(ppy)$_3$ [mol %]	conversion	M_n (exp) [g/mol]	M_n (theo) [g/mol]	Đ
1[b]	0.005	76%	14,400	15,200	1.45
2	0.005	79%	16,000	15,800	1.39
3	0.01	76%	15,200	15,200	1.30
4	0.05	63%	12,500	12,600	1.25
5	0.1	54%	10,900	10,800	1.32
6[c]	0.05	0%	--	--	--
7	0	43%	240,000[d]	8,600	1.76

[a] Reaction conditions: MA (1 equiv.), Ir(ppy)$_3$ (0 – 0.1 mol %), **1** (0.004 equiv), DMA (3.5 M of MA) at room temperature with irradiation from 380 nm LEDs for 4 h (M_n = number average molecular weight; M_w = weight average molecular weight). Đ, or M_w / M_n, determined using size exclusion chromatography (SEC). M_n determined by NMR except where noted; [b] reaction run at 2 M [c] reaction run in the dark; [d] M_n determined by SEC.
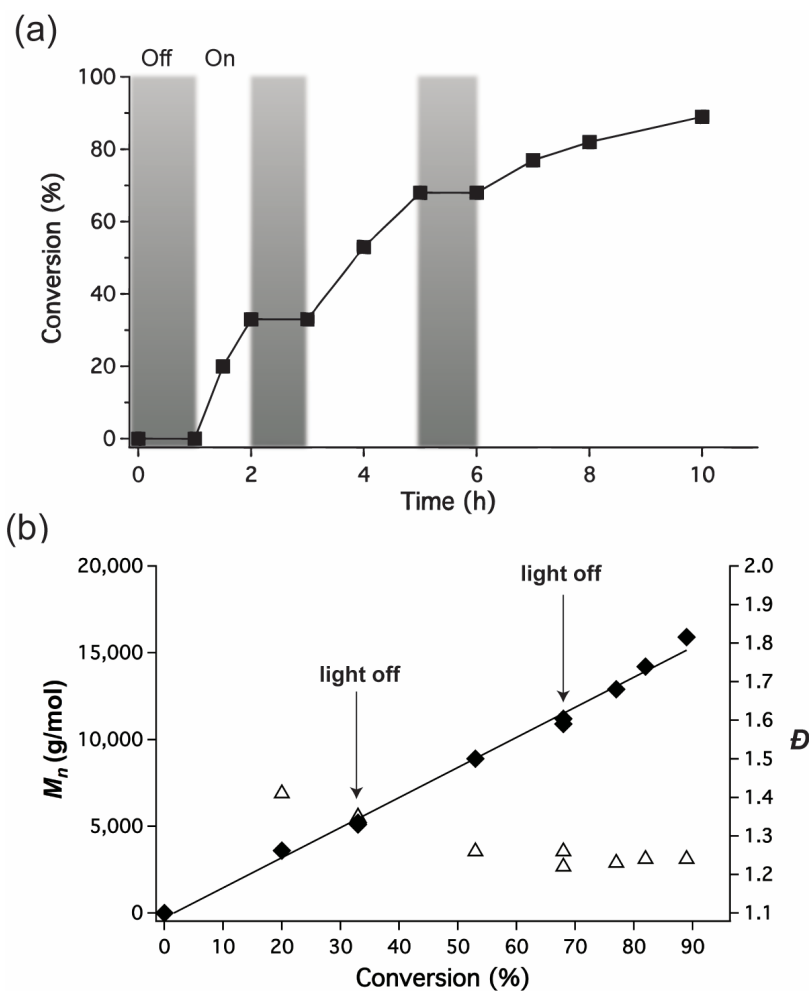
Figure 2.3 Polymerization of MA with Ir(ppy)$_3$ while cycling the reaction's exposure to light. (a) Conversion vs. time; (b) Molecular weight (M_n) vs. conversion and Đ vs. conversion (Đ = M_w / M_n).

B. Kinetic Analysis

By analogy with the methacrylate system previously reported, the absence of reaction in the dark allows for temporal influence over the polymerization process. To demonstrate the capability to turn the polymerization "on" and "off" while maintaining control, methyl acrylate, initiator **1**, and Ir(ppy)$_3$ were combined and kept in the dark for 1 hour, with no polymerization being observed. The reaction was then exposed to light, reaching 33%

conversion after 1 hour (Figure 2.3a). When irradiation was subsequently removed from the system, the polymerization became dormant and no conversion was observed. On re-exposure to light, the polymerization process was re-activated and this cycle could be repeated multiple times with no conversion observed in the absence of irradiation. Significantly, a linear relationship between molecular weight and conversion was observed up to high (>90%) conversion even with multiple on/off cycles (Figure 2.3b). Finally, a linear relationship for $\ln([M]_0/[M]_t)$ versus time of light exposure indicated that a constant radical concentration exists throughout the polymerization (Figure S2.2) illustrating the stimuli-responsive and living nature of these Ir(ppy)$_3$ based acrylate polymerizations.

C. Extension of Scope

To further expand the range of polymerizable acrylate monomers and to demonstrate control of molecular weight for a variety of acrylate structures, the ratio of initiator to monomer was varied for methyl, *n*-butyl, and *t*-butyl acrylate as shown in Table 2.2.[35-40]

Table 2.2 Molecular weight control of alkyl substituted acrylates[a]
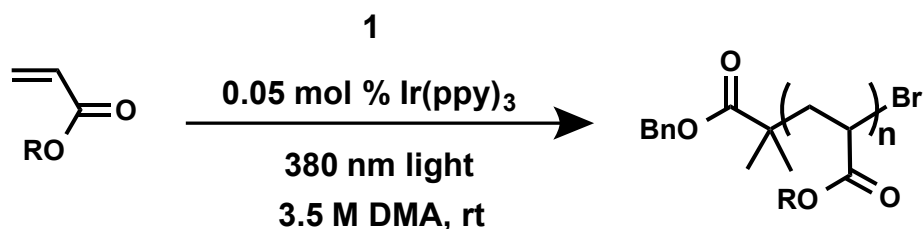
Entry	Monomer	M_n (exp) [g/mol]	M_n (theo) [g/mol]	Đ
1	methyl acrylate	900	800	1.42
2		3,000	2,800	1.32
3		7,900	8,200	1.19
4		18,400	18,000	1.22
5		28,900	29,000	1.37
6	*n*-butyl acrylate	2,400	2,500	1.34
7		5,100	4,800	1.25
8		11,300	10,600	1.24
9		24,800	27,600	1.31
10		42,600	38,400	1.45
11	*t*-butyl acrylate	3,900	3,600	1.37
12		7,000	7,200	1.26
13		14,300	14,600	1.27
14		32,300	28,800	1.29
15		40,600	40,200	1.36
16		62,700	60,000	1.42
17		109,000	108,000	1.46
18		200,000	193,000	1.44

[a] Reaction conditions: methyl acrylate, *n*-butyl acrylate, *t*-butyl acrylate (1 equiv.), Ir(ppy)₃ (0.05 mol %), **1** (0.00043 - 0.026 equiv), DMA (3.5 M of monomer) at room temperature with irradiation from 380 nm LEDs for 3-5 h (M_n = number average molecular weight; M_w = weight average molecular weight). Đ, or M_w / M_n, determined using SEC. M_n determined by NMR.

In all cases, excellent agreement is observed between experimental and theoretical values for molecular weights of less than 1,000 g/mol to greater than 100,000 g/mol (Table 2.2, entry 1, 17, and 18). These results clearly demonstrate that molecular weight can be controlled by adjusting initiator to monomer ratio and, importantly, that the optimized conditions lead to low polydispersities for a variety of acrylate monomers.

D. Acrylic acid Copolymerizations

With the successful polymerization of a variety of acrylate monomers, we next addressed the challenge of incorporating functional initiators or monomers directly into the polymer backbone. As a test case, carboxylic acid units were examined as they are traditionally difficult to control under standard ATRP conditions. This difficulty is due to the Cu-catalysts for ATRP being formed *in-situ* through coordination chemistry which is in direct contrast to the covalent nature of *fac*-[Ir(ppy)$_3$]. The stability of *fac*-[Ir(ppy)$_3$] should therefore result in a more robust system with an increased tolerance to acidic groups. To demonstrate this, the synthesis of chain end functionalized poly(*n*-butyl acrylate) from 3-bromopropionic acid as an initiator was examined. Over a wide range of initiator/monomer ratios, accurate control over molecular weight and narrow polydispersities were obtained (supporting information).

Synthetically more demanding is the copolymerization of acrylic acid (AA) and ethyl acrylate (EA) which was examined at feed ratios of up to 50 mol% acrylic acid (Table 2.3).

Table 2.3 Random copolymerizations of acrylic acid (AA) and ethyl acrylate (EA)[a]

Entry	AA:EA	% AA incorp	M_n (exp) [g/mol]	M_n (theo) [g/mol]	Đ
1	0:100	0	7,700	7,600	1.28
2	5:95	2	12,300	12,400	1.28
3	10:90	8	9,500	10,600	1.38
4	10:90	8	17,300	21,600	1.44
5	10:90	7	38,300	37,200	1.45
6	20:80	15	13,800	12,200	1.38
7	30:70	21	13,500	11,100	1.51
8	40:60	36	16,300	12,100	1.65
9	50:50	46	20,500	11,500	1.90

[a] Reaction conditions: EA (1 equiv.), AA (0 – 1 equiv.), Ir(ppy)$_3$ (0.05 mol %), **1** (0.004 equiv), DMA (3.5 M of monomer) at room temperature with irradiation from 380 nm LEDs for 2-5 h (M_n = number average molecular weight; M_w = weight average molecular weight). % AA incorp= mol % acrylic acid incorporation. Đ, or M_w / M_n, determined using SEC. M_n determined by NMR. For characterization of the acid functionalized copolymers, methylation with trimethylsilyldiazomethane was performed prior to analysis.

For feed ratios of 5-20 mol%, excellent agreement between experimental and theoretical molecular weights is observed with low polydispersities between 1.25 and 1.40. Increasing the molecular weight for 10 mol% feed ratios resulted in a similar level of molecular weight control with the polydispersity increasing to ca. 1.40-1.50. Only at higher incorporations of AA (30-50 mol %) was increased polydispersities observed.

This capacity to incorporate acrylic acid directly into acrylate backbones at moderate loading levels while retaining control over the polymerization process is significant and offers a wide range of opportunities in the design of functional macromolecules.

E. Block Copolymerizations

The ability to polymerize acrylates coupled with the prior demonstration of the controlled polymerization of methacrylates prompted an investigation into the utility of Ir-catalyzed polymerizations for producing block copolymers. Initially, simple re-initiation was studied by the chain extension of a methyl acrylate homopolymer (M_n = 7,600 g/mol; Đ= 1.31) with *n*-butyl acrylate to yield a block copolymer (M_n = 30,200 g/mol; Đ= 1.24). Size exclusion chromatography (SEC) shows minimal residual homopolymer after chain-extension, indicating excellent fidelity and reactivation of the alkyl bromide chain-end (Figure 2.4a).
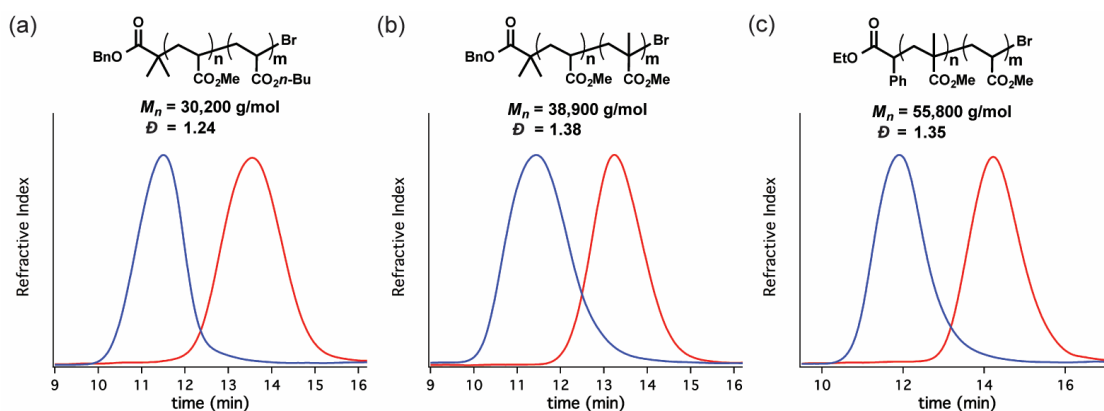
Figure 2.4 Block copolymer synthesis and corresponding SEC traces (red trace = homopolymer, blue trace = block copolymer) (a) PMA-*b*-*n*-PBA (b) PMA-*b*-PMMA (c) PMMA-*b*-PMA

For the more complex, acrylate-methacrylate diblock copolymer systems, the sequence of monomer polymerization can have a dramatic influence on the fidelity of the process. In traditional ATRP, the use of comonomers[41] or halogen exchange[42] is necessary when chain extending polyacrylate macroinitiators with methacrylates. In this case, a PMA homopolymer was synthesized and used as a macroinitiator to polymerize methyl

63

methacrylate under the conditions previously reported[27] to yield a PMA-*b*-PMMA block copolymer with a polydispersity of 1.38 and little tailing in the homopolymer regime of the SEC trace (Figure 2.4b). For the reverse case, a poly(methyl methacrylate) homopolymer was synthesized under our photocontrolled conditions and chain extended with methyl acrylate to yield the inverse block copolymer with accurate control over molecular weight and polydispersity (Figure 2.4c). This high level of control in both cases further illustrates the robust nature and simplicity of this catalyst system and the absence of a required monomer sequence is a potential advantage over traditional ATRP systems.

IV. Conclusion

In conclusion, we have demonstrated the light mediated, controlled radical polymerization of a variety of acrylate monomers using an Ir-based photoredox catalyst. Linear increases in molecular weight with conversion and first order reaction rates for a wide range of molecular weights demonstrates a well-behaved system with efficient chain capping and re-initiation in response to light. The robust nature of this polymerization system was illustrated by tolerance to acidic functional groups and the ability to control the copolymerization of acrylic acid. An added advantage of the Ir-based photoredox system is the lack of specific monomer order for block copolymer formation with well-defined materials being formed from both MA-MMA and MMA-MA sequences. This work demonstrates an expanding range of compatible monomers for Ir-based photoredox polymerizations and the significant potential that externally regulated systems offer.

V. Acknowledgements

VI. References

[1]   C. J. Hawker, A. W. Bosman, E. Harth, *Chem. Rev.* **2001**, *101*, 3661–3688.

[2]   J. Nicolas, Y. Guillaneuf, C. Lefay, D. Bertin, D. Gigmes, B. Charleux, *Progress in Polymer Science* **2013**, *38*, 63–235.

[3]   G. Moad, E. Rizzardo, S. H. Thang, *Polymer* **2008**, *49*, 1079–1131.

[4]   K. Matyjaszewski, *Macromolecules* **2012**, *45*, 4015–4039.

[5]   F. A. Leibfarth, K. M. Mattson, B. P. Fors, H. A. Collins, C. J. Hawker, *Angew. Chem. Int. Ed.* **2012**, *52*, 199–210.

[6]   J. Yan, B. Li, B. Yu, W. T. S. Huck, W. Liu, F. Zhou, *Angew. Chem. Int. Ed.* **2013**, *52*, 9125–9129.

[7]   B. Li, B. Yu, W. T. S. Huck, F. Zhou, W. Liu, *Angew. Chem. Int. Ed.* **2012**, *51*, 5092–5095.

[8]   B. Li, B. Yu, W. T. S. Huck, W. Liu, F. Zhou, *J. Am. Chem. Soc.* **2013**, *135*, 1708–1710.

[9]   N. Bortolamei, A. A. Isse, A. J. D. Magenau, A. Gennaro, K. Matyjaszewski, *Angew. Chem. Int. Ed.* **2011**, *50*, 11391–11394.

[10]   A. Goto, J. C. Scaiano, L. Maretti, *Photochem. Photobiol. Sci.* **2007**, *6*, 833.

[11]   D.-L. Versace, Y. Guillaneuf, D. Bertin, J.-P. Fouassier, J. Lalevée, D. Gigmes, *Org. Biomol. Chem.* **2011**, *9*, 2892.

[12]   Y. Guillaneuf, D. Bertin, D. Gigmes, D.-L. Versace, J. Lalevée, J.-P. Fouassier, *Macromolecules* **2010**, *43*, 2204–2212.

[13]   E. Yoshida, *Colloid Polym Sci* **2009**, *288*, 73–78.

[14]   J. Lalevée, M.-A. Tehfe, F. Dumur, D. Gigmes, N. Blanchard, F. Morlet-Savary, J.-P. Fouassier, *ACS Macro Lett.* **2012**, *1*, 286–290.

[15]   G. Zhang, I. Y. Song, K. H. Ahn, T. Park, W. Choi, *Macromolecules* **2011**, *44*, 7594–7599.

[16]   J. Lalevée, N. Blanchard, M.-A. Tehfe, M. Peter, F. Morlet-Savary, D. Gigmes, J.-P. Fouassier, *Polym. Chem.* **2011**, *2*, 1986.

[17]   Y. Yagci, S. Jockusch, N. J. Turro, *Macromolecules* **2010**, *43*, 6245–6260.

[18]   G. Liu, H. Shi, Y. Cui, J. Tong, Y. Zhao, D. Wang, Y. Cai, *Polym. Chem.* **2013**, *4*, 1176.

[19]   Y. Shi, G. Liu, H. Gao, L. Lu, Y. Cai, *Macromolecules* **2009**, *42*, 3917–3926.

[20]   J. Xu, K. Jung, A. Atme, S. Shanmugam, C. Boyer, *J. Am. Chem. Soc.* **2014**, *136*, 5508–5519.

[21]   M. A. Tasdelen, M. Uygun, Y. Yagci, *Macromol. Rapid Commun.* **2010**, *32*, 58–62.

[22]   M. A. Tasdelen, M. Uygun, Y. Yagci, *Macromolecular Chemistry and Physics* **2010**, *211*, 2271–2275.

[23]   D. Konkolewicz, K. Schröder, J. Buback, S. Bernhard, K. Matyjaszewski, *ACS Macro Lett.* **2012**, 1219–1223.

[24]   J. Mosnáček, M. Ilčíková, *Macromolecules* **2012**, 120719062410009.

[25]   A. Ohtsuki, A. Goto, H. Kaji, *Macromolecules* **2013**, *46*, 96–102.

[26]   X. Zheng, M. Yue, P. Yang, Q. Li, W. Yang, *Polym. Chem.* **2012**, *3*, 1982.

[27]   Y. Zhao, M. Yu, X. Fu, *Chem. Commun.* **2013**, *49*, 5186.

[28]   S. Yamago, Y. Ukai, A. Matsumoto, Y. Nakamura, *J. Am. Chem. Soc.* **2009**, *131*, 2100–2101.

[29]   B. P. Fors, C. J. Hawker, *Angew. Chem. Int. Ed.* **2012**, *51*, 8850–8853.

[30]   J. E. Poelma, B. P. Fors, G. F. Meyers, J. W. Kramer, C. J. Hawker, *Angew. Chem. Int. Ed.* **2013**, *52*, 6844–6848.

[31]   J. E. Mark, Ed., *Polymer Data Handbook,* (Oxford Univ. Press, New York, 1999), pp. 252–253.

[32]   J. W. Taylor, J. N. Argyropoulos, J. J. Lear, *United States Patent* **1993**, 1–17.

[33]   W. Tang, K. Matyjaszewski, *Macromolecules* **2007**, *40*, 1858–1863.

[34]   We do not believe that autopolymerization plays a role under the optimized conditions due to the high molar absorptivity of $Ir(ppy)_3$ causing nearly all of the light to be absorbed by the catalyst (see ref 30).

[35]   Q. Ma, K. L. Wooley, *J. Polym. Sci. A Polym. Chem.* **2000**, *38*, 4805–4820.

[36]   J. N. Brantley, K. M. Wiggins, C. W. Bielawski, *Science* **2011**, *333*, 1606–1609.

[37]   J. M. Jethmalani, W. T. Ford, *Chem. Mater.* **1996**, *8*, 2138–2146.

[38]   I. Sondi, T. H. Fedynyshyn, R. Sinta, E. Matijević, *Langmuir* **2000**, *16*, 9031–9034.

[39]   O. Colombani, M. Ruppel, F. Schubert, H. Zettl, D. V. Pergushov, A. H. E. Müller, *Macromolecules* **2007**, *40*, 4338–4350.

[40]   Y. Amamoto, J. Kamada, H. Otsuka, A. Takahara, K. Matyjaszewski, *Angew.*

Chem. Int. Ed. **2011**, *50*, 1660–1663.

[41]   L. Mueller, W. Jakubowski, W. Tang, K. Matyjaszewski, *Macromolecules* **2007**, *40*,

6464–6472.

[42]   D. A. Shipp, J.-L. Wang, K. Matyjaszewski, *Macromolecules* **1998**, *31*, 8005–8008.

VII. *Supplementary Information*

A. General Reagent Information

All polymerizations were carried out under an argon atmosphere. Anhydrous N,N-dimethylacetamide and anhydrous 1-methyl-2-pyrrolidinone were purchased from Sigma-Aldrich and used as received. Methyl acrylate, *n*-butyl acrylate, *t*-butyl acrylate, and ethyl acrylate were purchased from Sigma-Aldrich and passed through a plug of basic alumina before use. Acrylic acid was purchased from Sigma-Aldrich and distilled under reduced pressure prior to use.   [fac-Ir(ppy)$_3$], ethyl α-bromophenylacetate, benzyl alcohol, triethylamine, dimethylaminopyridine, bromoisobutyryl bromide, and (trimethylsilyl)diazomethane solution (2.0 M in diethyl ether) were purchased from Sigma-Aldrich and used as received.

B. General Analytical Information

Nuclear magnetic resonance spectra were recorded on either a Varian 400 MHz, a Varian 500 MHz, or a Varian 600 MHz instrument. All ^{1}H NMR experiments are reported in δ units, parts per million (ppm), and were measured relative to the signals for residual chloroform (7.26 ppm) in the deuterated solvent, unless otherwise stated. All ^{13}C NMR

spectra are reported in ppm relative to deuterochloroform (77.23 ppm), unless otherwise stated, and all were obtained with ^{1}H decoupling. Gel permeation chromatography (GPC) was performed on a Waters 2695 separation module with a Waters 2414 refractive index detector in chloroform with 0.25% triethylamine. Number average molecular weights (M_n) and weight average molecular weights (M_w) were calculated relative to linear polystyrene standards for calculation of M_w/M_n. The molecular weight (M_n) was calculated using ^{1}H NMR by comparing the integration of the benzyl peak in the initiator to the methyl peak in the polymer side chain unless otherwise noted.

C. Light Source

LED strips (380 nm) were bought from elemental led (see www.elementalled.com) and used as shown below (Figure S2.1). Reactions were placed next to the LED light strips under vigorous stirring while cooling with compressed air. The light intensity was measured to be 0.65 µW/cm^2.
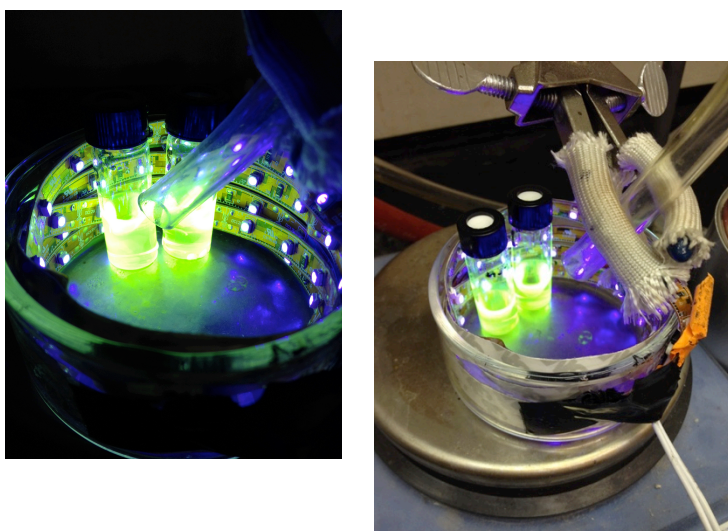
Figure S2.1 General setup with reactions vigorously stirring in an LED-lined crystallization dish while cooling with compressed air.

D. Synthesis of benzyl 2-bromoisobutyrate
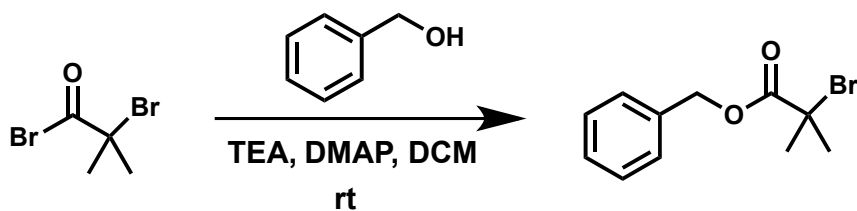
The following procedure was adopted from Long et al.[1] To a flame dried flask equipped with a magnetic stir bar was added benzyl alcohol (1.24 mL, 12 mmol), triethylamine (1.9 mL, 13.2 mmol), N,N-dimethylaminopyridine (19 mg, 0.16 mmol), and anhydrous CH_2Cl_2 (25 mL). The flask was then cooled to 0 °C and bromoisobutyryl bromide (1.63 mL, 13.2 mmol) was added dropwise over 15 min. After stirring at room temperature for 16 h, the reaction was washed with dilute HCl three times (200 mL total) and dilute Na_2CO_3 three times (150 mL total). The organic phase was then dried using Mg_2SO_4 and concentrated on a rotary evaporator. The crude product was purified on a silica-packed chromatography column (5 % EtOAc/Hexanes) to give benzyl 2-bromoisobutyrate as a clear oil (1.76 g, 57% yield). ^{1}H NMR (500 MHz, CDCl$_3$) δ: 7.39 (d, J = 5 Hz, 4H), 7.35 (m, 1H), 5.22 (s, 2H), 1.96 (s, 6H) ppm. ^{13}C NMR (125 MHz, CDCl$_3$) δ: 171.7, 135.7, 128.8, 128.5, 128.1, 67.8, 55.9, 31.0 ppm. IR (neat, cm^{-1}): 2976, 1732, 1455, 1388, 1270, 1153, 1106, 1010, 734, 695. HRMS $C_{11}H_{13}O_2Br$ Found 256.0099, Calc'd 256.0105.

E. General Procedure for Table 2.1
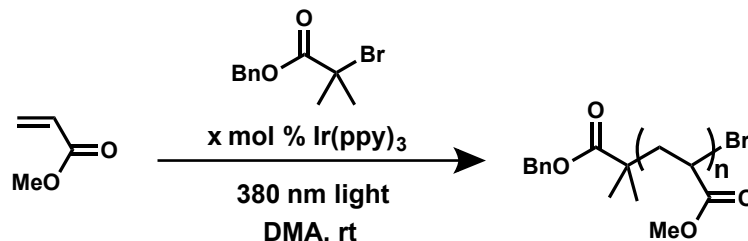
A vial equipped with a magnetic stir bar and fitted with a teflon screw cap septum was charged with methyl acrylate (338 µL, 3.75 mmol), *fac*-Ir(ppy)$_3$ (0.005 - 0.1 mol %) and N,N-dimethylacetamide (2 M – 3.5 M). The reaction mixture was degassed with three freeze-pump-thaw cycles. The vial was then backfilled with argon and benzyl α-bromoisobutyrate (3 µL, 0.018 mmol) was injected via syringe. The reaction was vigorously stirred in front of 380 nm LEDs while cooling with compressed air to maintain ambient temperature. The reaction was allowed to proceed to ca. 50% conversion of methyl acrylate as monitored by ^{1}H NMR. The molecular weight was calculated using ^{1}H NMR and an aliquot was taken and analyzed using GPC to give the molecular weight distribution (M_w/M_n) of the polymer.

F. Polymerization Using 50 Watt Fluorescent Lamps
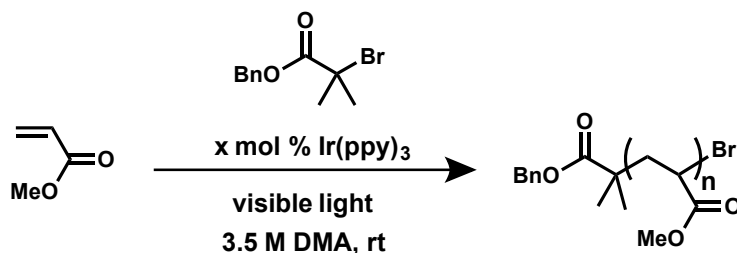
Entry	Ir(ppy)$_3$ [mol %]	M_n (experimental) [g/mol]	M_n (theoretical) [g/mol]	PDI
1	0.05	13,200	12,600	1.35
2	0	271,000	6,600	1.33

A vial equipped with a magnetic stir bar and fitted with a teflon screw cap septum was charged with methyl acrylate (324 µL, 3.75 mmol), *fac*-Ir(ppy)$_3$ (0 or 1.2 mg, 0 or 0.05 mol %) and N,N-dimethylacetamide (3.5 M). The reaction mixture was degassed with three freeze-pump-thaw cycles. The vial was then backfilled with argon and benzyl α-bromoisobutyrate (3 µL, 0.016 mmol) was injected via syringe. The reaction was stirred in front of a 50 W fluorescent lamp while cooling with compressed air to maintain ambient temperature. The reaction was allowed to proceed to 63% (Entry 1) conversion of methyl acrylate as monitored by ^{1}H NMR. The molecular weight was calculated using ^{1}H NMR. An aliquot was taken and analyzed using GPC to give the molecular weight distribution (M_w/M_n) of the polymer.

G. Procedure for Figure 2.3

A vial equipped with a magnetic stir bar and fitted with a teflon screw cap septum was charged with methyl acrylate (338 µL, 3.75 mmol), *fac*-Ir(ppy)$_3$ (1.2 mg, 0.05 mol %) and

N,N-dimethylacetamide (733 μL, 3.5 M). The reaction mixture was degassed with three freeze-pump-thaw cycles. The vial was then backfilled with argon, and brought into a glove box containing a nitrogen atmosphere. It was then covered with aluminum foil, and benzyl α-bromoisobutyrate (3 μL, 0.018 mmol) was injected via syringe. After 1 h of stirring in the dark, an aliquot was taken. The reaction was then vigorously stirred in front of 380 nm LEDs while cooling with a portable fan to maintain ambient temperature. After 30 minutes stirring under light, another aliquot was taken from the reaction mixture. At 1 h, the reaction was immediately wrapped in aluminum foil and an aliquot was taken. This process was repeated multiple times (see Figure 2.3). Conversion was monitored by ^{1}H NMR. The molecular weight was calculated using ^{1}H NMR. GPC was used to obtain the molecular weight distribution (M_w/M_n) of the polymer.
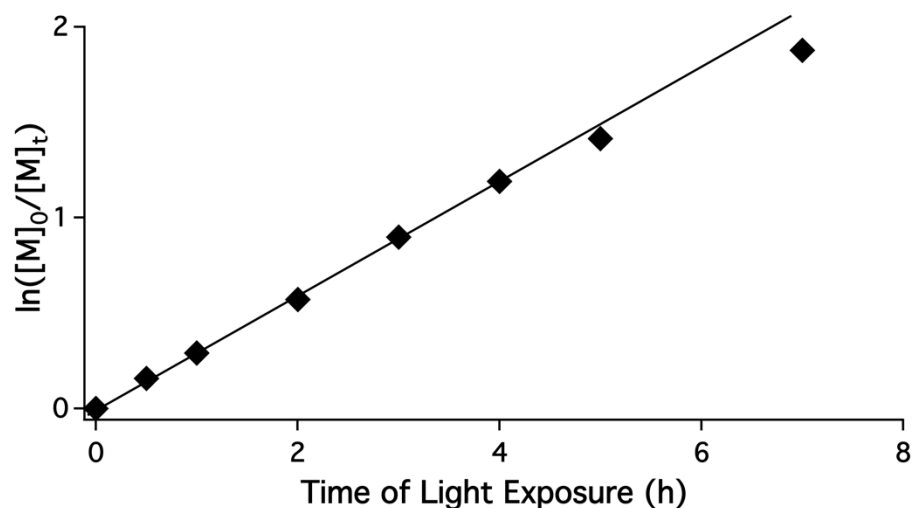
Figure S2.2 Ln($[M]_0/[M]_t$) vs. time of light exposure for kinetic reaction (see Figure 2.3)

H. General Procedure for Table 2.2
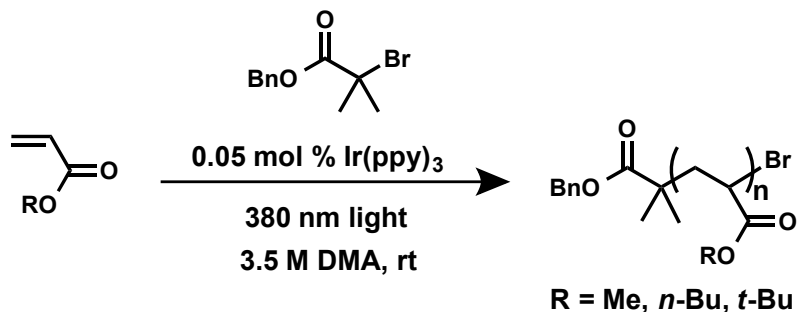
A vial equipped with a magnetic stir bar and fitted with a teflon screw cap septum was charged with methyl, *n*-butyl, or *t*-butyl acrylate (3.75 mmol), *fac*-Ir(ppy)$_3$ (1.2 mg, 0.05 mol %) and N,N-dimethylacetamide (3.5 M). The reaction mixture was degassed with three freeze-pump-thaw cycles. The vial was then backfilled with argon and degassed benzyl α-bromoisobutyrate (0.0016 – 0.096 mmol) was injected via syringe. The reaction was vigorously stirred in front of 380 nm LEDs while cooling with compressed air to maintain ambient temperature. The reaction was allowed to proceed to ca. 50% conversion of monomer as monitored by ^{1}H NMR. The molecular weight was calculated using ^{1}H NMR. An aliquot was taken and analyzed using GPC to give the molecular weight distribution (M_w/M_n) of the polymer.

I. Procedures for Table 2.3
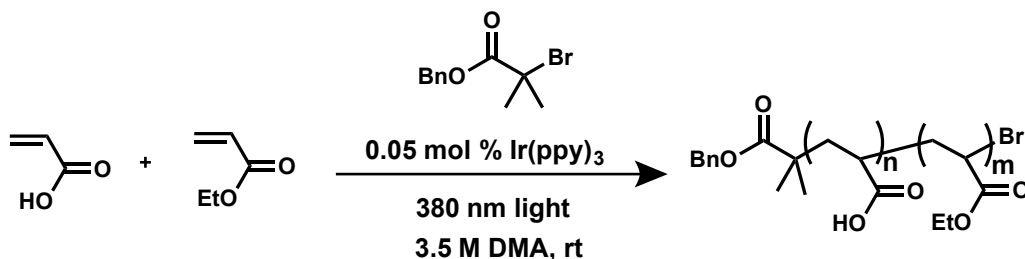
Poly(ethyl acrylate-ran-acrylic acid) (Table 2.3, entry 3) A vial equipped with a magnetic stir bar and fitted with a teflon screw cap septum was charged with ethyl acrylate (369 µL, 3.38 mmol), acrylic acid (27 µL, 0.38 mmol), *fac*-Ir(ppy)$_3$ (1.2 mg, 0.05 mol %) and N,N-dimethylacetamide (675 µL, 3.5 M). The reaction mixture was degassed with three freeze-pump-thaw cycles. The vial was then backfilled with argon and benzyl α-bromoisobutyrate (3.4 µL, 0.018 mmol) was injected via syringe. The reaction was vigorously stirred in front of 380 nm LEDs while cooling with compressed air to maintain ambient temperature. In 1.5 h, the reaction reached 57% conversion as monitored by ^{1}H NMR. The molecular weight was calculated using ^{1}H NMR (M_n = 9,500 g/mol). The product was slowly dropped into a flask of vigorously stirring methanol. A yellow oil precipitated out, the solvent was decanted off, and the product was then dried under vacuum.
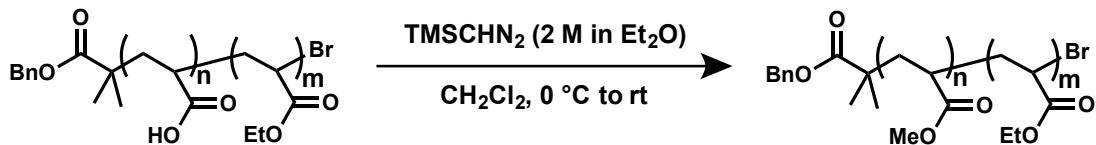
In order to fully characterize the polymer, TMS-diazomethane was used to methylate the acrylic acid units.[2] A stir bar was added to the previous vial and diluted with 5 mL of CH_2Cl_2. The mixture was cooled to 0 °C and TMS diazomethane (1 mL of 2.0 M in diethyl ether) was added dropwise. The reaction was stirred for 3 h. Glacial acetic acid (0.5 mL) was then added slowly to quench the excess TMSCHN$_2$ (^{1}H NMR of the crude reaction mixture showed ca. 8% incorporation of the acrylic acid). The solvent and byproducts were then removed under reduced pressure to give the desired product, analyzed by GPC (M_w/M_n = 1.37). ^{1}H NMR (400 MHz, CDCl3) δ: 7.34 (m, 0.1H), 5.07 (s, 0.1H), 4.10 (bs, 2H), 3.65 (bs, 0.38H), 2.29 (bs, 0.9H), 1.91 (bs, 0.68H), 1.65 (bs, 1.22H), 1.49 (bm, 0.63H), 1.24 (s, 2.78H) ppm.

Poly(ethyl acrylate-ran-acrylic acid) (Table 2.3, entry 1) Procedure identical to that described above using the following conditions: ethyl acrylate (409 µL, 3.75 mmol), acrylic acid (0 mmol), *fac*-Ir(ppy)$_3$ (1.2 mg, 0.05 mol %), N,N-dimethylacetamide (662 µL, 3.5 M), and benzyl α-bromoisobutyrate (3.5 µL, 0.018 mmol). In 2.25 h, the reaction reached 38% conversion as monitored by ^{1}H NMR. The molecular weight (M_n) was calculated using ^{1}H NMR. After methylation, the % acrylic acid incorporation was calculated using ^{1}H NMR and the molecular weight distribution (M_w/M_n) by GPC.

Poly(ethyl acrylate-ran-acrylic acid) (Table 2.3, entry 2) Procedure identical to that described above using the following conditions: ethyl acrylate (388 µL, 3.56 mmol), acrylic acid (13 µL, 0.19 mmol), *fac*-Ir(ppy)$_3$ (1.2 mg, 0.05 mol %), N,N-dimethylacetamide (670 µL, 3.5 M), and benzyl α-bromoisobutyrate (3.4 µL, 0.0184 mmol). In 3 h, the reaction reached 63% conversion as monitored by ^{1}H NMR. The molecular weight (M_n) was calculated using ^{1}H NMR. After methylation, the % acrylic acid incorporation was calculated using ^{1}H NMR and the molecular weight distribution (M_w/M_n) by GPC.

Poly(ethyl acrylate-ran-acrylic acid) (Table 2.3, entry 4) Procedure identical to that described above using the following conditions: ethyl acrylate (369 µL, 3.38 mmol), acrylic acid (27 µL, 0.37 mmol), *fac*-Ir(ppy)$_3$ (1.2 mg, 0.05 mol %), N,N-dimethylacetamide (675 µL, 3.5 M), and benzyl α-bromoisobutyrate (1.7 µL, 0.009 mmol). In 5.5 h, the reaction reached 43% conversion as monitored by ^{1}H NMR. The molecular weight (M_n) was calculated using ^{1}H NMR. After methylation, the % acrylic acid incorporation was calculated using ^{1}H NMR and the molecular weight distribution (M_w/M_n) by GPC.

Poly(ethyl acrylate-ran-acrylic acid) (Table 2.3, entry 5) Procedure identical to that described above using the following conditions: ethyl acrylate (369 µL, 3.38 mmol), acrylic acid (27 µL, 0.37 mmol), *fac*-Ir(ppy)$_3$ (1.2 mg, 0.05 mol %), N,N-dimethylacetamide (675 µL, 3.5 M), and benzyl α-bromoisobutyrate (0.8 µL, 0.00452 mmol). In 3 h, the reaction reached 49% conversion as monitored by ^{1}H NMR. The molecular weight (M_n) was calculated using ^{1}H NMR. After methylation, the % acrylic acid incorporation was calculated using ^{1}H NMR and the molecular weight distribution (M_w/M_n) by GPC.

Poly(ethyl acrylate-ran-acrylic acid) (Table 2.3, entry 6) Procedure identical to that described above using the following conditions: ethyl acrylate (327 µL, 3 mmol), acrylic acid (54 µL, 0.75 mmol), *fac*-Ir(ppy)₃ (1.2 mg, 0.05 mol %), N,N-dimethylacetamide (690 µL, 3.5 M), and benzyl α-bromoisobutyrate (3.3 µL, 0.0176 mmol). In 1.5 h, the reaction reached 64% conversion as monitored by ^{1}H NMR. The product was precipitated into ether. The molecular weight (M_n) was calculated using ^{1}H NMR. After methylation, the % acrylic acid incorporation was calculated using ^{1}H NMR and the molecular weight distribution (M_w/M_n) by GPC.

Poly(ethyl acrylate-ran-acrylic acid) (Table 2.3, entry 7) Procedure identical to that described above using the following conditions: ethyl acrylate (287 µL, 2.63 mmol), acrylic acid (77 µL, 1.12 mmol), *fac*-Ir(ppy)₃ (1.2 mg, 0.05 mol %), N,N-dimethylacetamide (707 µL, 3.5 M), and benzyl α-bromoisobutyrate (3.2 µL, 0.0171 mmol). In 1.5 h, the reaction reached 62% conversion as monitored by ^{1}H NMR. The product was precipitated into ether. The molecular weight (M_n) was calculated using ^{1}H NMR. After methylation, the % acrylic acid incorporation was calculated using ^{1}H NMR and the molecular weight distribution (M_w/M_n) by GPC.

Poly(ethyl acrylate-ran-acrylic acid) (Table 2.3, entry 8) Procedure identical to that described above using the following conditions: ethyl acrylate (246 µL, 2.25 mmol), acrylic acid (103 µL, 1.5 mmol), *fac*-Ir(ppy)₃ (1.2 mg, 0.05 mol %), N,N-dimethylacetamide (722 µL, 3.5 M), and benzyl α-bromoisobutyrate (3 µL, 0.0160 mmol). In 1.5 h, the reaction

reached 67% conversion as monitored by ^{1}H NMR. The product was precipitated into ether. The molecular weight (M_n) was calculated using ^{1}H NMR. After methylation, the % acrylic acid incorporation was calculated using ^{1}H NMR and the molecular weight distribution (M_w/M_n) by GPC.

Poly(ethyl acrylate-ran-acrylic acid) (Table 2.3, entry 9) Procedure identical to that described above using the following conditions: ethyl acrylate (205 µL, 1.875 mmol), acrylic acid (129 µL, 1.875 mmol), *fac*-Ir(ppy)$_3$ (1.2 mg, 0.05 mol %), N,N-dimethylacetamide (737 µL, 3.5 M), and benzyl α-bromoisobutyrate (2.9 µL, 0.016 mmol). In 1 h, the reaction reached 71% conversion as monitored by ^{1}H NMR. The product was precipitated into ether. The molecular weight (M_n) was calculated using ^{1}H NMR. After methylation, the % acrylic acid incorporation was calculated using ^{1}H NMR and the molecular weight distribution (M_w/M_n) by GPC.

J. Procedure for Acid Functionalized Initiator Polymerizations
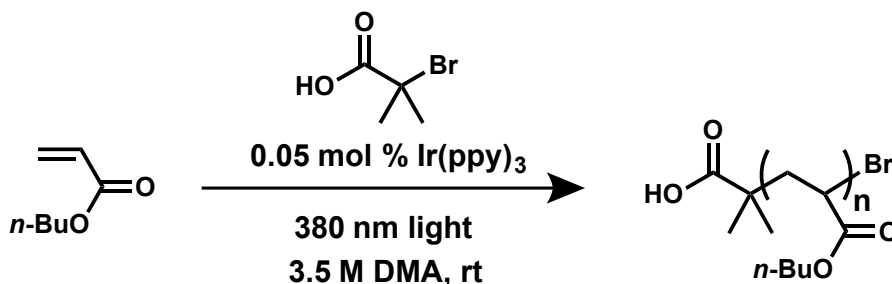
Poly(n-butyl acrylate) A vial equipped with a magnetic stir bar and fitted with a teflon screw cap septum was charged with *n*-butyl acrylate (535 µL, 3.75 mmol), *fac*-Ir(ppy)$_3$ (1.2 mg, 0.05 mol %) and N,N-dimethylacetamide (436 µL). The reaction mixture was degassed

with three freeze-pump-thaw cycles. The vial was then backfilled with argon. In a separate

vial, 3-bromopropionic acid (0.024-0.048 mmol) was combined with N,N-dimethylacetamide (100 µL) and degassed with three freeze-pump-thaw cycles before

transferring to the vial containing monomer and catalyst via syringe. The reaction was

vigorously stirred in front of 380 nm LEDs while cooling with compressed air to maintain

ambient temperature. The reaction conversion was monitored by ^{1}H NMR. The product was

slowly dropped into a flask of vigorously stirring hexanes. A yellow oil precipitated out,

and the solvent was decanted off. The product was then dried under reduced pressure.
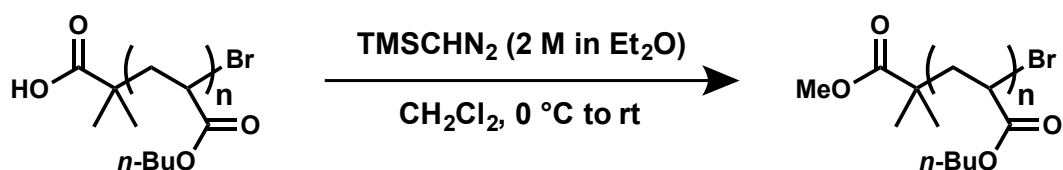
In order to fully characterize the polymer, TMS-diazomethane was used to methylate the

acidic functional groups.[2] A stir bar was added to the previous vial and diluted with 5 mL

of CH_2Cl_2. The mixture was cooled to 0 °C and TMS diazomethane (0.3 mL of 2.0 M in

diethyl ether) was added dropwise. The reaction was stirred for 3 h. Glacial acetic acid (0.3

mL) was then added slowly to quench the reaction of excess $TMSCHN_2$. The solvent and

byproducts were then removed under reduced pressure to give the desired product, which

was analyzed by GPC (M_n and M_w/M_n).

K. Procedure for Figure 2.4

Poly(methyl acrylate) A vial equipped with a magnetic stir bar and fitted with a teflon screw cap septum was charged with methyl acrylate (631 μL, 7 mmol), *fac*-Ir(ppy)$_3$ (2.3 mg, 0.05 mol %) and N,N-dimethylacetamide (925 μL, 4.5 M). The reaction mixture was degassed with three freeze-pump-thaw cycles. The vial was then backfilled with argon and benzyl α-bromoisobutyrate (4.5 μL, 0.024 mmol) was injected via syringe. The reaction was stirred in front of 380 nm LEDs while cooling with compressed air to maintain ambient temperature. The reaction was stirred in front of the light for 2.5 h and then put into the dark by wrapping it in aluminum foil. A syringe wrapped in aluminum foil was then used to transfer the reaction mixture in the dark into a stirring solution of methanol (also wrapped in aluminum foil). A yellow oil crashed out, and the solution was placed into a freezer (ca. -20 °C) for 1 h. The methanol was then decanted and the residual solvent was evaporated to yield 130 mg of a yellow oil. M_n = 7,600 g/mol, M_w/M_n = 1.31; ^{1}H NMR (400 MHz, CDCl3) δ: 7.35 (m, 0.1H), 5.08 (m, 0.08H), 3.66 (s, 3H), 2.31 (bs, 1.2H), 1.92 (bm, 0.6H), 1.68 (bs, 1H), 1.50 (bm, 0.5H), 1.25 (s, 0.12H), 1.18 (s, 0.06H), 1.15 (s, 0.07H) ppm.
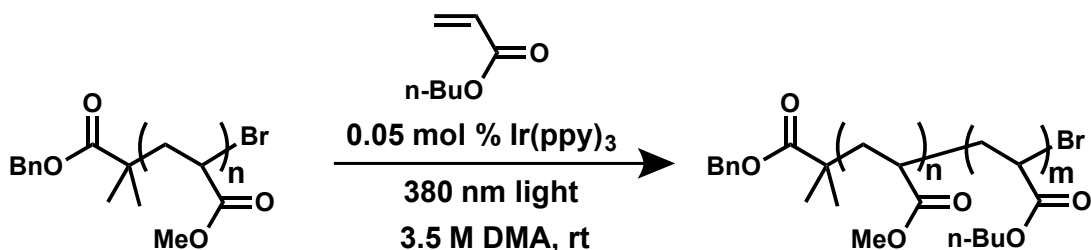
Poly(methyl acrylate)-*b*-(n-butyl acrylate) A vial equipped with a magnetic stir bar and fitted with a teflon screw cap septum was charged with n-butyl acrylate (392 µL, 2.74 mmol), *fac*-Ir(ppy)$_3$ (0.9 mg, 0.05 mol %) and N,N-dimethylacetamide (191 µL). In another flask, 200 µL of dimethyl acetamide was added to the poly(methyl acrylate) macroinitiator (51 mg, 0.0088 mmol). Both reaction mixtures were degassed with three freeze-pump-thaw cycles. Special care was taken to handle the macroinitiator in the dark as residual Ir(ppy)$_3$ may degrade chain ends in the presence of light. Using a syringe, the macroinitiator was then transferred to the flask containing n-butyl acrylate. The reaction was stirred in front of 380 nm LEDs while cooling with compressed air to maintain ambient temperature. After 5.5 h the reaction was stopped by opening to air and precipitated into MeOH (20 mL). A yellow oil crashed out, and the solution was placed into a freezer (ca. -20 °C) for 1 h. The methanol was then decanted off and the residual solvent was removed under reduced pressure. This process was repeated 3 times to yield 45 mg of a yellow oil. M_n = 30,200 g/mol, M_w/M_n = 1.24; ^{1}H NMR (600 MHz, CDCl3) δ: 5.07 (m, 0.1H), 4.04 (bm, 2H), 3.66 (s, 0.87H), 2.27 (bm, 1.47H), 1.91 (bm, 0.81H), 1.60 (bs, 3.04H), 1.48 (bm, 0.43H), 1.37 (bs, 1.93H), 1.25 (s, 0.14H), 0.93 (t, 2.67H) ppm.
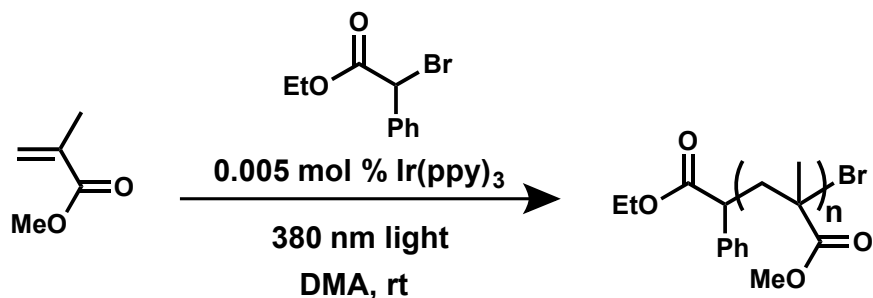
Poly(methyl methacrylate) A vial equipped with a magnetic stir bar and fitted with a rubber septum was charged with methyl methacrylate (2.4 mL, 22.5 mmol), *fac*-Ir(ppy)$_3$ (0.7 mg, 0.005 mol %) and N,N-dimethylacetamide (8.4 mL). The reaction mixture was degassed with three freeze-pump-thaw cycles. The vial was then backfilled with argon and benzyl α-bromoisobutyrate (16.9 μL, 0.09 mmol) was injected via syringe. The reaction was stirred in front of 380 nm LEDs while cooling with compressed air to maintain ambient temperature. The reaction was stirred in front of the light for 3 h and then put into the dark by wrapping it in aluminum foil. A syringe wrapped in aluminum foil was used to transfer the reaction mixture in the dark into a stirring solution of hexanes (50 mL, also wrapped in aluminum foil). The white precipitate was filtered, and re-dissolved in dichloromethane before precipitating again into hexanes to yield 610 mg of a white powder. M_n = 7,200 g/mol, M_w/M_n = 1.36.

Poly(methyl methacrylate)-*b*-(methyl acrylate) A vial equipped with a magnetic stir bar and fitted with a teflon screw cap septum was charged with methyl acrylate (506 µL, 5.61 mmol), *fac*-Ir(ppy)$_3$ (0.37 mg, 0.01 mol %) and N,N-dimethylacetamide (600 µL). In another flask, 500 µL of dimethyl acetamide was added to the poly(methyl methacrylate) macroinitiator (87 mg, 0.0121 mmol). Both reaction mixtures were degassed with three freeze-pump-thaw cycles. Using a syringe, the monomer and catalyst were then transferred to the flask containing macroinitiator. The reaction was stirred in front of 380 nm LEDs while cooling with compressed air to maintain ambient temperature. After 8 h the reaction was stopped by opening to air and precipitated into MeOH (20 mL). A yellow oil crashed out, and the solution was placed into a freezer (ca. -20 °C) for 1 h. The methanol was then decanted off and the residual solvent was removed under reduced pressure. This process was repeated once to yield 102 mg of a yellow oil. M_n = 55,800 g/mol, M_w/M_n = 1.35.
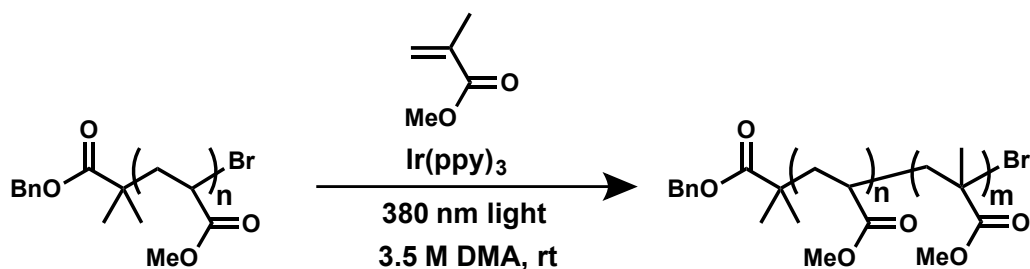
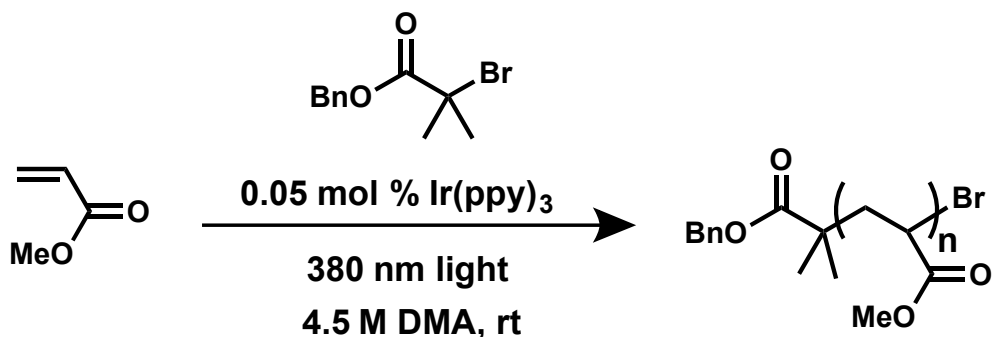**Poly(methyl acrylate)-*b*-(methyl methacrylate)** A vial equipped with a magnetic stir bar and fitted with a teflon screw cap septum was charged with methyl methacrylate (458 µL, 4.29 mmol), and N,N-dimethylacetamide (400 µL). In another flask, 368 µL of dimethyl acetamide was added to the poly(methyl acrylate) macroinitiator (90 mg, 0.0107 mmol). Residual Ir(ppy)$_3$ from the poly(methyl acrylate) macroinitiator was sufficient to catalyze

block copolymerization. Both reaction mixtures were degassed with three freeze-pump-thaw cycles. Special care was taken to handle the macroinitiator in the dark as residual Ir(ppy)$_3$ may degrade chain ends in the presence of light. Using a syringe, the macroinitiator was then transferred to t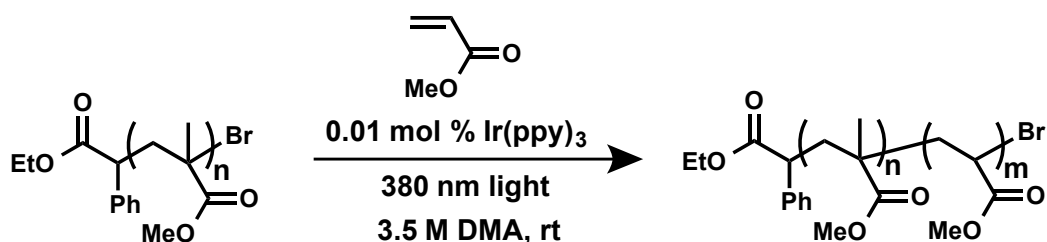he flask containing methyl methacrylate. The reaction was stirred in front of 380 nm LEDs while cooling with compressed air to maintain ambient temperature. After 7 h the reaction was stopped by opening to air and precipitated into MeOH (20 mL). A yellow oil crashed out, and the solution was placed into a freezer (ca. -20 °C) for 1 h. The methanol was then decanted off and the residual solvent was removed under reduced pressure This process was repeated 2 times to yield 100 mg of a yellow oil. M_n = 38,900 g/mol, M_w/M_n = 1.38.

L.   Supplementary References

[1]   M. Long, D. W. Thornthwaite, S. H. Rogers, G. Bonzi, F. R. Livens, S. P. Rannard, *Chem. Commun.* **2009**, 6406.

[2]   E. Kühnel, D. D. P. Laffan, G. C. Lloyd-Jones, T. Martínez del Campo, I. R. Shepperson, J. L. Slaughter, *Angew. Chem. Int. Ed.* **2007**, *46*, 7075–7078.

3. Metal-Free Atom Transfer Radical Polymerization

I. *Abstract*

Overcoming the challenge of metal contamination in traditional ATRP systems, a metal-free ATRP process, mediated by light and catalyzed by an organic-based photoredox catalyst is reported. Polymerization of vinyl monomers are efficiently activated and deactivated with light leading to excellent control over the molecular weight, polydispersity and chain ends of the resulting polymers. Significantly, block copolymer formation was facile and could be combined with other controlled radical processes leading to structural and synthetic versatility. We believe that these new organic-based photoredox catalysts will enable new applications for controlled radical polymerizations and also be of further value in both small molecule and polymer chemistry.
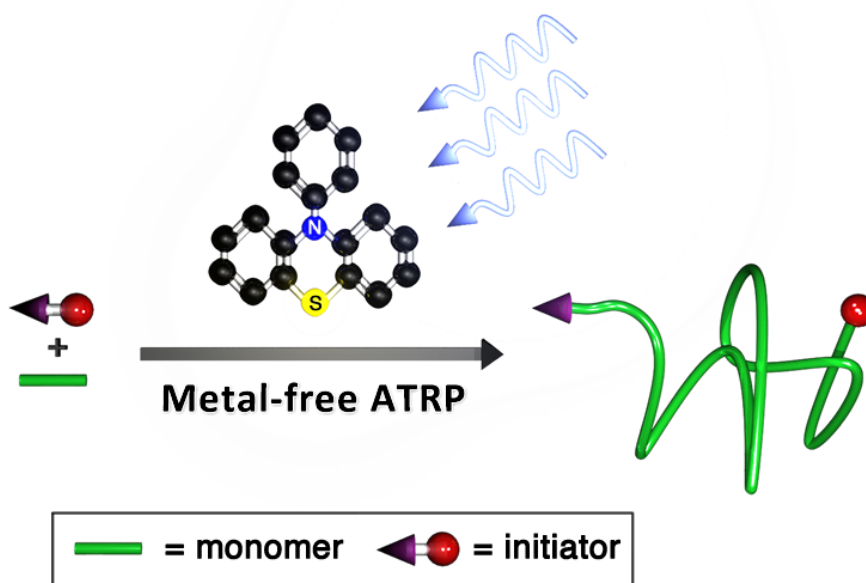
Figure 3.1   Representation of light mediated metal-free atom transfer radical polymerization

II. Introduction

Controlled free radical polymerizations (CRP) represent one of the most far reaching developments in polymer synthesis, allowing non-experts facile access to functionalized polymers with well-defined structure and architecture.[1-6] Of the CRP techniques, Atom Transfer Radical Polymerization (ATRP) is arguably the most utilized and operates via a redox equilibrium process mediated by a ligated metal catalyst (i.e. Cu(I), Ru(II), Fe(II)). For a variety of applications, such as microelectronics, biomaterials, etc., a key limiting factor in using ATRP is metal contamination.[1-13] A significant focus for the ATRP field since the initial discovery[1,2,4,6,8-14] has therefore been directed towards lowering catalyst loadings[2,4,6,8-13] and/or removal of residual metals.[15-18] Although catalyst loadings can be decreased to parts per million (ppm), we envisaged that a much more viable and ambitious solution to this grand challenge would be the development of a metal-free catalyst system for atom transfer radical polymerization.

In recent years our group has disclosed the photomediated ATRP of methacrylates and acrylates using Ir-based photoredox catalysts.[19-21] This system provides for excellent spatial and temporal control over the chain-growth process, enabling the formation of complex 3-dimensional nanostructures in a single step.[19,22] However, as in ATRP, the use of ppm levels of metal catalyst limited the practicality of this system. Although the emergent field of photoredox catalysis has primarily utilized transition metals (i.e. Iridium and Ruthenium),[23] organic catalysts have recently attracted significant attention[24] and, in some cases, have been shown to be more efficient than metal-based systems.[25] We saw this as an opportunity to establish a metal-free ATRP process by developing an organic-based catalyst that could replace Ir(ppy)$_3$ in photomediated, controlled radical polymerizations. The

ultimate aim is an organic photoredox system that is reducing in the excited state and effectively catalyzes controlled radical polymerization processes in an analogous manner to traditional ATRP systems (Scheme 3.1).

Traditional ATRP: Metal Catalyst (Previous Work)

CuBr, Ligand

R$-$Br + Monomer   R$-$P$_n$$-$Br

PTH, Light

Metal-free ATRP: Organic Photocatalyst (This Work)
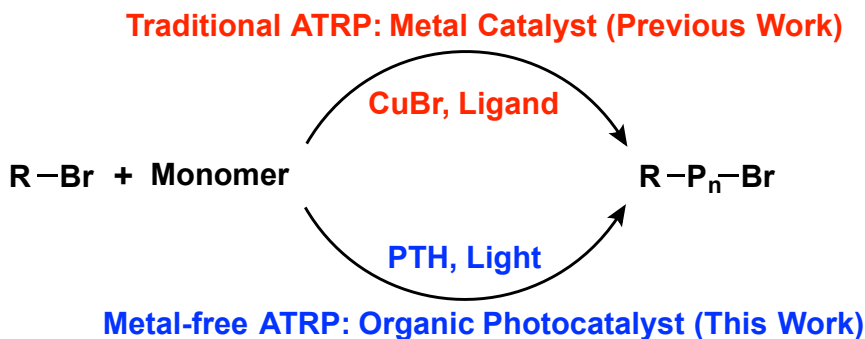
Scheme 3.1 Previous ATRP systems rely on metal catalysts (i.e. CuBr) with ligands for control; metal-free ATRP relies on an organic photoredox catalyst (i.e. PTH) to produce identical polymers.

III. Results and Discussion

A. Catalyst Identification

An immediate challenge in developing a metal-free ATRP is designing an organic catalyst that is highly reducing in the excited state. The majority of organic based dyes, currently used as photoredox catalysts, are oxidizing in the excited state and would not possess the desired reduction potentials required to reduce the alkyl bromide initiator or subsequent polymer chain ends to a propagating radical. We therefore reasoned that an organic catalyst is needed that has an excited state reduction potential on par with Ir(ppy)$_3$, as well as a stable radical cation species, which is formed after reduction of the alkyl bromide (Figure 3.2). After surveying a range of possible organic dyes, phenothiazine

derivatives were chosen as candidates for our initial studies due to the desired photophysical properties (*vide supra*), low cost, ready availability, and facile modification chemistry.[26]
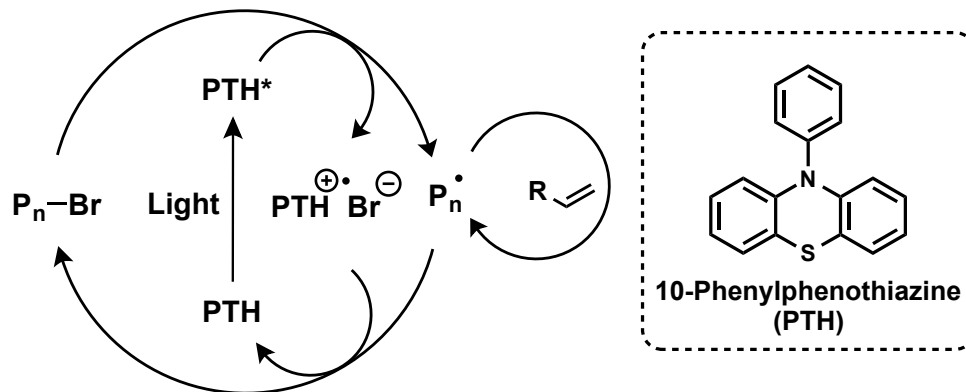
Figure 3.2 Proposed mechanism of metal-free photomediated ATRP with 10-phenylphenothiazine as the catalyst (P_n = polymer chain).

Initially, we examined the use of commercially available 10-methylphenothiazine (**Me-PTH**) for the polymerization of methyl methacrylate (MMA) under 380 nm irradiation at room temperature. Encouragingly, polymerization was observed with good agreement between theoretical and experimental molecular weight, albeit with poor control over the molecular weight distribution (Table 1, entry 1). We postulated that tuning the nitrogen substituent on the phenothiazine ring would reduce catalyst decomposition, allowing for greater control over the polymerization process. To this end, we synthesized 10-phenylphenothiazine, **PTH**, from commercially available phenothiazine and chlorobenzene using C-N cross-coupling chemistry followed by repeated purification to obtain highly pure **PTH**[27] (see SI, E_{red}(**PTH**$^+$/**PTH***) = -2.1 V vs. SCE[28]). Significantly, we found that the controlled polymerization of MMA could be achieved in the presence of a traditional ATRP initiator, **1**, and **PTH**. Of even greater encouragement was the observation of conventional CRP behavior with the molecular weight being determined by the initial monomer:initiator

ratio and low polydispersities being obtained in each case (Table 1, entries 2 – 6). These experiments establish that, for the first time, an atom transfer radical polymerization (ATRP) process could occur with a metal-free catalyst system.

Table 3.1 Optimization of a light-mediated polymerization of methyl methacrylate using organic photoredox catalysts.[a]

Entry	Catalyst	M_n (exp) [g/mol]	M_n (theo) [g/mol]	M_w / M_n
1	Me-PTH	8,300	7,400	1.74
2[b]	PTH	15,400	14,000	1.32
3[b]	PTH	12,000	11,000	1.25
4	PTH	6,200	7,200	1.30
5	PTH	2,400	2,600	1.18
6	PTH	1,300	1,800	1.20
7[c]	PTH	--	--	--
8[d]	PTH	42,300	--	2.00
9[e]	--	--	--	--
10[f]	Eosin Y	--	--	--
11[f]	Methylene Blue	--	--	--

[a] Reaction conditions: MMA (1 equiv.), photocatalyst (0.001 equiv.), **1** (0.008-0.01 equiv), DMA (2.7 M of MMA) at room temperature with irradiation from 380 nm LEDs for 4 h (M_n = number average molecular weight; M_w = weight average molecular weight). M_n and M_w / M_n determined using size exclusion chromatography (SEC) or ^{1}H NMR; [b] reaction run with benzyl methacrylate (1 equiv.) for 7 h [c] reaction run in the dark [d] reaction run in the absence of **1** [e] reaction run in the absence of catalyst [f] irradiated with visible light (50 W fluorescent bulbs).

To further support the controlled nature of this polymerization, a range of experimental conditions were examined. When the polymerization was conducted in the absence of light, initiator, or catalyst, either no or uncontrolled polymerization was observed (Table 1, entries 7–9), demonstrating that this is indeed a photomediated process that is initiated by 1 and catalyzed by PTH. Moreover, when other organic-based photoredox catalysts were employed (Eosin Y and Methylene Blue), which are oxidizing in the excited state, no reaction occurred (Table 1, entries 8 and 9). This further corroborates that a catalyst that is highly reducing in the excited state is needed to activate the alkyl bromide chain-end.
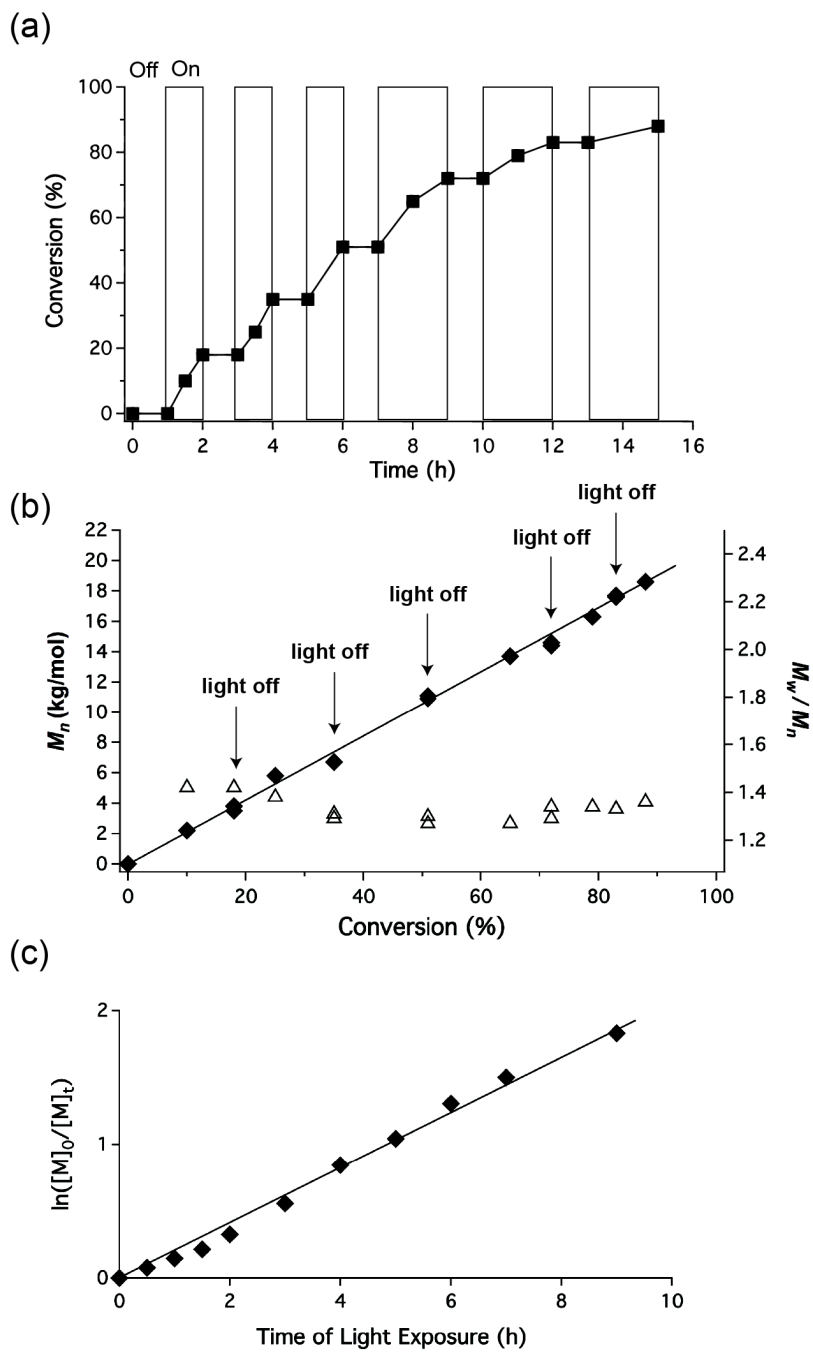
Figure 3.3 Polymerization of BnMA using PTH with repeated 'on-off' cycling of the reaction to light.

B. Kinetic Analysis

The lack of reaction in the dark suggested that the polymerization could be activated/deactivated by light leading to controlled regulation of the polymerization process. To investigate this responsive nature, **PTH** was combined with the initiator, **1**, and benzyl methacrylate (BnMA). Upon observing no conversion after 1 hour in the dark, the reaction was exposed to 380 nm light, reaching 18% conversion in 1 hour (Figure 3.3a). After removal of the light source, no further conversion was observed during the course of 1 hour; however, re-exposure to 380 nm light led to further reaction progress. This cycle could be repeated several times up to high conversions (~ 90%) indicating very efficient activation and deactivation of the polymerization process. Significantly, a linear increase in molecular weight vs. conversion is obtained even with multiple 'on-off' light switching cycles (Figure 3.3b), and the observation of first order kinetics through the course of the reaction demonstrated a controlled polymerization process (Figure 3.3c). In analogy with traditional ATRP processes, this data indicates that when light is removed from the system the chain-ends are oxidized to the stable and dormant alkyl bromides and upon re-exposure to light in the presence of **PTH**, the chain-ends are efficiently and reversibly converting to propagating radicals.

C. Scope Extension

In contrast to Ir(ppy)$_3$ and traditional metal-catalyzed ATRP processes, a unique feature of **PTH** is its highly reducing excited state, which may allow a wider selection of functional groups to be tolerated during the polymerization. We sought to take advantage of this feature by polymerizing monomer-types that were inaccessible with the Ir-based system. The test vehicle chosen was 2-(dimethylamino)ethyl methacrylate (DMAEMA); a monomer utilized

ubiquitously for its stimuli-responsive properties.[29-32] In the presence of Ir(ppy)$_3$ under the previously optimized conditions, very broad polydispersities were observed (Table S1, $M_w/M_n > 3$). We surmised that the uncontrolled polymerization was a result of radical formation through oxidation of the amine; this is a well-known reaction pathway for photoredox catalysts.[33] In direct contrast, for the less oxidizing **PTH** ($E_{1/2}^{ox} = 0.68$ V vs. SCE, see SI)**,** irradiation resulted in a well-defined polymerization process with accurate control over molecular weight and low polydispersities (~1.1) (Scheme 3.2). Moreover, this system allows precise control over the M_n of these polymers by varying the initiator to monomer ratio, as well as enabling the synthesis of functional materials (block copolymers) – both of which could not be achieved using the Ir-based catalyst system (see SI). Therefore, this system not only avoids metal contamination, but extends the scope of the photomediated ATRP in general.
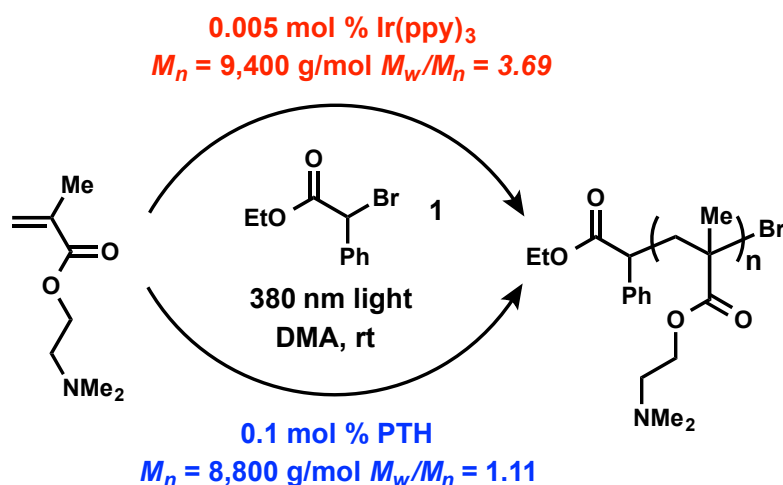
Scheme 3.2 Dimethylaminoethyl methacrylate (DMAEMA) gives uncontrolled polymerization with Ir-based system and controlled polymerization with PTH, demonstrating the broad scope of photomediated ATRP

D. Chain-end Fidelity

A fundamental key to the success of any controlled radical process, such as ATRP, is chain-end fidelity. Achieving high chain-end fidelity allows for effective block copolymer formation, chain end functionalization, and the successful synthesis of a wide variety of well-defined macromolecules. It was therefore critical to determine chain-end fidelity in these reactions. Initially, a low molecular weight PMMA (M_n = 1,400 g/mol, M_w/M_n = 1.08) was synthesized by **PTH**-mediated, metal-free ATRP under the optimized conditions described above and analyzed using electrospray ionization mass spectrometry (ESI-MS) (Figure 3.4a). Of particular note is the correlation of observed molecular weight with the expected values for the individual PMMA oligomers based on the presence of the initiating unit at one chain end and a bromine atom at the propagating chain end with each peak separated by the mass of one monomer unit (100 amu). Further evidence for chain-end fidelity is supplied by the isotopic splitting for the respective molecular ions, clearly indicating the presence of a single Br atom at one chain end (Figure S3.4).
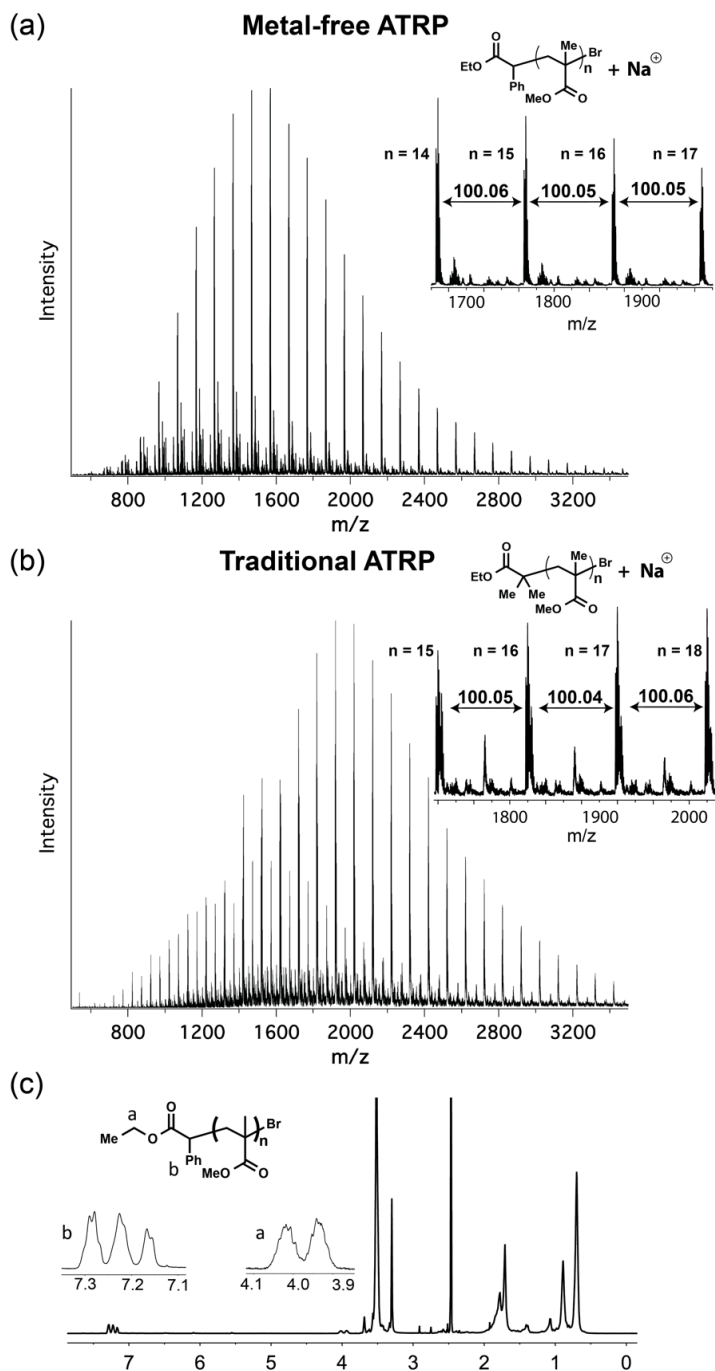
Figure 3.4 (a) ESI-MS of PMMA produced under optimized metal-free ATRP conditions with major peaks separated by molecular weight of the monomer; (b) ESI-MS of PMMA produced using reported conditions of traditional ATRP; (c) ^{1}H NMR of PMMA sample showing initiator-derived protons.

To illustrate the similarity of polymers obtained from this new process and traditional ATRP procedures, a low molecular weight PMMA derivative was prepared using CuBr as catalyst and 4,4'-dinonyl-2,2'-dipyridyl as ligand at 90 °C (M_n = 1,100 g/mol, M_w/M_n = 1.20). Analysis by ESI-MS again showed the expected oligomer distribution and chain ends with a very similar peak distribution and profile (Figure 3.4b).

^{1}H NMR was used to further confirm the level of incorporation and fidelity of the chain ends with resonances for the initiating ethyl 2-phenylacetate group being observed at ~ 4.0 and 7.2 ppm. Integration of these resonances and comparison with resonances for the backbone allowed molecular weights to be calculated that were in full agreement with values obtained by both MS and GPC analysis (Figure 3.4c). This data firmly establishes that **PTH**-mediated, metal-free ATRP procedures give a similar degree of control over chain ends as that observed for traditional ATRP systems with the polymers obtained from both process being analogous.

E. Block Copolymerizations

Although ESI-MS and NMR give evidence for a and w chain ends, successful block copolymerization provides definitive proof that a controlled polymerization system has been achieved. To examine the utility of this metal-free process, the polymerization of **1** and MMA with 0.1 mol % **PTH**, was conducted to give a starting PMMA homopolymer (M_n = 5,100 g/mol, M_w/M_n = 1.12). After standard purification and storage, the stable homopolymer was examined as a macroinitiator for the polymerization of benzyl methacrylate under metal-free ATRP conditions (0.1 mol % **PTH**, 380 nm irradiation for 4 h) leading to a well-defined PMMA-*b*-PBnMA block copolymer (Figure 3.5, M_n = 25,900 g/mol, M_w/M_n = 1.31). The size exclusion chromatogram (SEC) clearly shows a shift to

97

higher molecular weight species with little tailing in the homopolymer regime, indicating excellent alkyl bromide chain-end fidelity in the PMMA macroinitiator and a high re-initiation efficiency. To further explore the scope of this process, a PMMA-*b*-PBnMA copolymer could also be prepared (Figure S3.5, M_n = 27,900 g/mol, M_w/M_n = 1.28) starting from ethyl 2-bromoisobutyrate as initiator, illustrating the versatility of this process.

Block and random copolymerizations with other monomer families were then conducted to demonstrate the broad scope of this system. The presence of bromo chain ends suggest potential orthogonality for combining metal-free ATRP with other controlled radical processes, increasing the range of block copolymers that can be prepared. To demonstrate the ability of metal-free ATRP to be combined with other catalyst systems, the starting PMMA homopolymer (M_n = 3,600 g/mol, M_w/M_n = 1.19) was used to polymerize methyl acrylate under Ir(ppy)$_3$ catalyst conditions.[20] Significantly, a well-defined block copolymer (Figure 3.5, M_n = 20,200 g/mol, M_w/M_n = 1.24) with virtually no tailing in the homopolymer regime of the SEC trace was obtained. Taking this concept even further, the same **PTH**-derived PMMA macroinitiator could be used for the polymerization of styrene under traditional ATRP conditions employing CuBr as the catalyst. The resulting block copolymer (Figure 3.5, M_n = 11,100 g/mol, M_w/M_n = 1.06) again revealed a monomodal shift in retention time of the chromatogram. Finally, the reverse CRP order - Cu-based ATRP to produce a PMMA macroinitiator followed by chain extension with BnMA using **PTH** as catalyst was also shown to be a facile process leading to well-defined diblock copolymers (Figure S3.6). Under our standard conditions several random copolymers were also synthesized with varying incorporations of styrene, as well as methyl acrylate, while

maintaining good agreement between theoretical and experimental molecular weights (Tables S3.2 and S3.3).
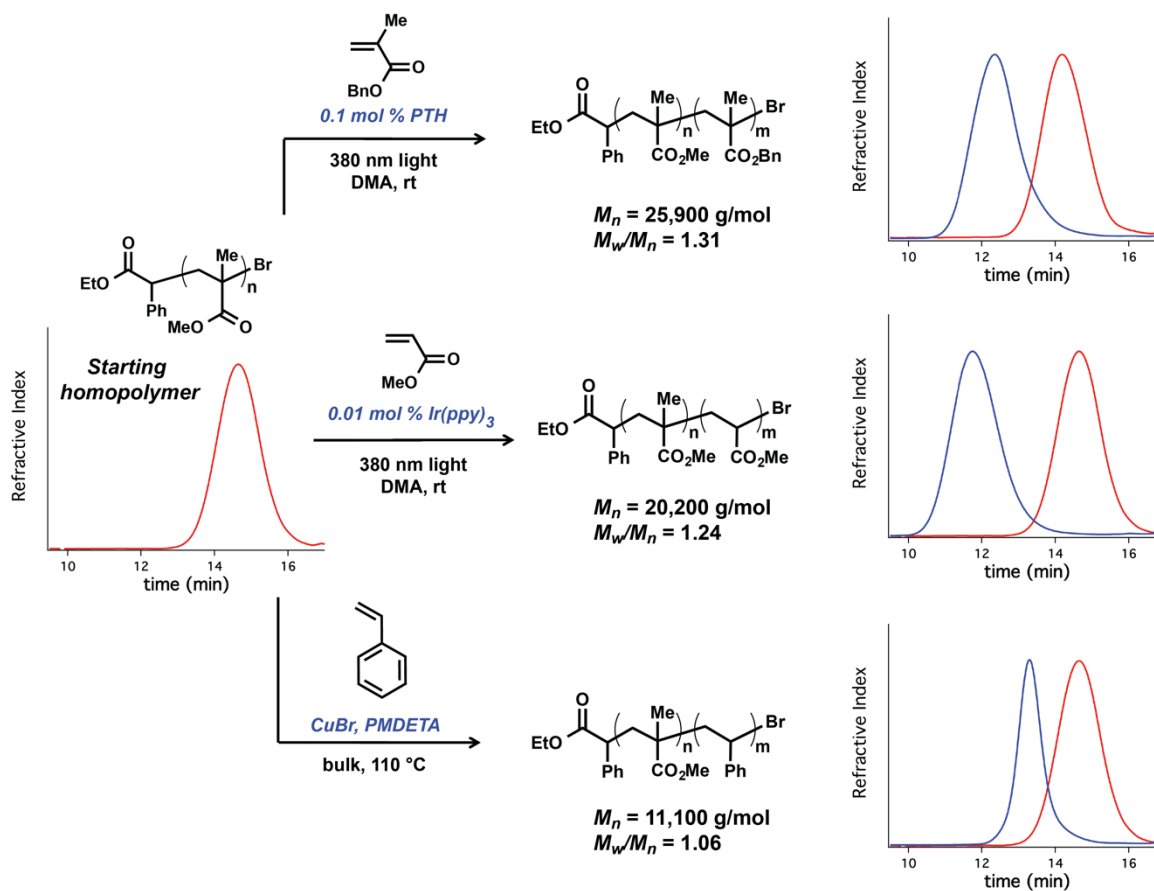
Figure 3.5 Synthesis of block copolymers starting from a PMMA macroinitiator prepared by metal-free ATRP conditions and accompanying SEC traces of various blocks produced using different combinations of catalyst systems (red trace = starting PMMA macroinitiator, blue trace = block copolymer)

IV. Conclusion

In conclusion, we have demonstrated a successful metal-free, atom transfer radical polymerization. Use of an affordable, easily prepared organic catalyst, **PTH**, leads to a controlled, photomediated process that bears many characteristics of traditional ATRP procedures including accurate control over molecular weight, low polydispersity, and high retention of chain end groups. This allows a variety of block copolymers to be prepared in a sequential manner as well as in combination with other ATRP processes (traditional Cu-catalyzed and photomediated Ir-based systems). This organic-based catalyst system circumvents issues of metal contamination in polymers made using ATRP and allows for the production of a variety of functional materials, pushing the field of CRP into new areas and applications. We further anticipate that the unique properties of this new class of organic-based photoredox catalysts, specifically their highly reducing nature, will find applications in both small molecule and polymer functionalization chemistry.

V. Acknowledgements

VI. References

[1]   K. Matyjaszewski, N. V. Tsarevsky, *J. Am. Chem. Soc.* **2014**, *136*, 6513–6533.

[2]   W. Jakubowski, K. Matyjaszewski, *Angew. Chem. Int. Ed.* **2006**, *45*, 4482–4486.

[3]   G. Moad, E. Rizzardo, S. H. Thang, *Polymer* **2008**, *49*, 1079–1131.

[4]   W. Jakubowski, K. Min, K. Matyjaszewski, *Macromolecules* **2006**, *39*, 39–45.

[5]   J. Nicolas, Y. Guillaneuf, C. Lefay, D. Bertin, D. Gigmes, B. Charleux, *Progress in Polymer Science* **2013**, *38*, 63–235.

[6]   K. Matyjaszewski, W. Jakubowski, K. Min, W. Tang, J. Huang, W. A. Braunecker, N. V. Tsarevsky, *Proceedings of the National Academy of Sciences* **2006**, *103*, 15309–15314.

[7]   C. J. Hawker, A. W. Bosman, E. Harth, *Chem. Rev.* **2001**, *101*, 3661–3688.

[8]   K. Min, H. Gao, K. Matyjaszewski, *Macromolecules* **2007**, *40*, 1789–1791.

[9]   Y. Gnanou, G. Hizal, *J. Polym. Sci. A Polym. Chem.* **2004**, *42*, 351–359.

[10]   S. Fleischmann, B. M. Rosen, V. Percec, *J. Polym. Sci. A Polym. Chem.* **2010**, *48*, 1190–1196.

[11]   Y. Kwak, A. J. D. Magenau, K. Matyjaszewski, *Macromolecules* **2011**, *44*, 811–819.

[12]   H. Dong, K. Matyjaszewski, *Macromolecules* **2008**, *41*, 6868–6870.

[13]   A. J. D. Magenau, N. C. Strandwitz, A. Gennaro, K. Matyjaszewski, *Science* **2011**, *332*, 81–84.

[14]   M. Ouchi, T. Terashima, M. Sawamoto, *Chem. Rev.* **2009**, *109*, 4963–5050.

[15]   K. Matyjaszewski, T. Pintauer, S. Gaynor, *Macromolecules* **2000**, *33*, 1476–1478.

[16]   S. Munirasu, R. Aggarwal, D. Baskaran, *Chem. Commun.* **2009**, 4518.

[17]   G. Kickelbick, H.-J. Paik, K. Matyjaszewski, *Macromolecules* **1999**, *32*, 2941–2947.

[18]   Y. Shen, S. Zhu, *Macromolecules* **2001**, *34*, 8603–8609.

[19]   B. P. Fors, C. J. Hawker, *Angew. Chem. Int. Ed.* **2012**, *51*, 8850–8853.

[20]   N. J. Treat, B. P. Fors, J. W. Kramer, M. Christianson, C.-Y. Chiu, J. R. de Alaniz, C. J. Hawker, *ACS Macro Lett.* **2014**, *3*, 580–584.

[21]   Boyer and coworkers have elegantly extended the use of photoredox catalysts for photomediated RAFT. (a) Xu, J.; Jung, K.; Atme, A.; Shanmugam, S.; Boyer, C. *J. Am. Chem. Soc.* **2014**, *136*, 5508. (b) Xu, J.; Jung, K.; Boyer, C. *Macromolecules* **2014**, *47*, 4217. (c) Shanmugam, S.; Xu, J.; Boyer, C. *Macromolecules* **2014**, *47*, 4930. (d) Xu, J.; Jung, K.; Corrigan, N. A.; Boyer, C. *Chem. Sci.* **2014**, *5,* 3568.

[22]   J. E. Poelma, B. P. Fors, G. F. Meyers, J. W. Kramer, C. J. Hawker, *Angew. Chem. Int. Ed.* **2013**, *52*, 6844–6848.

[23]   C. K. Prier, D. A. Rankic, D. W. C. MacMillan, *Chem. Rev.* **2013**, 130319115037002.

[24]   D. A. Nicewicz, T. M. Nguyen, *ACS Catal.* **2014**, *4*, 355–360.

[25]   S. P. Pitre, C. D. McTiernan, H. Ismaili, J. C. Scaiano, *J. Am. Chem. Soc.* **2013**, *135*, 13286–13289.

[26]   **2001**, 1–10.

[27]   D. Maiti, B. P. Fors, J. L. Henderson, Y. Nakamura, S. L. Buchwald, *Chem. Sci.* **2010**, *2*, 57.

[28]   Excited state reduction potential estimated using oxidation potential of ground state catalyst and photoluminescence emission maximum (see SI).

[29]   F. A. Plamper, A. Schmalz, A. H. E. Müller, *J. Am. Chem. Soc.* **2007**, *129*, 14538–14539.

[30]   Y.-Z. You, D. S. Manickam, Q.-H. Zhou, D. Oupický, *Journal of Controlled Release* **2007**, *122*, 217–225.

[31]   X.-S. Wang, T. E. Dykstra, M. R. Salvador, I. Manners, G. D. Scholes, M. A. Winnik, *J. Am. Chem. Soc.* **2004**, *126*, 7784–7785.

[32]   V. L. Cunningham, *United States Patent* **1978**, 1–5.

[33]   J. D. Nguyen, E. M. D'Amato, J. M. R. Narayanam, C. R. J. Stephenson, *Nature Chem* **2012**, *4*, 854–859.

VI. Supporting Information

A. General Reagent Information

All polymerizations were carried out under an argon atmosphere. Methyl methacrylate, benzyl methacrylate, methyl acrylate, and styrene were purchased from Sigma-Aldrich and passed through a plug of basic alumina before use. Anhydrous *N,N*-dimethylacetamide, Methylene blue, Eosin Y, ethyl α-bromophenylacetate, ethyl α-bromoisobutyrate, 10-methyl phenothiazine, phenothiazine, RuPhos, *N,N,N',N',N''*-pentamethyldiethylenetriamine, 4,4'-dinonyl-2,2'-dipyridyl, *fac*-[Ir(ppy)$_3$], sodium *tert*-butoxide, and anhydrous chlorobenzene were purchased from Sigma-Aldrich and used as received. CuBr was purchased from Sigma-Aldrich and purified by washing with acetic acid, followed by ethanol and ether. The resulting CuBr was kept under an argon atmosphere. RuPhos Precatalyst was purchased from Strem Chemicals Inc.

B. General Analytical Information

Nuclear magnetic resonance spectra were recorded on a Varian 400 MHz, a Varian 500 MHz, or a Varian 600 MHz instrument. All ^{1}H NMR experiments are reported in δ units, parts per million (ppm), and were measured relative to the signals for residual chloroform (7.26 ppm) in the deuterated solvent, unless otherwise stated. All ^{13}C NMR spectra are reported in ppm relative to deuterochloroform (77.23 ppm), unless otherwise stated, and all were obtained with ^{1}H decoupling. Gel permeation chromatography (GPC) was performed on a Waters 2695 separation module with a Waters 2414 refractive index detector eluting with 0.25 wt% triethylamine/chloroform and a Waters Alliance HPLC System, 2695 separation module with combined Wyatt DAWN HELEOS-II light scattering/Wyatt Optilab rEX refractive index detectors. Number average molecular weights (M_n) and weight average molecular weights (M_w) were calculated relative to linear polystyrene standards or from light scattering. Reported molecular weights (M_n) were calculated using ^{1}H NMR by comparing the integration of the ethyl protons on the initiating chain end to the polymer side chain peaks unless otherwise noted. Mass spectrometry was performed on a Micromass QTOF2 Quadrupole/Time-of-Flight Tandem instrument. Cyclic voltammetry was carried out on a VMP Multichannel Potentiostat with EC lab software.

C. Light Source

LED strips (380 nm) were bought from elemental led (see www.elementalled.com) and used as shown below (Figure S3.1). Note: 380 nm LED strips are no longer sold by elemental led, but may be bought from LEDlightinghut.com. Reactions were placed next to the 380 nm lights under vigorous stirring while cooling with compressed air. The light intensity was measured to be 0.65 mW/cm^2.
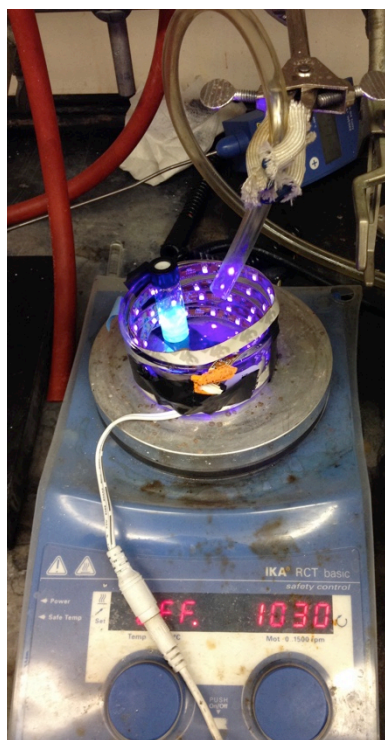
Figure S3.1 Representative configuration comprising reaction vial surrounded by 380 nm LEDs with a tube blowing compressed air for cooling.

D. Synthesis of 10-phenylphenothiazine (PTH)
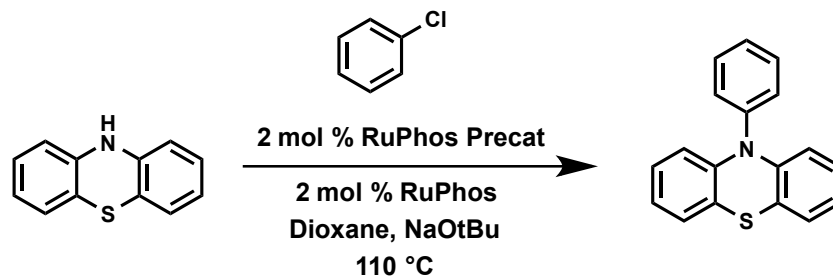
The following procedure was adopted from Maiti et al.[1] To a vial armed with a magnetic stir bar was added NaOtBu (134 mg, 1.4 mmol), phenothiazine (199 mg, 1 mmol), RuPhos Precat (14 mg, 0.02 mmol, 2 mol %), and RuPhos (8 mg, 0.02 mmol, 2 mol %). The vial was evacuated and backfilled 3x with argon before adding dry Dioxane (1 mL). Lastly, anhydrous chlorobenzene (143 mL, 1.4 mmol) was added. The vial was then placed in an oil bath at 110 °C with stirring for 5 h. The vial was then cooled to room temperature, diluted with CH_2Cl_2, washed with water, brine, dried with Mg_2SO_4, and purified using column chromatography (5 % EtOAc/Hexanes). The product was dried under reduced pressure to yield 267 mg of a white solid (97 % yield). ^{1}H NMR (600 MHz, $CDCl_3$) δ: 7.60 (t, J = 8 Hz, 2H), 7.49 (t, J = 8 Hz, 1H), 7.40 (d, J = 7 Hz, 2H), 7.02 (d, J = 8 Hz, 2H), 6.86-6.79 (m, 4 H), 6.20 (d, J = 8 Hz, 2 H) ppm. ^{13}C NMR (151 MHz, $CDCl_3$) δ: 144.5, 141.2, 131.1, 130.9, 128.4, 127.0, 126.9, 122.7, 120.4, 116.3 ppm. HRMS $C_{18}H_{13}NS$ Found 275.0753, Calc'd 275.0769.

E. Determination of Excited State Reduction Potential
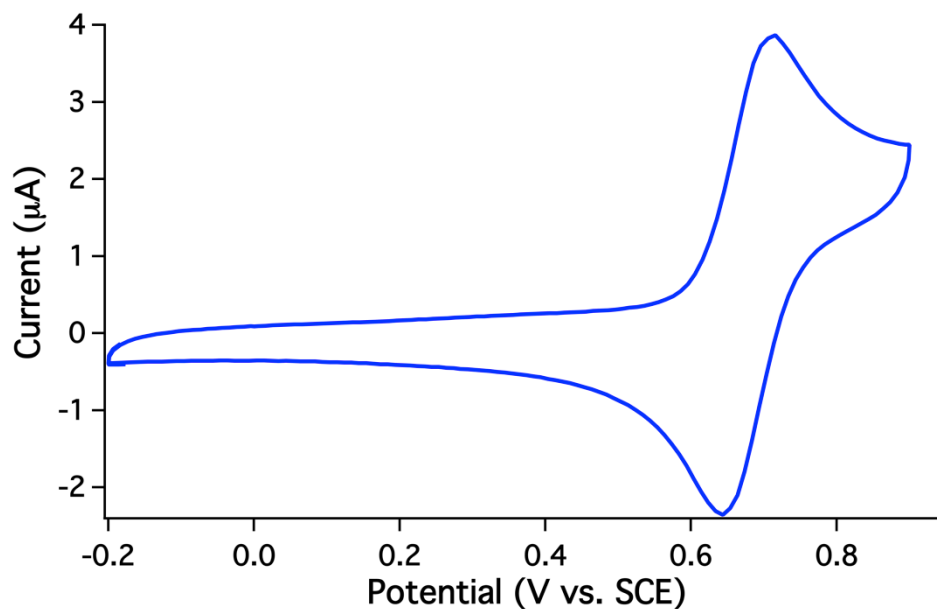
Figure S3.2 Cyclic voltammetry of 10-phenylphenothiazine showing reversible oxidation peak at +0.68 V

Cyclic voltammetry was conducted using 0.1 M tetrabutylammonium hexafluorophosphate as electrolyte in acetonitrile at 25 °C with a standard calomel reference electrode (E^{ox} = +0.68 V vs. SCE).
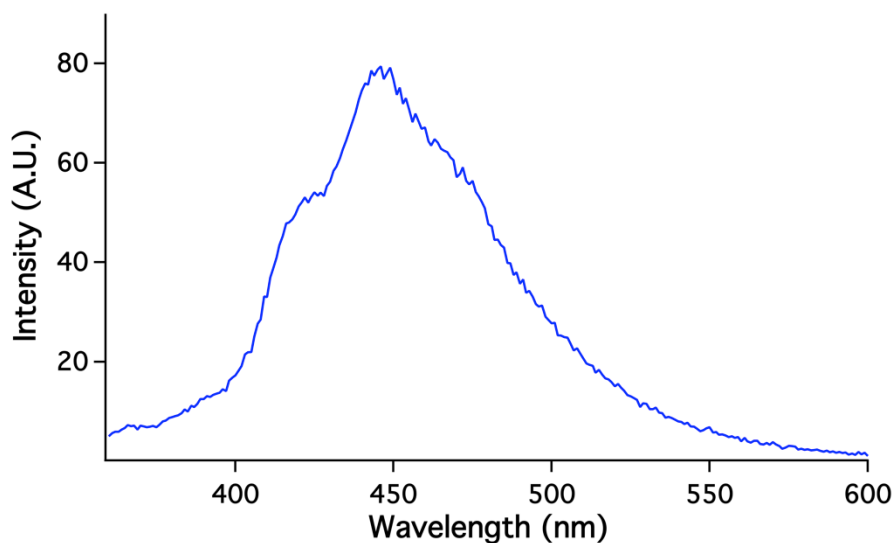
Figure S3.3 Fluorescence spectrum of PTH in *N,N*-dimethylacetamide (0.17 mM)

107

A Varian Cary Eclipse Fluorescence Spectrophotometer was used to measure fluorescence. Photoluminescence max was estimated to be 445 nm (see Figure S3.3). Using the photoluminescence λ_{max} and E^{ox}, the excited state reduction potential was estimated for **PTH** ($E_{1/2}$ (PTH$^{+\cdot}$/PTH*) = -2.1 V) using the following equations:

$$E_{1/2}\,(\text{PTH}^{+\cdot}/\text{PTH*}) = E^{ox} - E_{0,0}$$

$$\text{where } E_{0,0} = hc\,/\,\lambda_{max} = 1240\text{ nm}\,/\,\lambda_{max}.$$

F. General Procedure for Table 3.1
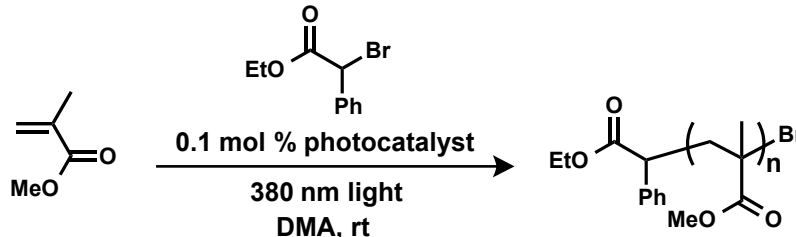
A vial equipped with a magnetic stir bar and fitted with a teflon screw cap septum was charged with methyl methacrylate (401 μL, 3.75 mmol), photocatalyst (0.1 mol %) and *N,N*-dimethylacetamide (1 mL). The reaction mixture was degassed with three freeze-pump-thaw cycles. The vial was then backfilled with argon and ethyl α-bromophenylacetate (0.0188 - 0.075 mmol) was injected via syringe. The reaction was vigorously stirred in front of 380 nm LEDs or 50 W compact fluorescent bulbs while cooling with compressed air to maintain ambient temperature. The reaction was allowed to proceed to ca. 50 % conversion of MMA

as monitored by ^{1}H NMR. An aliquot was taken and analyzed using ^{1}H NMR to give the molecular weight (M_n) and GPC to give the molecular weight distribution (M_w/M_n) of the polymer.

G. Procedure for Figure 3.3

A vial equipped with a magnetic stir bar and fitted with a teflon screw cap septum was charged with benzyl methacrylate (762 µL, 4.5 mmol), **PTH** (1.2 mg, 0.1 mol %) and *N,N*-dimethylacetamide (1.2 mL). The reaction mixture was degassed with three freeze-pump-thaw cycles. The vial was then backfilled with argon, and brought into a glove box containing a nitrogen atmosphere. It was then covered with aluminum foil, and ethyl α-bromophenylacetate (6.9 µL, 0.0396 mmol) was injected via syringe. After 1 h of stirring in the dark, an aliquot was taken. The reaction was then vigorously stirred in front of 380 nm LEDs while cooling with a portable fan to maintain ambient temperature. After 0.5 h and 1 h stirring under light, aliquots were taken from the reaction mixture and, at 1 h, the reaction was immediately wrapped in aluminum foil. This process was repeated multiple times (see Figure 3.3). Conversion was monitored by ^{1}H NMR. The molecular weight was calculated using ^{1}H NMR. GPC was used to obtain the molecular weight distribution (M_w/M_n) of the polymer.

Table S3.1 Polymerization of Dimethylaminoethyl methacrylate[a]

Entry	Photocatalyst	conversion	M_n (exp) [g/mol]	M_w / M_n
1[b]	Ir(ppy)$_3$	50%	9,400	3.69
2	PTH	73%	8,800	1.11
3	PTH	33%	5,100	1.26

[a] Reaction conditions: DMAEMA (1 equiv.), photocatalyst (0.001 equiv.), **1** (0.01 equiv), DMA (2.7 M of DMAEMA) at room temperature with irradiation from 380 nm LEDs for 0.5-2 h (M_n = number average molecular weight; M_w = weight average molecular weight). M_n and M_w / M_n determined using size exclusion chromatography (SEC) or ^{1}H NMR; [b] used 0.00005 equiv. Ir(ppy)$_3$ (0.005 mol % relative to monomer)

H. General Procedure for Table S3.1

A vial equipped with a magnetic stir bar and fitted with a teflon screw cap septum was charged with 2-(dimethylamino)ethyl methacrylate (634 μL, 3.75 mmol), photocatalyst (0.1 mol % **PTH** or 0.005 mol % Ir(ppy)$_3$) and *N,N*-dimethylacetamide (1 mL). The reaction mixture was degassed with three freeze-pump-thaw cycles. The vial was then backfilled with argon and ethyl α-bromophenylacetate (10.3 μL, 0.059 mmol) was injected via syringe. The reaction was vigorously stirred in front of 380 nm LEDs and conversion monitored by ^{1}H NMR. An aliquot was taken and analyzed using ^{1}H NMR to give the molecular weight (M_n) and GPC to give the molecular weight distribution (M_w/M_n) of the polymer.

I. Procedure for Figure 3.4

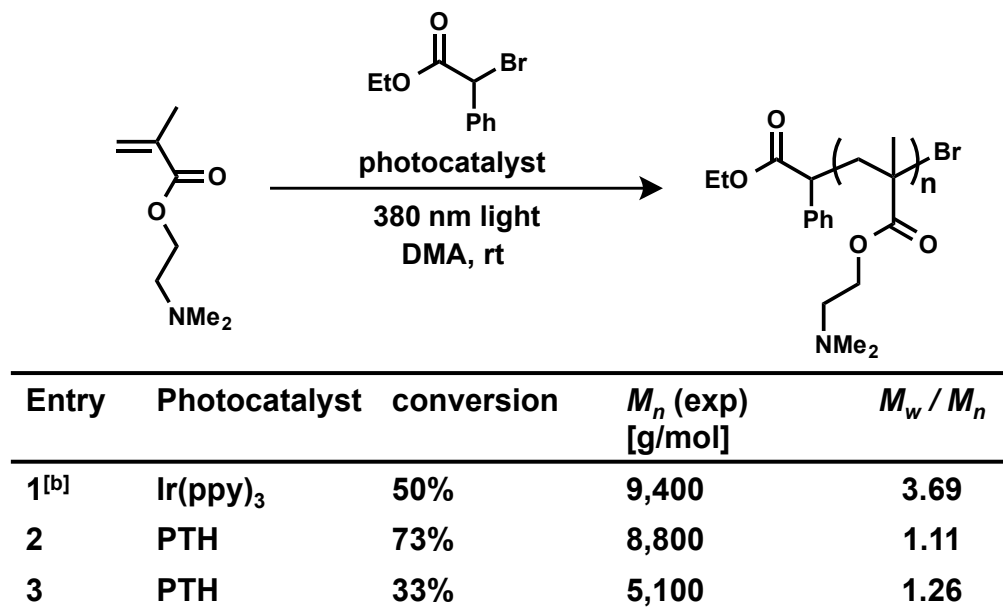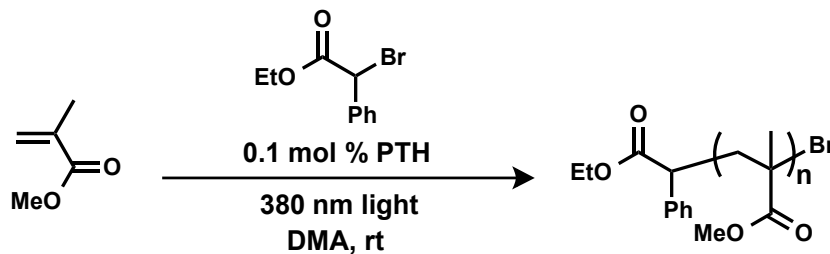
Figure 3.4a: Poly(methyl methacrylate) by metal-free ATRP: A vial equipped with a magnetic stir bar and fitted with a teflon screw cap septum was charged with methyl methacrylate (401 mL, 3.75 mmol), **PTH** (1 mg, 0.1 mol %) and N,N-dimethylacetamide (1 mL). The reaction mixture was degassed with three freeze-pump-thaw cycles. The vial was then backfilled with argon and ethyl α-bromophenylacetate (13.1 μL, 0.075 mmol) was injected via syringe. The reaction was stirred in front of 380 nm LEDs while cooling with compressed air to maintain ambient temperature. The reaction was stirred in front of the light for 7.5 h (25 % conv.) and then put into the dark by wrapping it in aluminum foil. A syringe wrapped in aluminum foil was used to transfer the reaction mixture in the dark into a stirring solution of hexanes (15 mL, also wrapped in aluminum foil). The solution was put into a freezer (ca. -40 °C) for 1 h. The white precipitate was decanted, and re-dissolved in dichloromethane before precipitating again into hexanes to yield 24 mg of a white powder. M_n = 1,400 g/mol, M_w/M_n = 1.08.
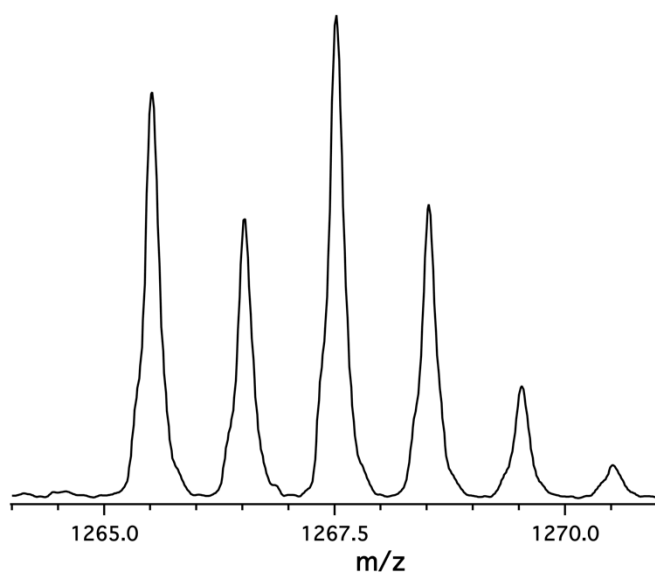
Figure S3.4 Zoomed in spectrum of ESI-MS for PMMA prepared using metal-free

ATRP indicating bromine isotopic splitting pattern
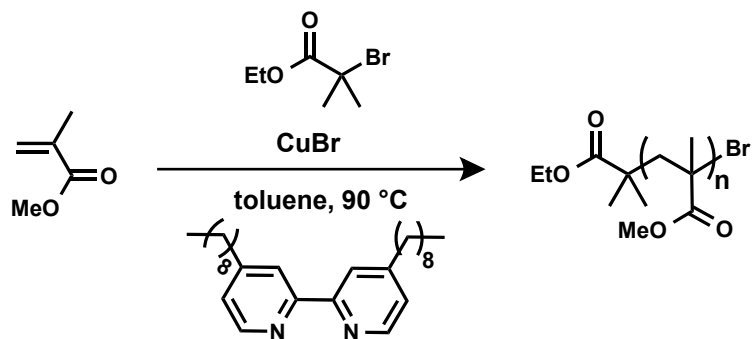
Figure 3.4b: Poly(methyl methacrylate) by traditional Cu-catalyzed ATRP: A vial

equipped with a magnetic stir bar and fitted with a teflon screw cap septum was charged

with methyl methacrylate (401 mL, 3.75 mmol), **CuBr** (5.4 mg, 0.0375 mmol), 4,4'-

dinonyl-2,2'-dipyridyl (30.7 mg, 0.075 mmol), and toluene (400 mL, 50 vol %). The

reaction mixture was degassed with three freeze-pump-thaw cycles. The vial was then

backfilled with argon and ethyl α-bromoisobutyrate (11 µL, 0.075 mmol) was injected via

syringe. The reaction was stirred in a 90 °C oil bath for 2 h (38 % conv.), cooled to room temperature, diluted with dichloromethane, and filtered through an alumina plug before precipitating into 20 mL of hexanes. The precipitate was filtered, and redissolved in dichloromethane before re-precipitating into hexanes to obtain 5 mg of a white powder. M_n = 1,100 g/mol, M_w/M_n = 1.20.

Figure 3.4c: Poly(methyl methacrylate) A vial equipped with a magnetic stir bar and fitted with a rubber septum was charged with methyl methacrylate (2.4 mL, 22.5 mmol), **PTH** (6.2 mg, 0.1 mol %) and *N,N*-dimethylacetamide (6 mL). The reaction mixture was degassed with three freeze-pump-thaw cycles. The vial was then backfilled with argon and ethyl α-bromophenylacetate (39 μL, 0.225 mmol) was injected via syringe. The reaction was stirred in front of 380 nm LEDs while cooling with compressed air to maintain ambient temperature. The reaction was stirred in front of the light for 2.5 h (14 % conv.) and then put into the dark by wrapping it in aluminum foil. A syringe wrapped in aluminum foil was used to transfer the reaction mixture in the dark into a stirring solution of hexanes (50 mL, also wrapped in aluminum foil). The white precipitate was decanted, and re-dissolved in dichloromethane before precipitating again into hexanes to yield 197 mg of a white powder. M_n = 2,600 g/mol, M_w/M_n = 1.33.

J. Procedure for Figure 3.5

Poly(methyl methacrylate) (P1) A vial equipped with a magnetic stir bar and fitted with a rubber septum was charged with methyl methacrylate (2.4 mL, 22.5 mmol), **PTH** (6.2 mg, 0.1 mol %) and *N,N*-dimethylacetamide (6 mL). The reaction mixture was degassed with three freeze-pump-thaw cycles. The vial was then backfilled with argon and ethyl α-bromophenylacetate (39 μL, 0.225 mmol) was injected via syringe. The reaction was stirred in front of 380 nm LEDs while cooling with compressed air to maintain ambient temperature. The reaction was stirred in front of the light for 5.5 h (36 % conv.) under a positive pressure of Argon and then put into the dark by wrapping it in aluminum foil. A syringe wrapped in aluminum foil was used to transfer the reaction mixture in the dark into a stirring solution of hexanes (80 mL, also wrapped in aluminum foil). The precipitate was decanted, and re-dissolved in dichloromethane before precipitating again into hexanes to yield 677 mg of a white powder. M_n = 5,100 g/mol, M_w/M_n = 1.12.

BnO

0.1 mol % PTH

380 nm light
DMA, rt

EtO

Br

n

Ph

MeO O

O

P1

EtO

O

Br

n m

Ph CO₂Me CO₂Bn

Poly(methyl methacrylate)-*b*-(benzyl methacrylate) A vial equipped with a magnetic stir bar and fitted with a teflon screw cap septum was charged with benzyl methacrylate (630 μL, 3.72 mmol), **PTH** (1 mg, 0.1 mol %) and *N,N*-dimethylacetamide (500 μL). In another flask, 500 μL of *N,N*-dimethylacetamide was added to the poly(methyl methacrylate) macroinitiator (**P1**, 83.5 mg, 0.0164 mmol). Both reaction mixtures were degassed with three freeze-pump-thaw cycles. Using a syringe, the monomer and catalyst were then transferred to the flask containing macroinitiator. The reaction was stirred in front of 380 nm LEDs while cooling with compressed air to maintain ambient temperature. After 5 h (61 % conv.), the reaction was stopped by opening to air and precipitated into methanol (20 mL). The precipitate was filtered and redissolved in CH_2Cl_2 before reprecipitating into methanol. The product was analyzed by ^1H NMR and GPC. (yield: 189 mg of a white powder) GPC M_n = 25,900 g/mol, M_w/M_n = 1.31.
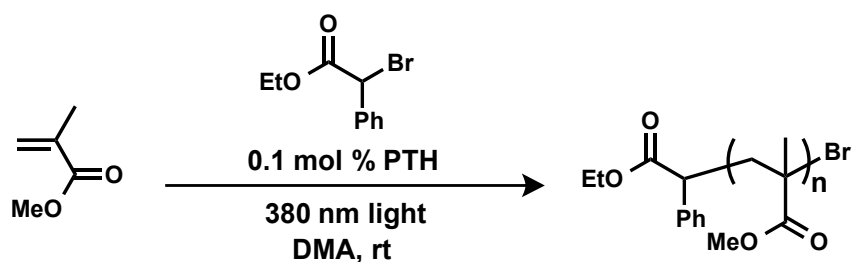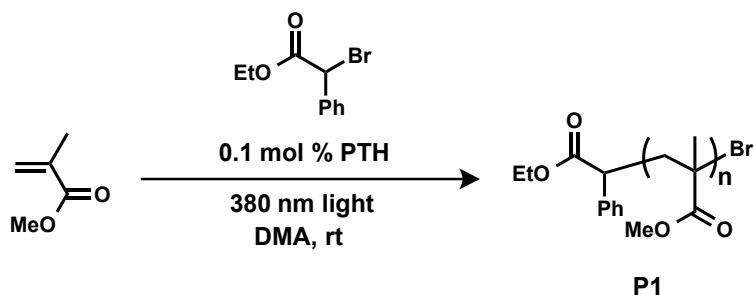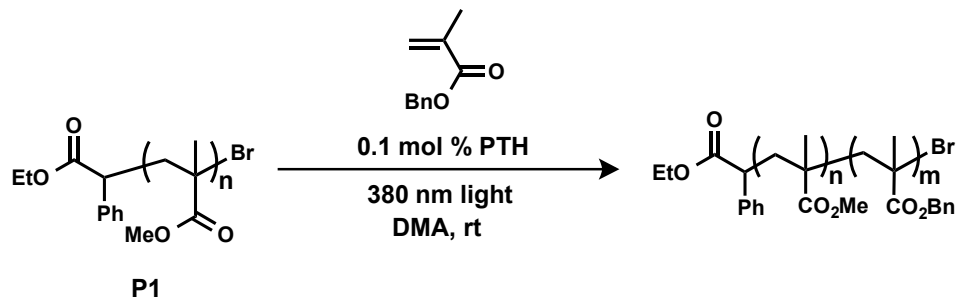
P2

Poly(methyl methacrylate) (P2) A vial equipped with a magnetic stir bar and fitted with a rubber septum was charged with methyl methacrylate (2.4 mL, 22.5 mmol), **PTH** (6.2 mg, 0.1 mol %) and *N,N*-dimethylacetamide (6 mL). The reaction mixture was degassed with three freeze-pump-thaw cycles. The vial was then backfilled with argon and ethyl α-bromophenylacetate (39 μL, 0.225 mmol) was injected via syringe. The reaction was stirred in front of 380 nm LEDs while cooling with compressed air to maintain ambient temperature. The reaction was stirred in front of the light for 5 h (25 % conv.) and then put into the dark by wrapping it in aluminum foil. A syringe wrapped in aluminum foil was used to transfer the reaction mixture in the dark into a stirring solution of hexanes (50 mL, also wrapped in aluminum foil). The white precipitate was decanted, and re-dissolved in dichloromethane before precipitating again into hexanes to yield 655 mg of a white powder. M_n = 3,600 g/mol, M_w/M_n = 1.19.
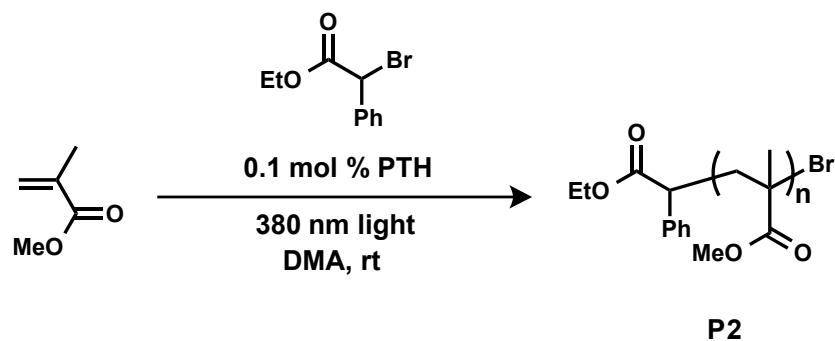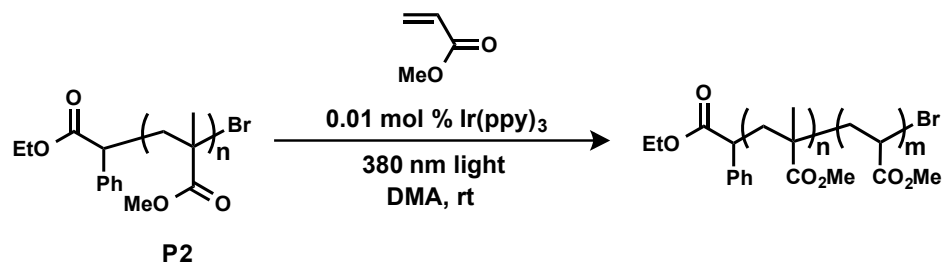
P2

Poly(methyl methacrylate)-*b*-(methyl acrylate) A vial equipped with a magnetic stir bar and fitted with a teflon screw cap septum was charged with methyl acrylate (511 µL, 5.67 mmol), *fac*-Ir(ppy)₃ (0.37 mg, 0.01 mol %) and *N,N*-dimethylacetamide (600 µL). In another flask, 500 µL of *N,N*-dimethylacetamide was added to the poly(methyl methacrylate) macroinitiator (**P2**, 30.7 mg, 0.0122 mmol). Both reaction mixtures were degassed with three freeze-pump-thaw cycles. Using a syringe, the monomer and catalyst were then transferred to the flask containing macroinitiator. The reaction was stirred in front of 380 nm LEDs while cooling with compressed air to maintain ambient temperature. After 4 h (45 % conv.) the reaction was stopped by opening to air and precipitated into MeOH (20 mL). A yellow oil crashed out, and the solution was placed into a freezer (ca. -20 °C) for 1 h. The methanol was then decanted off and the residual solvent was removed under reduced pressure. This process was repeated once to yield 47 mg of a yellow oil. M_n =20,200 g/mol, M_w/M_n = 1.24.

EtO–C(=O)...Me...Br **P2** (Ph, MeO, CO) + CH₂=CH–Ph $\xrightarrow[\text{toluene, 110 °C}]{\text{CuBr, PMDETA}}$ EtO–C(=O)...Me...Br (Ph, CO₂Me, Ph)
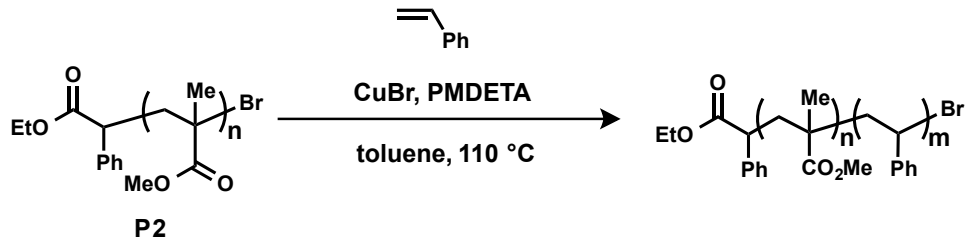
P2

Poly(methyl methacrylate)-*b*-(styrene) A vial equipped with a magnetic stir bar and fitted with a Teflon screw cap septum was charged with Styrene (290 mL, 2.52 mmol), poly(methyl methacrylate) macroinitiator (**P2**, 46 mg, 0.0131 mmol), *N,N,N',N',N''*-pentamethyldiethylenetriamine (PMDETA, 5.5 mL, 0.0262 mmol), and toluene (290 mL). The reaction mixture was degassed with three freeze-pump-thaw cycles. The vial was then backfilled with argon and frozen before adding CuBr (1.9 mg, 0.0131 mmol). After adding CuBr, the vial was evacuated-backfilled with Argon 2 times. The mixture was thawed, and placed into an oil bath heated to 110 °C for 4.5 h (17 % conv.). The reaction was cooled, opened to air, diluted with dichloromethane, and filtered through alumina before precipitating into hexanes. The precipitate was filtered, redissolved in dichloromethane, and re-precipitated into hexanes to yield 10 mg of a white powder. NMR M_n = 11,100 g/mol, GPC M_n = 4,800 g/mol, M_w/M_n = 1.06.
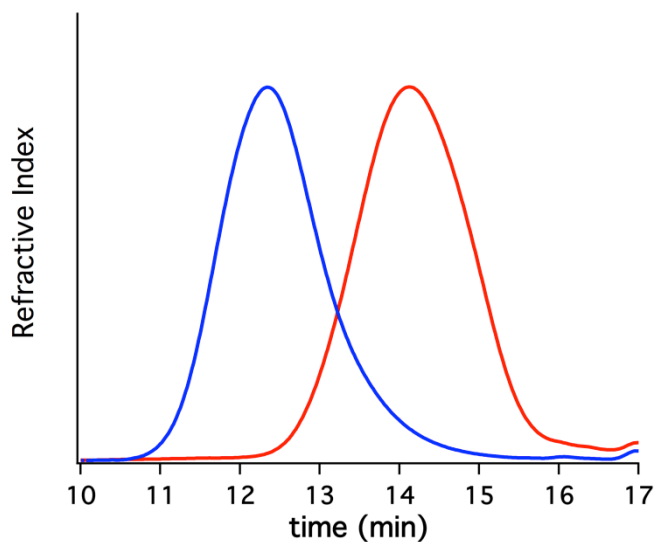
Figure S3.5 Block copolymerization SEC traces with PMMA (red trace, starting homopolymer) blocked with PBnMA (blue trace, block copolymer), using ethyl α-bromoisobutyrate as initiator.

K. Procedure for Figure S3.5
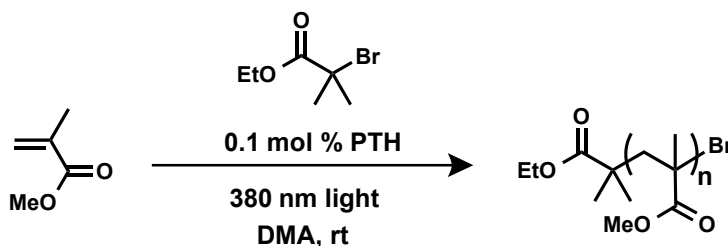
Poly(methyl methacrylate) A vial equipped with a magnetic stir bar and fitted with a rubber septum was charged with methyl methacrylate (2.4 mL, 22.5 mmol), **PTH** (6.2 mg, 0.1 mol %) and *N,N*-dimethylacetamide (6 mL). The reaction mixture was degassed with three freeze-pump-thaw cycles.   The vial was then backfilled with argon and ethyl α-bromoisobutyrate (33 μL, 0.225 mmol) was injected via syringe. The reaction was stirred in front of 380 nm LEDs while cooling with compressed air to maintain ambient temperature. The reaction was stirred in front of the light for 5 h (19 % conv.) and then put into the dark

by wrapping it in aluminum foil. A syringe wrapped in aluminum foil was used to transfer the reaction mixture in the dark into a stirring solution of hexanes (50 mL, also wrapped in aluminum foil). The white precipitate was decanted, and re-dissolved in dichloromethane before precipitating again into hexanes to yield 273 mg of a white powder. M_n = 5,300 g/mol, M_w/M_n = 1.30.
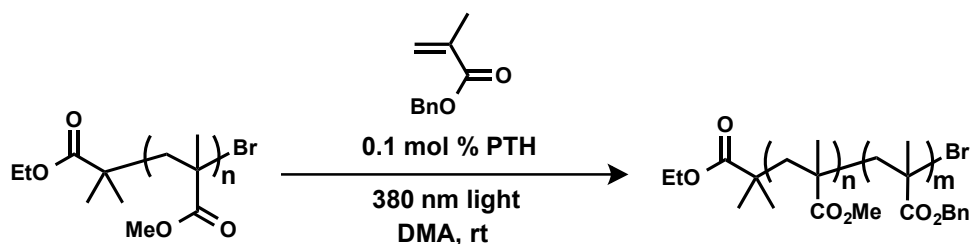
Poly(methyl methacrylate)-*b*-(benzyl methacrylate) A vial equipped with a magnetic stir bar and fitted with a teflon screw cap septum was charged with benzyl methacrylate (461 µL, 2.62 mmol), **PTH** (0.7 mg, 0.1 mol %) and *N,N*-dimethylacetamide (350 µL). In another flask, 350 µL of *N,N*-dimethylacetamide was added to the poly(methyl methacrylate) macroinitiator (57.6 mg, 0.0115 mmol). Both reaction mixtures were degassed with three freeze-pump-thaw cycles. Using a syringe, the monomer and catalyst were then transferred to the flask containing macroinitiator. The reaction was stirred in front of 380 nm LEDs while cooling with compressed air to maintain ambient temperature. After 6 h (62 % conv.) the reaction was stopped by opening to air and precipitated into methanol (20 mL). The precipitate was filtered and redissolved in CH_2Cl_2 before reprecipitating into methanol. The product was analyzed by ^{1}H NMR and GPC. (yield: 163 mg of a white powder) M_n = 27,900 g/mol, M_w/M_n = 1.28.
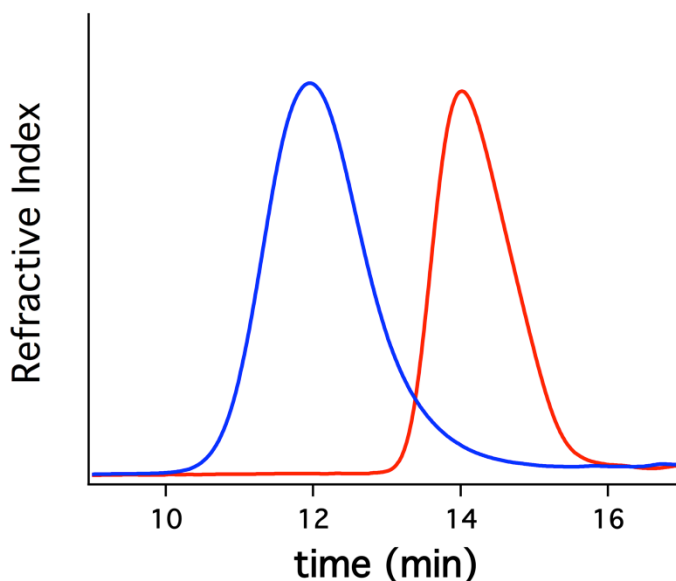
Figure S3.6 Block copolymerization SEC traces with PMMA (red trace, starting homopolymer) synthesized with traditional ATRP conditions and chain extending with BnMA (blue trace, block copolymer), using metal-free photomediated ATRP conditions.

L. Procedure for Figure S3.6
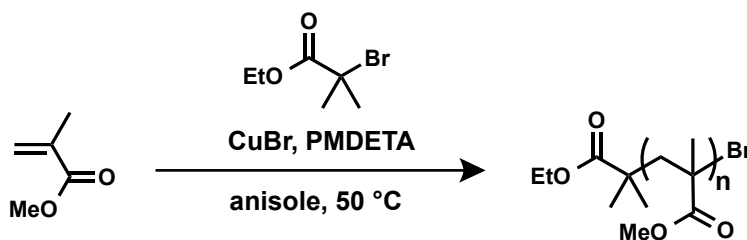
Poly(methyl methacrylate) A vial equipped with a magnetic stir bar and fitted with a teflon screw cap septum was charged with methyl methacrylate (2.4 mL, 22.5 mmol), **CuBr** (16.1 mg, 0.113 mmol), *N,N,N',N',N''*-pentamethyldiethylenetriamine (47 mL, 0.225 mmol), and anisole (2.4 mL, 50 vol %). The reaction mixture was degassed with three freeze-pump-thaw cycles. The vial was then backfilled with argon and degassed ethyl α-

bromoisobutyrate (33 μL, 0.225 mmol) was injected via syringe. The reaction was stirred in a 50 °C oil bath for 2.5 h (27 % conv.), cooled to room temperature, diluted with dichloromethane, and filtered through an alumina plug before precipitating into 100 mL of hexanes. The precipitate was filtered, and redissolved in dichloromethane before re-precipitating into hexanes to obtain 363 mg of a white powder. M_n = 3,000 g/mol, M_w/M_n = 1.13.
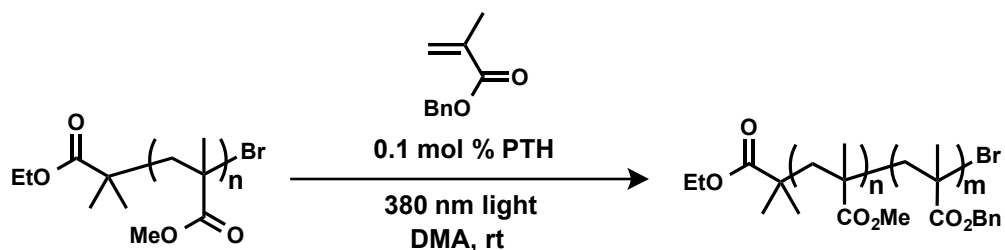
Poly(methyl methacrylate)-b-(benzyl methacrylate) A vial equipped with a magnetic stir bar and fitted with a teflon screw cap septum was charged with benzyl methacrylate (590 μL, 3.48 mmol), **PTH** (1 mg, 0.1 mol %) and N,N-dimethylacetamide (500 μL). In another flask, 500 μL of N,N-dimethylacetamide was added to the poly(methyl methacrylate) macroinitiator (46 mg, 0.0153 mmol). Both reaction mixtures were degassed with three freeze-pump-thaw cycles. Using a syringe, the monomer and catalyst were then transferred to the flask containing macroinitiator. The reaction was stirred in front of 380 nm LEDs while cooling with compressed air to maintain ambient temperature. After 4 h (57 % conv.) the reaction was stopped by opening to air and precipitated into methanol (20 mL). The precipitate was filtered and redissolved in CH$_2$Cl$_2$ before reprecipitating into methanol. The

product was analyzed by ^{1}H NMR and GPC. (yield: 230 mg of a white powder) GPC $M_n =$ 34,500 g/mol, $M_w/M_n = 1.33$.
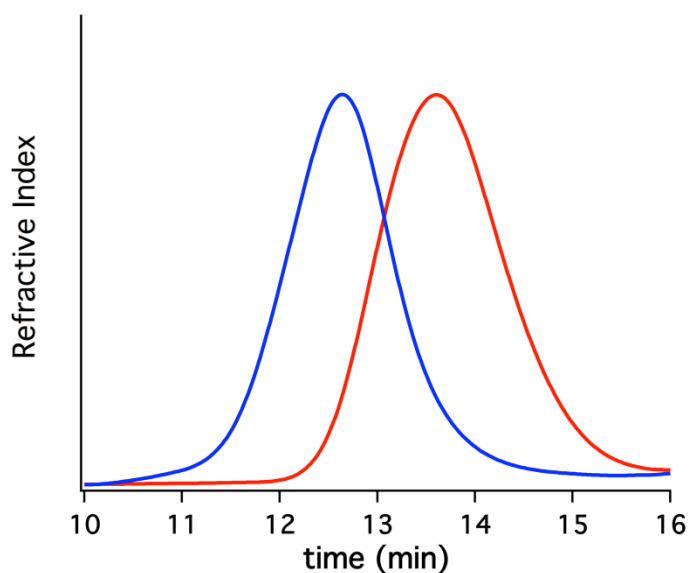
Figure S3.7 SEC traces with P*t*-BuMA (red trace, starting homopolymer) synthesized using metal-free ATRP conditions and chain extending with DMAEMA (blue trace, block copolymer), using metal-free photomediated ATRP conditions.

M. Procedure for Figure S3.7
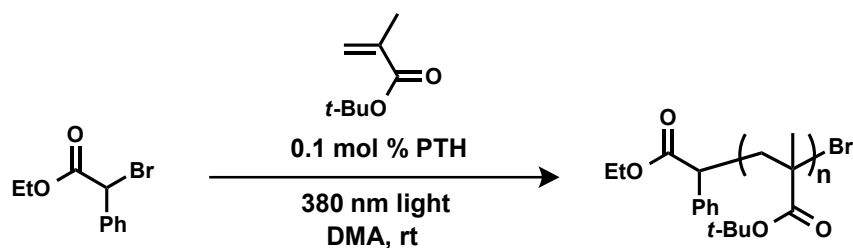
Poly(*t*-butyl methacrylate) A vial equipped with a magnetic stir bar and fitted with a rubber septum was charged with *t*-butyl methacrylate (5 mL, 30.8 mmol), **PTH** (8.5 mg, 0.1 mol %) and dimethylacetamide (8.2 mL). The reaction mixture was degassed with three freeze-pump-thaw cycles.   The vial was then backfilled with argon and ethyl α-bromophenylacetate (38 µL, 0.218 mmol) was injected via syringe. The reaction was stirred in front of 380 nm LEDs while cooling with compressed air to maintain ambient temperature. The reaction was stirred in front of the light for 6 h (41 % conv.) and then put into the dark by wrapping it in aluminum foil. A syringe wrapped in aluminum foil was used to transfer the reaction mixture in the dark into a stirring solution of methanol:water (9:1) (250 mL, also wrapped in aluminum foil). The white precipitate was decanted, and re-dissolved in dichloromethane before precipitating again into methanol:water (9:1) to yield 1.7 g of a white powder. M_n = 8,900 g/mol, M_w/M_n = 1.24.
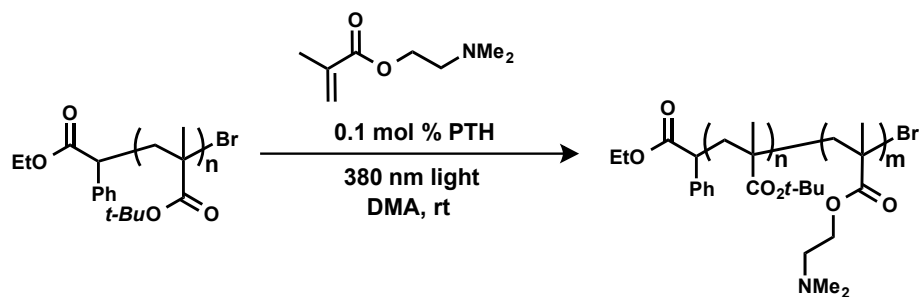
Poly(*t*-butyl methacrylate)-*b*-(dimethylaminoethyl methacrylate) A vial equipped with a magnetic stir bar and fitted with a teflon screw cap septum was charged with dimethylaminoethyl methacrylate (1.76 mL, 10.45 mmol), **PTH** (2.9 mg, 0.1 mol %) and N,N-dimethylacetamide (1 mL). In another flask, 4.6 mL of N,N-dimethylacetamide was added to the poly(*t*-butyl methacrylate) macroinitiator (1.45 g, 0.164 mmol). Both reaction

mixtures were degassed with three freeze-pump-thaw cycles. Using a syringe, the monomer and catalyst were then transferred to the flask containing macroinitiator. The reaction was stirred in front of 380 nm LEDs while cooling with compressed air to maintain ambient temperature. After 30 min (36 % conv.) the reaction was stopped by opening to air and precipitated into cold hexanes (200 mL). A white oil crashed out, the hexanes was then decanted off and the oil was redissolved in dichloromethane before precipitating into cold hexanes again. Yield: 800 mg of a white oil. M_n =22,500 g/mol, M_w/M_n = 1.30.

Table S3.2 Methacrylate/Acrylate Copolymerizations[a]
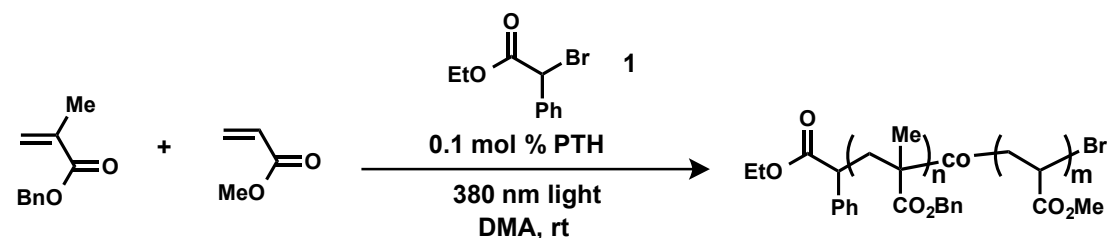
Entry	BnMA:MA [mol %]	% MA incorp [mol %]	Time	conversion	M_n (exp) [g/mol]	M_n (theo) [g/mol]	M_w / M_n
1	90:10	6	6 h	71 % BnMA 49 % MA	15,300	13,800	1.28
2	50:50	32	4.5 h	69 % BnMA 36 % MA	12,800	11,600	1.25
3	10:90	82	3 h	86 % BnMA 47 % MA	12,100	10,800	1.45

[a] Reaction conditions: BnMA & MA (1 equiv.), photocatalyst (0.001 equiv.), **1** (0.0047-0.008 equiv), DMA at room temperature with irradiation from 380 nm LEDs for 3-6 h (M_n = number average molecular weight; M_w = weight average molecular weight). M_n and M_w / M_n determined using size exclusion chromatography (SEC) or ^{1}H NMR. % MA incorporation determined using ^{1}H NMR.

N. General Procedure for Table S3.2

A vial equipped with a magnetic stir bar and fitted with a teflon screw cap septum was charged with benzyl methacrylate and methyl acrylate (combined 3.75 mmol), **PTH** (1 mg, 0.1 mol %) and *N,N*-dimethylacetamide (1 mL). The reaction mixture was degassed with three freeze-pump-thaw cycles. The vial was then backfilled with argon and ethyl α-bromophenylacetate (0.0178 - 0.0315 mmol) was injected via syringe. The reaction was vigorously stirred in front of 380 nm LEDs while cooling with compressed air to maintain ambient temperature. An aliquot was taken and analyzed using ^{1}H NMR to give the conversion. Molecular weight (M_n) and molecular weight distribution (M_w/M_n) of the polymer were determined by SEC and ^{1}H NMR.

Table S3.3 Methacrylate/Styrene Copolymerizations[a]
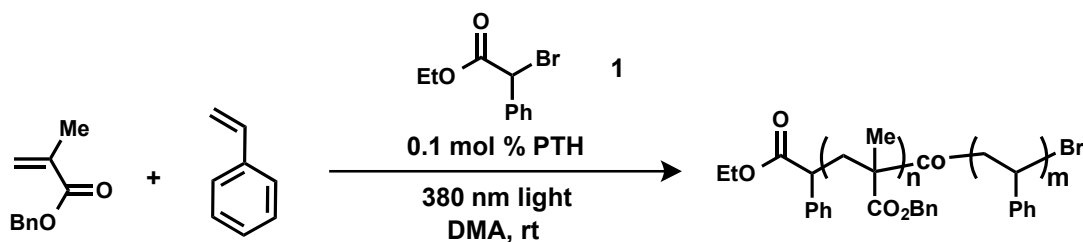
Entry	BnMA:Styrene [mol %]	% Styrene incorp [mol %]	Time	conversion	M_n (exp) [g/mol]	M_n (theo) [g/mol]	M_w / M_n
1	99:1	3	5 h	68 % BnMA 85 % Styrene	9,800	13,600	1.39
2	95:5	11	5 h	34 % BnMA 88 % Styrene	5,900	7,100	1.41
3	90:10	19	7 h	45 % BnMA 78 % Styrene	15,200	9,400	1.65

126

[a] Reaction conditions: BnMA & Styrene (1 equiv.), photocatalyst (0.001 equiv.), **1** (0.00847-0.00877 equiv), DMA at room temperature with irradiation from 380 nm LEDs for 5-7 h (M_n = number average molecular weight; M_w = weight average molecular weight). M_n and M_w / M_n determined using size exclusion chromatography (SEC). % Styrene incorporation determined using ^{1}H NMR.

O. General Procedure for Table S3.3

A vial equipped with a magnetic stir bar and fitted with a teflon screw cap septum was charged with benzyl methacrylate and styrene (combined 3.75 mmol), **PTH** (1 mg, 0.1 mol %) and *N,N*-dimethylacetamide (1 mL). The reaction mixture was degassed with three freeze-pump-thaw cycles. The vial was then backfilled with argon and ethyl α-bromophenylacetate (0.0318 - 0.0329 mmol) was injected via syringe. The reaction was vigorously stirred in front of 380 nm LEDs while cooling with compressed air to maintain ambient temperature. An aliquot was taken and analyzed using ^{1}H NMR to give the conversion. Molecular weight (M_n) and molecular weight distribution (M_w/M_n) of the polymer were determined by SEC.

P. Supplementary References

[1]   D. Maiti, B. P. Fors, J. L. Henderson, Y. Nakamura, S. L. Buchwald, *Chem. Sci.* **2010**, *2*, 57.

4. A Highly Reducing Metal-free Photoredox Catalyst: Design and Application in Radical Dehalogenations

I. Abstract

The synthetic utility of photoredox catalysis for a wide variety of chemical transformations has seen exponential growth in recent years. However, current state-of-the-art photocatalysts, typically based on transition metals, have inherent limitations, including high cost, sensitivity to air, and restricted scope. Herein, we report 10-phenylphenothiazine (PTH) as an inexpensive, highly reducing metal-free photocatalyst for the reduction of of carbon-halogen bonds via the trapping of reactive carbon-centered radical intermediates with a mild hydrogen atom donor. Using this catalyst, reductive dehalogenations were carried out on a variety of iodo, bromo, and chloro substrates with excellent yields at room temperature in the presence of air. This new class of organic photocatalyst opens doors to previously inaccessible photoredox transformations.
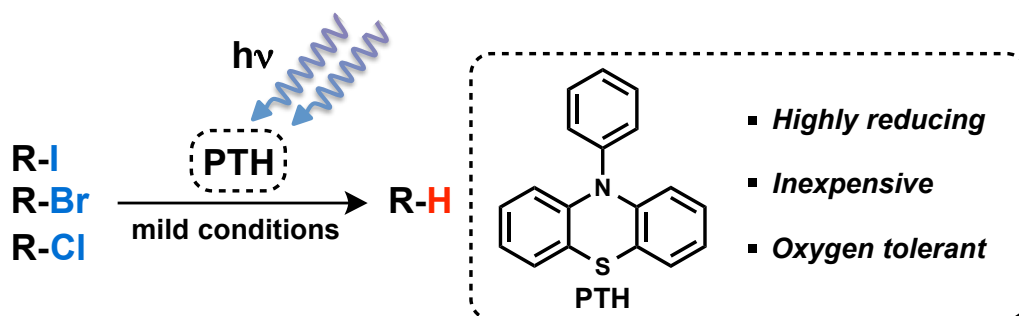
Figure 4.1 Phenyl phenothiazine as a highly reducing organic photocatalyst

II. Introduction

In recent years, photoredox chemistry has enabled the development of a wide variety of synthetic transformations.[1-6] These methods are based on photocatalysts which, upon absorption of light, enter either a highly reducing or oxidizing excited state capable of facilitating redox-based transformations. In particular, the reduction of activated carbon-halide (C–X) bonds has generated wide interest, largely because of the broad synthetic utility of resulting carbon-centered radical intermediates.[7-37] One example includes subsequent trapping of these intermediates with a mild H-atom source to achieve radical dehalogenations.[1-10] In this case, the power of using a photoredox approach is that it offers a more efficient and safer alternative to traditional dehalogenation protocols involving metal-halogen exchange,[2,4,6,11-40] stoichiometric tin hydride,[41] and various other highly toxic reagents.[42-44] However, despite the notable advantages of photoredox catalysis,[1,3] a number of major challenges still exist. This includes the use of catalysts based on rare-earth transition metals such as Ru and Ir, which have inherent limitations due to the cost of the catalyst itself (~$1/mg for Ir(ppy)$_3$),[45] as well as the high cost associated with the removal of trace metals from the desired products - critical for applications extending from pharmaceuticals to micro-electronics. In addition, although a assortment of activated carbon-halogen bonds have been accessed using these catalysts,[1] higher energy unactivated halides are a significantly more challenging task, with only unactivated iodides being explored to date.[4,19] To this end, a more affordable gold-based photocatalyst has been developed,[37] and although offering a broader substrate scope than Ir and Ru, the disadvantages of metal-based systems remain. To overcome

this, the use of an organic perylene diimide (PDI)-based photocatalyst was recently reported, and while providing a valuable metal-free alternative, it requires elevated temperatures to achieve a scope limited to activated aryl-halides.[18] In this context, we envisioned the development of a highly reducing, inexpensive, metal-free photocatalyst that could offer access to unactivated carbon-halogen substrates under markedly mild conditions (Figure 4.2). Our group previously employed 10-phenylphenothiazine (PTH) as a metal-free catalyst for photomediated atom transfer radical polymerizations (ATRP).[28] In this system, PTH acts as a photoreductant in a similar manner to Ir(ppy)$_3$ with a reduction potential ($E^*_{1/2}$ = - 2.1 V vs. SCE) significantly higher than Ir(ppy)$_3$ ($E^*_{1/2}$ = -1.7 V vs. SCE). Based on our interest in metal-free ATRP, we envisioned that the same radical based processes enabled by PTH could also be used to access a variety of carbon-centered radical intermediates that could be used for subsequent synthetic transformations, such as the reduction of carbon-halogen bonds. Highlighted by its use of mild reagents, a readily accessible light source, as well its high degree of oxygen tolerance, we believe this novel metal-free system will serve as a platform for expanding the synthetic utility of photoredox chemistry.
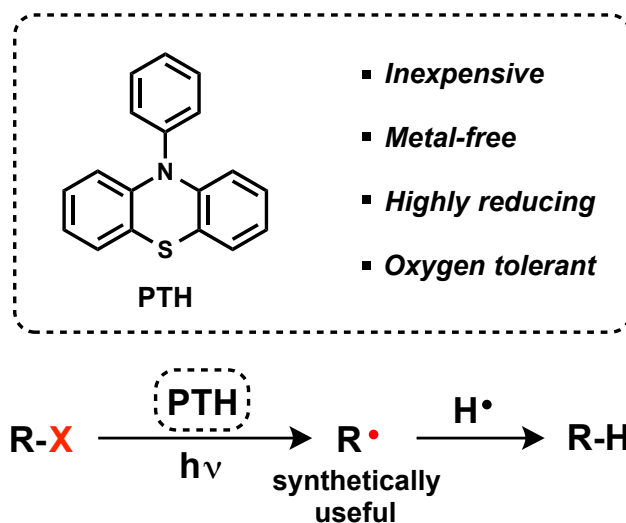
Figure 4.2 Characteristics and application of 10-phenylphenothiazine (PTH)

III. Results and Discussion

A. Optimization of Conditions
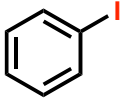
The initial test system chosen for investigation was the reduction of iodobenzene, employing PTH as the photocatalyst. After optimization (Tables S4.1-3), quantitative reduction of iodobenzene (**1**) to benzene (98% yield) could be achieved in 1 h under 380 nm LED irradiation (Table 4.1) in the presence of 5 mol % PTH and 5 equivalents each of tributylamine and formic acid. Significantly, the reaction was compatible with a range of solvents as well as amine sources leading to similar yields and reaction rates. Notably, quantitative reduction could also be achieved with catalyst loadings as low as 0.5 mol %, albeit at a slower reaction rate. Full conversion of iodobenzene was also observed using visible light sources, such as 25 W CFLs and blue LEDs (Table S4.1 and S4.3). This demonstrates the inherent flexibility of PTH as a photoredox catalyst platform, which was further enhanced by the use of a
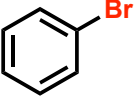
commercially available N-Me phenothiazine derivative for the successful reduction of iodobenzene (see SI).

B. Comparison with Other Photocatalyst Systems

To further validate PTH as an organic photoredox catalyst, a series of control experiments in the absence of light, catalyst, or amine were conducted. In each case, no reaction was observed (Table S4.2). We next sought to compare the performance of PTH with widely used photoredox systems such as Ir(ppy)$_3$, as well as the metal-free PDI based system, and in both cases we observed higher reactivity.[46] For example, only 23% yield was obtained after 1 h for the reduction of iodobenzene using Ir(ppy)$_3$ when compared to the quantitative reduction observed for PTH (Table 4.1). It is worth noting that the 380 nm LED light source matches the excitation maximum of Ir(ppy)$_3$ (378 nm),[1] while the absorption spectrum of PTH has only a small shoulder at this wavelength (Figure S4.2). However, this does not appear to hinder reactivity.[47] Similarly, comparison of the perylene diimide-based photocatalyst also showed no reduction of iodobenzene after 1 h.

Table 4.1 Comparison of reduction capabilities of Ir(ppy)$_3$, PDI with PTH for the reduction of iodo- and bromobenzene.[a]

$$\text{Ph-X} \xrightarrow[\text{h}\nu,\ \textbf{conditions}]{\textbf{Photocatalyst}} \text{Ph-H}$$

Substrate	Time	Photocatalyst	Yield
(iodobenzene) **1**	1 h	PTH	98 %
		Ir(ppy)$_3$	23 %
		PDI	0 %
(bromobenzene) **2**	72 h	PTH	85 %
		Ir(ppy)$_3$	0 %
		PDI	0 %

[a] Reaction conditions using PTH and Ir(ppy)$_3$: Iodobenzene or bromobenzene (1 equiv.), PTH (5 mol %) or Ir(ppy)$_3$ (1 mol %)[29], formic acid (5 equiv.) and tributylamine (5 equiv.), acetonitrile (0.08 M of substrate) at room temperature with irradiation from 380 nm LEDs (1.8 μW/cm^2). ^{1}H NMR yield determined using 1,3,5-trimethoxybenzene or 1,2,4,5-tetramethylbenzene as internal standard. Reaction conditions using PDI: Iodobenzene or bromobenzene (1 equiv.), PDI (5 mol %), triethylamine (8 equiv), dimethylformamide (0.02 M of substrate) at 40 °C with irradiation from 465 nm LEDs (5 μW/cm^2). ^{1}H NMR yield determined using 1,2,4,5-tetramethylbenzene as internal standard.

This increased performance encouraged the examination of PTH as a photocatalyst for the reduction of more challenging unactivated brominated substrates, which to date has not been accessible using a metal-free photoredox system. Significantly, bromobenzene was successfully reduced in 85% yield after 72 h (by comparison, no reaction was observed after 72 h using Ir(ppy)$_3$ or PDI). These results nicely

demonstrate that the higher-energy excited state reduction potential of PTH is necessary to activate more challenging C-Br bonds (E^{red} = -2.05 to -2.57).[48,49]

C. Substrate Scope

With a general protocol in place, we next set out to demonstrate the broad applicability of PTH as a photoredox catalyst for a library of aryl iodides and bromides including unactivated, or even deactivated derivatives (Table 4.2). Excellent activity was observed with compounds containing electron-rich substituents such as **3**, **4**, and **5** being dehalogenated in high yields. Additionally, achieving high fidelity reduction of substrates **4**, **6**, and **7** exemplifies the mildness of our protocol and its tolerance across many different functional groups including acids, phenolic alcohols, and amines. A range of more challenging aryl bromides (**8–18**) were then examined, with near quantitative conversion to the dehalogenated product being observed for substrates **8–11**. Extension to more synthetically interesting heterocyclic aryl bromides was also observed with excellent yields being obtained for brominated pyridine (**13**), benzothiazole (**14**), and thiophene systems (**15–16**). Particularly noteworthy was the application of PTH for the reduction of primary alkyl bromides (**17–18**), and even electron-rich aryl bromides such as 4-bromophenol (**12**) could be reduced in modest yield. The use of a single set of conditions for the reduction of both unactivated alkyl and aryl bromides further demonstrates the synthetic versatility of PTH-based organic photoredox catalysts.

Encouraged by the successful reduction of a wide range of C–Br bonds, we next explored the reduction of activated aryl chlorides. After 24 h of irradiation time in the presence of PTH, benzyl 4-chlorobenzoate was successfully reduced, with the desired

product being isolated in 83% yield. A variety of other activated aryl chlorides were subsequently examined with methyl benzoate, benzonitrile, and benzoic acid derivatives undergoing dechlorination in good yields (**20–22**).

Table 4.2 Substrate scope of reductive dehalogenations of iodides, bromides, and chlorides using PTH.[a]
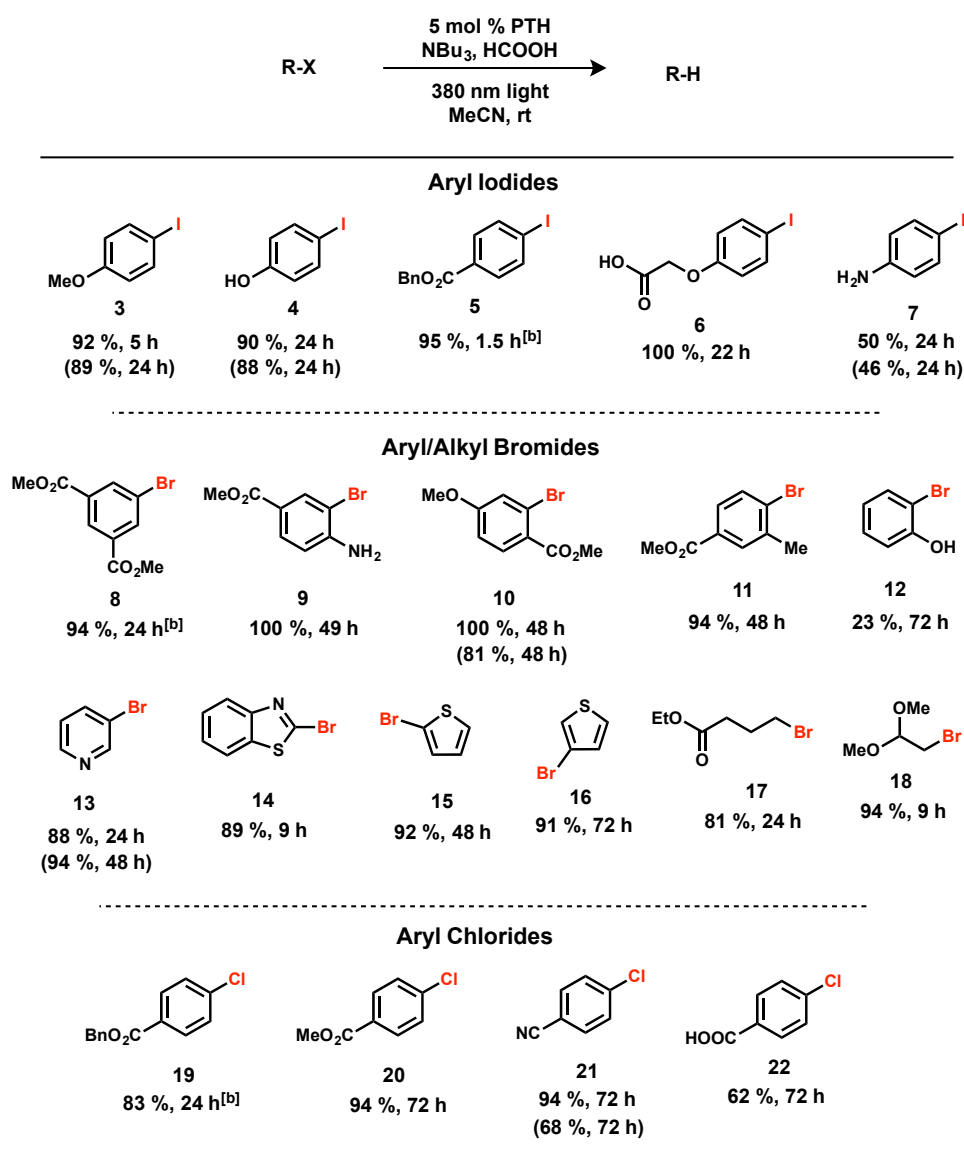
[a] Reaction conditions: substrate (1 equiv.), PTH (5 mol %), formic acid (5 equiv.), tributylamine (5 equiv.), acetonitrile (0.08 M of substrate) at room temperature with irradiation from 380 nm LEDs. ^{1}H NMR yield determined using 1,3,5-trimethoxybenzene or

1,2,4,5-tetramethylbenzene as internal standard. Yields and times in parentheses were run in the presence of air. [b] isolated yields run on 0.2 mmol scale

D. Physical Organic Insights

With a broad substrate scope and the potential of the new metal-free photoredox system established, the physical organic properties of PTH were studied in more detail, in particular the high excited state reduction potential, which is given by:

$$E^*_{1/2} = E_{1/2}{}^{ox} - hc / \lambda_{max}$$

where $E^*_{1/2}$ is the excited state reduction potential, $E_{1/2}{}^{ox}$ is the ground state oxidation potential, h is Planck's constant, c is the speed of light and λ_{max} is the photoluminescence maximum.[50] While the ground state oxidation potential of PTH ($E_{1/2}{}^{ox} = 0.68$ vs. SCE)[28] is only slightly lower than that of Ir(ppy)$_3$ ($E_{1/2}{}^{ox} = 0.77$ V vs. SCE), the photoluminescence maximum of PTH ($\lambda_{max} = 445$ nm, Figure 4.3a) is significantly lower (Ir(ppy)$_3$ $\lambda_{max} = 500$ nm).[1] In contrast to the triplet emission of Ir(ppy)$_3$, the higher-energy emission from PTH is the result of fluorescence from the singlet state, with an observed lifetime of < 3 ns (see SI). To confirm, we also measured the energy of the triplet excited state of PTH at 77 K, and under these conditions it more closely resembled the energy of Ir(ppy)$_3$ (Figure 4.3a, $\lambda_{max} = 510$ nm). This implies that the higher excited state energy of the singlet is the primary origin of PTH's ability to access higher energy bonds.
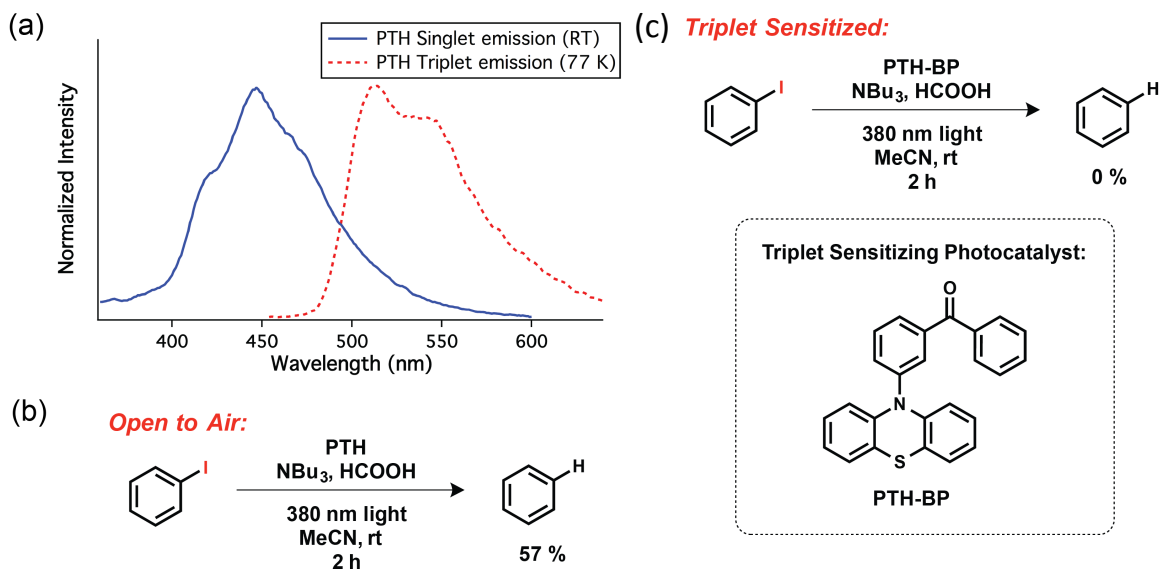
Figure 4.3 Evidence for singlet state catalysis using PTH (a) Photoluminescence spectroscopy at room temperature and 77 K suggests no triplet emission at RT (b) Reaction in the presence of air (triplet quencher) proceeds, (c) while no reaction is observed when using a triplet sensitizing catalyst (PTH-BP).

To probe whether the singlet excited state of PTH could be responsible for the catalysis observed in this system, the reduction of iodobenzene was performed open to air, with oxygen acting as a potent triplet quencher.[38] Under these conditions where triplet pathways should be inhibited, a 57% yield was observed after 2 h, suggesting that the singlet state may be the primary mode of catalysis. Further, the reaction proceeded to 90% yield within 15 h, and while a decrease in reaction rate was observed, it is noteworthy that any reactivity occurs. For traditional photoredox systems, complete inhibition is expected as the reaction pathway involves a triplet state mechanism. To further examine this feature, control experiments were conducted using reported optimized conditions for Ir(ppy)₃,[4] but in the presence of

137

air and, as expected, no reduction of iodobenzene was observed after 2 h. Encouraged by these results, we further examined the oxygen tolerance of PTH with a range of substrates from each aryl halide class. Significantly, a variety of aryl iodides (**3-4**, **7**), bromides (**10**, **13**), and chlorides (**21**) could be successfully dehalogenated in moderate to good yields (Table 4.2), confirming the oxygen tolerance of PTH. It should be noted that the yields were similar in all cases to those obtained for carefully deoxygenated solutions.

After observing reactivity in the presence of air, this phenomenon was further probed by the use of a designer PTH-based catalyst functionalized with a triplet-sensitizing moiety (Figure 4.3c). In this case, conjugation with benzophenone, a well-known triplet sensitizer, was expected to greatly increase the rate of intersystem crossing leading to an exclusive, triplet state excited catalyst, PTH-BP. To confirm that the catalyst acted as hypothesized, photoluminescence spectra were obtained both at room temperature and 77 K with luminescence observed only at 77 K, indicating that fluorescence from the singlet state had been completely deactivated (Figures S4.5-6). Moreover, the use of PTH-BP for the reduction of iodobenzene under our optimized conditions resulted in no reaction, suggesting that the singlet state is necessary for catalysis.[51]

E. Oxygen Tolerant Scale-up

To illustrate the scalability and practical nature of PTH as an organic photoredox catalyst, we conducted a multigram-scale reaction in the presence of air (Scheme 4.1). We envisioned a very rudimentary experimental set-up with no precautions taken to ensure an air or moisture-free environment. Using a 125-mL Erlenmeyer flask, we

138

scaled up our general conditions by 7000% using benzyl 4-iodobenzoate as our substrate, and observed 98% conversion by ^{1}H NMR after 20 h. It is noteworthy that although the penetration of light through the solution is a common issue in the scale-up of photochemical reactions, we obtained the dehalogenated product in a reasonable amount of time. The reaction was purified by column chromatography to yield the desired product in 87% yield (1.5 g), thoroughly demonstrating both the scalability and robustness of our protocol. Further, during the course of purification, we were also able to isolate the PTH catalyst used in the reaction. This catalyst sample was then re-used in the reduction of **5**, and quantitative conversion to the desired product was observed after 1.5 h. This again highlights the simplicity and inherent robustness of PTH.

Scheme 4.1 Preparative scale reaction conducted without degassing to demonstrate modularity and scalability of PTH-based reactions.

Gram-scale reaction in air:
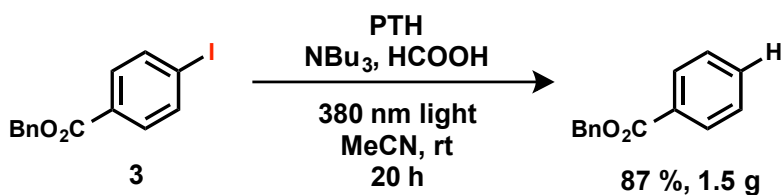
F. Mechanistic Studies

Based on the results above, the following tentative mechanism is proposed (Scheme 4.2a). Upon absorption of a photon, PTH enters a highly reducing excited state, and an oxidative quenching cycle ensues. The excited catalyst preferentially reduces the carbon-halide bond, subsequently transforming the catalyst to an oxidized radical

cation before it is reduced back to its native form by tributylamine, completing the catalytic cycle. To provide evidence that the reaction indeed occurs through the oxidative quenching cycle rather than reductive quenching, Stern-Volmer studies were conducted (Figures S4.3-4). Upon addition of iodobenzene to a solution of PTH, dynamic quenching was observed, implying a reductive process between the catalyst and substrate. However, when tributylamine was added to a solution of PTH, no decrease in photoluminescence occurred. This suggests that PTH is not reduced by tributylamine, and further supports that the oxidative quenching cycle is the mechanism for generation of the reactive intermediate. Furthermore, evidence of a radical-based mechanism was obtained via a successful radical cyclization of substrate **23** (Scheme 4.2b). The desired product **24** was obtained in 47% yield, providing strong support that the reaction proceeds through a radical process, as well as preliminary evidence illustrating that radical intermediates generated by PTH can be used for carbon–carbon bond forming reactions.

Scheme 4.2 Proposed mechanism for metal-free photoredox radical dehalogenations and radical cyclization
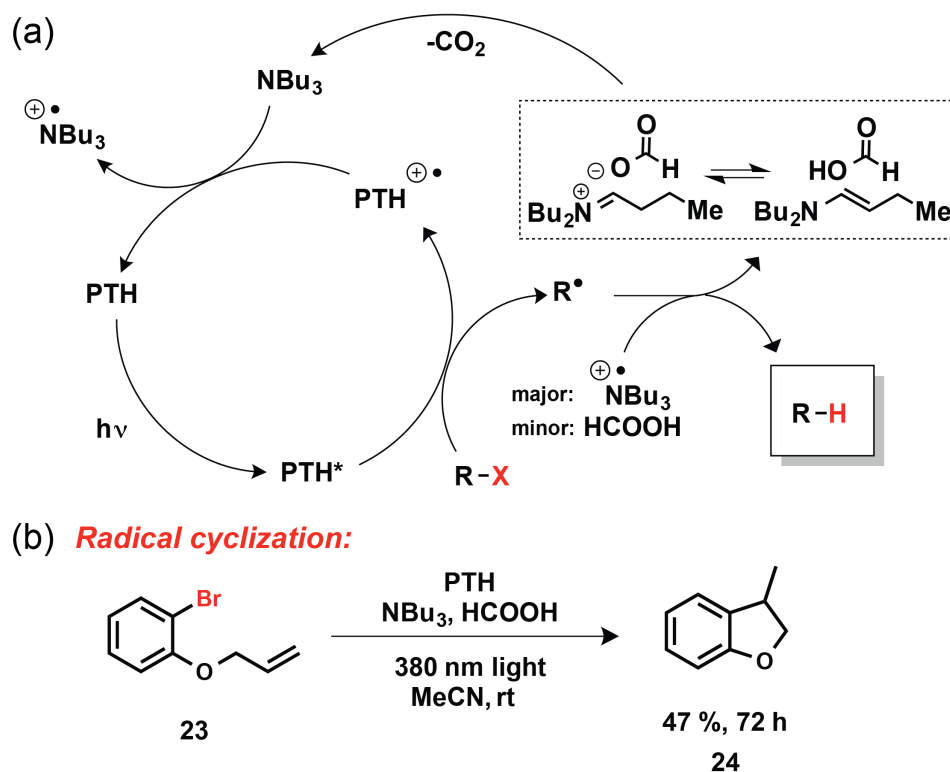
Lastly, we were also interested in understanding subsequent steps of our proposed mechanism, including the primary source of the H-atom that eventually replaces the halide. In a series of control experiments with PTH/iodobenzene in the presence and absence of formic acid and tributylamine, reactions conducted with no formic acid, a reagent generally reported as a source for H-atom abstraction,[2,4] did indeed lead to reduction of iodobenzene (71% yield after 2 h). This suggests that in addition to serving as reducing agent for the oxidized PTH, tributylamine may be the primary source of labile H-atoms. Subsequent experiments with deuterated NEt_3, HCOOH, and MeCN provided additional evidence suggesting that the tertiary amine served as

the primary H-atom source (see SI). Interestingly, when deuterated formic acid was employed under the optimized conditions, deuterium incorporation was observed in the alpha and beta positions of tributylamine, indicating that an imine/enamine equilibrium was occurring in the reaction, with the formic acid playing a role in regenerating the amine (Figures S4.7-8).

IV. Conclusions

In conclusion, we have developed a highly reducing, organic photocatalytic platform with broad applicability for the generation of carbon-centered radical intermediates on route to efficient dehalogenations of aryl and alkyl iodides, bromide and chlorides. In addition to offering an inexpensive, metal-free alternative to current halide reductions, this approach is highlighted by a robust and facile nature with high yields being obtained even in the presence of air. Moreover, in contrast to classic photoredox systems, preliminary evidence suggests that PTH is primarily operating through the singlet state. Further investigations regarding the mechanism, the tunability of the catalyst, selectivity for polyhalogenated systems and its potential to open doors for new organic bond forming transformations are currently in progress.

V. Acknowledgements

VI. References

[1] C. K. Prier, D. A. Rankic, D. W. C. MacMillan, *Chem. Rev.* **2013**, *113*, 5322–5363.

[2] J. M. R. Narayanam, J. W. Tucker, C. R. J. Stephenson, *J. Am. Chem. Soc.* **2009**, *131*, 8756–8757.

[3] D. M. Schultz, T. P. Yoon, *Science* **2014**, *343*, 1239176–1239176.

[4] J. D. Nguyen, E. M. D'Amato, J. M. R. Narayanam, C. R. J. Stephenson, *Nature Chem* **2012**, *4*, 854–859.

[5] J. M. R. Narayanam, C. R. J. Stephenson, *Chem. Soc. Rev.* **2010**, *40*, 102.

[6] S. M. Senaweera, A. Singh, J. D. Weaver, *J. Am. Chem. Soc.* **2014**, *136*, 3002–3005.

[7] J. Xuan, W.-J. Xiao, *Angew. Chem. Int. Ed.* **2012**, *51*, 6828–6838.

[8] C. D. McTiernan, S. P. Pitre, H. Ismaili, J. C. Scaiano, *Adv. Synth. Catal.* **2014**, *356*, 2819–2824.

[9] D. A. Nicewicz, T. M. Nguyen, *ACS Catal.* **2014**, *4*, 355–360.

[10] M. J. Schnermann, L. E. Overman, *Angew. Chem. Int. Ed.* **2012**, *51*, 9576–9580.

[11] S. Fukuzumi, K. Hironaka, T. Tanaka, *J. Am. Chem. Soc.* **1983**, *105*, 4722–4727.

[12] W. F. Bailey, J. J. Patricia, *Journal of organometallic chemistry* **1988**, *352*, 1–46.

[13] S. Fukuzumi, S. Mochizuki, T. Tanaka, *Journal of Physical Chemistry* **1990**, *94*, 722–726.

[14] P. Knochel, W. Dohle, N. Gommermann, F. F. Kneisel, F. Kopp, T. Korn, I. Sapountzis, V. A. Vu, *Angew. Chem. Int. Ed.* **2003**, *42*, 4302–4320.

[15]   D. A. Nicewicz, D. W. C. Macmillan, *Science* **2008**, *322*, 77–80.

[16]   D. A. Nagib, M. E. Scott, D. W. C. MacMillan, *J. Am. Chem. Soc.* **2009**, *131*, 10875–10877.

[17]   H.-W. Shih, M. N. Vander Wal, R. L. Grange, D. W. C. MacMillan, *J. Am. Chem. Soc.* **2010**, *132*, 13600–13603.

[18]   I. Ghosh, T. Ghosh, J. I. Bardagi, B. Konig, *Science* **2014**, *346*, 725–728.

[19]   H. Kim, C. Lee, *Angew. Chem. Int. Ed.* **2012**, *51*, 12303–12306.

[20]   C.-J. Wallentin, J. D. Nguyen, P. Finkbeiner, C. R. J. Stephenson, *J. Am. Chem. Soc.* **2012**, *134*, 8875–8884.

[21]   J. D. Nguyen, J. W. Tucker, M. D. Konieczynska, C. R. J. Stephenson, *J. Am. Chem. Soc.* **2011**, *133*, 4160–4163.

[22]   N. Iqbal, S. Choi, E. Ko, E. J. Cho, *Tetrahedron Letters* **2012**, *53*, 2005–2008.

[23]   E. J. Cho, C. Yu, N. Iqbal, S. Park, *Chem. Commun.* **2014**, *50*, 12884–12887.

[24]   J. W. Tucker, C. R. J. Stephenson, *Org. Lett.* **2011**, *13*, 5468–5471.

[25]   J. W. Tucker, J. M. R. Narayanam, S. W. Krabbe, C. R. J. Stephenson, *Org. Lett.* **2010**, *12*, 368–371.

[26]   L. Furst, B. S. Matsuura, J. M. R. Narayanam, J. W. Tucker, C. R. J. Stephenson, *Org. Lett.* **2010**, *12*, 3104–3107.

[27]   B. P. Fors, C. J. Hawker, *Angew. Chem. Int. Ed.* **2012**, *51*, 8850–8853.

[28]   N. J. Treat, H. Sprafke, J. W. Kramer, P. G. Clark, B. E. Barton, J. Read de Alaniz, B. P. Fors, C. J. Hawker, *J. Am. Chem. Soc.* **2014**, *136*, 16096–16101.

[29]   G. M. Miyake, J. C. Theriot, *Macromolecules* **2014**, *47*, 8255–8261.

[30]   J. W. Tucker, J. D. Nguyen, J. M. R. Narayanam, S. W. Krabbe, C. R. J.

Stephenson, *Chem. Commun.* **2010**, *46*, 4985.

[31]   M. Neumann, S. Füldner, B. König, K. Zeitler, *Angew. Chem. Int. Ed. Engl.* **2011**, *50*, 951–954.

[32]   M. Cherevatskaya, M. Neumann, S. Füldner, C. Harlander, S. Kümmel, S. Dankesreiter, A. Pfitzner, K. Zeitler, B. König, *Angew. Chem. Int. Ed.* **2012**, *51*, 4062–4066.

[33]   Y. Su, L. Zhang, N. Jiao, *Org. Lett.* **2011**, *13*, 2168–2171.

[34]   M. Pirtsch, S. Paria, T. Matsuno, H. Isobe, O. Reiser, *Chem. Eur. J.* **2012**, 7336–7340.

[35]   P. Kohls, D. Jadhav, G. Pandey, O. Reiser, *Org. Lett.* **2012**, *14*, 672–675.

[36]   T. Maji, A. Karmakar, O. Reiser, *J. Org. Chem.* **2011**, *76*, 736–739.

[37]   G. Revol, T. McCallum, M. Morin, F. Gagosz, L. Barriault, *Angew. Chem. Int. Ed.* **2013**, *52*, 13342–13345.

[38]   C. D. McTiernan, S. P. Pitre, J. C. Scaiano, *ACS Catal.* **2014**, *4*, 4034–4039.

[39]   A. Singh, A. Arora, J. D. Weaver, *Org. Lett.* **2013**, *15*, 5390–5393.

[40]   S. Fukuzumi, H. Kotani, K. Ohkubo, S. Ogo, N. V. Tkachenko, H. Lemmetyinen, *J. Am. Chem. Soc.* **2004**, *126*, 1600–1601.

[41]   W. P. Neumann, *Synthesis* **1987**, 665–683.

[42]   A. Krief, A.-M. Laval, *Chem. Rev.* **1999**, *99*, 745–778.

[43]   K. Miura, Y. Ichinose, K. Nozaki, K. Fugami, K. Oshima, K. Utimoto, *Bulletin of the Chemical Society of Japan* **1989**, *62*, 143–147.

[44]   M. R. Medeiros, L. N. Schacherer, D. A. Spiegel, J. L. Wood, *Org. Lett.* **2007**, *9*, 4427–4429.

[45]   Based on Sigma-Aldrich price on January 21, 2015.

[46]   To eliminate any question of difference in catalyst loading causing the increased performance, 5 mol % Ir(ppy)$_3$ was also tested and gave a slightly lower yield after 1 h (19 %).

[47]   J.-B. Xia, C. Zhu, C. Chen, *Chem. Commun.* **2014**, *50*, 11701–11704.

[48]   A. J. Fry, R. L. Krieger, *J. Org. Chem.* **1976**, *41*, 54–57.

[49]   S. Rondinini, P. R. Mussini, P. Muttini, G. Sello, *Electrochimica acta* **2001**, *46*, 3245–3258.

[50]   J. W. Tucker, C. R. J. Stephenson, *J. Org. Chem.* **2012**, *77*, 1617–1622.

[51]   Although these results in the presence of oxygen support singlet catalysis, it is important to note that a combination of both singlet and triplet states operating under our oxygen free conditions cannot be completely ruled out at this time.

VII. *Supplementary Information*

A. General Reagent Information

All reactions were carried out under an argon atmosphere unless otherwise noted.   All commercially obtained reagents were used as received unless otherwise noted. All reactions were performed at room temperature (ca. 23 °C), unless otherwise noted. Aryl halides **5**, **19,** and **23** were prepared according to literature procedures.[1,2] Aryl halides **1-4**, **6-18**, **20-22** were purchased from commercial sources.   Acetonitrile was purchased from Fisher Scientific and used as received. Phenothiazine, chlorobenzene, sodium *tert*-butoxide, anhydrous dioxane, *fac*-Ir(ppy)$_3$, tributylamine, N,N-diisopropylethylamine, Triethylamine,

formic acid, RuPhos, 1,3,5-trimethoxybenzene, and 1,2,4,5-tetramethylbenzene were purchased from Sigma-Aldrich and used as received. RuPhos Precatalyst (Chloro-(2-Dicyclohexylphosphino-2′,6′-diisopropoxy-1,1′-biphenyl)[2-(2-aminoethyl)phenyl]palladium(II) - methyl-*t*-butyl ether adduct) was purchased from Strem Chemicals Inc.

B. General Analytical Information

Nuclear magnetic resonance spectra were recorded on a Varian 400 MHz, a Varian 500 MHz, or a Varian 600 MHz instrument. All ^{1}H NMR experiments are reported in δ units, parts per million (ppm), and were measured relative to the signals for residual chloroform (7.26 ppm) in the deuterated solvent, unless otherwise stated. All ^{13}C NMR spectra are reported in ppm relative to deuterochloroform (77.23 ppm), unless otherwise stated, and all were obtained with ^{1}H decoupling. For quantitative NMR a 15-second relaxation delay parameter and 1,3,5-trimethoxybenzene or 1,2,4,5-tetramethylbenzene was used as internal standard to monitor yields, unless otherwise stated.

C. Light Source

LED strips (380 nm) were bought from elemental led (see www.elementalled.com) and used as shown below (Figure S4.1). Reactions were placed next to the 380 nm lights under vigorous stirring while cooling with compressed air. The light intensity was measured to be 1.8 μW/cm^2.
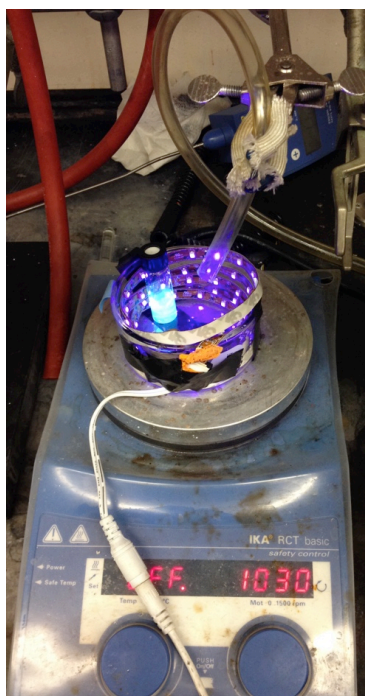
Figure S4.1 Representative reaction set-up comprising reaction vial surrounded by 380 nm LEDs with a tube blowing compressed air for cooling.

D. Synthesis of 10-phenylphenothiazine
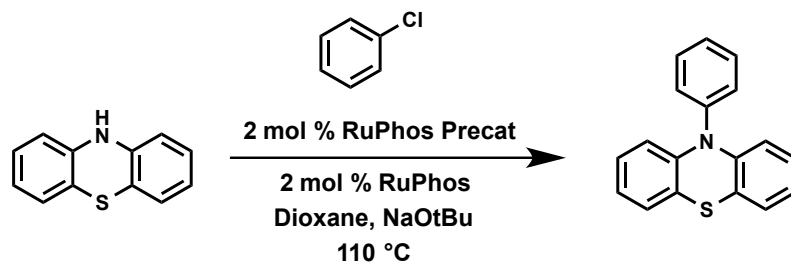
The following procedure was adopted from Maiti et al.[3] To a vial armed with a magnetic stir bar was added NaOtBu (134 mg, 1.4 mmol), phenothiazine (199 mg, 1 mmol), RuPhos Precat (14 mg, .02 mmol, 2 mol %), and RuPhos (8 mg, 0.02 mmol, 2 mol %). The vial was evacuated and backfilled 3x with argon before adding anhydrous Dioxane (1 mL). Lastly, anhydrous chlorobenzene (143 µL, 1.4 mmol) was added. The vial was then placed in an oil bath at 110 °C and let react for 5 h. The vial was then cooled to room temperature, diluted with CH_2Cl_2, washed with water, brine, dried with Mg_2SO_4, and run through a silica plug (5 % EtOAc/Hexanes). The product was then dried under reduced pressure to yield 267 mg of a white solid (97 % yield). ^{1}H NMR (600 MHz, CDCl$_3$) δ: 7.60 (t, J = 8 Hz, 2H), 7.49 (t, J = 8 Hz, 1H), 7.40 (d, J = 7 Hz, 2H), 7.02 (d, J = 8 Hz, 2H), 6.86-6.79 (m, 4 H), 6.20 (d, J = 8 Hz, 2 H) ppm. ^{13}C NMR (151 MHz, CDCl$_3$) δ: 144.5, 141.2, 131.1, 130.9, 128.4, 127.0, 126.9, 122.7, 120.4, 116.3 ppm. HRMS C$_{18}$H$_{13}$NS Found 275.0753, Calc'd 275.0769.

E. General Procedure for Table 1 using Ir(ppy)₃ or PTH
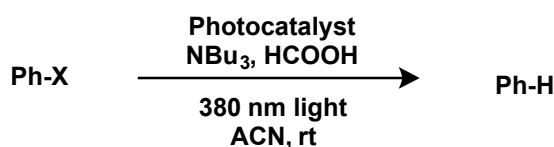
A vial equipped with a magnetic stir bar and fitted with a teflon screw cap septum was charged with iodo- or bromobenzene (0.1 mmol), PTH (5 mol %) or Ir(ppy)₃ (1 mol %), formic acid (19 μL, 0.5 mmol), tributylamine (119 μL, 0.5 mmol), 1,2,4,5-tetramethylbenzene (NMR standard, 13.4 mg, 0.1 mmol) and acetonitrile (1 mL). The reaction mixture was degassed with three freeze-pump-thaw cycles. The vial was then backfilled with argon and vigorously stirred in front of 380 nm LEDs while cooling with compressed air to maintain ambient temperature. The reaction conversion was monitored by ¹H NMR.

F. Synthesis of PDI Photocatalyst
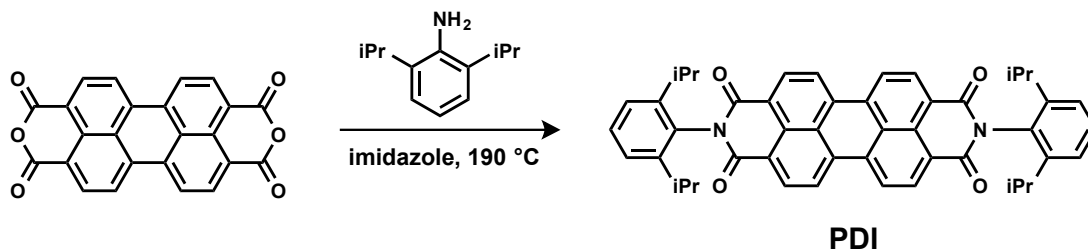
The following procedure was adopted from Ghosh et al.[4] To a dry 100 mL round bottomed flask equipped with a magnetic stir bar was added perylene-3,4,9,10-tetracarboxylic dianhydride (392 mg, 1 mmol), 2,6-diisoprpylaniline (785 μL, 4.16 mmol), and imidazole (2.9 g). The flask was immersed in an oil bath at 190 °C for 20 h. The reaction was then stopped by cooling the flask to room temperature and adding EtOH (25 mL) and 2 M HCl (25 mL), sonicating, and filtering. The filtrate was washed with 1:1 EtOH/HCl (2 M) and 1:1 EtOH/H₂O mixtures before purifying by silica column chromatography using hexanes/dichloromethane (1:1 to 30:70 hexanes/dichloromethane). PDI was obtained as a red solid (35 mg). ¹H NMR (600 MHz, CDCl₃) δ: 8.80 (d, J = 7.9 Hz, 4H), 8.75 (d, J = 8.0 Hz, 4H), 7.51 (t, J = 7.8 Hz, 2H), 7.36 (d, J = 7.7 Hz, 4H), 2.82 –

2.70 (m, 4H), 1.19 (d, J = 6.8 Hz, 24H) ppm. ^{13}C NMR (126 MHz, CDCl$_3$) δ: 163.7, 145.9, 135.3, 132.3, 130.8, 130.4, 129.9, 127.1, 124.3, 123.7, 123.6, 29.5, 24.2 ppm. HRMS C$_{48}$H$_{42}$N$_2$O$_4$ Found 710.3129, Calc'd 710.3145.

G. General Procedure for Table 1 using PDI

A vial equipped with a magnetic stir bar and fitted with a teflon screw cap septum was charged with iodo- or bromobenzene (0.05 mmol), PDI (1.8 mg, 0.0025 mmol, 5 mol %), 1,2,4,5-tetramethylbenzene (NMR standard, 6.7 mg, 0.05 mmol) and *N,N*-dimethylformamide (3 mL). The reaction mixture was degassed with three freeze-pump-thaw cycles. The vial was then backfilled with argon and triethylamine (56 μL, 0.4 mmol) was added under argon before vigorously stirring in front of blue LEDs (λ_{max} = 465 nm, 5 μW/cm^2) while cooling with compressed air to maintain 40 °C. The reaction yields were monitored by ^{1}H NMR.

H. General Procedure for Table 2
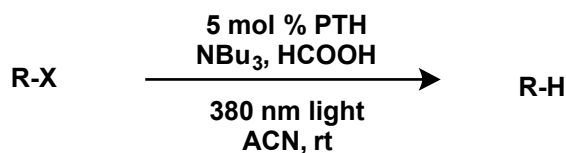
A vial equipped with a magnetic stir bar and fitted with a teflon screw cap septum was charged with substrate (0.1 mmol), PTH (1.4 mg, 5 mol %), formic acid (19 μL, 0.5 mmol), tributylamine (119 μL, 0.5 mmol), 1,3,5-trimethoxybenzene (33.6 mg, 0.2 mmol) and acetonitrile (1 mL). The reaction mixture was degassed with three freeze-pump-thaw cycles. The vial was then backfilled with argon and vigorously stirred in front of 380 nm LEDs

while cooling with compressed air to maintain ambient temperature. The reaction yield was monitored by ^{1}H NMR.

I. General Procedure for Isolation of Dehalogenated Products of 5, 8, and 19

$$\text{R-X} \xrightarrow[\substack{\textbf{380 nm light} \\ \textbf{ACN, rt}}]{\substack{\textbf{5 mol \% PTH} \\ \textbf{NBu}_3\textbf{, HCOOH}}} \text{R-H}$$
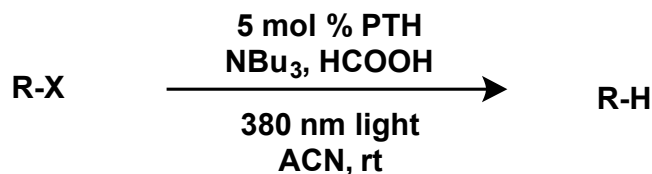
A vial equipped with a magnetic stir bar and fitted with a teflon screw cap septum was charged with substrate (0.2 mmol), PTH (2.8 mg, 5 mol %), formic acid (38 μL, 1 mmol), tributylamine (238 μL, 1 mmol), and acetonitrile (2 mL). The reaction mixture was degassed with three freeze-pump-thaw cycles. The vial was then backfilled with argon and vigorously stirred in front of 380 nm LEDs while cooling with compressed air to maintain ambient temperature. The reaction conversion was monitored by ^{1}H NMR, and stopped by opening the reaction to air. The acetonitrile was removed *in vacuo* before redissolving in ethyl acetate and washing with 2 M HCl. The aqueous layer was washed again with ethyl acetate, and the organic layers were combined and washed with 1 M NaCO$_3$, brine, and dried over Mg$_2$SO$_4$. The solvent was removed *in vacuo* and the resulting mixture was purified by silica gel column chromatography eluting with 99:1 hexane:ethyl acetate.

PTH
NBu$_3$, HCOOH

380 nm light
ACN, rt

BnO$_2$C ... I ... 3 → BnO$_2$C ... H
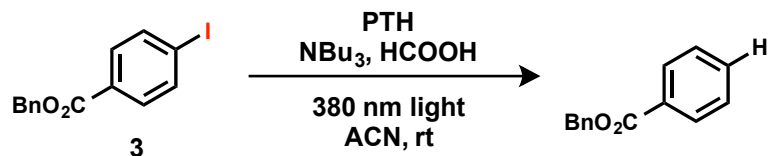
Benzyl benzoate (5): Spectral data matched that of commercially available reagents (see Sigma-Aldrich). ^{1}H NMR (600 MHz, CDCl$_3$) δ: 8.09 (d, J = 7.6 Hz, 2H), 7.56 (t, J = 7.5 Hz, 1H), 7.45 (m, 4H), 7.40 (t, J = 7.4 Hz, 2H), 7.35 (t, J = 7.3 Hz, 1H), 5.37 (s, 2H) ppm. ^{13}C NMR (126 MHz, CDCl$_3$) δ: 166.6, 136.3, 133.2, 130.4, 129.9, 128.8, 128.6, 128.5, 128.4, 66.9 ppm. HRMS C$_{14}$H$_{12}$O$_2$ Found 212.0830, Calc'd 212.0837.

PTH
NBu$_3$, HCOOH

380 nm light
ACN, rt

MeO$_2$C ... Br ... CO$_2$Me ... 8 → MeO$_2$C ... H ... CO$_2$Me
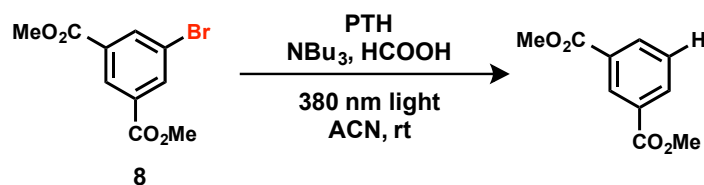
Dimethyl Isophthalate (8): Spectral data matched that of commercially available reagents (see Sigma-Aldrich). ^{1}H NMR (600 MHz, CDCl$_3$) δ: 8.69 (s, 1H), 8.23 (d, J = 7.8 Hz, 1H), 7.54 (t, J = 7.8 Hz, 1H), 3.95 (s, 6H) ppm. ^{13}C NMR (126 MHz, CDCl$_3$) δ: 166.5, 134.0, 131.0, 130.8, 128.8, 52.6 ppm. HRMS C$_{10}$H$_{10}$O$_4$ Found 194.0573, Calc'd 194.0579.

PTH
NBu$_3$, HCOOH

380 nm light
ACN, rt

BnO$_2$C ... Cl ... 19 → BnO$_2$C ... H
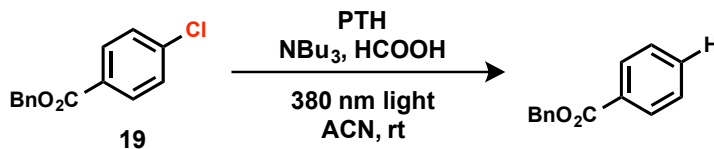
Benzyl benzoate (19): Spectral data matched that of commercially available reagents (see Sigma-Aldrich). ^{1}H NMR (600 MHz, CDCl$_3$) δ: ^{1}H NMR (600 MHz, CDCl$_3$) δ: 8.09 (d, J = 7.6 Hz, 2H), 7.56 (t, J = 7.5 Hz, 1H), 7.45 (m, 4H), 7.40 (t, J = 7.4 Hz, 2H), 7.35 (t, J = 7.3 Hz, 1H), 5.37 (s, 2H) ppm.

J. Dehalogenation Using Commercially Available Catalyst
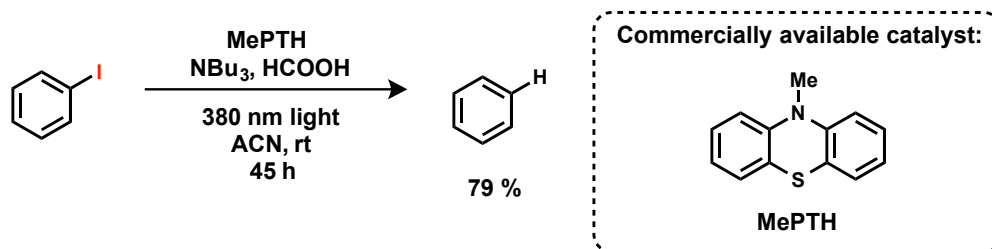
A vial equipped with a magnetic stir bar and fitted with a teflon screw cap septum was charged with iodobenzene (11.2 μL, 0.1 mmol), MePTH (1.1 mg, 5 mol %), formic acid (19 μL, 0.5 mmol), tributylamine (119 μL, 0.5 mmol), 1,2,4,5-tetramethylbenzene (13.4 mg, 0.1 mmol) and acetonitrile (1 mL). The reaction mixture was degassed with three freeze-pump-thaw cycles. The vial was then backfilled with argon and vigorously stirred in front of 380 nm LEDs while cooling with compressed air to maintain ambient temperature. The reaction yield was monitored by ^{1}H NMR.

Table S4.1 Optimization table using iodobenzene and PTH[a]
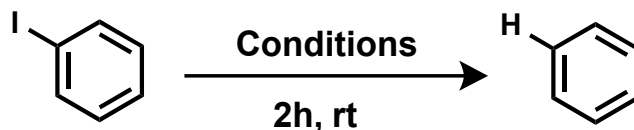
Entry	Conditions	% Yield
1	TBA(5eqv.), HCOOH(5eqv.) in ACN	94
2	TBA(5eqv.), HCOOH(5eqv.) in **DMA**	47
3	TBA(5eqv.), HCOOH(5eqv.) in **DMF**	67
4	TBA(5eqv.), HCOOH(5eqv.) in **THF**	10
5	TBA(5eqv.), HCOOH(5eqv.) in **Hexane**	12
6	**TEA(5eqv.),** HCOOH(5eqv.) in ACN	44
7	**DIPEA(5eqv.),** HCOOH(5eqv.) in ACN	93
8*	**Compact Fluorescent Lamp**, TBA(5eqv.), HCOOH(5eqv.) in ACN	45
9*	**465 nm LED**, TBA(5eqv.), HCOOH(5eqv.) in ACN	53

[a] Reaction conditions: Iodobenzene (1 equiv.), PTH (5 mol %), formic acid (5 equiv), tributylamine (5 equiv), Acetonitrile (0.08 M of substrate) at room temperature for 2 h with irradiation from 380 nm LEDs (1.8 mW/cm^2) unless otherwise stated. ^{1}H NMR yield determined using 1,2,4,5-tetramethylbenzene as an internal standard. *24 hour reaction time

Table S4.2 Control Experiments[a]
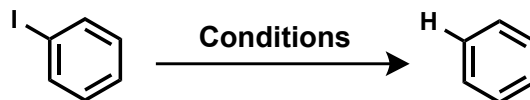
Entry	Conditions	% Yield
1	**NO CATALYST,** TBA(5eqv.), HCOOH(5eqv.) in ACN, 2hrs	0
2	**NO LIGHT**, TBA(5eqv.), HCOOH(5eqv.) in ACN, 2hrs	0
3	**NO TBA**, HCOOH(5eqv.) in ACN, 2hrs	0
4	TBA(5eqv.), **NO HCOOH** in ACN, 2hrs	71
5	**NO TBA**, **NO HCOOH** in ACN, 2hrs	0

[a] Reaction conditions: Iodobenzene (1 equiv.), PTH (5 mol %)), formic acid (5 equiv), tributylamine (5 equiv), Acetonitrile (0.08 M of substrate) at room temperature for 2 h with irradiation from 380 nm LEDs (1.8 mW/cm^2) unless otherwise stated. ^{1}H NMR yield determined using 1,3,5-trimethoxybenzene as an internal standard.

Table S4.3 Optimization of Catalyst Loadings[a]
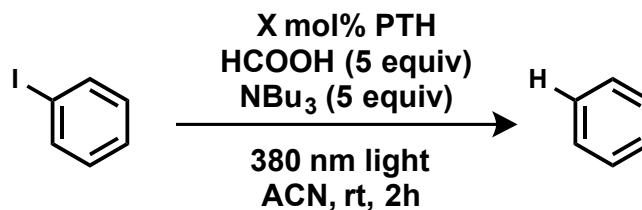
Entry	Catalyst loading (mol %)	Yield (%)
1	5	> 95
2	1	90
3	0.5	85
4	0.1	42

[a] Reaction conditions: Iodobenzene (1 equiv.), PTH (0.1-5 mol %), Formic acid (5 equiv.), tributylamine (5 equiv.), Acetonitrile (0.08 M of iodobenzene) at room temperature with irradiation from 380 nm LEDs for 2 h. Yield tracked using 1,3,5-trimethoxybenzene as an internal standard.
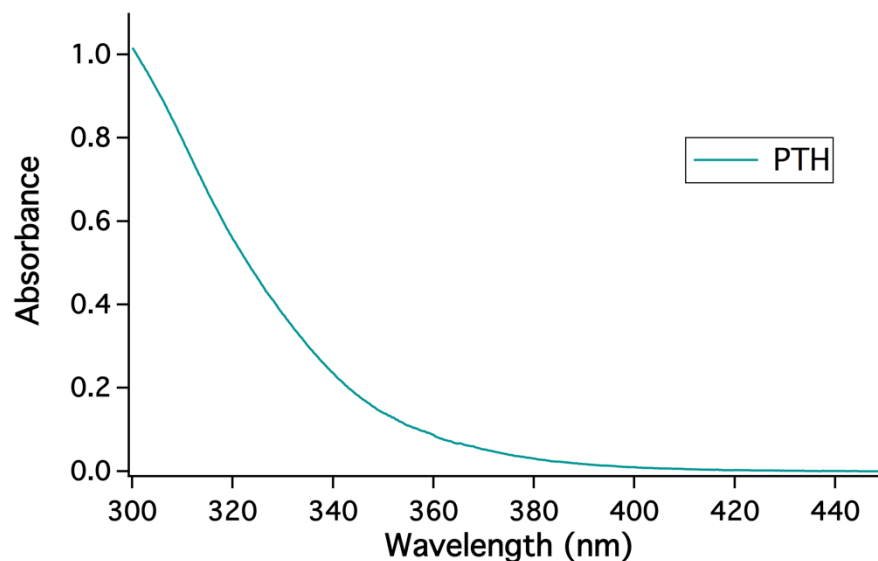
Figure S4.2 Absorbance spectrum of PTH (0.17 mM in ACN) recorded on a Shimadzu 3600 UV-Vis-NIR spectrometer

K. Fluorescence quenching studies

A Varian Cary Eclipse Fluorescence Spectrophotometer was used in the quenching studies. The PTH solutions were excited at 350 nm. The emission of a 0.17 mM solution of PTH was first measured with varying concentrations of iodobenzene. As can be seen in Figure S4.3, the intensity of the peak emission was decreased with increasing concentration of iodobenzene, giving evidence for the direct reduction of iodobenzene upon irradiation of PTH. Next, the emission of a 0.17 mM solution of PTH was measured with varying concentrations of tributylamine. Figure S4.4 shows the raw emission data, demonstrating no quenching from the amine source.

Figure S4.3 Stern-Volmer quenching study with iodobenzene (quencher) and PTH (0.17 mM in ACN)

Figure S4.4 Emission spectra of 0.17 mM PTH solution in ACN with varying concentrations of tributylamine

L. Lifetime measurements

PTH (0.17 mM in ACN) lifetime measurements were performed using Time-Correlated Single Photon Counting (TCSPC) technique. Approximately 200 femtosecond (fs) excitation pulses with wavelength 380 nm and ~10 pJ energy were generated b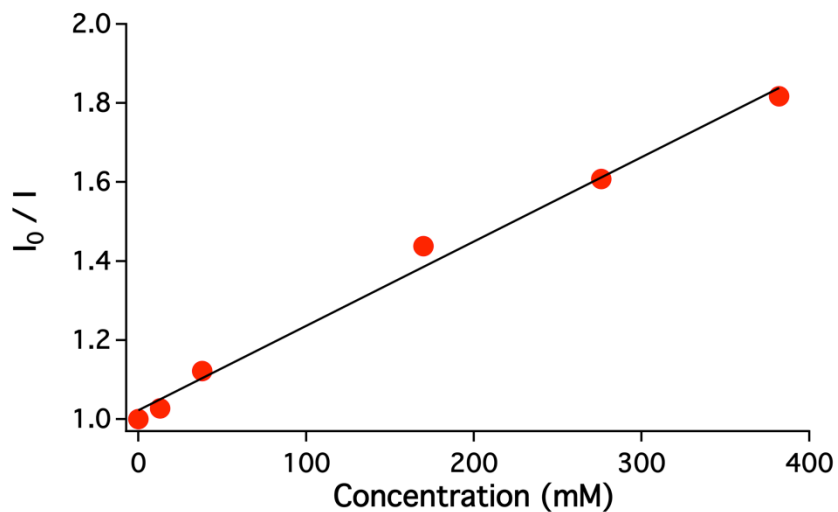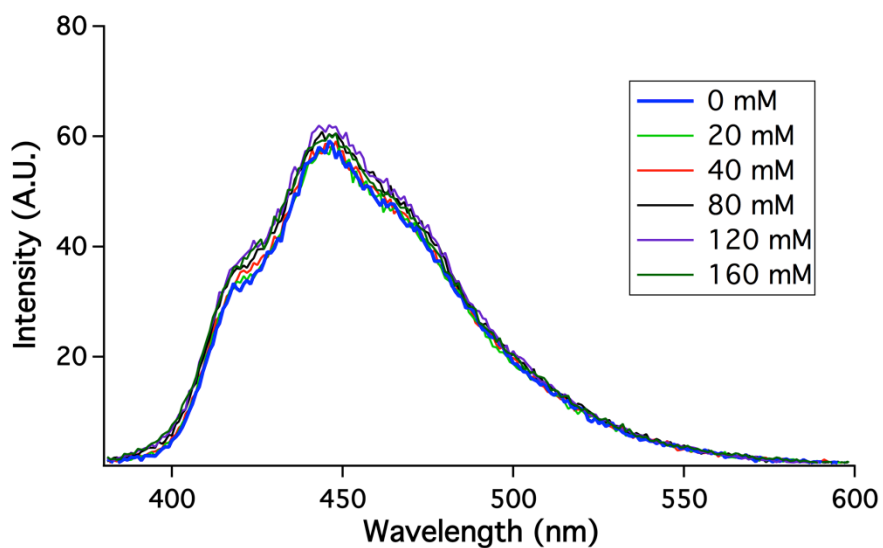y doubling the fundamental frequency of fs Ti:Sapphire laser (Coherent Mira 900) pulses in a commercial optical harmonic generator (Inrad). The laser repetition rate was reduced to 2 MHz by a home-made acousto-optical pulse picker in order to avoid saturation of the chromophore. TCSPC system is equipped with an ultrafast microchannel plate photomultiplier tube detector (Hamamatsu R3809U-51) and electronics board (Becker & Hickl SPC-130) and has instrument response time about 60-65 picoseconds. Triggering signal for the TCSPC board was generated by sending a small fraction of the laser beam onto a fast (400 MHz bandwidth) Si photodiode (Thorlabs Inc.). Fluorescence signal was dispersed in Acton Research SPC-500 monochromator after passing through a pump blocking, long wavelength-pass, autofluorescence-free, interference filter (Omega Filters, ALP series). The monochromator is equipped with a CCD camera (Roper Scientific PIXIS-400) allowing for monitoring of the time-averaged fluorescence spectrum.

A biexponential decay of the emission at 450 nm was observed to be $\tau_1 = 0.81$ ns (54 %) and $\tau_2 = 2.3$ ns (46 %).

M. Synthesis of PTH-BP

159
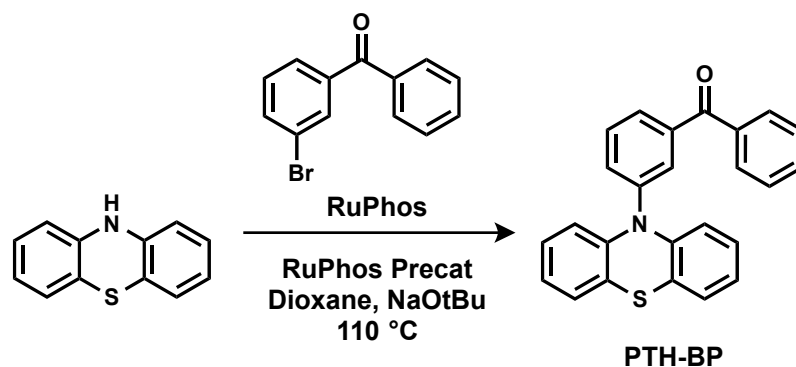
To a 10 mL round-bottom flask with stir bar and condenser was added phenothiazine (0.5 g, 2.5 mmol), *m*-bromobenzophenone (0.78 g, 3.0 mmol), RuPhos (5.9 mg, 0.013 mmol), RuPhos Precatalyst (10.3 mg, 0.013 mmol) and sodium *tert*-butoxide (0.29 g, 3.0 mmol). The flask was evacuated and backfilled with argon three times before 2.5 mL degassed 1,4-dioxane was added. The mixture was heated to 110 ºC for 1 hour, then cooled to room temperature and partitioned between EtOAc and water. The EtOAc layer was washed twice more with water and once with brine, then the organic layer was dried with $MgSO_4$, filtered, and concentrated. The product was recrystallized from EtOAc/hexanes to give 727 mg PTH-BP as a yellow solid (76% yield) ^{1}H NMR (600 MHz, CDCl$_3$) δ 7.92 (d, J = 7.6 Hz, 1H), 7.84 (d, J = 7.6 Hz, 2H), 7.72 (t, J = 7.6 Hz, 1H), 7.63 (d, J = 8.2 Hz, 1H), 7.61 (t, J = 7.6 Hz, 1H), 7.50 (t, J = 8.2 Hz, 2H), 7.08 (d, J = 7.6 Hz, 2H), 6.93 (t, J = 8.2 Hz, 2H), 6.87 (t, J = 7.6 Hz, 2H), 6.34 (d, J = 8.2 Hz, 2H) ppm; ^{13}C NMR (150 MHz, CDCl$_3$) δ 195.6, 143.8, 141.5, 140.2, 137.1, 134.0, 132.7, 131.3, 130.7, 130.0, 129.2, 128.4, 127.1, 129.9, 123.0, 121.6, 116.9 ppm; HRMS (ESI) calculated for C$_{25}$H$_{17}$NNaOS [M+Na]$^+$: 402.0923, found 402.0919.

N. PTH-BP Photoluminescence at Room Temperature and 77 K
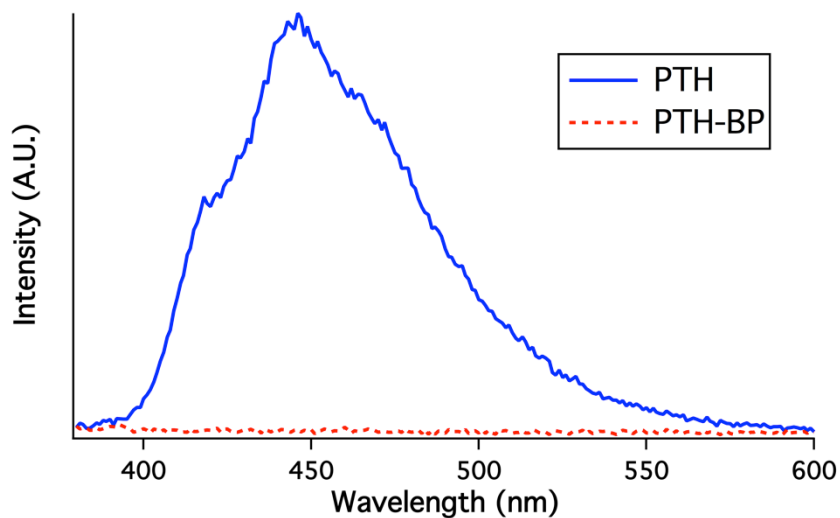

Figure S4.5 Comparison of photoluminescence between PTH (0.17 mM in ACN) and

BP-PTH (0.17 mM in ACN), giving evidence for no singlet state emission
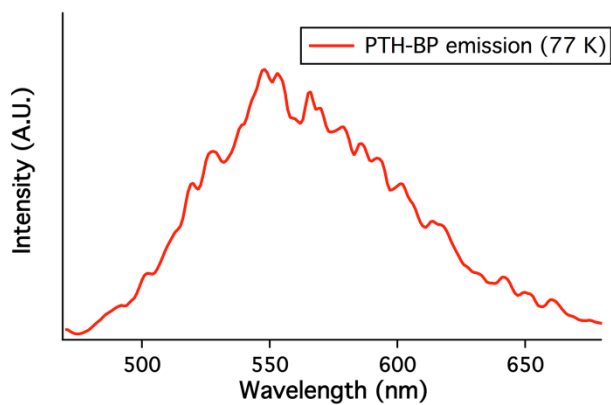
Figure S4.6 Photoluminescence of PTH-BP (0.17 mM in ACN) at 77 K, showing triplet

emission

O. Dehalogenation Procedure in the Presence of Air

A vial equipped with a magnetic stir bar and fitted with a screw cap was charged with substrate (0.1 mmol), PTH (1.4 mg, 5 mol %), formic acid (19 µL, 0.5 mmol), tributylamine (119 µL, 0.5 mmol), 1,2,4,5-tetramethylbenzene (13.4 mg, 0.1 mmol) and acetonitrile (1 mL). Without degassing, the reaction mixture was vigorously stirred in front of 380 nm LEDs while cooling with compressed air to maintain ambient temperature. The reaction yield was monitored by ^{1}H NMR.

Note: Iodobenzene was first tested using the above procedure, observing 90 % yield in 16 h with a capped vial. To be sure that the catalyst could operate in an "infinite" amount of oxygen, the reaction was also run continuously open to air and 90 % yield was observed after 15 h.

P. Procedure for Radical Cyclization
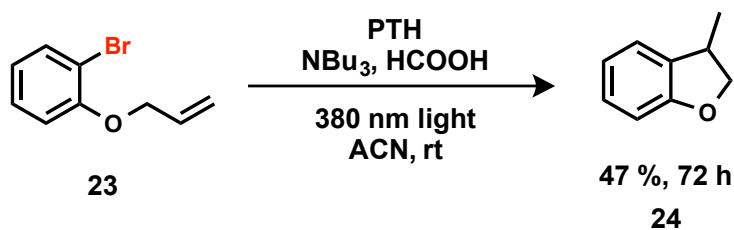
A vial equipped with a magnetic stir bar and fitted with a teflon screw cap septum was charged with **23** (0.1 mmol), PTH (1.4 mg, 5 mol %), formic acid (19 µL, 0.5 mmol), tributylamine (119 µL, 0.5 mmol), 1,3,5-trimethoxybenzene (33.6 mg, 0.2 mmol) and acetonitrile (1 mL). The reaction mixture was degassed with three freeze-pump-thaw cycles. The vial was then backfilled with argon and vigorously stirred in front of 380 nm LEDs

while cooling with compressed air to maintain ambient temperature. The reaction yield was monitored by ^{1}H NMR.

Q. Deuterated Studies
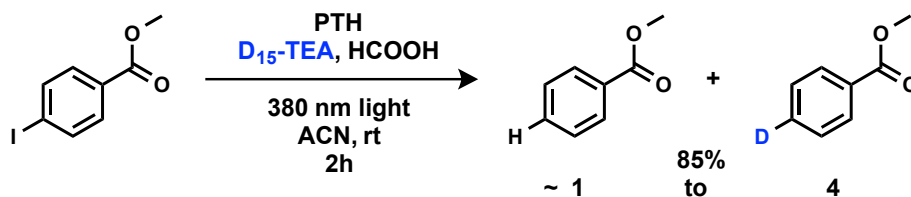
D$_{15}$-TEA: A vial equipped with a magnetic stir bar and fitted with a teflon screw cap septum was charged with methyl 4-iodobenzoate (0.1mmol), PTH (5 mol %), formic acid (19 µL, 0.5 mmol), D$_{15}$-triethylamine (80 µL, 0.5 mmol), 1,3,5-trimethoxybenzene (33.6 mg, 0.2 mmol) and acetonitrile (1 mL). The reaction mixture was degassed with three freeze-pump-thaw cycles. The vial was then backfilled with argon and vigorously stirred in front of 380 nm LEDs while cooling with compressed air to maintain ambient temperature. The reaction yield was monitored by ^{1}H NMR.

DCOOD: A vial equipped with a magnetic stir bar and fitted with a teflon screw cap septum was charged with methyl 4-iodobenzoate (0.1 mmol), PTH (5 mol %), D$_2$-formic acid (19 µL, 0.5 mmol), tributylamine(119 µL, 0.5 mmol), 1,3,5-trimethoxybenzene (33.6

mg, 0.2 mmol) and acetonitrile (1 mL). The reaction mixture was degassed with three freeze-pump-thaw cycles. The vial was then backfilled with argon and vigorously stirred in front of 380 nm LEDs while cooling with compressed air to maintain ambient temperature. The reaction yield was monitored by ^{1}H NMR.

D$_3$-ACN: A vial equipped with a magnetic stir bar and fitted with a teflon screw cap septum was charged with methyl 4-iodobenzoate (0.1mmol), PTH (5 mol %), D$_2$-formic acid (19 µL, 0.5 mmol), tributylamine (119 µL, 0.5 mmol), 1,3,5-trimethoxybenzene (33.6 mg, 0.2 mmol) and acetonitrile (1 mL). The reaction mixture was degassed with three freeze-pump-thaw cycles. The vial was then backfilled with argon and vigorously stirred in front of 380 nm LEDs while cooling with compressed air to maintain ambient temperature. The reaction yield was monitored by ^{1}H NMR.

DCOOD and D$_3$-ACN: A vial equipped with a magnetic stir bar and fitted with a teflon screw cap septum was charged with methyl 4-iodobenzoate (0.1mmol), PTH (5 mol %), D$_2$-formic acid (19 µL, 0.5 mmol), tributylamine (119 µL, 0.5 mmol), 1,3,5-trimethoxybenzene

164

(33.6 mg, 0.2 mmol) and D₃-acetonitrile (1 mL). The reaction mixture was degassed with three freeze-pump-thaw cycles. The vial was then backfilled with argon and vigorously stirred in front of 380 nm LEDs while cooling with compressed air to maintain ambient temperature. The reaction yield was monitored by ^{1}H NMR.
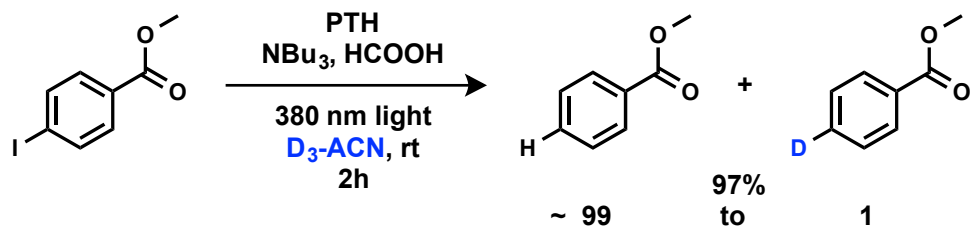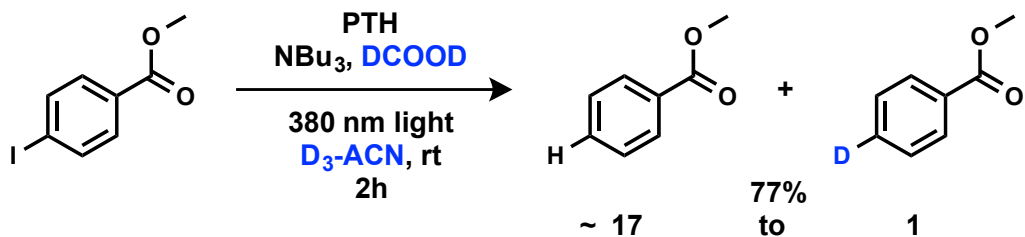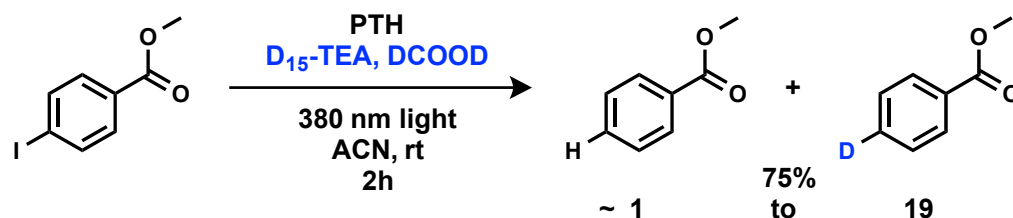

D₁₅-TEA and DCOOD: A vial equipped with a magnetic stir bar and fitted with a teflon screw cap septum was charged with methyl 4-iodobenzoate (0.1mmol), PTH (5 mol %), D₂-formic acid (19 µL, 0.5 mmol), D₁₅-triethylamine (80 µL, 0.5 mmol), 1,3,5-trimethoxybenzene (33.6 mg, 0.2 mmol) and acetonitrile (1 mL). The reaction mixture was degassed with three freeze-pump-thaw cycles. The vial was then backfilled with argon and vigorously stirred in front of 380 nm LEDs while cooling with compressed air to maintain ambient temperature. The reaction yield was monitored by ^{1}H NMR.
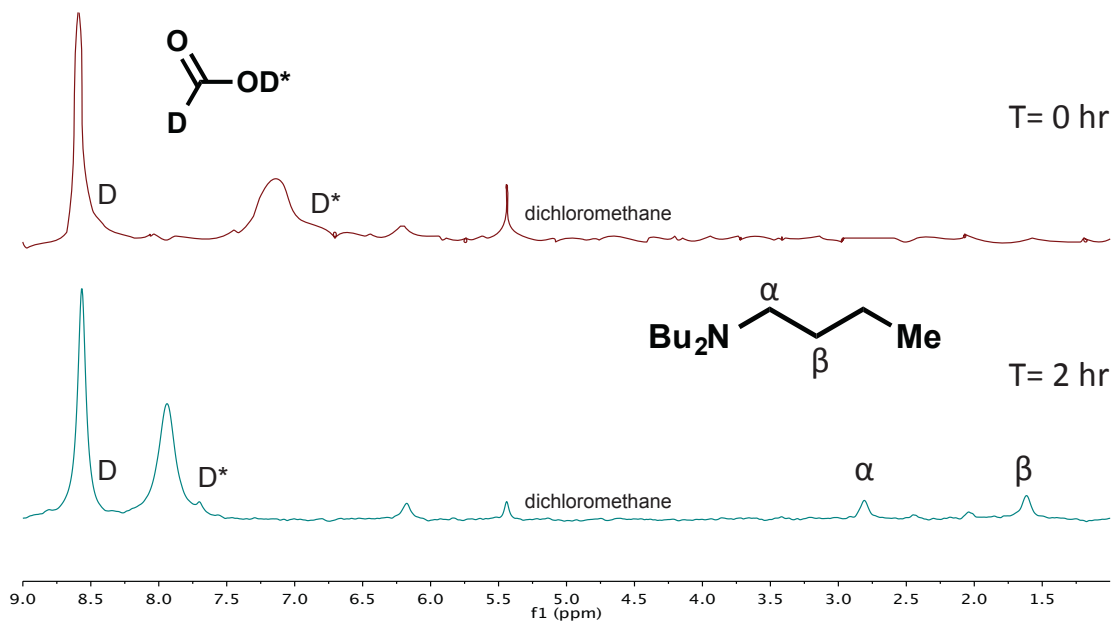
Figure S4.7 Deuterium NMR (in CH$_2$Cl$_2$) of reaction mixture (see above, DCOOD) at 0 h and 2 h, showing deuterium incorporation at the alpha and beta position of tributylamine
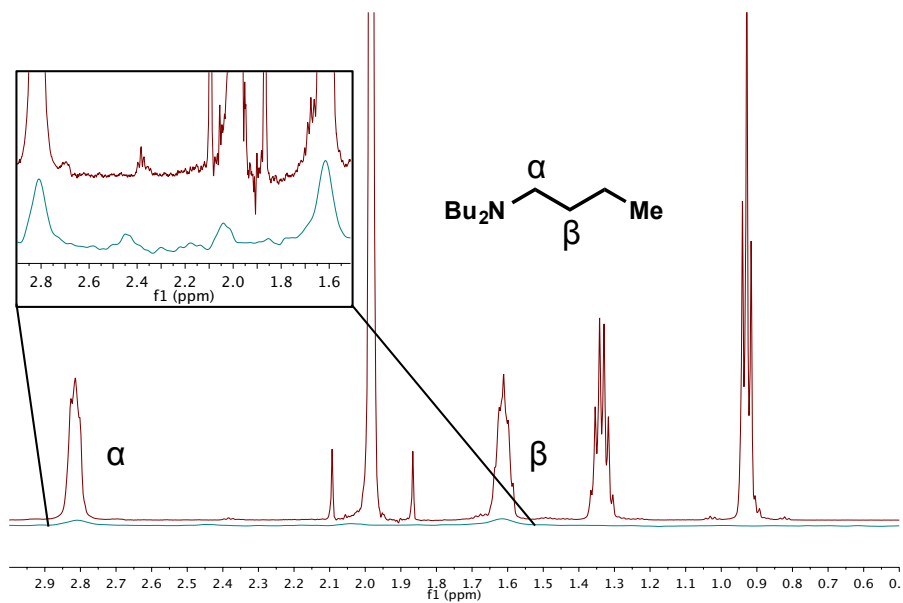
Figure S4.8 Comparison of ^{1}H and deuterium NMR of reaction mixture (see above, **DCOOD**) after 2 h to confirm that deuterium is incorporated in the alpha and beta positions of tributylamine

R. Preparative Scale Reaction Conducted in Air
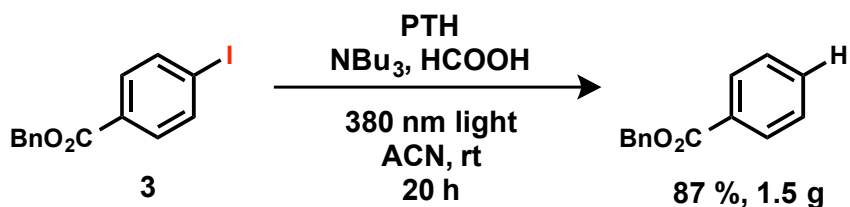
To a 125mL Erlenmeyer flask equipped with a magnetic stir bar was added benzyl 4-iodobenzoate (2.37 g, 7.0 mmol), PTH (96.4 mg, 0.35 mmol, 5 mol %), formic acid (1.32 mL, 35 mmol), tributylamine (8.32 mL, 35 mmol), and acetonitrile (70 mL). The flask was capped with a rubber septum and was stirred vigorously while irradiating with 380 nm LEDs and cooling with compressed air for 20 hours. The acetonitrile was removed *in vacuo* before redissolving in ~100mL of ethyl acetate and washing with ~100mL of 2M HCl. After extracting the aqueous layer with ethyl acetate (100 mL), the organic layer was combined and washed with 1 M NaCO$_3$ (100 mL) and brine before drying with Na$_2$SO$_4$. The solvent was removed *in vacuo* and the resulting mixture was purified by silica gel column chromatography eluting with 99:1 hexane:ethyl acetate to give 1.49 g of a pale yellow liquid (87%).

Recycled catalyst: 56 mg of PTH was isolated and purity was confirmed by ^{1}H and C^{13} NMR. ^{1}H NMR (600 MHz, DMSO) δ: : 6.86 (t, *J* = 6.9 Hz, 2H), 6.73 (t, *J* = 12 Hz, 1H), 6.61 (d, *J* = 7.7 Hz, 2H), 6.27 (d, *J* = 7.5 Hz, 2H), 6.12 (t, *J* = 7.8 Hz, 2H), 6.05 (t, *J* = 7.5

Hz, 2H), 5.35 (d, *J* = 8.2 Hz, 2H) ppm. ^{13}C NMR (101 MHz, DMSO) δ: 143.7, 140.4, 131.2, 130.4, 128.6, 127.4, 126.8, 122.9, 119.5, 116.2 ppm.
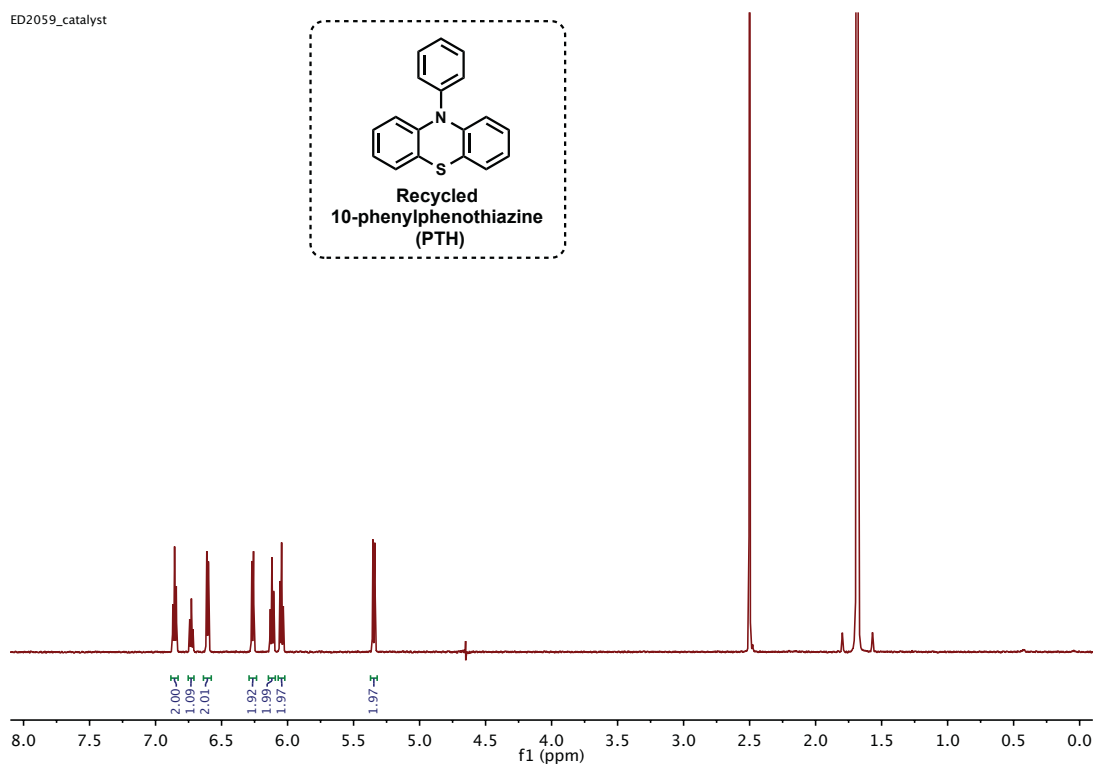
Figure S4.9 ^{1}H NMR in DMSO of the isolated PTH after preparative scale reaction

S. Reductive Dehalogention Using Recycled PTH
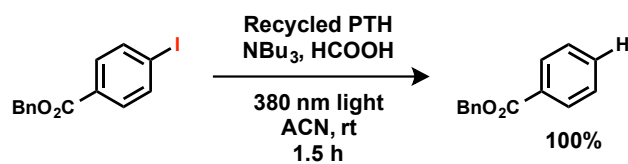
A vial equipped with a magnetic stir bar and fitted with a teflon screw cap septum was charged with benzyl 4-iodobenzoate (33.8 mg, 0.1 mmol), PTH (1.4 mg, 5 mol %), formic acid (19 μL, 0.5 mmol), tributylamine (119 μL, 0.5 mmol), 1,2,4,5-tetramethylbenzene (13.4 mg, 0.1 mmol) and acetonitrile (1 mL). The reaction mixture was degassed with three freeze-pump-thaw cycles. The vial was then backfilled with argon and vigorously stirred in front of 380 nm LEDs while cooling with compressed air to maintain ambient temperature. The reaction yield was monitored by ^{1}H NMR.

T. Supplementary References

[1]   C. A. Ocasio, T. S. Scanlan, *Bioorganic & Medicinal Chemistry* **2008**, *16*, 762–770.

[2]   E. C. Taylor, C.-M. Yoon, *J. Org. Chem.* **1994**, *59*, 7096–7098.

[3]   D. Maiti, B. P. Fors, J. L. Henderson, Y. Nakamura, S. L. Buchwald, *Chem. Sci.* **2010**, *2*, 57.

[4]   I. Ghosh, T. Ghosh, J. I. Bardagi, B. Konig, *Science* **2014**, *346*, 725–728.

5. Oxygen Tolerance of Phenothiazine-based Metal-free Atom Transfer Radical Polymerizations

I. Introduction

For an introduction to controlled radical polymerizations, and why metal-free atom transfer radical polymerizations are important, see chapters 1 and 3. The focus of this chapter is to describe the use of 10-phenyl phenothiazine as a photocatalyst for metal-free ATRP without degassing, or in the presence of oxygen.

Conducting controlled polymerizations without degassing would allow non-experts even greater access to functional materials due to its simplicity, and would provide greater opportunity for industrial adoption. Within the field of ATRP, others have previously used both light[1] and reducing agents[2,3] in combination with transition metal catalysts for conducting polymerization in the presence of air. Although useful, these methods relied on the use of transition metals, limiting applications in biological or electronic materials. To date, it has not been demonstrated that a metal-free ATRP system can be conducted in the presence of air.

II. Results and Discussion

A. Optimization of Conditions

Initially, different catalyst loadings of 10-phenylphenothiazine (PTH) were screened for the polymerization of benzyl methacrylate without degassing. In the case of 0.5-1 mol % catalyst loadings, control was observed, with approximate agreement between theoretical

and experimental molecular weights and low polydispersities. This is significant, as it demonstrates that maintaining control over polymerization only requires a simple 5-fold increase in catalyst loadings, with no external additives. As controls, when the light was off, no polymerization occurred, and in the absence of initiator or catalyst, only uncontrolled polymerization occurred (Table 1).

Table 5.1 Optimization of a light-mediated polymerization of benzyl methacrylate without degassing using 10-phenylphenothiazine.[a]
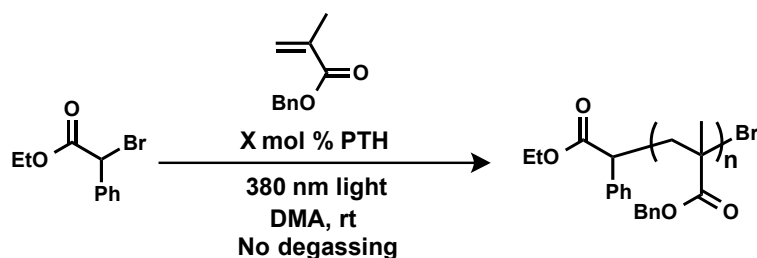
Entry	Catalyst loading [mol %]	M_n (exp) [g/mol]	M_n (theo) [g/mol]	M_w / M_n
1	0.1	30,300	4,600	2.81
2	0.5	17,600	14,600	1.26
3	1	11,500	7,000	1.25
4[b]	1	--	--	--
5[c]	1	65,300	--	1.82
6[d]	1	24,300	--	1.90

[a] Reaction conditions: BnMA (1 equiv.), 10-phenylphenothiazine (0.001-0.01 equiv.), initiator (0.009 equiv), DMA (2.7 M of BnMA) at room temperature with irradiation from 380 nm LEDs for 4 h (M_n = number average molecular weight; M_w = weight average molecular weight). M_n and M_w / M_n determined using size exclusion chromatography (SEC) or ^{1}H NMR; [b] reaction run in the dark [c] reaction run in the absence of photocatalyst [d] reaction run in the absence of initiator

B. Kinetic Analysis

Next, the kinetic behavior of these polymerizations in the presence of air were explored under the optimized conditions of 0.5 mol % PTH (Figure 5.1). An initial inhibition period

of ~1 h occurred, potentially due to the time necessary for eliminating the presence of oxygen in the reaction. Following this, the polymerization occurred in a controlled manner as indicated by linear increase in molecular weight with conversion, with the ability to be temporally controlled with light. The reaction could be stopped and started by simply placing it in the dark, and no loss in control was observed due to cycling the reaction's exposure to light. Approximately linear first order kinetics indicate a constant radical concentration when the light is on. These results demonstrate that this system has very similar attributes to the degassed version of polymerization, while offering a great amount of operational ease for non-experts.
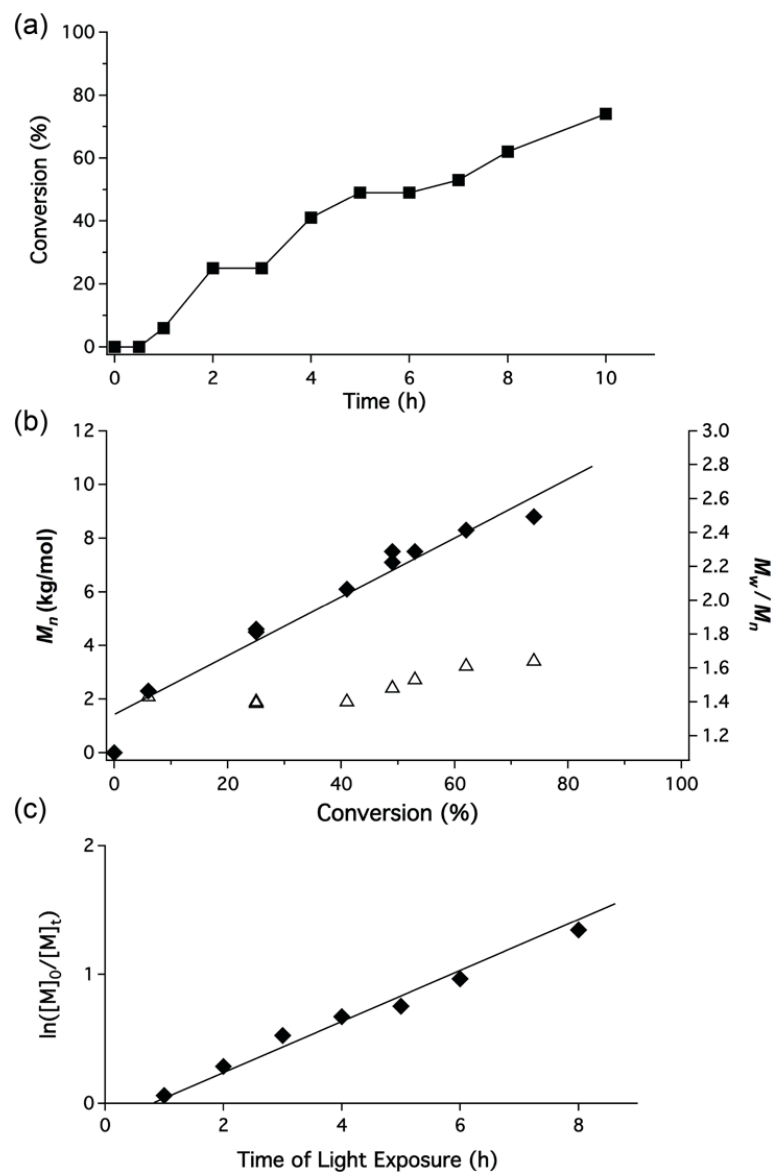
Figure 5.1 Polymerization of BnMA using PTH with repeated 'on-off' cycling of the reaction to light.
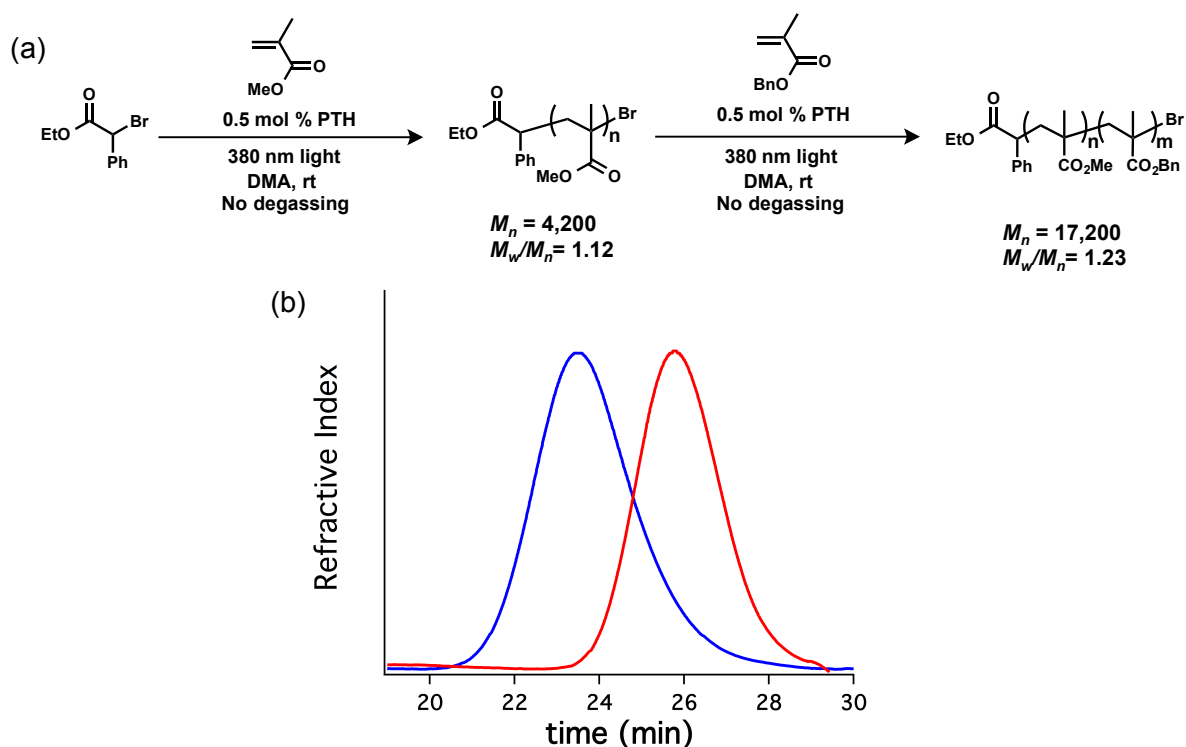
Figure 5.2   Block copolymerization experiment demonstrating chain extension of PMMA with PBnMA without degassing reaction mixtures for both homopolymerization and chain extension.   Red trace = homopolymer (PMMA).   Blue trace = block copolymer (PMMA-*b*-PBnMA)

C. Block Copolymerizations

Controlled behavior is important to obtain accurate molecular weights, but perhaps the most useful attribute of controlled polymerizations is the ability to synthesize block copolymers, allowing access to complex molecular architectures.   To provide evidence for the existence of living chain ends, a homopolymer of polymethylmethacrylate was synthesized under the optimized conditions, isolating by precipitation (M_n = 4,200, M_w/M_n = 1.12).   Following this, the PMMA sample was resubjected to the optimized conditions with benzyl methacrylate, taking no precautions to eliminate air from the reaction.   The chain

extension showed little to no tailing in the homopolymer regime (Figure 5.2b), indicating that living chain ends were present.   This is significant as it indicates that oxygen did not irreversibly terminate the polymer chain ends, even whenever the polymerization is conducted with no degassing.

D. Catalyst Degradation Studies

The origin of polymerization control in the presence of oxygen was next explored, with particular focus on understanding the need for higher catalyst loadings. An initial hint was found by analyzing the ^{1}H NMR of a crude polymerization mixture, whereby it was observed that a large portion of catalyst had been converted to the sulfoxide (PTH-SO, Figure S5.1). This was confirmed by independently synthesizing PTH-SO and comparing the respective ^{1}H NMR spectra. Subsequently, to test for controlled polymerization when using PTH-SO, a polymerization was conducted using only PTH-SO as photocatalyst, and no control was observed (Figure S5.2). Further, very little conversion was observed during the polymerization (10 % after 3 h), indicating that although present during the reaction, PTH-SO may not be involved mechanistically as it is not a highly reducing photocatalyst.

Next, a series of control experiments were conducted to gain insight into PTH oxidation (Scheme 5.1). First, a solution containing PTH was irradiated without degassing in the presence of the polymerization initiator, and after 2 h it was completely converted to the sulfoxide form. PTH was then irradiated without added initiator, and after 6 h no conversion to the sulfoxide was observed. Based on these results, a mechanistic hypothesis for catalyst degradation is proposed in Scheme 5.2. Upon irradiation, PTH enters an excited state and undergoes a single electron transfer in the presence of an alkyl bromide. The resulting radical cation is then highly susceptible to reaction with oxygen, and undergoes degradation

175

to PTH-SO. When using higher catalyst loadings, the oxygen will be consumed in the initial portion of the reaction, causing no significant chain end degradation and leaving a portion of catalyst to undergo controlled polymerization.
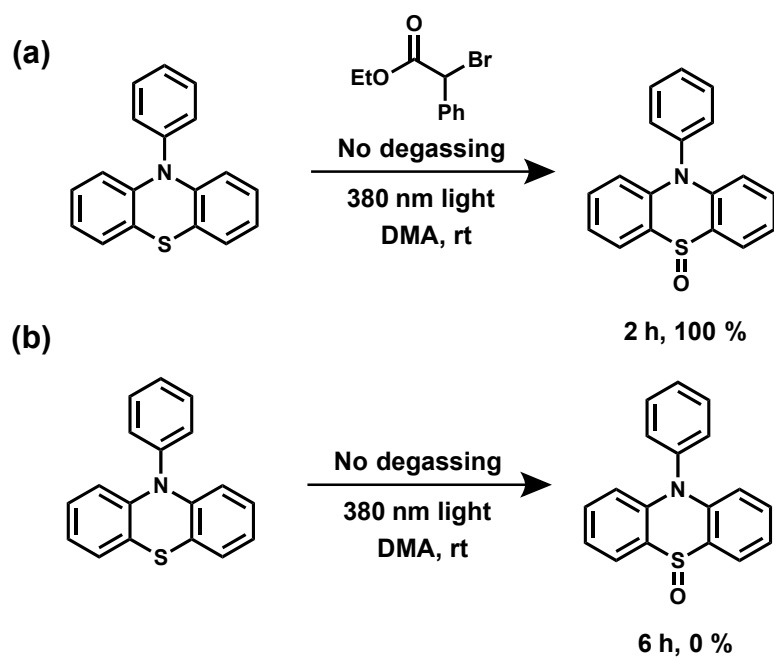
Scheme 5.1 Reactions conducted with only PTH and initiator and (b) just phenothiazine with no degassing
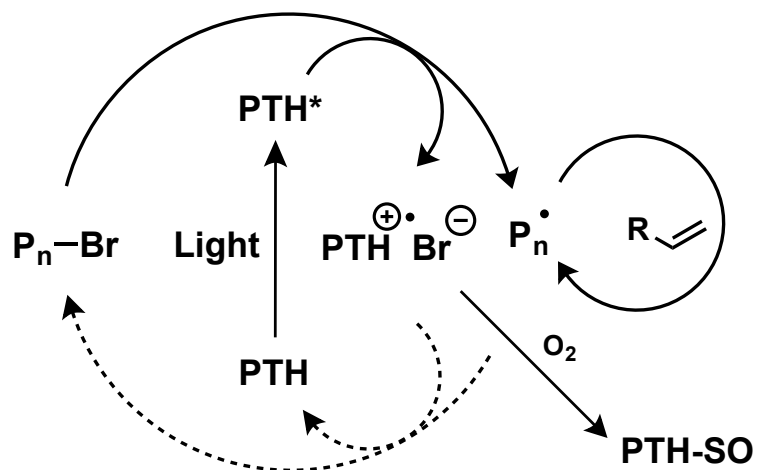
Scheme 5.2 Proposed mechanism of catalyst degradation due to oxygen reacting with oxidized PTH. PTH-SO = 10-phenyl phenothiazine sulfoxide

To test this, it was hypothesized that higher volumes of air in a reaction should thus lead to complete catalyst degradation to the sulfoxide, and uncontrolled polymerization. Indeed, when the headspace of the reaction flask was increased (Table 5.2), a drastic increase in dispersity was observed. Further, ^{1}H NMR confirmed complete conversion of PTH to PTH-SO.

Table 5.2 Polymerization of benzyl methacrylate with increasing headspace volume, thus including more oxygen[a]
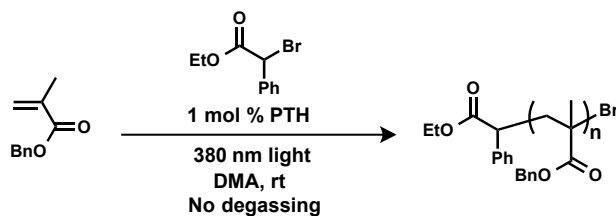
Entry	Reaction flask	Headspace volume	Conversion	GPC M_n (g/mol)	M_n (theoretical) (g/mol)	M_w / M_n
1	1 dram vial	3.4 mL	57 %	7,700	11,400	1.62
2	3 dram vial	7.4 mL	57 %	10,100	11,400	2.02
3	Scintillation vial	23.4 mL	49 %	17,300	9,800	2.06

[a] Reaction conditions: BnMA (1 equiv.), 10-phenylphenothiazine (0.01 equiv.), initiator (0.009 equiv), DMA (2.7 M of BnMA) at room temperature with irradiation from 380 nm LEDs for 4 h (M_n = number average molecular weight; M_w = weight average molecular weight). M_n and M_w / M_n determined using size exclusion chromatography (SEC) or ^{1}H NMR

III. Conclusions

In conclusion, we have demonstrated a successful oxygen tolerant metal-free, atom transfer radical polymerization. By simply raising catalyst loadings to overcome oxygen effects, degassing could be avoided altogether, opening the doors for non-experts to conduct these polymerizations to synthesize a variety of complex materials.

IV. References

[1]   J. Mosnáček, A. Eckstein-Andicsová, K. Borská, *Polym. Chem.* **2015**, *6*, 2523–2530.

[2]   K. Min, W. Jakubowski, K. Matyjaszewski, *Macromol. Rapid Commun.* **2006**, *27*, 594–598.

[3]   K. Matyjaszewski, H. Dong, W. Jakubowski, J. Pietrasik, A. Kusumo, *Langmuir* **2007**, *23*, 4528–4531.

V. *Supplementary Information*

A. General Reagent Information

All polymerizations were carried out under an argon atmosphere.   Anhydrous *N,N*-Dimethylacetamide was purchased from Sigma-Aldrich and used as received.   Methyl methacrylate and benzyl methacrylate were purchased from Sigma-Aldrich and passed through a plug of basic alumina before use.   Ethyl α-bromophenylacetate, phenothiazine, RuPhos, and chlorobenzene were purchased from Sigma-Aldrich and used as received. RuPhos Precatalyst was purchased from Strem Chemicals Inc.

B. General Analytical Information

Nuclear magnetic resonance spectra were recorded on a Varian 400 MHz, aVarian 500 MHz, or a Varian 600 MHz instrument. All ^{1}H NMR experiments are reported in δ units, parts per million (ppm), and were measured relative to the signals for residual chloroform (7.26 ppm) in the deuterated solvent, unless otherwise stated. All ^{13}C NMR spectra are reported in ppm relative to deuterochloroform (77.23 ppm), unless otherwise stated, and all were obtained with ^{1}H decoupling. Gel permeation chromatography (GPC) was performed on a Waters 2695 separation module with a Waters 2414 refractive index detector in chloroform with 0.25% triethylamine. Number average molecular weights (M_n) and weight average molecular weights (M_w) were calculated relative to linear polystyrene standards for calculation of M_w/M_n.

C. Light Source

LED strips (380 nm) were bought from elemental led (see www.elementalled.com) and used as shown below (Figure S1). Reactions were placed next to the 380 nm lights under vigorous stirring while cooling with compressed air. The light intensity was measured to be 1.6 mW/cm^2.

Figure S5.1. General reaction setup.

D. General Procedure for Table 5.1:
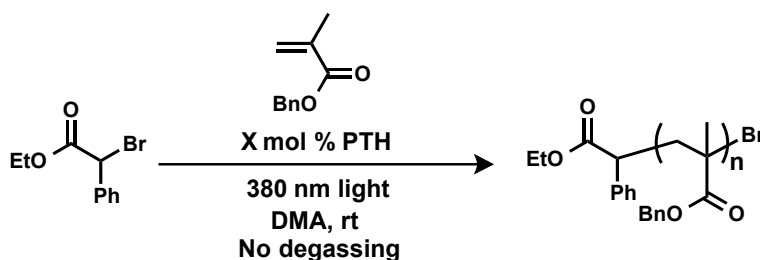
A vial equipped with a magnetic stir bar and fitted with a teflon screw cap septum was charged with benzyl methacrylate (635 μL, 3.75 mmol), photocatalyst (0.1-1 mol %) and dimethylacetamide (1 mL). The reaction mixture was capped without any degassing precautions taken. Lastly, ethyl α-bromophenylacetate (5.8 μL, 0.033 mmol) was added. The reaction was vigorously stirred in front of 380 nm LEDs while cooling with compressed

air to maintain ambient temperature. The reaction was allowed to proceed to ca. 50 %

conversion of benzyl methacrylate as monitored by ^{1}H NMR. An aliquot was taken and

analyzed using GPC to give the molecular weight (M_n) and molecular weight distribution

(M_w/M_n) of the polymer.

E. Procedure for Figure 5.1:

A vial equipped with a magnetic stir bar and fitted with a teflon screw cap septum was

charged with benzyl methacrylate (635 µL, 3.75 mmol), PTH (5.2 mg, 0.5 mol %)

dimethylacetamide (1 mL), and ethyl α-bromophenylacetate (5.8 µL, 0.033 mmol), with the

initiator being added last. The reaction was then vigorously stirred in front of 380 nm LEDs

while cooling with compressed air to maintain ambient temperature. Aliquots were taken

throughout the reaction using degassed syringes in order to avoid further introduction of

oxygen. The reaction was turned off periodically by wrapping the vial in aluminum foil.

Conversion was monitored by ^{1}H NMR. The molecular weight and molecular weight

distribution (M_w/M_n) of the polymer were found using GPC.

F. Procedure for Figure 5.2:

Poly(methyl methacrylate) A vial equipped with a magnetic stir bar and fitted with a rubber septum was charged with methyl methacrylate (2.4 mL, 22.5 mmol), 10-phenylphenothiazine (31 mg, 0.5 mol %) and dimethylacetamide (6 mL). The reaction mixture was capped without any degassing precautions taken. Lastly, ethyl α-bromophenylacetate (39 μL, 0.225 mmol) was added. The reaction was stirred in front of 380 nm LEDs while cooling with compressed air to maintain ambient temperature. The reaction was stirred in front of the light for 3.5 h (29 % conversion), and stopped by precipitating into hexanes (250 mL). The white precipitate was decanted, and re-dissolved in dichloromethane before precipitating again into hexanes (250 mL) to yield 517 mg of a white powder. M_n = 4,200 g/mol, M_w/M_n = 1.12.

182

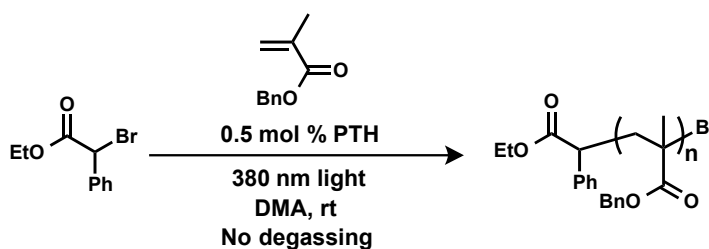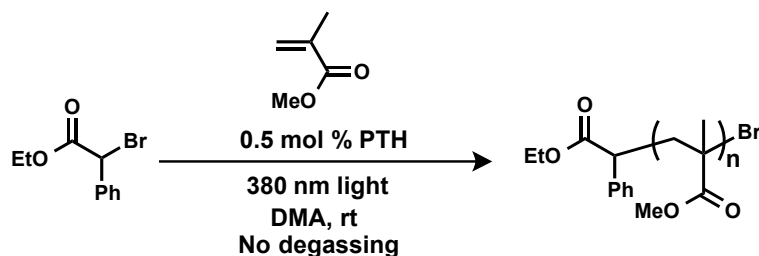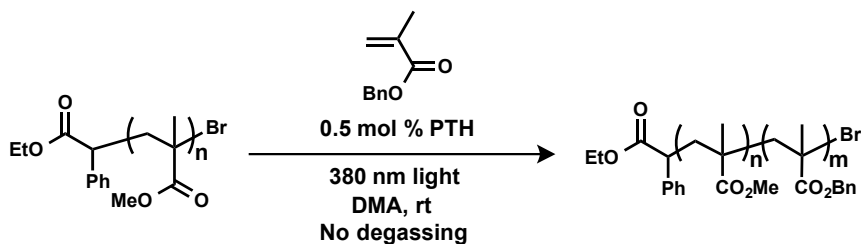**Poly(methyl methacrylate)-b-(benzyl methacrylate)** A vial equipped with a magnetic stir bar and fitted with a teflon screw cap septum was charged with benzyl methacrylate (617 µL, 3.64 mmol), PTH (5 mg, 0.5 mol %), poly(methyl methacrylate) macroinitiator (90 mg, 0.0214 mmol), and dimethylacetamide (1 mL). The reaction mixture was capped without any degassing precautions taken. The reaction was stirred in front of 380 nm LEDs while cooling with compressed air to maintain ambient temperature. After 4 h (33 % conv.) the reaction was stopped by opening to air and precipitated into methanol (20 mL). The precipitate was filtered and re-dissolved in CH_2Cl_2 before re-precipitating into methanol. The product was analyzed by ^{1}H NMR and GPC. (yield: 94 mg of a white powder) M_n = 17,200 g/mol, M_w/M_n = 1.23.
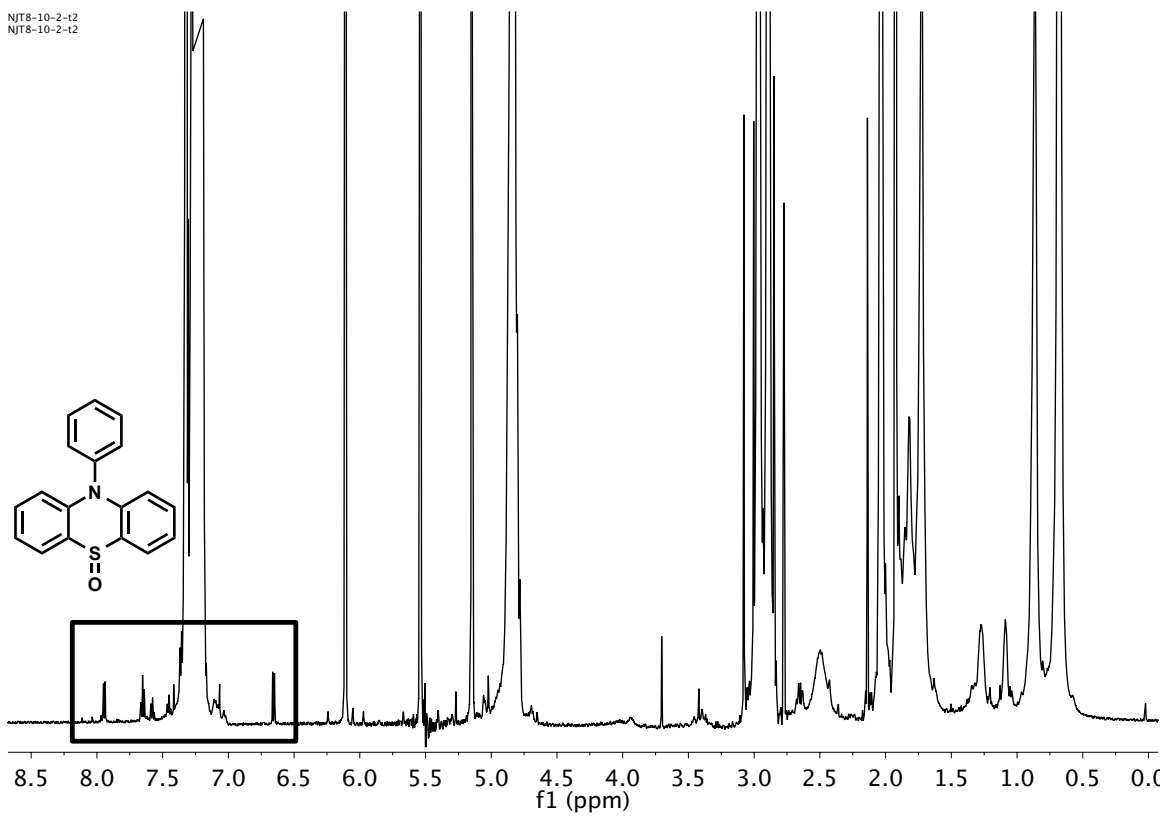
Figure S5.2 ^{1}H NMR of a polymerization using PTH with no degassing, highlighting the peaks corresponding to PTH-sulfoxide in the aromatic regime
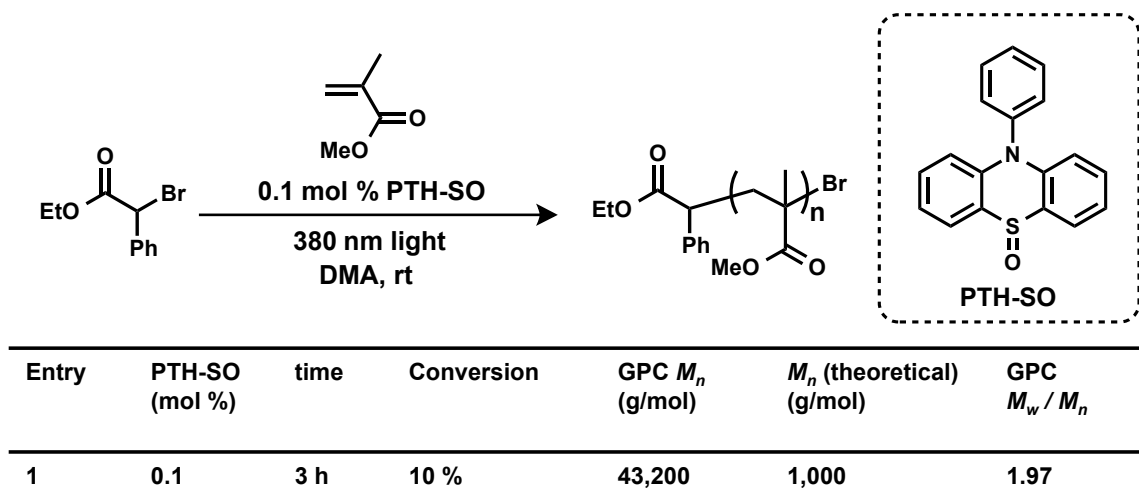
Figure S5.3 Polymerization conducted using 0.1 mol % PTH-SO, showing no control and a low conversion under typical conditions

Entry	PTH-SO (mol %)	time	Conversion	GPC M_n (g/mol)	M_n (theoretical) (g/mol)	GPC M_w / M_n
1	0.1	3 h	10 %	43,200	1,000	1.97

6. Exploring the Structure-Property Relationships of Phenothiazine-based Metal-free ATRP Photocatalysts

I. Introduction

This chapter will focus on the work conducted in an effort to optimize the photocatalyst used in metal-free ATRP. The motivation behind this work will be briefly described for each section, however the broader motivation was to design a photocatalyst system for lower dispersities, greater monomer tolerance, and higher molecular weights for metal-free ATRP. Motivation for the broader goal of conducting metal-free ATRP is discussed in chapter 3.

II. Results and Discussion

A. Electronic, Steric, and Heteroatom Variations

Figure 6.1 displays a variety of phenothiazine-based catalysts with various structural modifications in hopes of changing the properties of polymerization catalysis. These catalysts were tested for the polymerization of methyl methacrylate, with the hope of accessing lower dispersities, and targeting higher molecular weights, at high conversions. Catalysts **1-3** were synthesized in hopes of making a more electron deficient photocatalyst by installing an electron withdrawing group on the aryl ring conjugated to the phenothiazine core. Indeed, upon measuring the oxidation potential of the ground state and the luminescence, it could be seen that the excited state reduction potentials ($E_{1/2}$*, see Figure 6.1) were significantly raised from that of 10-phenylphenothiazine ($E_{1/2}$* = -2.1 V vs. SCE). Excited state reduction potentials were calculated according to the equation discussed in chapter 4:

$$E^{*}_{1/2} = E_{1/2}{}^{ox} - hc / \lambda_{max}$$

where $E^{*}_{1/2}$ is the excited state reduction potential, $E_{1/2}{}^{ox}$ is the ground state oxidation potential, h is Planck's constant, c is the speed of light and λ_{max} is the photoluminescence maximum.
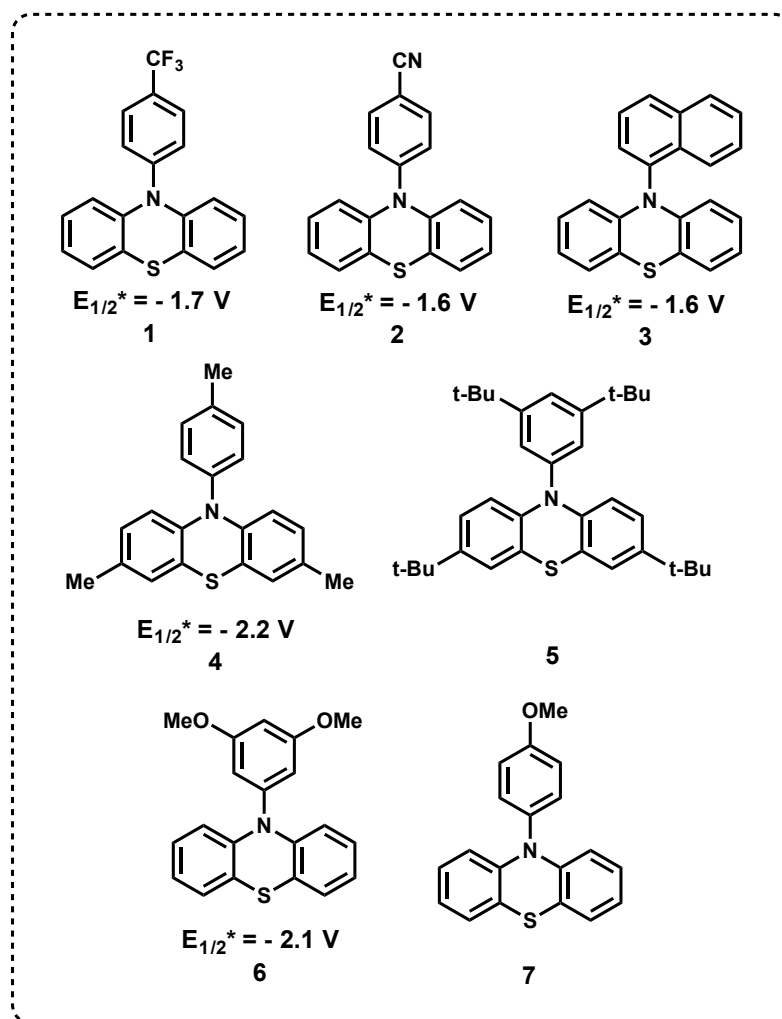

Figure 6.1 Various phenothiazine-based catalysts synthesized in hopes of improving metal-free ATRP. However, even when varying both electronics **1-3**, blocking substitution positions (**4**), changing the steric environment (**5**), or adding donating groups to the phenyl ring (**6-7**), polymerization characteristics showed little observable differences from the

original 10-phenyl phenothiazine photocatalyst discussed in chapter 3. (see SI for polymerization procedure)

The originally reported Ir(ppy)$_3$ catalyst system gave better polymerization characteristics than PTH (i.e. lower dispersities and access to higher molecular weights with control), thus, it was hypothesized that lower reduction potentials would aid the polymerization process. However, upon synthesizing and testing photocatalysts **1-3** with excited state reduction potentials in the range of Ir(ppy)$_3$ (E$_{1/2}$* = - 1.7 V vs. SCE), no improvement in control over the polymerization was observed. Although a controlled system was still in place for each of these catalysts, and block copolymers were made using catalyst **1** (Figure S6.1), no significant difference in the polymerization behavior (i.e. rates, dispersities, etc…) was observed.

It was then hypothesized that blocking photocatalyst degradation would help gain better control over polymerization. Catalyst **4** was thus synthesized in order to block the para-positions of the catalyst to avoid any substitution events during the polymerization. Unfortunately, catalyst **4** again gave polymerization characteristics very similar to that of the parent PTH system. Catalyst **5** was then synthesized in order to test whether having a sterically crowded environment around the photocatalyst would aid in the single electron process, giving more efficient polymerizations. Again, no observable difference from PTH occurred for the polymerization of methyl methacrylate. Finally, catalysts **6-7** were synthesized in order to test the effect of donating groups onto the phenothiazine scaffold, and no appreciable differences for the polymerization behavior were observed. In all cases for catalysts **1-7**, control over the polymerization of methyl methacrylate still occurred, but no legitimate differences were observed when compared to the parent PTH system.

Another catalyst that was synthesized and tested was a boron triphenothiazine derivative (Figure 6.2).[1] This derivative was known to have a stable radical cation, and was measured to have an excited state reduction potential ($E_{1/2}* = - 2.1$ V vs. SCE), similar to that of PTH. Indeed, at 0.05 mol % catalyst loading, controlled polymerization of methyl methacrylate was observed, with low dispersities ($M_w/M_n = 1.38$). Although just one working example is shown, this catalyst was shown to give control over polymerizations in a manner similar to PTH.

Entry	time	Conversion	GPC M_n (g/mol)	M_n (theoretical) (g/mol)	M_w / M_n
1	5 h	34 %	4,500	3,400	1.38
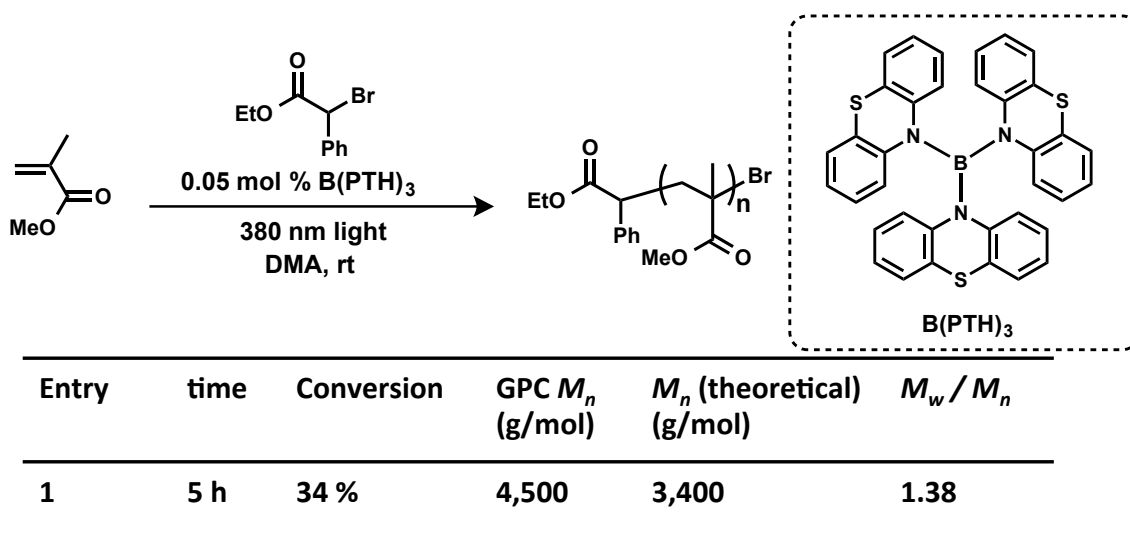
Figure 6.2 Working example of a boron-based phenothiazine catalyst, demonstrating that other catalyst scaffolds can control polymerizations

B. Failed Photocatalysts

Figure 6.3 displays a variety of catalysts that did not give any control over the polymerization under the conditions tested (using 0.1 mol % photocatalyst, see SI). A hypothesis for the reason for lack of control will be given in each case, however it should be pointed out that perhaps through further studies control may be achieved. The phenoxazine catalyst was synthesized to understand if the sulfur of the phenothiazine was essential to the

process. However, although it gave no control for the polymerization of methyl methacrylate, this is potentially due to its decreased absorbance at 380 nm. The other catalysts displayed in Figure 6.3 are hypothesized to be not reducing enough to undergo polymerization due to the fact that little or no polymerization of methyl methacrylate was observed in each case. Further, the bis-*meta*-CF₃-PTH and *para*-NO₂-PTH were both shown to have no emission. If no emission occurs, the catalyst is not able to undergo the single electron transfer to initiate polymerization.

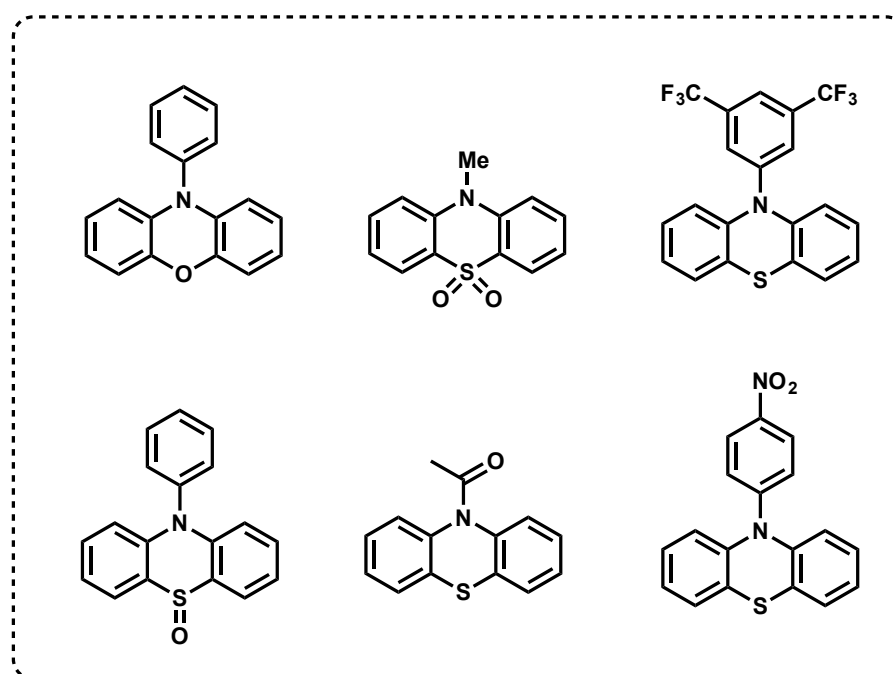**Figure 6.3** Photocatalysts that did not give control over polymerizations of methyl methacrylate (see SI for conditions)

C. Sulfur Free Photocatalysts

Next, a commercially available photocatalyst was tested to understand if the phenothiazine system was essential. Perhaps the simplest analogue to PTH is a triarylamine. A number of commercially available triarylamines were tested and found to give no control

over polymerization. In the case of triphenylamine, it is known that it can undergo dimerization leading to degradation when oxidized. Thus, by blocking the *para* position of triphenylamine with a methyl group (tritolylamine), some control over polymerization can be observed (Figure 6.4). After a brief screen of catalyst concentrations (0.01 – 5 mol %), it was found that 1 mol % tritolylamine gave some control, with dispersities near 1.5, and molecular weights near that of the theoretical value. Further, the molecular weight was shown to increase during the polymerization as a function of conversion. This gives initial support that the sulfur of phenothiazine is not necessary for polymerization control. However, further work is necessary to understand fully the potential of this system.
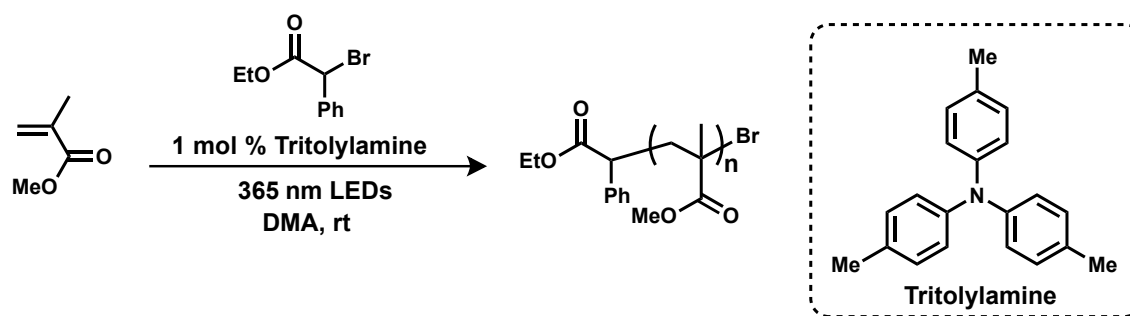
Entry	time	Conversion	GPC M_n (g/mol)	M_n (theoretical) (g/mol)	M_w/M_n
1	2 h	9 %	3,400	900	1.5
2	4 h	16 %	3,500	1,600	1.52
3	21 h	74 %	5,400	7,400	1.63

Figure 6.4 Initial results using tritolylamine as photocatalyst suggesting that control can be achieved over MMA polymerizations with simple, commercially available metal and sulfur free catalysts.

D. Visible Light Photocatalysts

Another goal for metal-free ATRP was to use a more mild source of energy than 380 nm LEDs (i.e. visible light). By synthesizing a visible light absorbing photocatalyst with similar redox properties, this may be achieved. Thus, bisacetoxy PTH was synthesized and measured to have an excited state reduction potential of -1.5 (vs. SCE), as well as absorb well into the visible regime (Figure 6.6). A variety of catalyst loadings were tested and it was found that 0.5 mol % catalyst could give some control over the polymerization process (Figure 6.5). Although this does not thoroughly demonstrate control over the process, it is some indication that this catalyst could gain control with more optimization. However, the Achilles heal of this catalyst appears to be it's sluggish kinetics (Entry 2, 16 h and 19 % conversion).
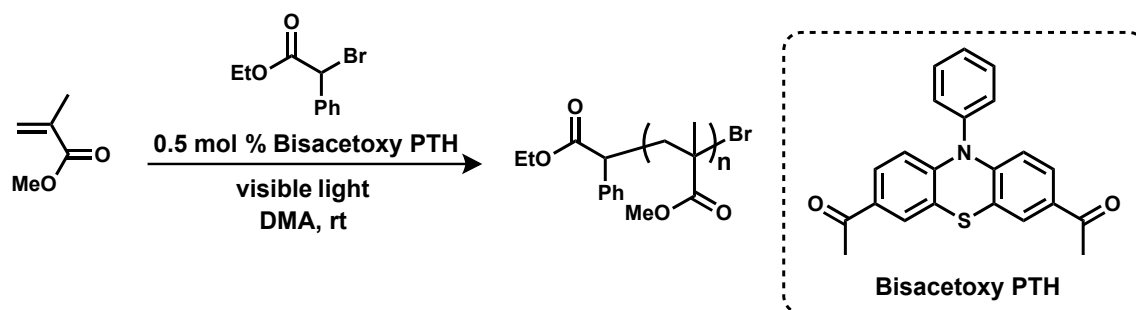
Entry	time	Conversion	GPC M_n (g/mol)	M_n (theoretical) (g/mol)	M_w / M_n
1	4 h	10 %	2,500	1,000	1.21
2	16 h	19 %	3,700	1,900	1.37

Figure 6.5 Bisacetoxy PTH polymerizations using visible light (465 nm LEDs), showing an initial proof of control over this process.
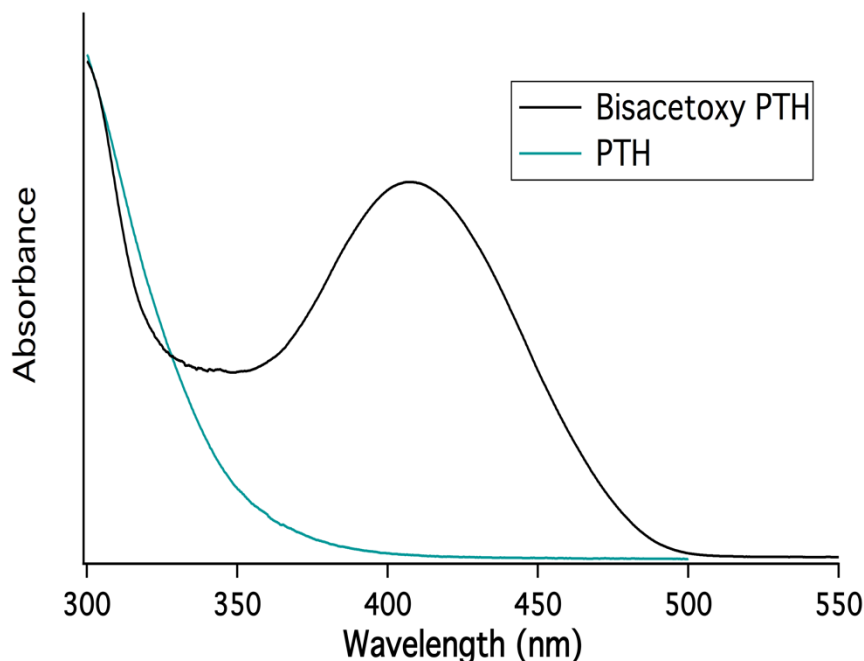
Figure 6.6 UV-Vis spectroscopy of PTH and Bisacetoxy PTH (~0.1 mM solutions), demonstrating visible light absorbance for Bisacetoxy PTH

III. Conclusions

The goal of this chapter was to summarize a significant portion of work conducted to optimize catalyst performance through varying the structure of the phenothiazine scaffold. Although these results are largely disappointing, they may be used as a reference for future research in the area, and they demonstrate some initial successes in exciting areas, such as visible light photopolymerizations and more simplified, commercially available catalyst systems. This is hoped to inspire the reader to look deeper into such systems, or to use the principles found and apply them to make other systems work more efficiently. Further, these results emphasize just how important it is to develop a better mechanistic understanding of metal-free ATRP, which will be the focus of chapter 7.

IV. Acknowledgements

Catalysts **4-5** were synthesized by Saemi Oh Poelma. Bisacetoxy PTH and catalyst **6** was synthesized by Zac Hudson and Joseph Mann. The PTH-sulfoxide was synthesized by Yingdong Luo. The para-NO$_2$-PTH and catalysts **2-3** were synthesized by Jelle Adan.

V. References

[1] S. Suzuki, K. Yoshida, M. Kozaki, K. Okada, *Angew. Chem. Int. Ed.* **2013**, *52*, 2499–2502.

VI. Supplementary Information

A. General Procedure for Figure 6.1
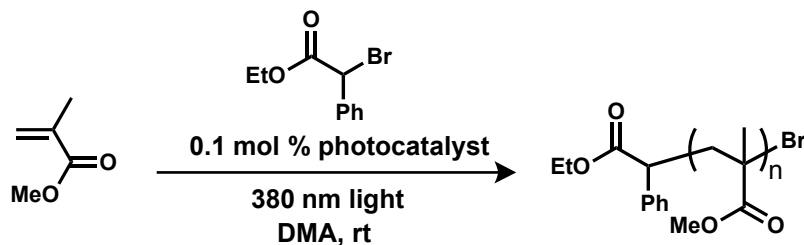
A vial equipped with a magnetic stir bar and fitted with a teflon screw cap septum was charged with methyl methacrylate (401 µL, 3.75 mmol), photocatalyst **1-7** (0.1 mol %) and dimethylacetamide (1 mL). The reaction mixture was degassed with three freeze-pump-thaw cycles. The vial was then backfilled with argon and ethyl α-bromophenylacetate (6.6 µL, 0.0375 mmol) was injected via syringe. The reaction was vigorously stirred in front of 380 nm LEDs while cooling with compressed air to maintain ambient temperature. The conversion of MMA was determined by ^{1}H NMR An aliquot was taken and analyzed using GPC to give the molecular and molecular weight distribution of the polymer.
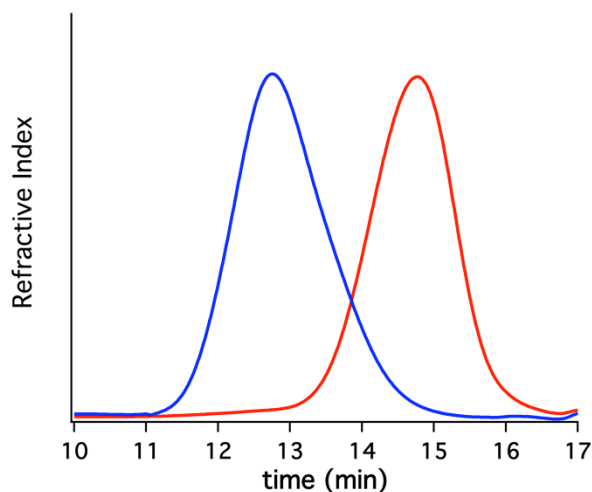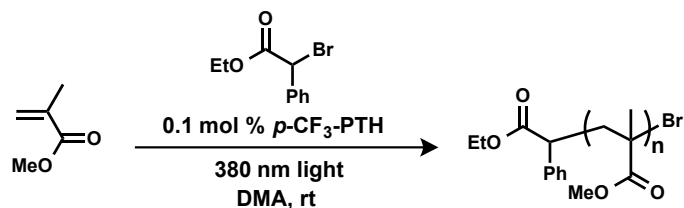
Figure S6.1 Block copolymer PMMA-*b*-PBnMA (blue trace) synthesized with ***p*-CF₃-PTH (1)** as catalyst. PMMA homopolymer is shown in red.

B. Procedure for Figure S6.1

Poly(methyl methacrylate) A vial equipped with a magnetic stir bar and fitted with a rubber septum was charged with methyl methacrylate (2.4 mL, 22.5 mmol), *p*-CF₃-PTH (**1**) (7.7 mg, 0.1 mol %) and dimethylacetamide (6 mL). The reaction mixture was degassed with three freeze-pump-thaw cycles. The vial was then backfilled with argon and benzyl α-bromophenylacetate (39 μL, 0.225 mmol) was injected via syringe. The reaction was stirred in front of 380 nm LEDs while cooling with compressed air to maintain ambient temperature. The reaction was stirred in front of the light for 2.5 h (17 % conv.) and then put into the dark by wrapping it in aluminum foil. A syringe wrapped in aluminum foil was used to transfer the reaction mixture in the dark into a stirring solution of hexanes (50 mL,

also wrapped in aluminum foil). The white precipitate was decanted, and re-dissolved in dichloromethane before precipitating again into hexanes to yield 280 mg of a white powder. M_n = 3,300 g/mol, M_w/M_n = 1.33.
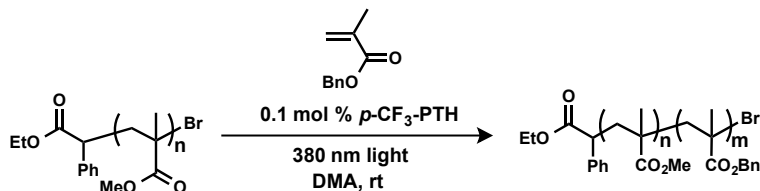
Poly(methyl methacrylate)-b-(benzyl methacrylate) A vial equipped with a magnetic stir bar and fitted with a teflon screw cap septum was charged with benzyl methacrylate (595 µL, 3.51 mmol), *p*-CF$_3$-PTH (**1**) (1.2 mg, 0.1 mol %) and dimethylacetamide (500 µL). In another flask, 500 µL of dimethylacetamide was added to the poly(methyl methacrylate) macroinitiator (49 mg, 0.031 mmol). Both reaction mixtures were degassed with three freeze-pump-thaw cycles. Using a syringe, the monomer and catalyst were then transferred to the flask containing macroinitiator. The reaction was stirred in front of 380 nm LEDs while cooling with compressed air to maintain ambient temperature. After 4 h the reaction was stopped by opening to air and precipitated into MeOH (20 mL). The product was filtered, redissolved in CH$_2$Cl$_2$, and precipitated into MeOH again (20 mL). (yield: 201 mg of a white powder) M_n = 10,800 g/mol, M_w/M_n = 1.44.
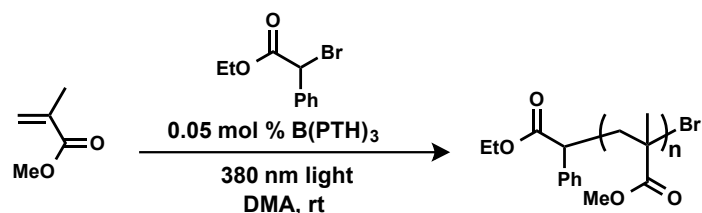
C. Procedure for Figure 6.2

A vial equipped with a magnetic stir bar and fitted with a teflon screw cap septum was charged with methyl methacrylate (401 µL, 3.75 mmol), **B(PTH)₃** (1.1 mg, 0.05 mol %) and dimethylacetamide (1 mL). The reaction mixture was degassed with three freeze-pump-thaw cycles. The vial was then backfilled with argon and benzyl α-bromophenylacetate (6.6 µL, 0.0375 mmol) was injected via syringe. The reaction was vigorously stirred in front of 380 nm LEDs for 5 h while cooling with compressed air to maintain ambient temperature. Conversion of MMA was determined by ^{1}H NMR to be 34%. An aliquot was taken and analyzed using GPC to give the molecular weight (M_n = 4,500 g/mol) and molecular weight distribution (M_w/M_n = 1.38) of the polymer.

D. General Procedure for Figure 6.3
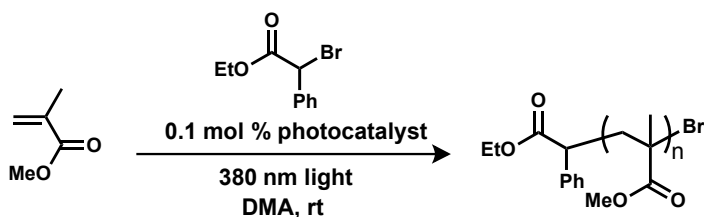
A vial equipped with a magnetic stir bar and fitted with a teflon screw cap septum was charged with methyl methacrylate (401 µL, 3.75 mmol), photocatalyst (0.1 mol %) and dimethylacetamide (1 mL). The reaction mixture was degassed with three freeze-pump-thaw cycles. The vial was then backfilled with argon and ethyl α-bromophenylacetate (6.6 µL,

0.0375 mmol) was injected via syringe. The reaction was vigorously stirred in front of 380 nm LEDs while cooling with compressed air to maintain ambient temperature. The conversion of MMA was determined by ^{1}H NMR An aliquot was taken and analyzed using GPC to give the molecular and molecular weight distribution of the polymer

E. Procedure for Figure 6.4

A vial equipped with a magnetic stir bar and fitted with a teflon screw cap septum was charged with methyl methacrylate (401 µL, 3.75 mmol), tritolylamine (1 mol %) and dimethylacetamide (1 mL). The reaction mixture was degassed with three freeze-pump-thaw cycles. The vial was then backfilled with argon and ethyl α-bromophenylacetate (6.6 µL, 0.0375 mmol) was injected via syringe. The reaction was vigorously stirred in front of 380 nm LEDs while cooling with compressed air to maintain ambient temperature. The conversion of MMA was determined by ^{1}H NMR An aliquot was taken and analyzed using GPC to give the molecular and molecular weight distribution of the polymer.

F. Procedure for Figure 6.5

A vial equipped with a magnetic stir bar and fitted with a teflon screw cap septum was charged with methyl methacrylate (401 µL, 3.75 mmol), bisacetoxy PTH (0.5 mol %) and dimethylacetamide (1 mL). The reaction mixture was degassed with three freeze-pump-thaw cycles. The vial was then backfilled with argon and ethyl α-bromophenylacetate (6.6 µL, 0.0375 mmol) was injected via syringe. The reaction was vigorously stirred in front of 380 nm LEDs while cooling with compressed air to maintain ambient temperature. The conversion of MMA was determined by ^{1}H NMR An aliquot was taken and analyzed using GPC to give the molecular and molecular weight distribution of the polymer.
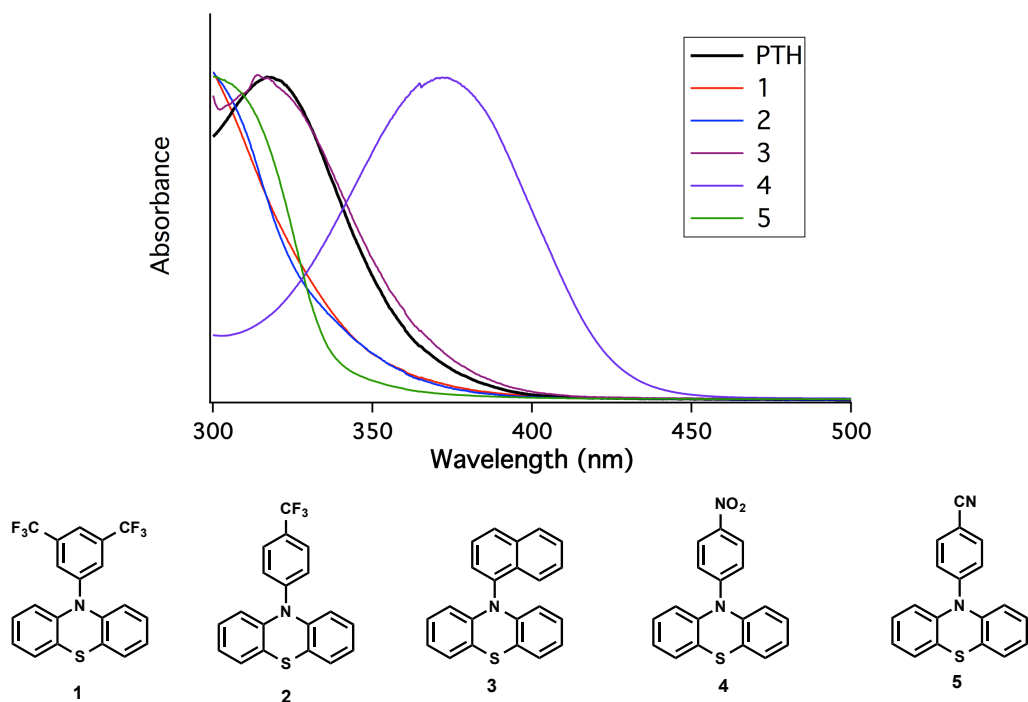
Figure S6.2 UV-Vis of a variety of phenothiazine derivatives (in MeCN at ~0.1 mM)

$E_{1/2}{}^* = -1.9$ V $E_{1/2}{}^* = -2.1$ V $E_{1/2}{}^* = -2.2$ V $E_{1/2}{}^* = -1.9$ V $E_{1/2}{}^* = -1.9$ V

$E_{1/2}{}^* = $ N/a
No emission

$E_{1/2}{}^* = $ N/a
No emission

$E_{1/2}{}^* = -2.1$ V

$E_{1/2}{}^* = -2.3$ V

Figure S6.3 Phenothiazine derivatives synthesized and studied, with excited state reduction

potentials listed beneath the catalysts. Due to no emission observed for some catalysts, there

was no way to estimate the potentials (see equation for calculating excited state reduction potentials).

7. Developing a Deeper Mechanistic Understanding of Metal-Free ATRP

I. Introduction

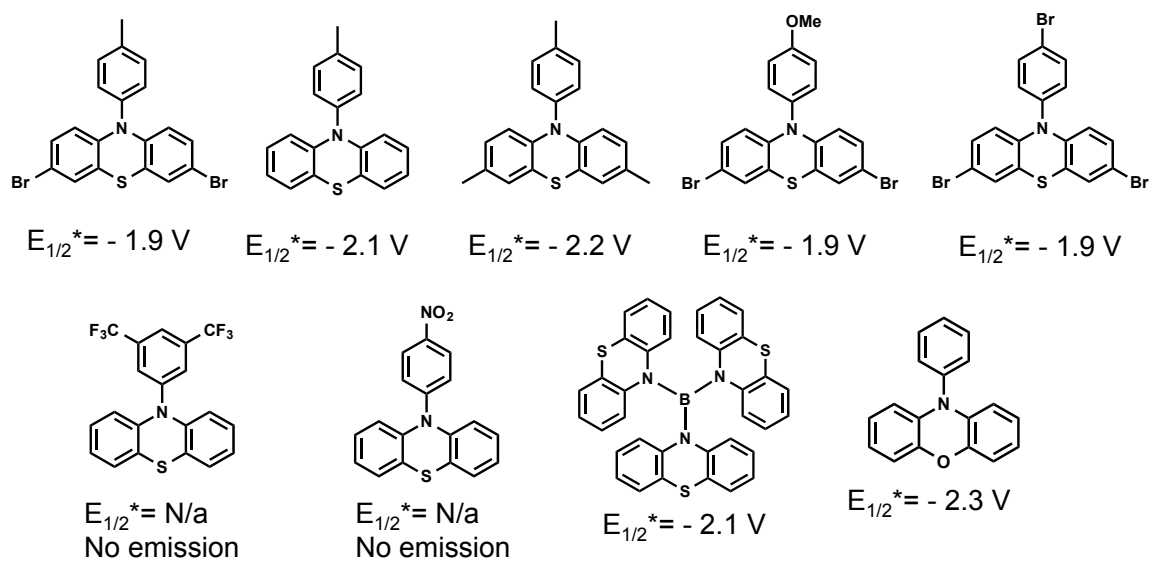Chapter 6 outlined a variety of attempts to gain better control over metal-free ATRP through catalyst optimization, and although many catalysts were synthesized and tested, no increase in control was observed. This spurred an interest in better understanding the mechanism of metal-free ATRP in order to more rationally design a system with better polymerization properties. Motivation for the broader goal of conducting metal-free ATRP is discussed in chapter 3.

Others, particularly the Matyjaszewski group, have also been keen to understand the mechanism of PTH-based metal-free ATRP.[1] Although a comprehensive study was conducted in order to understand the origin of control in metal-free ATRP, aspects of the mechanism remain unexplored. In particular, the aforementioned studies did not experimentally explore the deactivation step of metal-free ATRP.

It is known that chemically oxidized phenothiazine derivatives can be easily isolated and studied.[2,3] We hypothesized that by isolating the radical cation of PTH (Oxo-PTH), a variety of studies may be conducted to better understand the mechanism involved in metal-free ATRP and photoredox based ATRP polymerizations in general. Such mechanistic insight may one day lead to expanding the scope and control of these systems.

II. Results and Discussion

A. Understanding the Relationship of Oxo-PTH and Bromide Anions

Our initial interest in understanding the mechanism came out of a desire to draw from traditional ATRP systems, wherein a deactivator (Cu(II)) could be added in to gain control over certain systems. Thus, the stable radical cation of PTH (Oxo-PTH) was synthesized by combining PTH with tris(4-bromophenyl)ammoniumyl hexachloroantimonate and precipitating in ether (Scheme 7.1).[2,3]
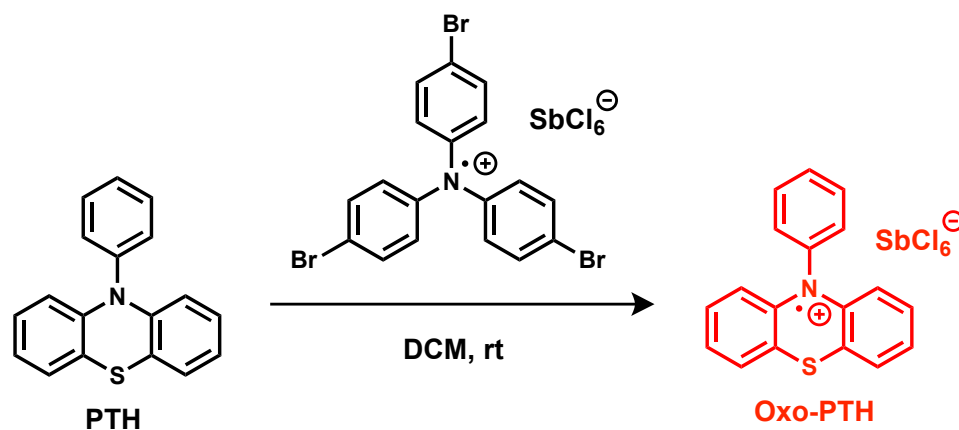
Scheme 7.1 Synthetic route to isolation of oxidized PTH

Having a bench stable form of the polymerization deactivator allows for a variety of studies to be conducted in order to better understand the mechanism. Because the polymerization occurs by PTH reducing a C-Br bond, the hexachloroantimonate counter-ion of the isolate species needed to be exchanged with a bromide. Thus, Oxo-PTH was taken up in acetonitrile, and tetrabutylammonium bromide was added. Upon addition of the bromide anion, a significant color change from deep red to slight yellow was immediately observed. This interesting result sparked further studies to understand the potential for reaction between Oxo-PTH and bromide anions. Initially, EPR spectroscopy was used to confirm

that Oxo-PTH was indeed a radical species in acetonitrile (Figure 7.1b). Following this, bromide anion was added to the same solution, and EPR was measured again, revealing no radical in solution (Figure 7.1c). This indicated that potentially a rapid bromide oxidation was occurring, forming Br-radicals, which will subsequently combine to form Br_2, and in the presence of excess Br anion, form tetrabutylammonium tribromide salts.
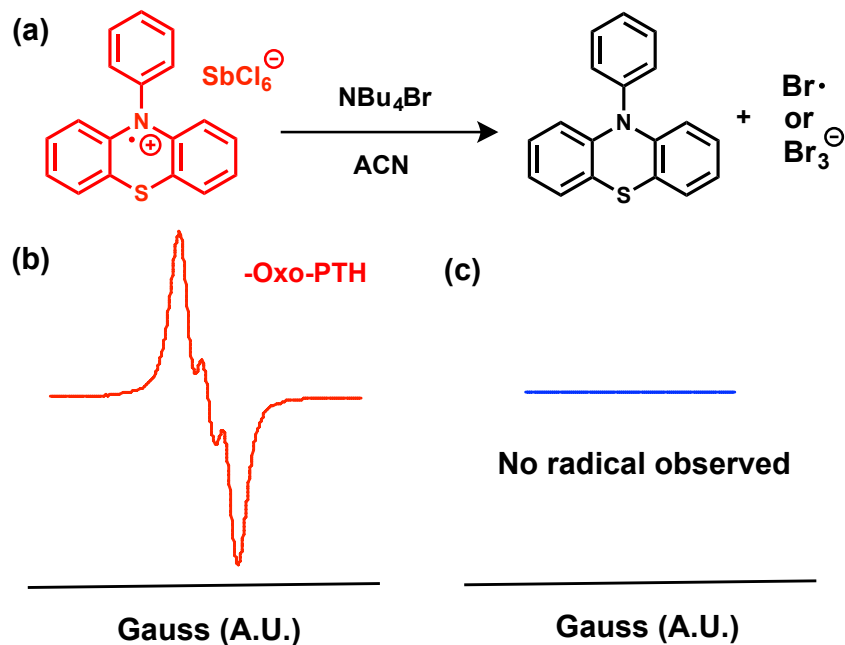

Figure 7.1 (a) Schematic of bromine oxidation by Oxo-PTH to form PTH and bromine radicals, bromine, or tribromide anions in the presence of excess bromide anion (b) EPR spectroscopy of Oxo-PTH, showing radical character in solution (c) EPR spectroscopy after adding in bromide anions, observing no radical character

To test further if the reaction of Oxo-PTH with bromide indeed formed PTH and bromine radicals or Br_2 in solution, UV-Vis and photoluminescence spectroscopy were conducted. When a solution of Oxo-PTH in acetonitrile (~0.1 mM) was analyzed by UV-Vis, the characteristic absorption was observed for a radical species, with absorbance in the

203

680-880 nm range (Figure 7.2). However, upon addition of tetrabutylammonium bromide to the solution, a drastic change in the UV-Vis was observed, with only a slight shoulder relative to that of the PTH spectra. This is indicative of a bromine species (i.e. Br_2 or Br_3 anion) coexisting in solution with the PTH catalyst.
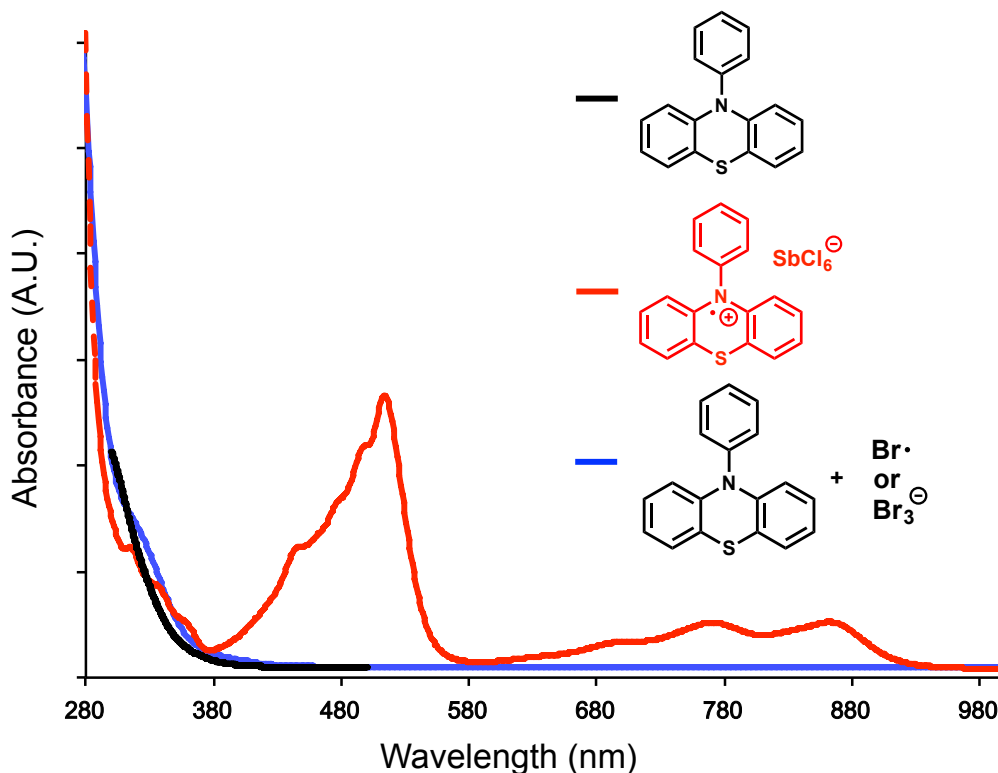

Figure 7.2 UV-Vis spectroscopy of PTH (black), Oxo-PTH (red), and the resulting solution after adding in bromide anion to Oxo-PTH in acetonitrile (blue)

Furthermore, when a luminescence spectrum of Oxo-PTH was obtained, a significantly different emission curve was observed relative to that of the PTH catalyst (Figure 7.3). However, upon addition of bromide anion to the solution, the emission spectrum was observed to shift to the luminescence spectrum of PTH. Again this indicates that immediate oxidation of bromide anions will occur when in the presence of Oxo-PTH (identical behavior for these experiments is observed in *N,N*-dimethylacetamide).
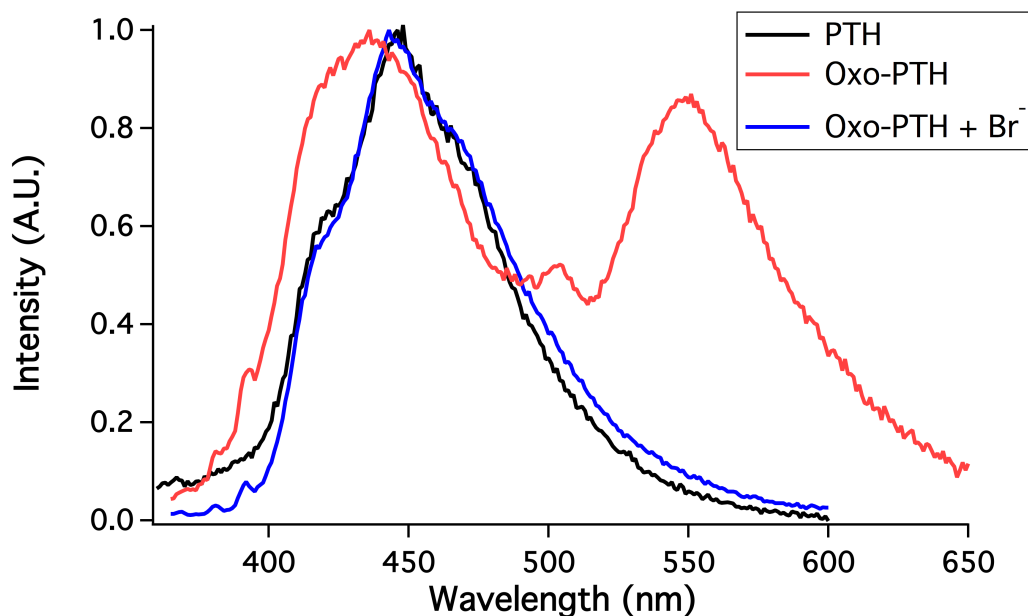
Figure 7.3 Fluorescence spectroscopy of PTH (black), Oxo-PTH (red), and the resulting solution after adding bromide anion to Oxo-PTH in acetonitrile (blue)

Finally, ^{1}H NMR was also employed to study this reaction. Interestingly, when sodium iodide was added to a solution of Oxo-PTH in acetonitrile, sharp peaks of the PTH catalyst were observed (Figure 7.4). However, when various bromide salts were added (LiBr and NBu$_4$Br), broad peaks in the aromatic regime were observed, indicating the potential for incomplete oxidation of the bromine salts. It is well known that a small amount of radical species will cause significant broadening of ^{1}H NMR.[4] Thus, it is hypothesized that an equilibrium exists between Oxo-PTH and the resulting bromine radical species (Scheme 7.2). Due to the previous spectroscopic results, it is likely that the equilibrium lies highly to the side of PTH being in the neutral state and bromine being oxidized. However, ^{1}H NMR indicates that it is also likely that a small amount of Oxo-PTH exists in solution. After 72 h, some bromination of PTH as well as PTH with sharp peaks can be observed in the spectra

(run in both deuterated chloroform and DMF). Thus, if the solution is allowed to reach true equilibrium, the catalyst appears to re-enter it's neutral form. It should be noted that there is also potential that aggregates are formed from the coordination of a bromine species to the catalyst, but further studies are necessary to fully understand this phenomenon.
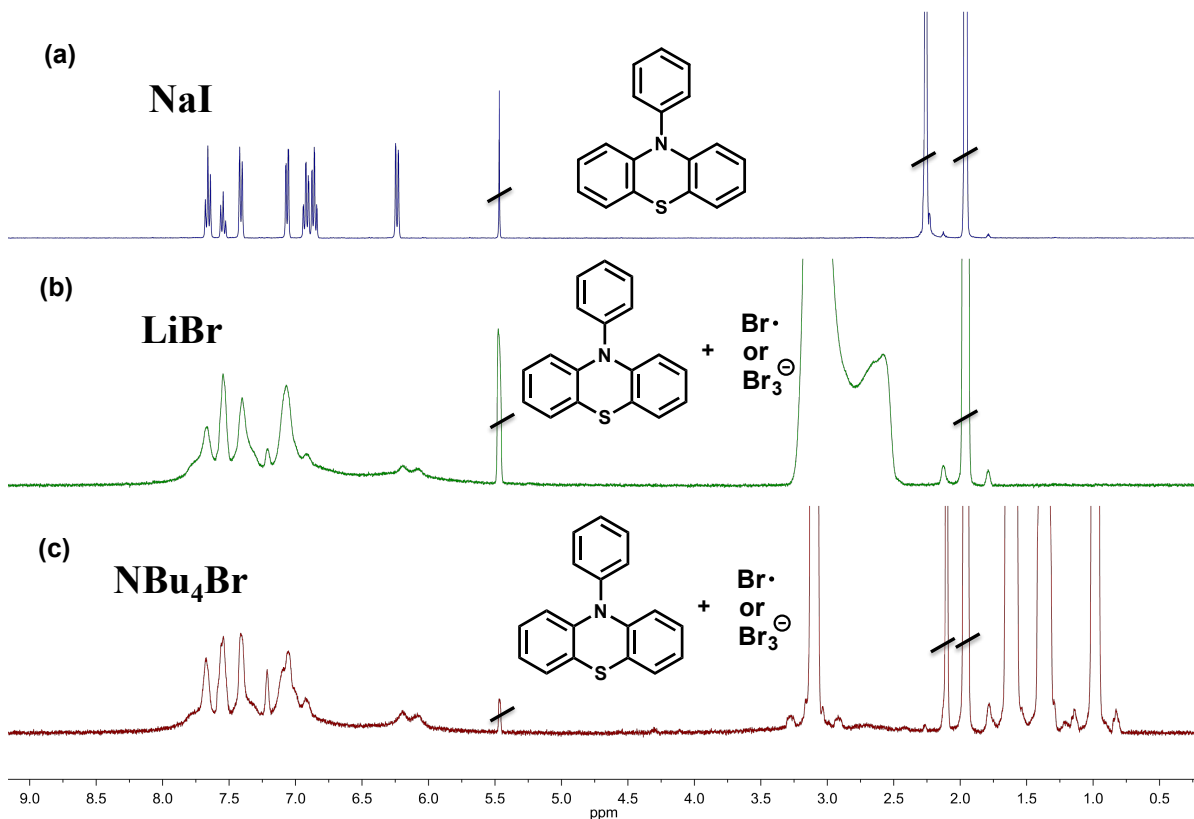

Figure 7.4 Representative ^{1}H NMR after reaction of Oxo-PTH with a variety of salts in acetonitrile.

Scheme 7.2 Equilibrium of bromine oxidation by Oxo-PTH. Based on above experiments, it is suggested that this equilibrium lies far to the right, and Br radicals likely form Br$_2$

As further evidence for the formation of either bromine radicals, bromine, or tribromide anions, a reaction was conducted wherein Oxo-PTH was combined with tetrabutylammonium bromide, and subsequently cyclohexene was added to the reaction. After monitoring with ^{1}H NMR, clear growth of peaks corresponding to the brominated product were observed. As it is well known that bromide anions will not brominate an alkene, this further confirms our hypothesis of a rapid oxidation of bromine by Oxo-PTH. Further, as the oxidation potential of cyclohexene is +2.37, it is thermodynamically highly unfavorable for Oxo-PTH to oxidize the alkene.[5]
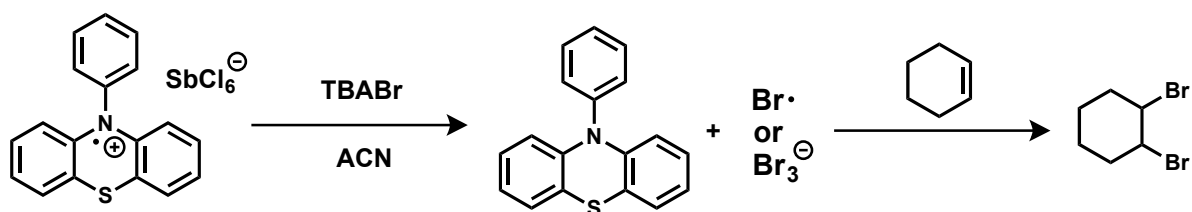
Scheme 7.3 Bromine oxidation by Oxo-PTH, with subsequent addition of cyclohexene giving the brominated product, providing evidence for the formation of bromine in solution

B. Altering Polymerization Properties with Oxo-PTH

The motivation for understanding the relationship of Oxo-PTH with bromide anions comes from the importance of the deactivation step for metal-free ATRP conducted with PTH. Thus, it was then sought to take advantage of this increased mechanistic understanding to alter polymerization characteristics. PTH (0.1 mol %) was combined with MMA in dimethylacetamide, and various amounts of Oxo-PTH (0-0.5 mol %) were added in with tetrabutylammonium bromide in order to observe different reactivity (Figure 7.5). After monitoring the polymerizations, measuring conversion, molecular weight, and dispersities, it was found that increasing amounts of the Oxo-PTH caused slower rates.

Further, the molecular weight vs. conversion were observed to increase linearly for these polymerizations, with dispersities on par with those previously reported, indicating that no control was lost whenever adding in the excess deactivator.

These initial studies indicate that by taking cues from mechanistic studies, polymerization properties could be changed. Further work is needed to understand if increased chain end fidelity is in place, and whether or not other additives (i.e. Br_2 or Br_3) could affect better polymerization properties.
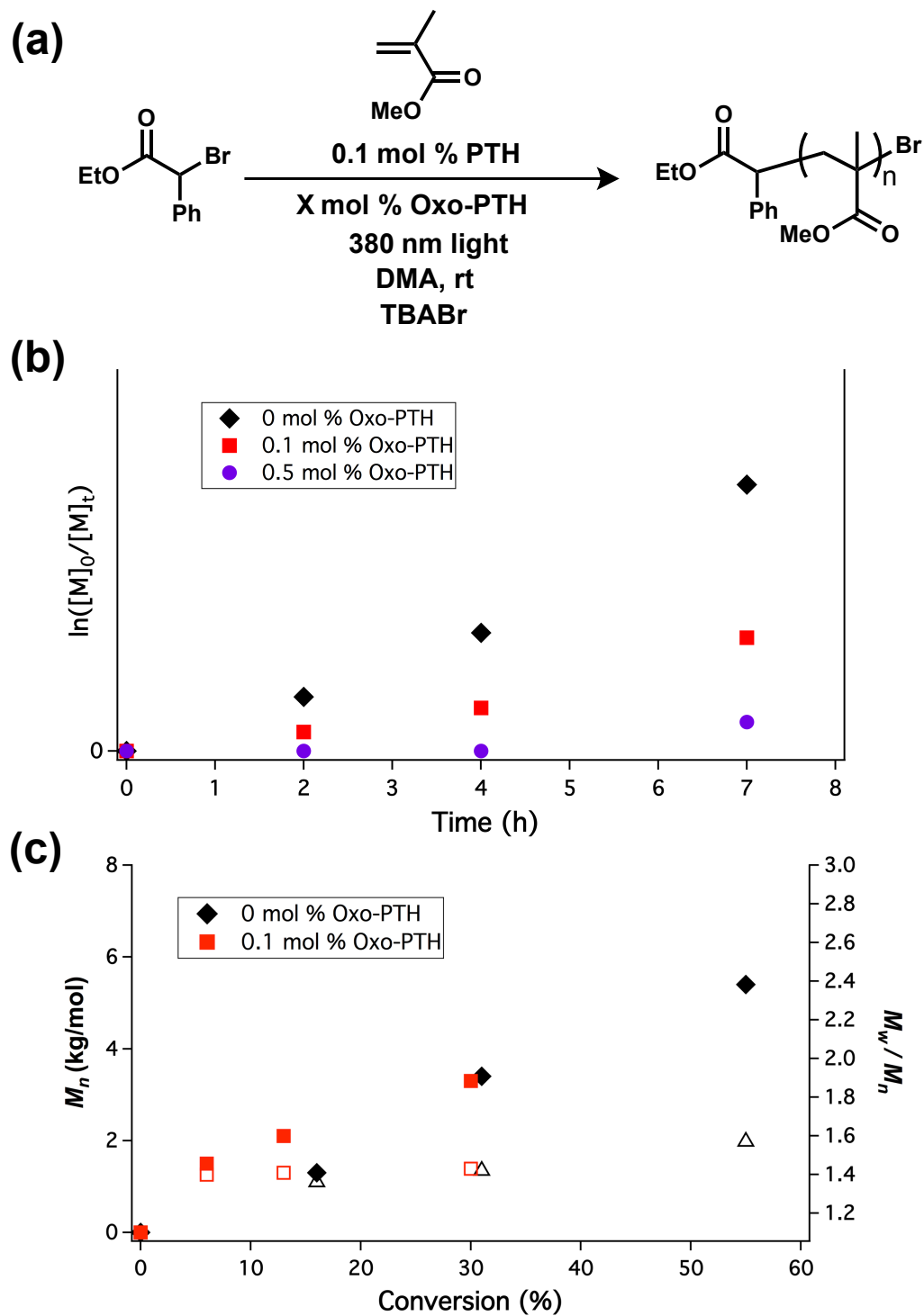
Figure 7.5 Polymerization kinetics of methyl methacrylate using typical metal-free ATRP conditions, while adding in various amounts of Oxo-PTH and bromide anion, observing a decrease in kinetic behavior when adding Oxo-PTH as deactivator

C. Uncovering the Highly Oxidizing Nature of Oxo-PTH

In seeking to better understand reactivity of Oxo-PTH, it was also uncovered that it can be highly oxidizing in the excited state ($E*^{ox}_{1/2} = +2.2$ V vs. SCE, see SI). As a proof of this highly oxidizing nature, a test reaction was conducted in the presence of *N,N*-dimethylformamide ($E^{ox} = +2.3$ V vs. SCE).[5] Thus, Oxo-PTH was added to *N,N*-dimethylacetamide, and monitored both in the presence of light and in darkness. In the dark no reaction was observed; however when irradiated, the presence of PTH in the ^{1}H NMR was observed after just 1 h (Figure S7.2). This is an initial proof that Oxo-PTH can be highly oxidizing in the excited state (Figure 7.7), even oxidizing amide bonds.
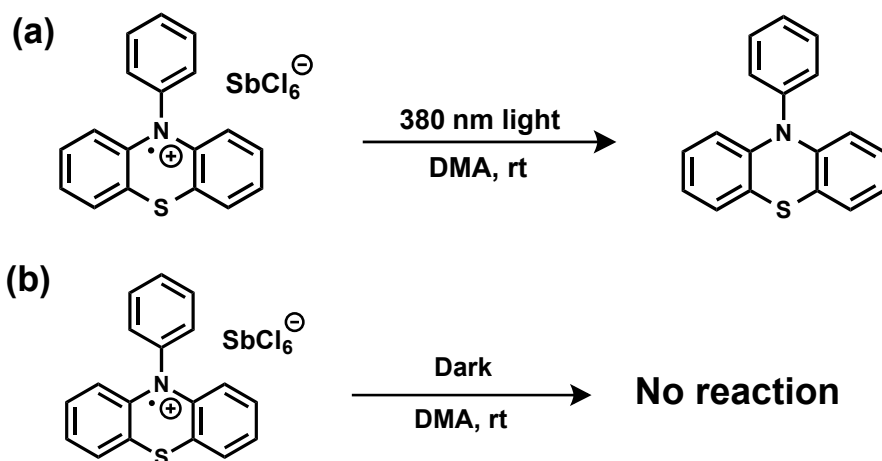

Figure 7.6 Experiments giving evidence of a photoexcited oxidation of DMA by Oxo-PTH where (a) in the presence of light the generation of PTH is observed, and (b) when placed in the dark, no generation of PTH occurs (see Figure S7.2)
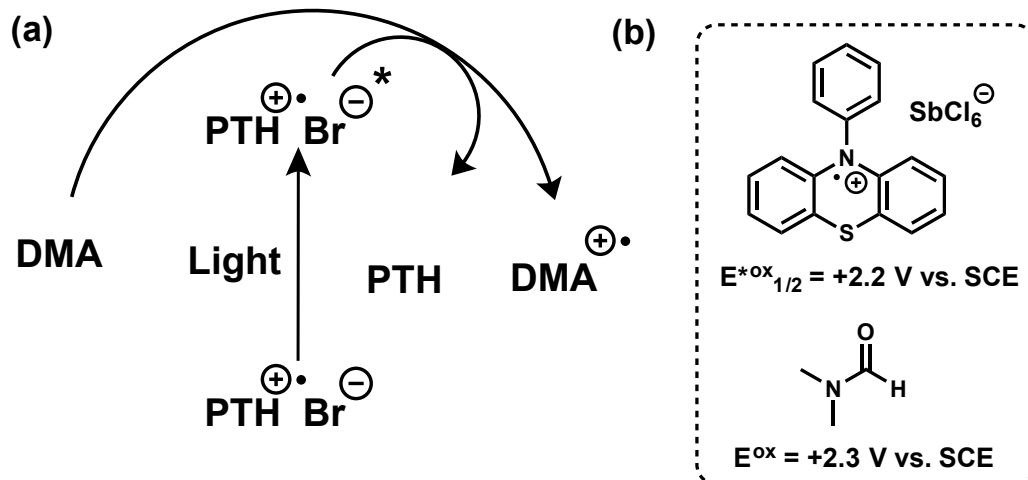
Figure 7.7 (a) Proposed mechanism for DMA oxidation by Oxo-PTH (b) with the excited state redox potentials listed for Oxo-PTH and DMF, suggesting that it is thermodynamically accessible to oxidize amides with Oxo-PTH

This initial proof of concept illustrates the potential power for PTH as a catalyst to act in both a highly oxidizing (Oxo-PTH $E^{*ox}_{1/2}$ = +2.2 V vs. SCE) and a highly reducing manner (PTH $E^{*red}_{1/2}$ = -2.1 V vs. SCE). Such highly oxidizing and reducing capabilities in a single catalyst have not been reported to date. However, taking advantage of either of these redox potentials will likely generate highly unstable intermediates, thus making it difficult to take full advantage of both oxidation and reduction in a single reaction. Perhaps by combining the catalyst with a transition metal these highly reactive intermediates may be intercepted before decomposition.

III. Conclusions

By taking advantage of the ability to isolate PTH in its oxidized form (Oxo-PTH), a variety of studies were conducted to understand its relationship to bromine. It was found that combination of Oxo-PTH with a variety of bromine anion sources all gave a rapid color

shift from red to yellow, and subsequent EPR, UV-Vis, Photoluminescence, and NMR studies all suggesting the rapid oxidation of bromine to a radical and the formation of ground state PTH. This increased mechanistic understanding opens the door for taking advantage of this knowledge to add in a deactivator to slow down the kinetics and obtain better chain end control. As an initial proof of concept, various amounts of Oxo-PTH were added to the polymerization of MMA in order to alter the kinetic profile of these polymerizations, while retaining control. This confirms the hypothesis that a better mechanistic understanding may lead to changing polymerization behavior. Future studies will focus on the use of other bromine radical sources (i.e. Br_2 or Br_3 anions) to modulate polymerization behavior.

IV. Acknowledgements

Yingdong Luo played a large role in much of the work discussed in this chapter. Many of the radical cation studies were conducted by him, and he worked hard to understand more deeply what was happening in these systems. This chapter would not have been possible without his expertise, tenacity, and passion.

V. References

[1]   X. Pan, C. Fang, M. Fantin, N. Malhotra, W. Y. So, L. A. Peteanu, A. A. Isse, A. Gennaro, P. Liu, K. Matyjaszewski, *J. Am. Chem. Soc.* **2016**, *138*, 2411–2425.

[2]   S. A. Odom, S. Ergun, P. P. Poudel, S. R. Parkin, *Energy Environ. Sci.* **2014**, *7*, 760.

[3]   S. Ergun, C. F. Elliott, A. P. Kaur, S. R. Parkin, S. A. Odom, *Chem. Commun.* **2014**, *50*, 5339.

[4]   K. A. Muszkat, I. Khait, *J. Chem. Soc., Chem. Commun.* **1986**, 446.

[5]   H. Roth, N. Romero, D. Nicewicz, *Synlett* **2016**, *27*, 714–723.

VI. *Supplementary Information*

A. General Reagent Information

All polymerizations were carried out under an argon atmosphere. Methyl methacrylate, benzyl methacrylate, methyl acrylate, and styrene were purchased from Sigma-Aldrich and passed through a plug of basic alumina before use.   Anhydrous *N,N*-dimethylacetamide, Methylene blue, Eosin Y, ethyl α-bromophenylacetate, ethyl α-bromoisobutyrate, 10-methyl phenothiazine, phenothiazine, RuPhos, *N,N,N',N',N''*-pentamethyldiethylenetriamine, 4,4'-dinonyl-2,2'-dipyridyl, *fac*-[Ir(ppy)₃], sodium *tert*-butoxide, and anhydrous chlorobenzene were purchased from Sigma-Aldrich and used as received. CuBr was purchased from Sigma-Aldrich and purified by washing with acetic acid, followed by ethanol and ether. The resulting CuBr was kept under an argon atmosphere. RuPhos Precatalyst was purchased from Strem Chemicals Inc. Oxo-PTH was synthesized according to a literature procedure.[2]

B. General Analytical Information

Nuclear magnetic resonance spectra were recorded on a Varian 400 MHz, a Varian 500 MHz, or a Varian 600 MHz instrument. All ^{1}H NMR experiments are reported in δ units, parts per million (ppm), and were measured relative to the signals for residual chloroform (7.26 ppm) in the deuterated solvent, unless otherwise stated. All ^{13}C NMR spectra are reported in ppm relative to deuterochloroform (77.23 ppm), unless otherwise stated, and all were obtained with ^{1}H decoupling. Gel permeation chromatography (GPC) was performed on a Waters 2695 separation module with a Waters 2414 refractive index detector eluting

with 0.25 wt% triethylamine/chloroform and a Waters Alliance HPLC System, 2695 separation module with combined Wyatt DAWN HELEOS-II light scattering/Wyatt Optilab rEX refractive index detectors. Number average molecular weights (M_n) and weight average molecular weights (M_w) were calculated relative to linear polystyrene standards or from light scattering. Reported molecular weights (M_n) were calculated using ^{1}H NMR by comparing the integration of the ethyl protons on the initiating chain end to the polymer side chain peaks unless otherwise noted. Mass spectrometry was performed on a Micromass QTOF2 Quadrupole/Time-of-Flight Tandem instrument. Cyclic voltammetry was carried out on a VMP Multichannel Potentiostat with EC lab software.

C. Determination of Excited State Oxidation Potential for Oxo-PTH

A Varian Cary Eclipse Fluorescence Spectrophotometer was used to measure fluorescence. Photoluminescence max of Oxo-PTH was estimated to be 440 nm (see Figure 7.3). The reduction potential of Oxo-PTH was measured with cyclic voltammetry to be E^{red} = - 0.6 V vs. SCE. Using the photoluminescence λ_{max} and E^{red}, the excited state reduction potential was estimated for Oxo-PTH ($E_{1/2}{}^{ox}* = +2.2$ V vs. SCE) using the following equations:

$$E_{1/2}*^{ox} = E^{red} + E_{0,0}$$

where $E_{0,0} = hc / \lambda_{max} = 1240$ nm $/ \lambda_{max}$.

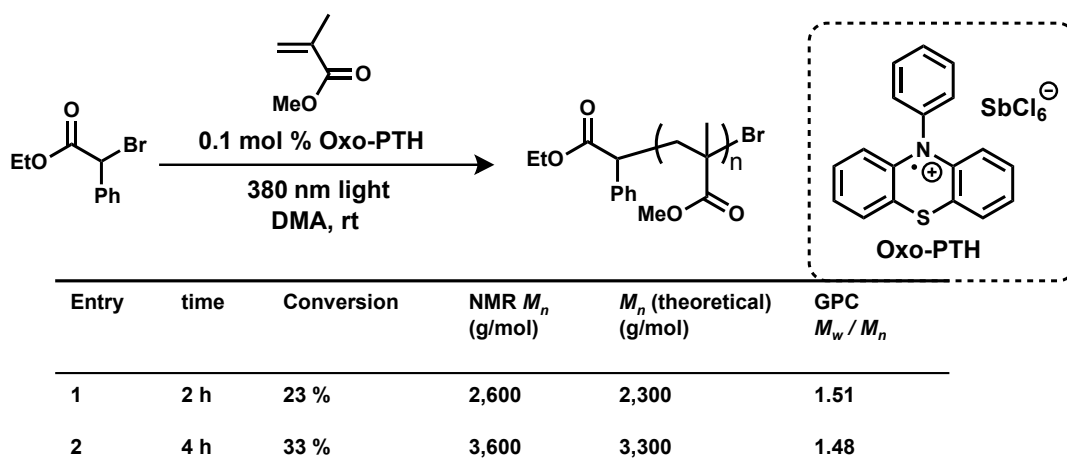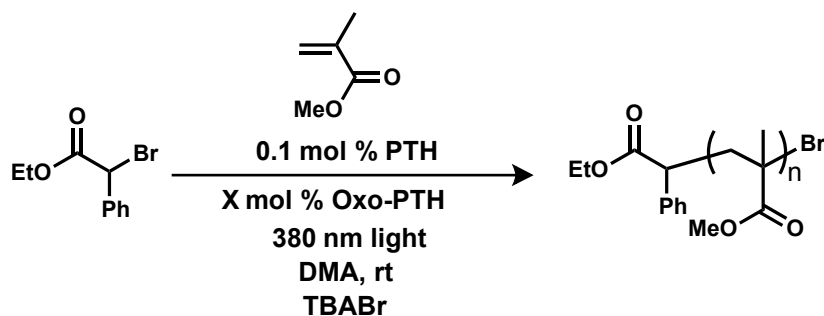| Entry	time	Conversion	NMR M_n (g/mol)	M_n (theoretical) (g/mol)	GPC M_w / M_n
1	2 h	23 %	2,600	2,300	1.51
2	4 h	33 %	3,600	3,300	1.48

Figure S7.1 Polymerization of methyl methacrylate using oxo-PTH, giving evidence for oxidation of DMA, leading to the formation of PTH to activate polymerization and gain control

D. Procedure for Figure 7.5

A vial equipped with a magnetic stir bar and fitted with a teflon screw cap septum was charged with Oxo-PTH (0.1-0.5 mol %), tetrabutylammonium bromide (12 mg, 0.0375 mmol, 1 mol %), methyl methacrylate (401 µL, 3.75 mmol), PTH (1 mg, 0.1 mol %) and *N,N*-dimethylacetamide (1 mL). Note: make sure to add both Oxo-PTH and TBABr together before adding DMA, as oxidation of Oxo-PTH can occur. The reaction mixture was degassed with three freeze-pump-thaw cycles. The vial was then backfilled with argon and ethyl α-bromophenylacetate (6.6 µL, 0.0375 mmol) was injected via syringe. The reaction

was vigorously stirred in front of 380 nm LEDs while cooling with compressed air to maintain ambient temperature. The reaction conversion of MMA was monitored by ^{1}H NMR. An aliquot was taken and analyzed using ^{1}H NMR or GPC to give the molecular weight (M_n) and GPC to give the molecular weight distribution (M_w/M_n) of the polymer.

E. Procedure for Figure S7.1

A vial equipped with a magnetic stir bar and fitted with a teflon screw cap septum was charged with methyl methacrylate (401 µL, 3.75 mmol), Oxo-PTH (0.1 mol %) and *N,N*-dimethylacetamide (1 mL). The reaction mixture was degassed with three freeze-pump-thaw cycles. The vial was then backfilled with argon and ethyl α-bromophenylacetate (0.075 mmol) was injected via syringe. The reaction was vigorously stirred in front of 380 nm LEDs while cooling with compressed air to maintain ambient temperature. The conversion of MMA was monitored by ^{1}H NMR. An aliquot was taken and analyzed using ^{1}H NMR to give the molecular weight (M_n) and GPC to give the molecular weight distribution (M_w/M_n) of the polymer.
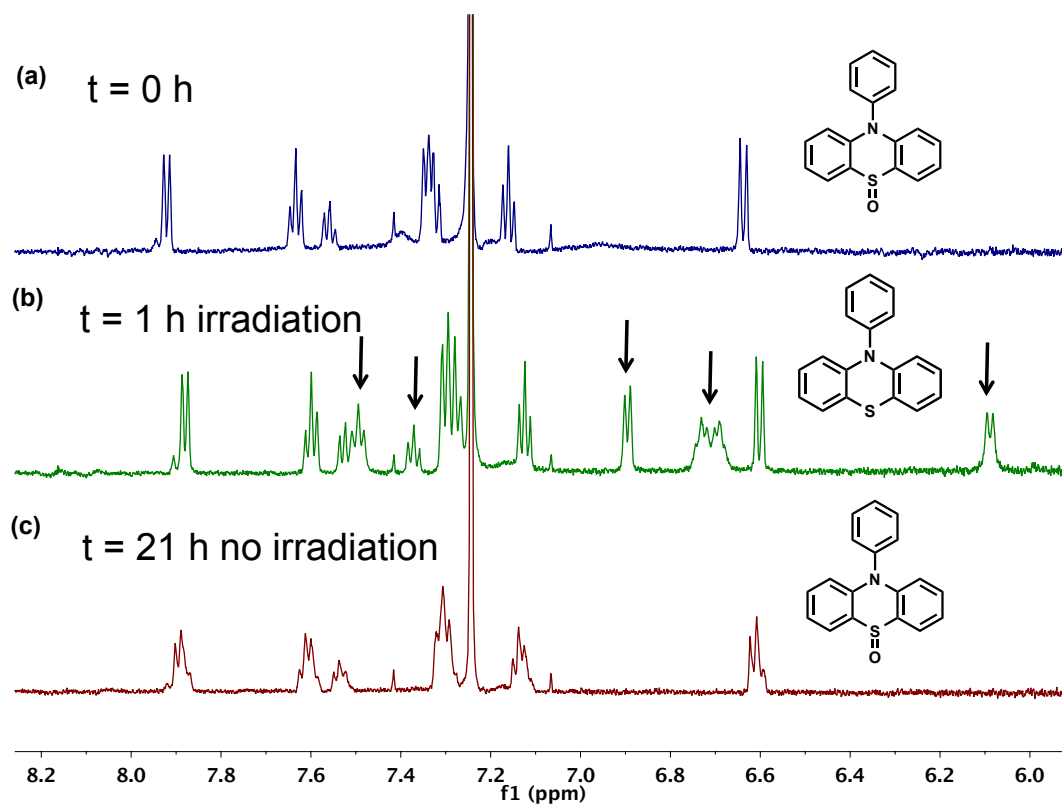
Figure S7.2 ^{1}H NMR for experiments shown in Figure 7.6, showing (a) the formation of PTH-SO initially due to oxygen reacting with the radical cation. (b) after 1 h of irradiation in dimethylacetamide the emergence of PTH peaks are indicated by arrows and (c) when the reaction is put in the dark, no change in the spectrum occurs